THE REDUCTION OF STRUCTURE-BORNE NOISE BY ACTIVE CONTROL OF VIBRATION

Promotoren : Prof. dr. ir. P. Sas
Prof. dr. ir. H. Van Brussel

Proefschrift voorgedragen tot het behalen van het doctoraat in de toegepaste wetenschappen door

ir. Wouter DEHANDSCHUTTER

97D7 December 1997

DANKWOORD

John Tyndall indachtig[1] word ik verondersteld met een combinatie van frustratie en opluchting terug te kijken op de voorbije jaren (vooral weken). Hoewel ik niet wil beweren dat ik met plezier wekenlang gekluisterd zat aan mijn tekstverwerker, durf ik zonder meer te stellen dat de term frustratie naast de kwestie is. Een doctoraat tot een goed einde brengen, is immers geen éénmanszaak. In eerste instantie is er de promotor die het werk begeleidt. In dit specifiek geval stonden zelfs twee promotoren in voor de begeleiding.

Professor Sas dank ik oprecht voor zijn blijvende interesse voor mijn werk. Zijn efficiënte pragmatische manier van problemen bekijken heeft tijdens onze talloze discussies bij herhaling nieuwe denkpistes opengegooid. Maar bovenal wil ik Paul Sas bedanken voor de sfeer van vertrouwen waarin ik jarenlang heb kunnen werken. Toen het ANRAVA-project lichtjes in mineur dreigde te eindigen stak hij, overtuigd van ons gelijk dat het beter kon, een diplomatiek en financieel tandje bij om het materiaal ter beschikking te krijgen voor aanvullende tests.

Het enthousiasme van Professor Van Brussel voor mechatronica, in al haar verschijningsvormen, is spreekwoordelijk. Onder zijn impuls werd reeds in het kader van mijn eindwerk mijn aandacht gewekt voor het aspect van het controle-ontwerp bij het ontwerp van mechatronische systemen. Zijn niet aflatende inspanningen om mij als onderzoeker te motiveren niet zomaar mee te spelen in dit domein maar zonder meer het betere werk te leveren heeft ongetwijfeld bijgedragen tot de kwaliteit van deze thesis.

Naast mijn promotoren wil ik ook Professor Vermeir bedanken als derde lid van mijn leescomité. De interessante suggesties die hij gaf bij de tekst betekenden dat een regelrechte meerwaarde voor deze thesis.

Furthermore I would like to express my gratitude for the effort made by Professor Elliott to read and evaluate my work as a member of the jury. Ook Professor Moonen en Professor De Schutter wil ik om die redenen bedanken.

---

[1] "I think I shall never undertake to write a book again. If one were a scamp, the work would be easy enough, but for an honest man it is dreadful" *J.T., 1859.*

Actieve controle is per definitie een multidisciplinair onderwerp, hetgeen als voordeel heeft dat je als onderzoeker niet steeds bij dezelfde mensen om raad moet. Tegelijkertijd impliceert het ook dat ik aan vele collega's schatplichtig ben voor de resultaten die ik de voorbije jaren wist te behalen.
Professor Van Herck is niet weg te denken uit elke vorm van onderzoek met enige praktisch-experimentele inslag. Zelfs de meest onverklaarbare "spoken" in een meetopstelling werden met doorslaggevende argumenten - te weten : het bord en een stuk krijt- uit de wereld geholpen.
De samenwerking met mijn meest naaste collega en zeer goede vriend Pieter Van den Braembussche nam een "vliegende" start bij de aanvang van onze thesis. Mijn huidig inzicht (...) in controletechnieken zoals H_∞ is zonder twijfel te danken aan alle inspanningen die Pieter reeds lang vóór mij had geleverd om zich in die theorie in te werken. Pieter was de voorbije jaren ook een aangenaam buro-genoot en gesprekspartner met wie ik meer dan alleen controleproblemen kon delen.
Bij Wim Desmet, hoegenaamd niet vies van een theoretische discussie ten gronde (en trouwens ook niet, het moet gezegd, van een frisse pint[2]), ging ik nooit tevergeefs aankloppen met om het even welk probleem. Van eenzelfde kaliber is Jan Swevers. Van hem zal me zowel zijn competentie bijblijven als de manier waarop hij "ik-kom-direkt-maar-hier-eerst-nog-efkes ...*klik*... een-berekeningske-opstarten" altijd aandacht kon hebben voor waar ik mee vast zat. Ook Ward Heylen ben ik veel dank verschuldigd voor het helpen zoeken naar oplossingen voor vraagstukken aangaande modale analyse in het algemeen, en het Cada-X® systeem[3] in het bijzonder.
Met plezier denk ik ook terug aan de samenwerking met alle collega's die deel uitmaken of uitmaakten van onze groep structuurdynamica, en de groep 'actieve controle' in het bijzonder. Allerhande discussies met hen hebben mij verplicht de theorie en praktijk van actieve controle beter te doorgronden. Chaoying Bao, Mr. Spox, introduced me to the adaptive signal processing techniques. Renaat Van Cauter was een prima eerste hulp bij de praktische gevallen die zich in de beginfase van het ANRAVA-project stelden. Zijn uitgebreide testwerk legde mee de basis voor de resultaten die we op het einde van het project wisten te behalen. Ook Joris Van Herbruggen, voorwaar een Matlab®-gymnast van het eerste garnituur, droeg wezenlijk bij tot het succes van dit project. De testresultaten die we op één 20-uren werkdag, en onder siberische omstandigheden, op verplaatsing in Wolfsburg behaalden gaven uiteindelijk de doorslag om "de Passat" niet

[2] Duvel is ook goed
[3] Vooral omdat het antwoord dikwijls letterlijk in de handleiding stond.

onmiddellijk na afloop van het project te verschroten. Pierre De Fonseca en Kris Henrioulle pakten kordaat verscheidene modellerings-problemen aan die ikzelf noodgedwongen op de lange baan had geschoven. Zij hebben het in zeer korte tijd mogelijk gemaakt dat wij als groep een hartig woordje kunnen meespreken over het modelleren, optimaliseren en controleren van verdeelde piezo-elektrische actuatoren en sensoren. Ook met René Boonen heb ik menig woordje kunnen wisselen betreffende het waarom van het hoe van controle. It was also a pleasure for me to work together with Roberto Arruda to develop the adaptive control approach to active control of power flow. I do hope we can extend our co-operation in future, more experimental work.
Ook mensen van buiten mijn eigen onderzoeksgroep leverden belangrijke bijdragen. Het was met de hulp van de DSP-wizards Luc Stevens en Lieven Demeestere dat ik de zevenkoppige draak in mijn C40-DSP-bord C-gewijs wist te bedwingen. Peter Van Overschee pakte de achilleshiel in het probleem van spectrale factorisatie op een doeltreffende manier aan. Verder wil ik zeker ook Katrien Wyckaert en Herman Van der Auweraer, van de firma LMS International, hartelijk danken voor de aangename én leerrijke samenwerking, zowel in het kader van Europese projecten als daarbuiten.
Daarnaast werd mijn onderzoek de voorbije vijf jaar voortgestuwd door het spel van wetenschappelijke vraag en aanbod dat gepaard gaat met het begeleiden van de laatstejaars thesisstudenten (met dank aan Bruno en Renaat, Francis en Philip, Michael, Joris en Gert, Bruno en Kris, Yves, Benoit en Tomas). Aangezien 4 van hen nadien besloten assistent te worden aan onze afdeling, ben ik zo vrij te veronderstellen dat de voldoening betreffende onze samenwerking wederzijds is geweest.
En natuurlijk had ook dit doctoraatswerk nergens gestaan zonder de daadwerkelijke en adequate bijstand van onze technische diensten, de mechanische en electronische werkplaats; en zonder de hulp van iedereen van de dienst informatica, en het secretariaat en de bibliotheek.

Mijn oprechte dank gaat ook uit naar iedereen op het thuisfront, (schoon)ouders, (schoon)broers en zussen, voor de regelmatige "en hoe zit het ermee?". Mijn bijzondere dank gaat naar mijn ouders, voor de inspanningen die ze hebben gedaan om het mij mogelijk te maken verder te studeren. Bedankt ook, mijn vrienden op en buiten het werk, Bruno, Michel, Luigi en Gudrun, Fulop, Thierry, Luc en Els, voor het beurtelings klaagmuur spelen. Bedankt Frank, voor de mens.

Een zeer bijzondere vermelding komt tenslotte toe aan mijn gezinnetje. Deze thesis is het resultaat van intensief thuiswerk. Terwijl ik zelf wekenlang tussen vrouw, kinderen en computer zapte, bleef mijn eigen zender maar al te dikwijls op beeld zonder klank staan. Lieve kleine Gitte, ik dank je voor je kordate "boekje nu toedoen, papa" op tijd en stond, en Idries, flink baasje, voor je gelaatsbrede glimlach de hele dag door. En Veerle, ik dank je voor alle begrip dat je op de juiste momenten wist op te brengen. Aan jullie drie is dit werk opgedragen.

ABSTRACT

This thesis deals with active control approaches to the reduction of structure-borne noise by controlling the vibration of the sound radiator. The latter specification emphasises the fact that the physical vibro-acoustic mechanisms dictate that maximum control efficiency will be attained by *reshaping* the vibration patterns of the radiating system (Active Structural Acoustic Control, or ASAC), rather than by reducing vibration levels at some selected points (Active Vibration Control, or AVC). The thesis considers basic control theory as well as the practical aspects of the implementation of active control systems, and discusses two strategies for ASAC in detail.

First, an LTI feedback controller is synthesised in the state space. The control objective is the global reduction of the total sound power radiated by a vibrating structure either to the free field or into an enclosure. The controller applies the appropriate control forces by means of point force actuators ; a measure of the vibration of the structure is used as a feedback signal. A model for the radiation behaviour of the structure is the basis for the design of the controller. This control strategy is validated, both on simulations and by means of experiments, for the case of a baffled, elastic, rectangular plate which radiates to the free field.

Secondly, an adaptive feedforward controller for the ASAC of structure-borne road noise in a passenger car is developed. The accelerations measured at the wheel centres serve as reference signals. Inertia shakers are used to control the vibration of car body ; microphones located in the car cabin are the error sensors. The control configuration is optimised by means of numerical simulations and laboratory tests, and is then validated in a series of road tests. This research work has initiated the development of a technique for the real-time enhancement of the reference signals for feedforward control. A numerical simulation of the control performance achieved with an enhanced reference set validates the technique.

NEDERLANDSE SAMENVATTING

Deze thesis behandelt actieve controle-strategieën voor de reductie van structuurgeluid door de trilling van de geluidsafstralende structuur op gepaste manier te controleren. Deze benadering wordt in het algemeen omschreven als "Actieve Structureel-Akoestische Controle" (ASAC). Deze aanpak verschilt wezenlijk van actieve trillingscontrole, aangezien het bij actieve trillingscontrole louter de bedoeling is het trillingsniveau van de structuur te reduceren, hetgeen niet noodzakelijk aanleiding geeft tot vergelijkbare reducties in afgestraald geluid. De thesis beschouwt zowel de theoretische aspecten van het ontwerp van de regelaar, als de praktische aspecten van de implementatie. Twee strategieën voor ASAC worden in detail behandeld.

Enerzijds wordt een lineaire, tijdsinvariante, modelgebaseerde regelaar ontworpen die de toestanden terugkoppelt van een toestandsruimtemodel dat zowel de structurele als de vibro-akoestische respons van het te controleren systeem beschrijft. De regelaar realiseert een globale reductie van het akoestisch vermogen dat de trillende structuur in het vrije veld of in een caviteit afstraalt. De regelaar maakt gebruik van een toestandsschatter om op basis van gemeten versnellingen de systeemtoestanden te schatten, en van een electrodynamische excitator om de controlekracht aan te leggen. De experimenten met een rechthoekige trillende plaat bevestigen het potentieel van deze benadering.

Daarnaast wordt het ontwerp besproken van een adaptieve vooruitgekoppelde regelaar voor de reductie van het rolgeluid in een wagen. De regelaar gebruikt tri-axiale accelerometers, bevestigd aan de wielassen, als referentie-sensoren, microfoons als foutsensoren, en inertiële actuatoren. De configuratie van het controlesysteem werd geoptimaliseerd d.m.v. numerieke simulaties en experimenten in het laboratorium. De resultaten van de wegtesten bevestigen de voorspelde controleperformantie. Aansluitend op dit werk werd een techniek ontwikkeld die de kwaliteit van de gebruikte referentiesignalen, en dus de maximaal haalbare reductie, alsook de convergentiesnelheid van het controle-algoritme verbetert. Deze techniek werd gevalideerd d.m.v. numerieke simulaties.

1. Inleiding en motivatie

Actieve controle is een techniek die erop gericht is het dynamisch gedrag te wijzigen van mechanische, akoestische, of vibro-akoestische systemen door gerichte controle-acties op het systeem uit te oefenen. Een *controle-eenheid* stuurt deze controle-acties. Deze controle-eenheid baseert zich daartoe op meetgegevens, afkomstig van een set *sensoren* die de respons van het systeem observeren, en eventueel op een systeemmodel. De *controle-actuatoren* oefenen de te nemen controle-acties (kracht, volumetrisch debiet, ...) uit op het systeem.
De term "actieve" controle lijkt enigszins contradictorisch voor controlespecialisten aangezien elke vorm van controle een zekere actie impliceert. Het predikaat "actief" wordt echter voornamelijk gebruikt om deze benadering te onderscheiden van de klassieke, de zogenaamde "passieve", trillings- en geluidscontroletechnieken. Actieve controle onderscheidt zich van passieve controle in die zin dat actieve controle energie toevoegt aan het systeem. Met uitzondering van de controle-eenheid en de toegevoegde sensoren en actuatoren, blijft het oorspronkelijke systeem echter ongewijzigd. Dit in tegenstelling tot de passieve controletechnieken, die het dynamisch gedrag van het systeem voornamelijk trachten te wijzigen door massa en/of dempingsmateriaal toe te voegen, of door de constructie aan te passen (toevoegen van verstijvers, e.a.). Vooral bij lage frequenties blijkt deze aanpak weinig efficiënt. Onder de beperkende voorwaarden van een maximum aan toegevoegde massa of aan constructieve wijzigingen kan enkel actieve controle aanzienlijke trillings- of geluidsreducties realiseren bij lage frequenties.

Deze thesis behandelt in hoofdzaak strategieën voor Actieve Structureel-Akoestische Controle, afgekort ASAC, met als doel het structuurgeluid te reduceren dat afgestraald wordt door trillende systemen. ASAC streeft, door gerichte controlekrachten aan te leggen, naar een optimale beïnvloeding van het trillingspatroon van de geluidsafstraler zodanig dat een maximale reductie van de afgestraalde akoestische energie behaald wordt met een minimum aan controle-energie. In die zin onderscheidt ASAC zich expliciet van actieve trillingscontrole (Active Vibration Control, kortweg AVC), waar louter de reductie van het trillingsniveau nagestreefd wordt, vermits ASAC in specifieke toepassingen een reductie van de afgestraalde akoestische energie realiseert door de trillingsniveaus te verhogen. Daarnaast werd ook aangetoond [34] dat ASAC in praktijk efficiënter blijkt dan actieve

geluidscontrole (Active Noise Control, of ANC), waarbij het afgestraalde geluidsveld gecontroleerd wordt m.b.v. akoestische controle-actuatoren.

Het werk in deze thesis wordt voornamelijk gemotiveerd door het potentieel dat ASAC biedt voor problemen waarbij de component structuurgeluid een belangrijk aandeel heeft. Met name : ASAC is efficiënter en biedt de mogelijkheid tot een ver doorgedreven integratie van de actuatoren en sensoren van het actieve controlesysteem in het gecontroleerde systeem. Meer specifiek heeft deze thesis als doel bij te dragen op het gebied van het ontwerp van aangepaste regelaars voor ASAC.
Hiertoe wordt vooreerst een degelijke basis gelegde onder de vorm van een overzicht van de controletheorie vanuit het standpunt van actieve controle. Dit overzicht heeft als voornaamste bedoeling de nodige inzichten te verschaffen in de fundamenten van de meest toegepaste controle-algoritmen. Enerzijds moet dit toelaten de ontwikkelingen in de daarop volgende hoofdstukken correct te interpreteren. Anderzijds werd er echter hoofdzakelijk naar gestreefd het overzicht dusdanig te organiseren en te documenteren met de nodige referenties dat het kan dienen als referentiewerk voor de ontwikkeling van regelaars in andere toepassingen dan de reductie van structuurgeluid, voor de evaluatie van de controlebenadering in aanverwant werk, enz. Dit overzicht vormt aldus een wezenlijk onderdeel van het doctoraatswerk en wordt beschouwd als een expliciete bijdrage tot het verwezenlijken van de doelstellingen van de thesis.
Daarnaast wordt het ontwerp van regelaars voor ASAC in detail besproken. Ten eerste wordt aangegeven hoe ASAC kan gerealiseerd worden met een controleconfiguratie die louter gebruik maakt van sensoren die een structurele respons meten, en voor het geval dat geen referentiesignaal voor de stoorbron voorhanden is. Om dit concreet probleem op te lossen wordt een procedure voorgesteld voor het ontwerp van een toestandsruimte-regelaar die een globale reductie realiseert van het totale geluidsvermogen dat een trillende structuur afstraalt. De voorgestelde benadering is gebaseerd op bestaand werk [51] dat echter moeilijk in praktijk toe te passen was. Door deze tekortkoming op te lossen werd in deze thesis de basis gelegd voor een controlestrategie die in principe zeer algemeen toepasbaar is. De praktische realisatie van de hier voorgestelde benadering voor een academisch voorbeeld, de reductie van het geluid afgestraald door een rechthoekige plaat, is de eerste in zijn soort.
Ten tweede wordt een controlestrategie ontwikkeld en geïmplementeerd voor een praktisch probleem, met name de reductie van het rolgeluid in een

wagen. Meer in het algemeen geldt deze toepassing als een voorbeeld van de reductie van structuurgeluid dat veroorzaakt wordt door meerdere, niet-coherente bronnen. De innovatieve benadering van dit probleem, met name het controleren van koetswerktrillingen m.b.v. inertiële actuatoren om het structuurgeluid tengevolge van het rijden over een ruw wegdek te reduceren, kreeg reeds navolging in aanverwant werk op een hoge-snelheidstrein [240]. Verder werd in dit kader een signaalverwerkingstechniek ontwikkeld die de kwaliteit verbetert van de vooruitgekoppelde referentiesignalen voor de controle van meerdere, niet-coherente stoorbronnen die niet onafhankelijk kunnen waargenomen worden. De toepassing van deze techniek voor actieve controle is zonder voorgaande en levert zeer goede resultaten op in de beschouwde toepassing.

2. Controletheorie

2.1 Inleiding

De realisatie van een regelaar voor actieve controle houdt meer in dan het uit een "kookboek" selecteren en rechtstreeks implementeren van een op maat geschreven controle-algoritme. Het vereist de nodige inzichten in de controletheorie om te komen tot een correcte keuze en implementatie van de controlestrategie. Dit hoofdstuk geeft daartoe een omstandig overzicht van de controletheorie. Dit overzicht is in geen enkel opzicht een voortzetting van de inleiding van de thesis, het hoofdstuk heeft een afgelijnde functie : leiden tot een beter ontwerp van regelaars voor actieve controle. De hierop volgende hoofdstukken zullen het overzicht tevens als vertrekbasis gebruiken voor de ontwikkeling van specifieke regelaars voor ASAC.

2.2 Terugkoppeling

Figuur 1 stelt het schema voor van een regelaar met terugkoppelketen. In het algemeen worden 4 types signalen onderscheiden : stooringangen $\mathbf{u}_w$, controle-ingangen $\mathbf{u}_c$, teruggekoppelde uitgangen $\mathbf{y}$ en de zogenaamde *performantie*-uitgangen $\mathbf{z}$. De performantie-uitgangen dienen om de vereisten voor de regelaar $\mathbf{C}(s)$ te specifiëren. Het is hierbij belangrijk op te merken dat de teruggekoppelde en performantie-uitgangen niet noodzakelijk samenvallen. Zo kan bijvoorbeeld de eindpuntverplaatsing van een robot geregeld worden door de hoekverdraaiing in de assen terug te koppelen.

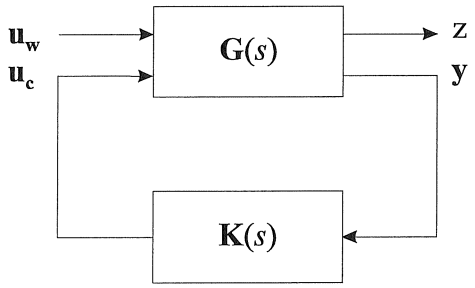

Figuur 1. Algemeen blokschema van een regelaar met terugkoppeling.

Met de intrede van de "moderne" controletheorie, begin jaren '60, werd een belangrijk formalisme geïntroduceerd welke een wiskundige basis legde voor het ontwerp van regelaars voor systemen van hogere orde, en met meerdere ingangen en uitgangen (MIMO systemen). Het ontwerp van de zogenaamde *toestandsruimte*regelaars bestaat uit drie fasen :
(i) opstellen van een toestandsruimtemodel van het systeem

$$\begin{aligned} \dot{\mathbf{x}} &= \mathbf{A}\cdot\mathbf{x}+\mathbf{B}\cdot\mathbf{u} \\ \mathbf{y} &= \mathbf{C}\cdot\mathbf{x}+\mathbf{D}\cdot\mathbf{u} \end{aligned} \tag{1}$$

(ii) uitdrukken van de specificaties voor de regelaar
(iii) de lineaire terugkoppelmatrix $\mathbf{K}$ berekenen die *(ii)* realiseert :

$$\mathbf{u}_c = -\mathbf{K}\cdot\mathbf{x}. \tag{2}$$

De meest algemene specificatie *(ii)* voor de regelaar is een kostenfunctie, die controleperformantie tegen benodigde controle-energie afweegt, en die door het vastleggen van de juiste $\mathbf{K}$-matrix geoptimaliseerd wordt. De meest gebruikte specificatie is de zogenaamde *Lineair Quadratische* (LQ) kostenfunctie (3)

$$J = \int_{t_0}^{t} \left(\mathbf{x}^T\mathbf{Q}_{ctr}\,\mathbf{x} + \mathbf{u}_c^T\mathbf{R}_{ctr}\,\mathbf{u}_c\right)d\tau\ . \tag{3}$$

Indien de toestanden van het systeemmodel overeenstemmen met structurele modale amplitudes, dan drukt (3) een som uit van trillings- en controle-energie. Maximale trillingsreductie zal worden bekomen indien de wegingsfactor van de controle-energie (bepaald door $\mathbf{R}_{ctr}$) verwaarsloosbaar is t.o.v. de weging van de trillingsenergie. Indien het systeem onderhevig is aan Gaussiaanse ruis, wordt de verwachte waarde van (3) berekend. De *LQG* (G voor Gaussiaans) regelaar die deze kostenfunctie optimaliseert, wordt bepaald door de oplossing van de zgn. *Ricatti* vergelijking.

De LQG regelaar blijkt in praktijk weinig robuust tegen modelfouten. De LQG/LTR (*Loop Transfer Recovery*) procedure verhelpt daar gedeeltelijk aan, maar in het algemeen blijft het zo dat de "moderne" controletheorie weinig instrumenten ter beschikking stelt om het aspect robuustheid systematisch in het ontwerp van de regelaar te beschouwen. De "robuuste" controletheorie is precies om die reden ontwikkeld vanaf het begin van de jaren '80. Dit gaf aanleiding tot een nieuwe controletechniek, de H_∞ controle. H_∞ controle is meer geschikt voor het ontwerp van robuuste regelaars ; het formalisme laat echter niet toe om de vereiste controleperformantie op een directe manier te specifiëren.

2.3 Voorwaartse koppeling

Het grote nadeel van regelaars met terugkoppeling is dat de performantie dikwijls sterk beperkt wordt door stabiliteitsproblemen. Deze zijn dan weer het gevolg van de tijdsvertragingen die in akoestische of vibro-akoestische optreden. In dergelijke systemen is regeling met voorwaartse koppeling eigenlijk meer aangewezen. Dergelijke regelaars berekenen de nodige controle-actie op basis van een gemeten *referentiesignaal*. Of, met andere woorden, het referentiesignaal wordt door een *controlefilter* gestuurd, hetgeen het controlesignaal oplevert. De controle-actie is erop gericht het uitgangssignaal van een set *foutsensoren* te minimaliseren.
Lineair tijdsinvariante (LTI) regelaars met voorwaartse koppeling worden eerder zelden aangetroffen in actieve controle toepassingen. Dit is voornamelijk ten gevolge van het feit dat de performantie van dergelijke regelaars aanzienlijk verslechtert indien het dynamisch gedrag van het te controleren systeem of de karakteristieken van de storing verandert. Adaptieve regelaars met voorwaartse koppeling, en meer specifiek het zogenaamde "Filtered-X LMS" controle-algoritme, worden daarentegen toegepast in het merendeel van de ANC, AVC en ASAC toepassingen. De voornaamste redenen hiervoor zijn dat het Filtered-X LMS algoritme betrekkelijk eenvoudig is, doch tegelijkertijd robuust en performant.
Het Filtered-X LMS algoritme is een adaptief algoritme dat iteratief de optimale (kleinste kwadraten, of *Least Mean Square*) oplossing zoekt van een kwadratische kostenfunctie in vooraf gespecifieerde foutsignalen die op hun beurt uitgedrukt worden als functie van de vrije parameters van de regelaar (de coëfficiënten van de controlefilter). Figuur 2 stelt het Filtered-X LMS algoritme schematisch voor. Het gebruik van het meerkanaals Filtered-X LMS algoritme voor actieve controle toepassingen werd voor het eerst voorgesteld door Elliott *et al.* in 1987 [122]. Verscheidene varianten van dit

algoritme werden in de loop van de jaren ontwikkeld, waaronder een frequentiedomein implementatie, een variante met variable convergentiesnelheid, enz.

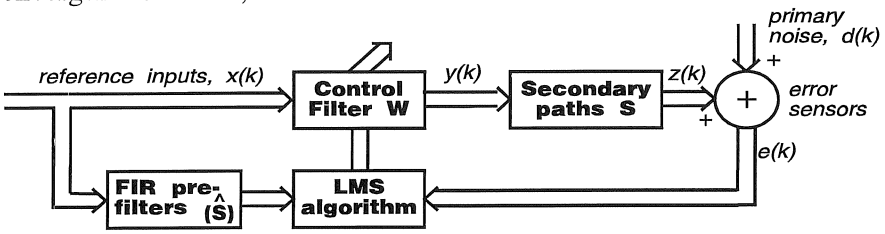

Figuur 2. Blokschema van het Filtered-X LMS adaptief regelschema met voorwaartse koppeling.

Een van de belangrijkste redenen om een adaptieve i.p.v. een LTI regelaar te gebruiken is het feit dat de controleperformantie op die manier niet, of minder, onderhevig is aan tijdsvariabiliteit van de verstoring, tijdsvariabiliteit van de dynamica van het systeem, e.a. De performantie van een regelaar met voorwaartse koppeling is in belangrijke mate functie van de "kwaliteit" van de referentiesignalen. In eerste instantie is het noodzakelijk een (set) referentie(s) te kiezen die een zo hoog mogelijke coherentie oplevert tussen referentie(s) en foutsignaal. Men kan aantonen dat de maximaal haalbare reductie, in dB, van het foutsignaal gelijk is aan

$$\Delta_{max} = -10\,log\left(1-\gamma^2_{d,\{x\}}\right). \tag{4}$$

Hierbij is $\gamma^2_{d,\{x\}}$ de (meervoudige) coherentie tussen de referentie(s) en het foutsignaal.

De keuze van de referentie(s) beïnvloedt echter ook in ruime mate de convergentie-eigenschappen, en bijgevolg ook weer de performantie, van het Filtered-X LMS algoritme. Tenslotte bepaalt de gekozen referentie of de regelaar al dan niet causaal is. Dit laatste begrip houdt voor een eenvoudig, 1-dimensionaal probleem, in dat het referentiesignaal ruim genoeg vooraf in de tijd gemeten wordt, zodanig dat de benodigde tijd om het controlesignaal te berekenen plus de tijd voor de controle-actie om de foutsensor te bereiken, kleiner is dan de tijd die de verstoring nodig heeft om van de referentiesensor naar de foutsensor te propageren. Voor een actief geluidscontrolesysteem in een ventilatiekanaal, bijvoorbeeld, houdt de causaliteitsbeperking dus in dat de referentiesensor voldoende ver ("stroomopwaarts") van de foutsensor moet verwijderd zijn.

2.4 Verschillen en equivalenties tussen voorwaartse koppeling en terugkoppeling

Bij de samenstelling van de controleconfiguratie -niet alleen in het geval van actieve controle- rijst dikwijls de pertinente vraag welke controlestrategie, voorwaartse koppeling of terugkoppeling, de "beste" is. Het is duidelijk dat niet zonder meer een in het algemeen "betere" strategie kan aangeduid worden, aangezien dit sterk afhangt van het soort toepassing. Deze vraag wordt nog het beste beantwoord door de expliciete verschillen, of voor- en nadelen, van beide technieken te overlopen. Een aantal argumenten worden hiervoor in de tekst behandeld.
Bij deze discussie rijst echter de vraag waar het onderscheid tussen beiden precies ligt. Op het eerste zicht lijkt dit een overbodige vraag, aangezien een regelaar met voorwaartse koppeling zich van terugkoppeling onderscheidt doordat hij gebruik maakt van een referentiesignaal om het controlesignaal te berekenen. Een regelaar met terugkoppeling, daarentegen, maakt hiervoor gebruik van een foutsignaal. Dit onderscheidt klopt echter niet volledig daar een adaptieve regelaar met voorwaartse koppeling, bv. het Filtered-X LMS algoritme, eveneens gebruik maakt van een foutsignaal, zij het in dit geval voor de aanpassing van de controleparameters. De berekening van het controlesignaal blijft enkel op basis van het referentiesignaal. Dit onderscheidt zich -in principe- van een foutsignaal voor teruggekoppelde regelaars door het feit dat een referentie in se gebruikt wordt om de verstoring op te meten. Dit terwijl een foutsignaal voor teruggekoppelde regelaars een bijdrage van de verstoring én de regelaar bevat. Echter, in toepassingen met voorwaartse koppeling is het niet onmogelijk dat de controle-actie ook in het referentiesignaal wordt gemeten. Zodoende kan dit soort configuratie eigenlijk ook als terugkoppeling worden aanzien. De thesis behandelt bijgevolg ook een aantal equivalenties tussen beide benaderingen.

3. Een regelaar met terugkoppeling voor Actieve Structureel-Akoestische Controle

3.1 Inleiding

Dit hoofdstuk behandelt het ontwerp van een regelaar voor ASAC van struktuurgeluid in toepassingen waarbij geen referentie voorhanden is voor de (breedband) verstoring. Dit impliceert het gebruik van een regelaar met terugkoppeling. De regelaar meet de trilling van de geluidsafstralende structuur en gebruikt deze als foutsignaal. De regelaar wordt ontworpen in de toestandsruimte. Dit ontwerp is gebaseerd op een model dat de manier beschrijft waarop de gegeven structuur geluid afstraalt ; hetzij in de vrije ruimte, hetzij in een caviteit. De benadering die in dit hoofdstuk voorgesteld wordt, is gebaseerd op het werk van Baumann *et al.* [51].

3.2 Een toestandsruimtemodel voor geluidsafstraling

De opbouw van het model start bij de vaststelling dat, om structuurgeluid te beschrijven, de snelheidsverdeling aan het oppervlak van de trillende structuur moet beschreven worden. Door deze snelheidsverdeling te ontbinden in de structurele moden is het mogelijk te komen tot een uitdrukking van de totale door de trillende structuur afgestraalde akoestische energie als functie van de vector $\mathbf{n}$ met de modale amplitudes en een matrix $\mathbf{M}$, als in (5)

$$E_{tot} = \frac{1}{2\pi\rho c}\int_0^\infty \int_S \mathbf{n}^H \mathbf{M}\,\mathbf{n}\, dS\, d\omega\,. \tag{5}$$

Deze $\mathbf{M}$-matrix bevat de modale stralingsefficiënties, op de diagonaal, en de modale koppelingsfactoren (alle niet-diagonaal elementen), en is functie van de modevormen van de structuur.

Door een spectrale factor van $\mathbf{M}$ te bepalen, d.i. een systeem $\mathbf{G}(s)$ waarvoor geldt dat $\mathbf{G}^T(-s)\mathbf{G}(s) = \mathbf{M}(s)$ op de imaginaire as $s = j\omega$, dan geldt, mede door het Parseval theorema, dat de totale akoestische energie kan uitgedrukt worden als

$$E_{tot} = \frac{1}{2\pi\rho c}\int_0^\infty \mathbf{n}^H \mathbf{G}^H \mathbf{G}\,\mathbf{n}\, d\omega = \frac{1}{2\pi\rho c}\int_0^\infty \mathbf{z}^H \mathbf{z}\, d\omega\,, \tag{6}$$

waarbij $z(t)$ de uitgang is van $\mathbf{G}(s)$ met als ingang de modale amplitudes $\psi(t)$.
Door $\mathbf{G}(s)$ in de toestandsruimte te beschrijven, en dit model te combineren met een toestandsruimtemodel dat de modale amplitudes weergeeft als functie van stoor- en controlekrachten, aangelegd op de structuur, wordt een toestandsruimtemodel bekomen dat de geluidsafstraling beschrijft in het tijdsdomein. Uit identificatie van (6) met (3) blijkt bovendien dat een voor de hand liggende regelwet, die het afgestraalde geluid reduceert, LQ-controle is.
In het algemeen is het bekomen van de spectrale factor $\mathbf{G}(s)$ niet evident. In [51] worden hiertoe een aantal methoden gesuggereerd, en toegepast om een model te bekomen voor de geluidsafstraling van een balk, waarvan de eerste 3 moden beschouwd werden. Voor praktische, en meer complexe toepassingen zijn deze methoden echter zeer omslachtig en bovendien numeriek slecht geconditioneerd. In deze thesis wordt een alternatieve benadering voorgesteld, waarbij de spectrale factor bekomen wordt door toepassing van een zogenaamde *subspace* identificatietechniek. Deze aanpak vereenvoudigt de synthese van de regelaar aanzienlijk.

3.3 Reductie van de geluidsafstraling van een rechthoekige plaat

Als illustratie wordt de voorgestelde strategie toegepast om een regelaar te bouwen die het geluid reduceert dat door een trillende rechthoekige plaat wordt afgestraald. Inertieshakers werden gebruikt, zowel om de stoorkracht als om de controlekracht aan de plaat aan te leggen. De thesis behandelt deze toepassing in twee fasen : ten eerste wordt, op basis van een analytisch model voor een eenvoudig opgelegde plaat, aangegeven hoe de voorgestelde procedure in zijn werk gaat. Vervolgens worden de nodige experimentele gegevens gebruikt om het bekomen model met de werkelijke proefopstelling te laten overeenstemmen. Hierbij betreft het vooral het opmeten van de experimentele modevormen, met overeenstemmende resonantiefrequentie en modale demping, en het opmeten en identificeren van een model voor de controle-actuatoren.
Figuur 3 stelt het resultaat voor van de identificatie van het model voor de geluidsafstraling : de volle lijn stelt de numeriek berekende waarden van $\mathbf{M}$ voor, de streeplijn de waarden die gesynthetiseerd werden op basis van een model voor $\mathbf{G}$. Het dient hierbij opgemerkt dat een aanvaardbare nauwkeurigheid werd behaald voor een relatief lage orde van het model (5 toestanden volstonden). Verder is het duidelijk dat de absolute waarden van de diagonaalelementen de matrix $\mathbf{M}$ uitdrukken welke moden efficiënt

geluid afstralen. De niet-diagonaal elementen welke verschillend zijn van nul, duiden op structurele moden die akoestisch met elkaar koppelen. Zoals bekend, treedt dit soort koppeling enkel op tussen moden van dezelfde groep (de [even, even] plaatmodes koppelen niet met de [even, oneven], [oneven, oneven] en [oneven, even] plaatmodes).

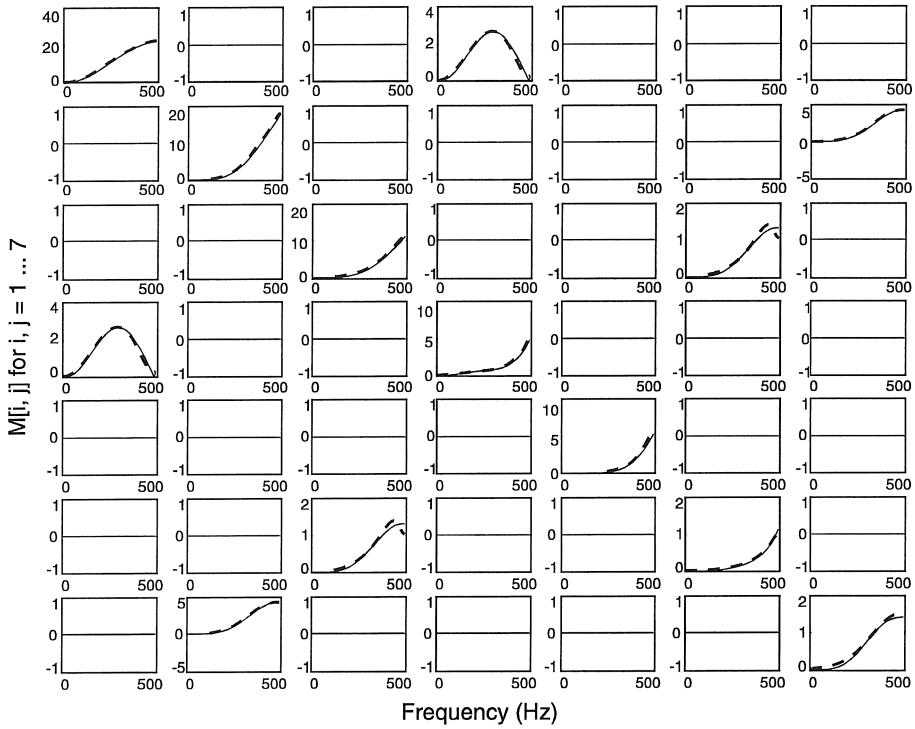

Figuur 3. Resultaat van *subspace* identificatie van een model voor de geluidsafstraling van de rechthoekige plaat.

De regelaar maakt van die eigenschappen gebruik door enerzijds de modale amplitudes te verlagen van moden met een hoge stralingsefficientie. Ten opzichte van actieve trillingscontrole betekent deze selectie een eerste "besparing" van controle-energie aangezien geen moden gecontroleerd worden die niet substantieel tot de afgestraalde akoestische energie bijdragen. Een extra reductie van de benodigde controle-energie volgt uit het feit dat de regelaar ook de koppeling tussen de structurele moden uitbuit. Door de fase tussen twee koppelende moden te wijzigen is het immers mogelijk om de direkte bijdrage, per mode, tot de geluidsafstraling (deels) teniet te doen met een invers gefaseerde bijdrage ten gevolge van de

koppeling tussen die moden. Bijgevolg is het zelfs mogelijk dat het trillingsniveau van de structuur stijgt, terwijl de totale afgestraalde akoestische energie daalt.
Figuur 4 stelt het resultaat voor van twee experimenten. Een eerste experiment leverde reductie op over de gehele bandbreedte waarvoor de regelaar ontworpen werd -met name tussen 0 en 315 Hz- maar de behaalde reductie was eerder gering. Een tweede experiment, met verhoogde kringversterking, leverde hogere reducties op de resonanties van de structurele moden. Een mode die het gevolg was van de koppeling tussen de plaat en de kelder waarboven de plaat was gemonteerd, werd in dit experiment echter versterkt. Deze mode was immers niet in het model opgenomen. Hogere orde moden, zoals bv. op 350 Hz, werden door de regelaar ongemoeid gelaten.

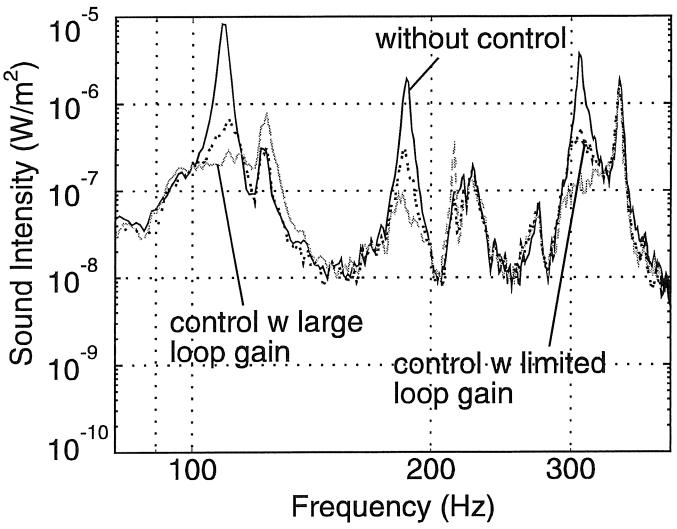

Figuur 4. Resultaat van de controle-experimenten op de rechthoekige plaat.

3.4 Besluit

Dit hoofdstuk introduceert een modelgebaseerde regelaar met terugkoppeling voor de reductie van geluidsafstraling. De experimenten op een rechthoekige plaat tonen het potentieel van de controlestrategie aan. Onder andere door het invoeren van een geavanceerde systeemidentificatie techniek is toepassing van de strategie op meer complexe problemen op realistische wijze verwezenlijkbaar.

4. Ontwerp van een regelaar met voorwaartse koppeling voor de reductie van rolgeluid in een wagen

4.1 Inleiding

Het geluid dat optreedt in een wagen heeft 3 componenten : rolgeluid, aandrijfgeluid en aerodynamisch geluid. In moderne wagens zijn, door aangepast ontwerp, de laatste twee componenten redelijk goed onder controle. Rolgeluid domineert bijgevolg het spectrum, vooral bij lagere frequenties. Bij die frequenties, met name onder de 600 Hz, is rolgeluid voornamelijk structuurgeluid. De trillingen van de wielen die ontstaan ten gevolge van het rijden over een (ruw) wegdek, planten zich voort doorheen de ophanging van de wagen tot aan het koetswerk, dat door die excitatie gaat trillen en bijgevolg geluid afstraalt in het interieur.
Dit hoofdstuk behandelt het ontwerp van een actief controlesysteem voor rolgeluid in detail. In feite worden twee systemen besproken. Ten eerste wordt een innovatieve aanpak voorgesteld, die eruit bestaat de trillingen van het koetswerk actief te controleren. Hiertoe worden trillingsexcitatoren, in dit geval inertiële shakers, op specifieke punten van de ophanging aangebracht. Dit controlesysteem is het zogenaamde ASAC systeem. Een tweede systeem, dat ter vergelijking werd ontwikkeld, gebruikt luidsprekers om het geluidsveld in het wageninterieur te controleren.
De ontwikkeling van beide systemen vormde het onderwerp van een Brite-EuRam project, "ANRAVA", waarin Elesa (It.), KUL (PMA), LMS International (B.), Metzeler Gimetall (D.), Volkswagen (D.), MONROE Belgium, de Univ. van Patras (Gr.), de Univ. van Manchester (GB.), en de Europese Unie participeerden.

4.2 Opbouw van het controlesysteem

Het controle-algoritme dat in dit probleem toegepast wordt, is het Filtered-X LMS algoritme. Bij de selectie van de referentiesignalen voor deze regelaar is het voornamelijk van belang de signalen te selecteren die de hoogste meervoudige coherentie tussen referenties en foutsignalen opleveren. Daarnaast moeten de referenties ook aan de causaliteitsvereisten van een regelaar met voorwaartse koppeling voldoen. Om die redenen werden de trillingen, gemeten aan de wielassen, als referentiesignalen gekozen. Vier microfoons, bevestigd tegen het plafond van de wagen, dienen als

foutsensoren. Het controle-algoritme werd geïmplementeerd op een systeem met vier parallel werkende digitale signaalprocessoren (DSPs).
Een belangrijk aspect bij het ontwerp van de controleconfiguratie was de bepaling van het aantal en de plaats van de controle-actuatoren. Daartoe werd een vibro-akoestische transferpad-analyse (TPA) uitgevoerd. TPA heeft tot doel om te kwantificeren welke transferpaden, van alle mogelijke transferpaden waarlangs trillingsenergie kan overgedragen worden, het meeste bijdragen tot het geluid, waargenomen in de wagen. In deze specifieke toepassing zijn de beschouwde transferpaden alle mogelijke verbindingspunt van de ophanging met het koetswerk van de wagen. De TPA levert bijgevolg een aantal (de meest belangrijke) verbindingspunten op waar controle van de transfer van trillingsenergie het meest invloed zal hebben op de reductie van het rolgeluid. Op zes van deze punten werden controle-actuatoren geplaatst.
Voor het actieve controle systeem met luidsprekers, werden vier luidsprekers geplaatst naast de vier passagiersplaatsen.
De controleconfiguratie werd uitvoerig geoptimaliseerd d.m.v. laboratoriumtesten en numerieke simulaties. In de laboratoriumtesten werd de haalbaarheid van de voorgestelde benadering geverifieerd. Een vereenvoudigde situatie werd hierbij getest. Eén wiel van de wagen werd geëxciteerd, een controleconfiguratie met 1 referentiesensor en maximaal 2 actuatoren en 2 foutsensoren werd in die omstandigheden getest. De numerieke simulaties gaven uitsluitsel over de meest optimale configuratie van een controlesysteem voor actieve controle van rolgeluid in een wagen die effectief over de weg rijdt. Een systeem met 6 referenties, 6 controle-actuatoren, en 4 foutsensoren werd hierbij geoptimaliseerd.

4.3 Wegtesten

Figuur 5 geeft het resultaat weer van de wegtest met het ASAC systeem, uitgevoerd op een relatief vlak wegdek bij een snelheid van 90 km/u. De figuur stelt vermogenspectra voor, gemeten aan de foutmicrofoon linksachter, zonder en met controle. In de frequentieband van 75 tot 105 Hz werd een gemiddelde reductie van 6.9 dB behaald. Met een microfoon ter hoogte van het oor van de passagier op deze positie werd een reductie van 6.1 dB gemeten. Het luidsprekersysteem leverde reducties van respectievelijk 10.2 en 8.8 dB op in de zelfde frequentieband. Deze reducties waren echter minder globaal aangezien de luidspreker zich meer uitgesproken als puntbronnen manifesteerden.

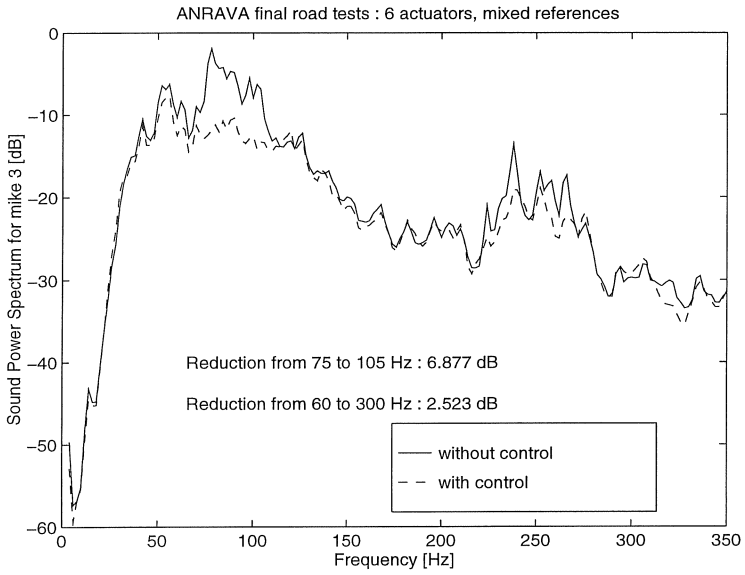

Figuur 5. Resultaat van de wegtest met het ASAC systeem.

4.4 Een algoritme voor de verbetering van de referentiesignalen

Uit wegtesten is duidelijk gebleken dat het noodzakelijk is een ruime set referentiesignalen te gebruiken om een goede meervoudige coherentie tussen foutsignaal en referenties te bekomen. Het beste resultaat, op simulatie, werd in die zin behaald door de accelaraties van elk wiel, in 3 richtingen gemeten, te gebruiken als referenties. Een dergelijk systeem met 12 referenties kon echter niet in praktijk gerealiseerd worden wegens beperkingen in beschikbare rekencapaciteit (ook al was die al aanzienlijk). Bovendien is het gebruik van een dergelijk groot aantal referentiesignalen uiterst nadelig voor de convergentiesnelheid van het controle-algoritme.
In deze paragraaf wordt een algoritme ontwikkeld dat zoveel mogelijk informatie, die vervat zit in een zo ruim mogelijke referentieset, "concentreert" in een beperktere set zogenaamde *virtuele* referenties. Hierbij wordt met name gezocht naar een transformatiematrix $\mathbf{T}(k)$ die de P oorspronkelijke referenties $\mathbf{x}(k)$ transformeert in N_S virtuele referenties $\mathbf{x}^{\circ}(k)$:

$$\left[\mathbf{x}^{\circ}(k)\right]_{N_S\times k} = \left[\mathbf{T}(k)\right]^{T}_{N_S\times P}\left[\mathbf{x}(k)\right]_{P\times k}. \qquad (7)$$

Als transformatiematrix wordt hiervoor de matrix met de singuliere vectoren van de covariantiematrix $\mathbf{COV}_{\mathbf{xx}}(k)$ van de oorspronkelijke referenties,

$$\begin{aligned}\left[\mathbf{COV}_{\mathbf{xx}}(k)\right]_{P\times P} &= \left[\mathbf{x}(k)\right]_{P\times k}\left[\mathbf{x}(k)\right]_{k\times P}^{T} \\ &= \begin{bmatrix} \sum_{n=0}^{k}\left(x_1^2(n)\right) & \cdots & \sum_{n=0}^{k}\left(x_1(n)x_P(n)\right) \\ \vdots & \ddots & \vdots \\ \sum_{n=0}^{k}\left(x_P(n)x_1(n)\right) & \cdots & \sum_{n=0}^{k}\left(x_P^2(n)\right) \end{bmatrix},\end{aligned} \tag{8}$$

genomen. Inderdaad, daar $\mathbf{COV}_{\mathbf{xx}}(k)$ symmetrisch is, is de singuliere waarden ontbinding gelijk aan

$$\begin{aligned}\left[\mathbf{COV}_{\mathbf{xx}}(k)\right]_{P\times P} &\approx \sum_{i=1}^{N_S}\left(\sigma_i(k)\left[\mathbf{u}_\mathbf{i}(k)\right]_{P\times 1}\left[\mathbf{u}_\mathbf{i}(k)\right]_{1\times P}^{T}\right) \\ &= \left[\mathbf{u}(k)\right]_{P\times N_S}\left[\Sigma(k)\right]_{N_S\times N_S}\left[\mathbf{u}(k)\right]_{N_S\times P}^{T}.\end{aligned} \tag{9}$$

Hierbij werden de P-N_S niet-significante singuliere waarden uit de ontbinding verwijderd.

Dus, met $\left[\mathbf{T}(k)\right]=\left[\mathbf{u}(k)\right]$ wordt de covariantiematrix van de virtuele referenties

$$\begin{aligned}\left[\mathbf{COV}_{\mathbf{x}^\circ\mathbf{x}^\circ}(k)\right]_{N_S\times N_S} &= \left[\mathbf{x}^\circ(k)\right]_{N_S\times k}\left[\mathbf{x}^\circ(k)\right]_{k\times N_S}^{T} \\ &= \left[\mathbf{u}(k)\right]_{N_S\times P}^{T}\left[\mathbf{COV}_{\mathbf{xx}}(k)\right]_{P\times P}\left[\mathbf{u}(k)\right]_{P\times N_S} \\ &\approx \left[\Sigma(k)\right]_{N_S\times N_S}.\end{aligned} \tag{10}$$

een diagonaalmatrix. M.a.w., een kleinere set van virtuele referenties wordt bekomen die toch de volledige informatie van de oorspronkelijke referenties reproduceren. Bovendien, aangezien $\Sigma(k)$ een diagonaalmatrix is, zijn de virtuele referenties onafhankelijk van elkaar, hetgeen impliceert dat geen informatie wordt gedupliceerd in de referenties. Deze laatste eigenschap geeft aanleiding tot verbeterde convergentie-eigenschappen van het adaptieve controle-algoritme.

Een belangrijk probleem bij deze benadering is het bekomen van de transformatiematrix. Hiertoe werd een recursief algoritme ontwikkeld dat op elke tijdstap k de transformatiematrix berekent op basis van de transformatiematrix die berekend werd op tijdstap k-1, en de gemeten referentiesignalen op tijdstap k.

Dit algoritme werd toegepast op twee data-sets. Een eerste set referenties werd bekomen uit een labo-test waarbij de 4 wielen van de wagen met een identiek breedband signaal geëxciteerd werden. Toepassing van de virtuele referenties-techniek gaf aan dat 1 virtuele referentie volstond om de excitatie volledig te beschrijven ; hetgeen ook werd aangetoond door de coherentie tussen deze virtuele referentie en het foutsignaal te vergelijken met de meervoudige coherentie tussen de oorspronkelijke referenties en het foutsignaal.
Een tweede set referenties bestond uit de 12 acceleraties, gemeten in 3 richtingen aan de 4 wielen tijdens een wegtest bij 90 km/h. Hieruit werd een set van 4 virtuele referenties geëxtraheerd die, na simulatie van de controle-performantie voor beide referentiesets, nagenoeg evenveel reductie opleverde dan de oorspronkelijke 12 referenties (figuur 6).

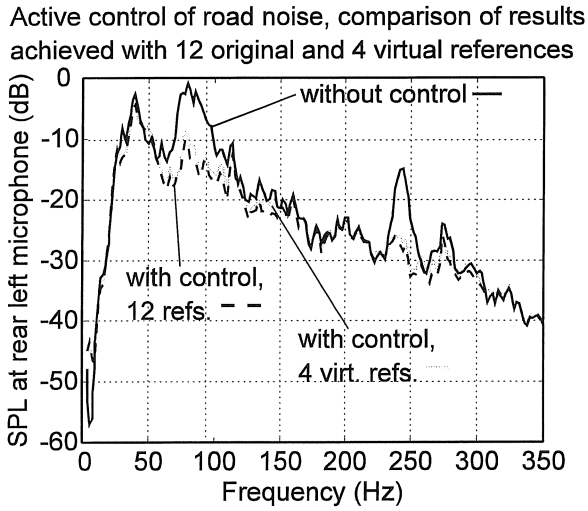

Figuur 6. Simulatie van actieve controle van rolgeluid, gebruik makend van een uitgebreide set van 12 referenties, en een beperkte set van 4 *virtuele* referenties.

4.5 Besluiten

Dit hoofdstuk bespreekt de reductie van rolgeluid in een wagen d.m.v. actieve controle. Hierbij werd een controlesysteem ontwikkeld, en getest, waarbij gebruik gemaakt wordt van inertiële actuatoren om het trillingsgedrag van het koetswerk zodanig te wijzigen dat het rolgeluid afneemt. Wegtesten hebben bewezen dat deze aanpak succesvol bleek in de

praktijk. Aansluitend op dit werk, werd een algoritme ontwikkeld dat op basis van een uitgebreide set referenties een beperkte set *virtuele* referenties berekent die dezelfde informatie bevatten maar minder rekencapaciteit vergen en bovendien aanleiding geven tot hogere convergentiesnelheden van het adaptief controle-algoritme. Deze techniek werd met succes op het probleem van rolgeluid toegepast.

5. Beschouwingen bij de implementatie van actieve controlesystemen

Dit hoofdstuk heeft enerzijds als bedoeling aan te geven welke de praktische beperkingen (kunnen) zijn in de implementatie-fase van een actief controlesysteem. Anderzijds wordt op die manier ook een -zij het beperkt- overzicht gegeven van de nieuwe technologische ontwikkelingen die de performantie verbeteren en de verdere integratie mogelijk maken van de actuatoren en sensoren van het actief controlesysteem.
Naast de technologieën voor actuatoren en sensoren, bespreekt dit hoofdstuk ook de optimalisatie zowel hard- als software van de digitale signaalprocessor waarop de digitale regelaar geïmplementeerd wordt.
Zie de thesistekst voor een gedetailleerde bespreking van deze technologische details.

6. Algemene besluiten

Deze thesis behandelt het ontwerp van actieve controlesystemen voor de reductie van structuurgeluid door actieve controle van de trillingen van het geluidsafstralend systeem. Twee controlebenaderingen worden uitgebreid behandeld.
Enerzijds wordt er een modelgebaseerde regelaar met terugkoppeling ontwikkeld, welke een globale reductie realiseert van het geluid dat een trillende structuur afstraalt in het vrije veld of in een caviteit. Deze benadering werd toegepast op een vrij academisch voorbeeld, maar het toepassingsgebied van de techniek is in principe zeer uitgebreid omdat het een oplossing biedt voor problemen van structuurgeluid dat te wijten is aan niet-harmonische stoorbronnen waar geen referentie voor voorhanden is.
Anderzijds wordt een zeer praktische toepassing behandeld, met name de reductie van rolgeluid in een wagen d.m.v. actieve controle. Hiervoor werd

een controlesysteem ontwikkeld, en getest, waarbij gebruik gemaakt wordt van inertiële actuatoren om het trillingsgedrag van het koetswerk zodanig te wijzigen dat het rolgeluid afneemt. Wegtesten hebben bewezen dat deze aanpak succesvol bleek in de praktijk. Aansluitend op dit werk, werd een algoritme ontwikkeld dat op basis van een uitgebreide set referenties een beperkte set *virtuele* referenties berekent die dezelfde informatie bevatten maar minder rekencapaciteit vergen en bovendien aanleiding geven tot hogere convergentiesnelheden van het adaptief controle-algoritme. Deze techniek werd met succes op het probleem van rolgeluid toegepast.

Als finaal besluit dient te worden opgemerkt dat, ongeacht het onbetwistbaar potentieel van de techniek, actieve controle geen wonderoplossing is voor om het even probleem van trillings- of geluidsoverlast. Actieve controlesystemen zijn typisch vrij complex, verbruiken energie, en vereisen steeds een minimum aan ontwikkeling in elke nieuwe toepassing. Daar tegenover staat dat met actieve controle dikwijls veel hogere performantie kan gehaald worden dan met passieve oplossingen -van redelijke omvang. Het relatief belang van kost tegenover vereiste performantie -dit laatste aspect is natuurlijk functie van de marktvraag, en bijgevolg van de bewustwording van het publiek voor de nadelen van te hoge geluidsniveaus- bepaalt bijgevolg of een probleem op een actieve, dan wel een passieve manier moet opgelost worden.

NOMENCLATURE

The most important symbols and abbreviations which are used in this text are explained below. One general rule applies to all symbols : bold face characters denote matrices. This includes vectors and rows.

LIST OF SYMBOLS

$\mathbb{C}$	field of complex numbers
$\mathbb{R}$	field of real numbers
$\mathcal{L}\{\cdot\}$	Laplace transform
$\mathcal{F}\{\cdot\}$	Fourier transform
ω	pulsation [rad/s]
s	Laplace variable
j	imaginary number, $j^2 = -1$
$\lvert\cdot\rvert$	magnitude
det	determinant of a matrix
sup	supremum, smallest upper limit
Tr	trace
$\overline{\sigma}$	largest singular value
$\underline{\sigma}$	smallest singular value
$E\{\cdot\}$	expectation operator
$(\cdot)^*$	complex conjugate
$(\cdot)^H$	hermitian, i.e. complex conjugate transpose
$\mathbf{A}$	state space system matrix
$\mathbf{B}$	state space input matrix
$\mathbf{C}$	state space output matrix
$\mathbf{D}$	direct feedthrough matrix
$\mathbf{u}_w$	exogenous input vector

$\mathbf{u}_c$	control input vector
$\mathbf{x}$	state vector
$\hat{\mathbf{x}}$	estimated system state
$\mathbf{z}$	performance output vector
$\mathbf{y}$	feedback output vector
$\mathbf{K}(s)$	continuous time feedback transfer function (matrix)
$\mathbf{K}$	constant state feedback matrix
$\mathbf{L}$	estimator gain matrix
$\mathbf{G}(s)$	continuous time system transfer function (matrix) or plant
$\tilde{\mathbf{G}}(s)$	continuous time closed loop system transfer function (matrix)
$S(s)$	sensitivity function
$T(s)$	complementary sensitivity function
$\mathbf{C}(z)$	discrete time controller transfer function
$\mathbf{H}(z)$	discrete time system transfer function (matrix)
$\mathbf{R}$	input auto-correlation matrix
$\mathbf{P}$	input cross-correlation matrix
μ	convergence coefficient
$\mathbf{w}$	control filter of adaptive feedforward controller
$\gamma^2_{d,\{x\}}$	multiple coherence between signal d and the set of references $\{x\}$
$\eta_i(t)$	modal amplitude
$\mathbf{COV}_{xx}$	covariance matrix
$\mathbf{x}^{\circ}(k)$	virtual reference signal
c	speed of sound in air [m/s]
k	acoustic wavenumber, $k = \omega/c$ [m^{-1}]
k_x, k_y	structural wavenumber [m^{-1}]

LIST OF ABBREVIATIONS

ANC	Active Noise Control
ANN	Artificial Neural Network
ARE	Algebraic Riccati Equation
ASAC	Active Structural Acoustic Control
AVC	Active Vibration Control
dB	decibel
DSAS	Discrete Structural Acoustic Sensing
DSP	Digital Signal Processor
FIR	Finite Impulse Response
HVAC	Heating, Ventilation and Air Conditioning
IIR	Infinit Impulse Response
IMSC	Independent Modal Space Control
LMS	Least Mean Squares
LQG	Linear Quadratic Gaussian
LQG/LTR	Linear Quadratic Gaussian with Loop Transfer Recovery
LQR	Linear Quadratic Regulator
LTI	Linear Time Invariant
MIMO	Multiple Input Multiple Output
PVDF	Piezovinylidenefluoride
RHP	Right Half Plane
RLMS	Recursive Least Mean Squares
RLS	Recursive Least Squares
SISO	Single Input Single Output
SVD	Singular Value Decomposition

TABLE OF CONTENTS

CHAPTER 1

INTRODUCTION

1.1 ACTIVE CONTROL OF VIBRATION AND SOUND

1.1.1 Basic principles

Active vs. passive control

Active control is the term used for all measures which aim at the reduction of a prespecified system response (acceleration, sound pressure level, ...) by applying control actions (force, volume velocity, ...) to that system. An active control system comprises a set of sensors, a control unit, and a set of control sources. As such, active control is a multi-disciplinary approach and implementation of any active control system requires a well-balanced investment in developing the appropriate hardware and software, and mastering signal processing techniques and control theory.

Active control is basically different from passive control in the sense that an active system adds energy to the system. Active approaches are thus capable of making a stable system unstable. They require a power source and are generally relatively complicated compared to passive methods. Passive control systems use only passive elements and do not add energy to the system. Typical passive control methods are surface treatments, mounts ("silent blocks"), tuned absorbers, resonators, etc. The application of passive control is very mature and there exist many efficient and cost effective passive solutions. However, they are often associated with an increase of the total weight, or dimension, of the original system. This is most certainly true in the low frequency domain, say, up to 500 Hz, as it is generally known that the thickness of an absorption material needs to be proportional to the acoustic wavelength in order to be effective. On the other hand, due to constraints related to available processing power in the controller and the physical constraints of the control mechanisms (there is, e.g., an upper limit to number of modes that can be controlled with a limited number of actuators), the typical bandwidth of an active control system is smaller than 500 Hz. From that perspective, active and passive control are perfectly complementary. In applications such as aircraft, or passenger cars, there is thus an opportunity for active control to enhance the acoustic comfort by reducing the vibration and sound levels down to relatively low frequencies. This is illustrated by the work of Fuller *et al.* on so-called *active foams* [1] which consist of a passive foam in which a distributed actuator (a PVDF foil, refer to paragraph 5.1) is embedded. They show that at low frequencies between 150 an 300 Hz, where the passive sound absorbing foam tends to be less efficient, the active foam still provides about 10 dB reduction of the sound level. A similar effect is observed in a headset with active control ([23], figure 12) where additional attenuation of 10 to 15 dB above the passive performance is provided by the active system up to a frequency of about 500 Hz ; above that frequency, noise reduction is achieved passively.
In addition, the almost limitless flexibility of computer-controlled active systems allows active control systems to provide a wide product differentiation to meet varying customer requirements [2].

There is, however, a group of noise and vibration control techniques which are neither active, nor purely passive, but lie in between the two extremes. Following the classification proposed by Bernhard [3], these systems can be classified as *adaptive-passive* and *hybrid active-passive* methods. Adaptive-passive methods utilise passive elements which can be tuned such that performance can be optimised over some specified range of conditions.

Typical examples are tuneable dampers in car suspensions [4] [5]. This type of suspension is often referred to as a *semi-active suspension*, as opposed to *active suspensions* which basically consist of 4 hydraulic pistons which replace the traditional damper-spring combination. Adaptive-passive, or semi-active, control systems do not add energy to the system. They are often less complicated, have the stability properties of a passive system and the adaptability of an active system. For these reasons, adaptive-passive systems are often preferred for the control of structural vibration in buildings, e.g. due to earthquakes [6] (in this application, they have the additional advantage that they require less control power than a fully adaptive system would do). However, as the adaptive-passive systems are often based on switching elements (switching from one damper state to another), their behaviour is intrinsically non-linear and hence difficult to analyse [4] [6].
Active-passive hybrids are active control systems where the passive system dynamics are designed such that they enhance the control performance or efficiency of the active system. The efficiency of an active control system utilising loudspeakers to control narrowband sound will be enhanced if the loudspeaker enclosure is optimised such that the power required by the electronic system is minimised. Other examples are active mounts consisting of a passive and an active element in parallel [7] (often the so-called active mount is a near-optimal system with an active system added to overcome the limitations of the passive system).

Control objectives

Active control systems can roughly be divided into 2 classes : systems for control of sound fields, and systems for control of structural vibration. The former group is generally called Active Noise Control (ANC) systems, while the latter is referred to as Active Vibration Control. In general, one could say that an ANC system is an active control system where the control sources are loudspeakers and the sensors are microphones, but this description is too restrictive to be used as a definition of ANC as there are various alternative configurations. The same remark applies to AVC systems, which generally use accelerometers to sense, and vibration actuators (shakers, ...) to control structural vibration. Another important class of active control systems are the Active Structural Acoustic Control (ASAC) systems which aim at reducing sound radiated by a vibrating structure by controlling its vibration. As will be shown in paragraph 1.2, ASAC is basically different from AVC (ASAC will sometimes even lead to increased vibration levels).

Regardless of the fact whether the active control system aims at reducing vibration or sound, the applied control mechanism depends on the control objective. The actual control objective can be thought of from different perspectives, some of which are explained below.

Active cancellation is the perspective from which active control is seen as an approach which relies on the creation of vibration or sound waves which are optimised in amplitude and phase such that they destructively interfere - at least at some observation point- with the field which is due to an external disturbance (vibration or sound). This perspective has led to the commonly used term *anti-noise* [8], which is a sound field which is equal in amplitude but 180^{o} out of phase with the disturbance.

Optimal global cancellation is achieved when the control objective is to simultaneously minimise the response at a number of locations. Other than in the case of active cancellation, it may not be possible to achieve perfect cancellation at each of these locations (this is a function of the number of target locations and the number of control sources) such that an optimum must be aimed at.

Confining the noise source within a volume is an approach which follows directly from the basic acoustical laws since the Helmholtz integral actually states that it is theoretically possible to cancel a primary sound field by a continuous distribution of monopole and dipole sources on a surface circumscribing the considered volume [9]. This approach divides the space into three separate regions : the space occupied by the disturbance source(s), the space to be made silent, and the space in between where the control sources are situated. An explicit formulation for this approach is provided by the JMC method (named after the first three pioneers of the method, namely Jessel, Mangiante and Canévet) [10]. The JMC method formulates the problem of active control of sound with general system theory. In this framework, the control action is realised by defining an operator (the so-called *modifier* or *reshaper*) which modifies the original field to the desired one. With this operator, the control source strengths can then be determined. In principle, whatever the original sound field is, it can be changed to any other field by using the JMC method. Hence the JMC method can also be applied such that, instead of surrounding a source volume, a sourceless part of the space can be surrounded with control sources for which an operator is determined which cancels the sound field inside this volume.

Control at the source is important in the sense that it can achieve global reduction. In acoustics, the control mechanism which realises this is acoustic coupling. The mutual coupling between the disturbance and the control source confines most of the acoustical volume flow in the nearfield

of these sources and hence the total radiated power is reduced (e.g. by adding a control source, a monopole disturbance source can be converted into a dipole which radiates less efficiently). The achievable sound power reduction has been shown to vary with the spatial separation between both sources [11]. A similar approach can be used to reduce the (vibrational) power input due to a disturbance force by applying a control force near to it. As illustrated by Jenkins *et al.* [12] for the case of point forces acting on an flexible thin plate, there is again a strict upper limit to the spatial separation between disturbance and control force in order to obtain worthwhile reductions in the total power output (of both forces).

Active boundary control refers to applications where the signal sent to the control source is determined by specification of the (surface) impedance of the source. A straightforward example is to use a loudspeaker and to control its surface impedance by controlling its velocity (using an accelerometer on the membrane) and the sound pressure above the membrane. Such an active acoustic absorber can be used to exert global control over the low frequency modes of an enclosed space [13]. However, in [14], it is shown that it is possible to specify the control source surface impedance associated with a number of standard active noise control objectives, such as active cancellation and optimal global cancellation.

Modal control is a term which is used when the control action is expressed in the modal domain and aimed at reducing modal amplitudes instead of physical responses. This formulation is restricted to applications where the system dynamics can accurately be modelled as a finite weighted sum of modal amplitudes (e.g. control of sound fields in lightly damped enclosures).

Perhaps the most general approach to active control is that active control allows to purposefully *modify the system dynamics* without actually changing the system (except for the addition of control sources and sensors). E.g., by applying a counteracting force which is proportional to a structure's displacement, the structure will respond to external forces as if it were stiffer ; similarly, its response will be more damped when the control force is proportional to the velocity of the structure. Active control thus changes the input impedance of the system with respect to external disturbances [15-16].

The various control objectives are realised by the control algorithm which is implemented in the control unit. The simplest way to think about the controller is that it is a filter which transforms the output of a measurement sensor into a control source drive signal. The two broad control strategies

for the implementation of active control, feedback and feedforward, are discussed in detail in chapter 2.

Location of actuators and sensors

For any active control system, the determination of the number and location of the control actuators is a key issue which largely determines the control performance. However, few generic methodologies exist that guide the control system designer to select an optimal actuator configuration. For most practical problems, it is not possible to analytically describe the control performance as a function of the control actuator configuration and thus one is often bound to ad-hoc solutions [17] such as enumerative schemes, Genetic Algorithms [18], or to use finite element models which properly describe the interaction of the control system with the structure [19].
The development and application of optimisation schemes for the location of actuators is beyond the scope of this thesis.

1.1.2 Short history

The start of the active control era is often associated with the publication of a patent by Paul Lueg[1] which describes a system to control sound waves in a duct by measuring the sound field with a microphone, electrically manipulating this signal and then feeding it to an electroacoustic control source. However, the fundamental concept of sound reduction by interference of a primary and a secondary wave was established by Lord Rayleigh [21]. The fact that this principle was recognised as a basis for noise control systems with commercial potential appears to be symptomatic of the field : the earliest publications on active noise control were patent applications, such as Paul Lueg's, whose patent was filed in the U.S.[2] on March 8, 1934, and granted June 6, 1936 [22].
This section will not repeat the many published reviews of the history of active control (an interesting review of the history of active noise control, highlighting the major deterrents and the major innovations of active noise

---

[1] It appears that this is historically incorrect : an identical patent has been filed by Henri Coanda, one year before Paul Lueg [20].
[2]More interestingly, the German patent was filed on 27 January 1933, but only granted on December 30, 1937. Also this appears to be symptomatic of the field...

control over the years, can be found in [23]), but will rather refer to a publication which describes the evolution of active control of noise and vibration at a large company (BBN Systems & Technologies) which has a large history in noise control services. This publication is illustrative in the sense that it presents some of the opportunities for active control in the domain of noise and vibration control engineering in general.

The early work at BBN on active control was performed in the framework of two PhD. thesisses (June 1968 and May 1968). Both studies address the active control of vibrations. Much of the early work also dealt with relatively low frequency vibration and control problems. For two decades, this work remained primarily at the study phase with little implementation. There were three reasons for that. First, microprocessors had not yet emerged as the omnipresent and inexpensive devices of today. Second, suitable actuators, particularly for active control of heavy structures at lower frequencies, were not available. Third, the point of diminishing returns on application of passive technology had not yet been reached for applications of concern (improvements in applied passive technology were often more affective with less risk than active control methods).

In 1985, at BBN (and elsewhere in the world), they began to move from theoretical studies to the laboratory demonstration of proof-of-principle systems. Examples of these Lab and Field experiments are : fan noise cancellation, hydraulic and pneumatic isolators, hybrid active/passive elastomeric isolators, etc. By about 1990, so-called Advanced Technology demonstrative systems were developed under the sponsorship of the US Department of Defense. Most of these applications, such as the control of aircraft engine sound generated in ground run-up tests, control of piping coupled fluid/structure borne noise, or the implementation of the complete control functionality on a multi-chip module, were classified programs, and system performance was never published in literature.

But from 1990 on, also operational active control systems were developed, such as a system for active machinery isolation (in marine ship), specialised actuators for vibration control (moving armature type), and a local airborne noise control system (installed in the sleeping compartment of the U.S. Navy's newest high-speed coastal patrol craft). The main difference between these latter examples and the early work lies in the fact that the active systems were not only developed for performance, but also for durability and reliability such that they would outperform passive measures in any aspect.

1.1.3 Applications of active control of vibration and sound

To make an overview of all current applications of active control is virtually impossible. First of all, unlike most other fields in physics, noise and vibration control is a subject where many researchers apply for patents before publishing their results in the open literature. This is even true for fundamental ideas [24]. These patents are not published in the conventional scientific journals. Another consequence of early submissions is that patents are sometimes immature as compared to later publications on the same subject. Furthermore, there is an enormous amount of scientific papers on the topic that are published each year. Guicking [25] [26] puts a large effort in compiling a reference bibliography on active control of noise and vibration (3rd edition 1988, 1704 citations; 1st supplement to 3rd edition 1991, 1752 citations), which lists scientific papers as well as patents. The applications which are presented here are taken from his review of the patent literature ([24], 320 citations ; the overview is based on more than 500 patents).

Active vibration control has not yet penetrated into a lot of applications as the domain of vibration control is dominated by passive treatments and structural modifications. However, an important application of active vibration control is *AVC of buildings* against earthquake and wind induced motions. Most of the implemented systems (in tall buildings, e.g. in Tokyo ; bridge heads in the US) rely on so-called active tuned mass dampers : a seismic mass is elastically connected to the top of the building so that the natural frequencies of building and mass are equal ; driving the mass in antiphase to the building vibration causes vibrationtal energy of the building to be absorbed (figure 1.1).
Active vibration isolation has often been demonstrated to be very effective and capable of providing lower force transmission than passive systems. This application is the subject of a large number of patents, most of them related to active mounts and active suspensions. Active mounts for the support of a truck cabin can reduce the vibration transmission to the cabin. A related application is *AVC for rotating machinery*, in which case the vibrations exhibited by rotating machines (due to unbalance, self excitation, etc.) are controlled actively. An example is the control of machine tool vibration (e.g. a boring bar) by an actuated mass in a sleeve holding the tool. Other applications of active vibration control are found in spacecraft (where the addition any mass is generally out of question), where the vibration of

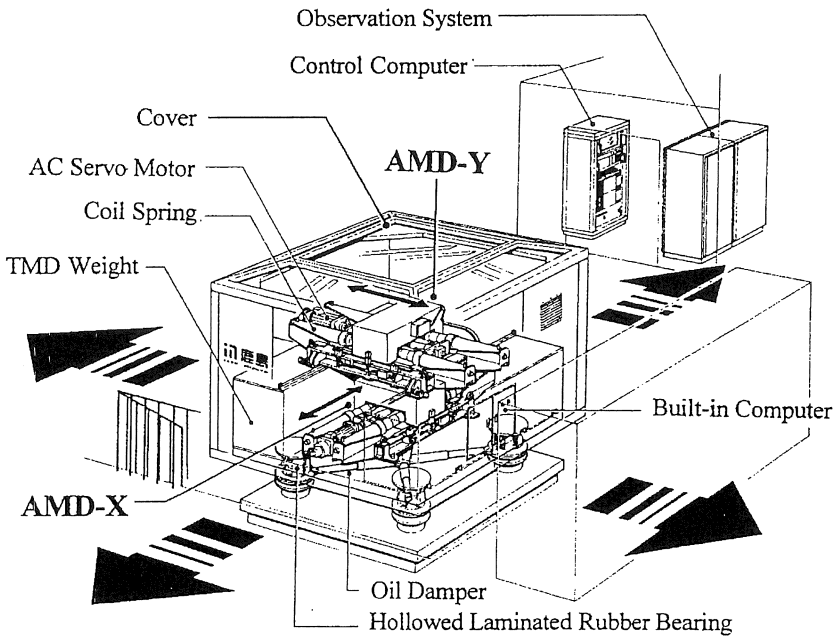

Figure 1.1. Actively tuned Mass Damper by Kajima, providing vibration attenuation in 2 directions. This device was installed in the 14-story, 68 m high office and residence Ando Nishikicho Building (Japan) in July 1993. The system was found to provide effective attenuation of the October 12, 1993 earthquake and the typhoon-like seasonal winds of February 21, 1994. (Figure taken from [328]).

large, flexible structures, such as a deployed antenna, is reduced by applying control forces to the structure.

ANC systems for low frequency sound control *in ducts* for HVAC as well as for air handling systems in industrial plants (figure 1.2) are commercially available at a very affordable cost, particularly as compared with passive silencers of equal performance. Technical applications of the cancellation of broadband duct noise became possible after the introduction of digital adaptive signal processing. Later-on; systems dealing with the cancellation of higher-order modes in ducts above the cut-on frequency of the first transverse mode have been developed. A related application is *ANC in mufflers* of internal combustion engines. A typical control system uses synchronisation signals from the engine, forms the cancelling signal by waveform synthesis, and radiates the cancelling sound from one or more loudspeakers which are radiated near the tail pipe. An interesting side-effect

is that also engine performance can be optimised by active control of inlet and/or outlet pressure fluctuations.

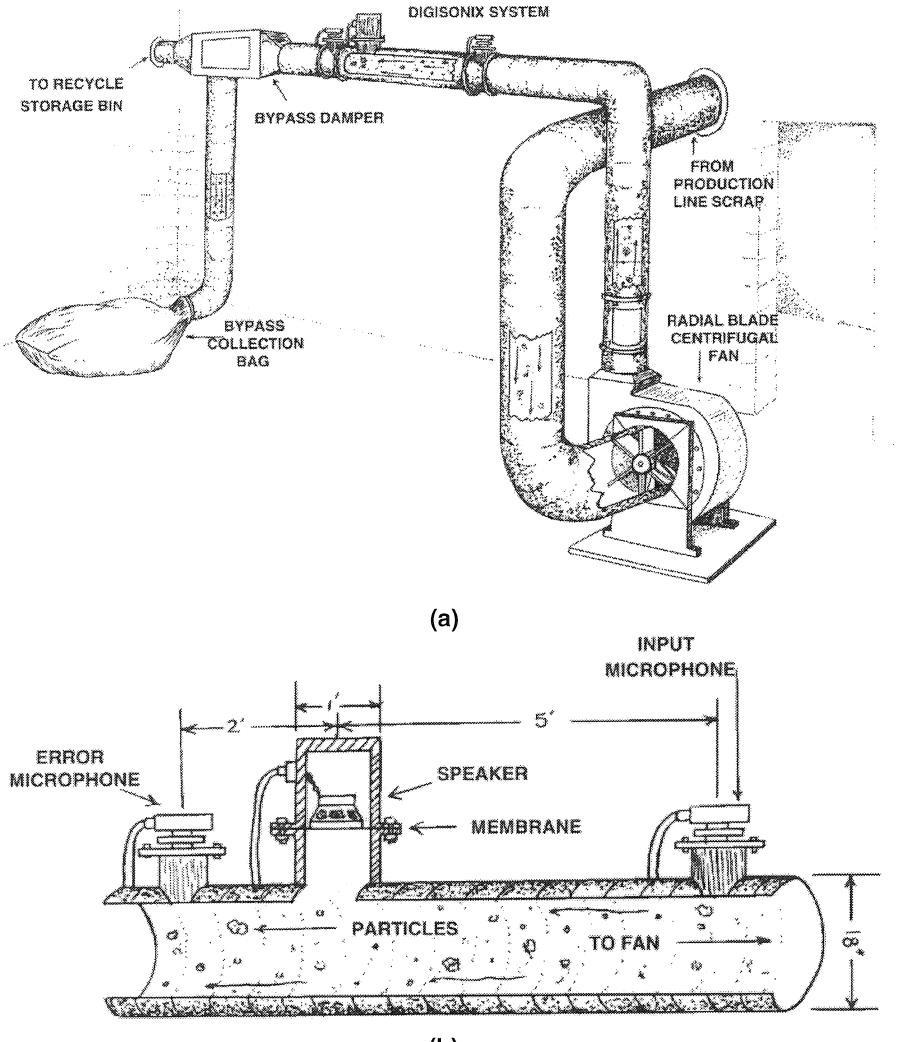

Figure 1.2. Illustration of ANC system installed in a material handling system. The noise source is a radial-blade centrifugal fan which draws scrap from paper-trim work stations in the plant and sends it to a collection bin for recycling. The exploded view (b) shows a DIGISONIX cancellation system which achieved 30 dB reduction at the blade passing frequency. (Figure taken from [334]).

An important application of *ANC in enclosures* is the sound reduction in automobiles and aeroplanes. A technically solved problem is the cancellation of the "boom"; an often annoying resonance of the air volume in the car cabin by an inherent unbalance of 4-cylinder internal combustion engines. The Nissan "Bluebird" car has been sold in Japan for some years with an optional active noise control system. The usual approach is feedforward control with the engine rotation frequency as synchronisation input, error microphones near the passengers' heads; and using the existing loudspeakers. Alternative control systems apply feedback control with microphones placed in Helmholtz resonators which are tuned to the car resonances. A more complicated problem is cancelling broadband noise in the cabin, originating from the tire rolling over a rough road surface (refer to chapter 4), wind noise, etc. The reduction of propeller generated tones inside an aircraft fuselage has been successfully demonstrated. Some systems use an array of loudspeakers which are controlled by error microphones located in the seat headrest ; other systems control fuselage vibrations.
A frequently discussed problem is the *cancellation of electric power transformer noise*, either by loudspeakers arranged around the site, by force input to the oil in which the transformer is immersed or to the surrounding tank walls, or by sound insulation panels enclosing the transformer. Other applications of ANC to three-dimensional exterior noise problems are still quite rare (one application from this category is the active control of lawnmower noise).
The application of *ANC in communication* is aimed at solving problems such as acoustic echoes and crosstalk, which are both relevant problems for hands-free telephoning to improve speech quality. Related applications are *ANC in hearing protectors* (prototype at PMA in 1987) *and headsets*. The latter are used by aircraft pilots (figure 1.3).
ANC for domestic appliances has resulted in a number of interesting products, such as silent refrigerators (offered by Toshiba in Japan), silent PC fans, silent kitchen exhausts etc.

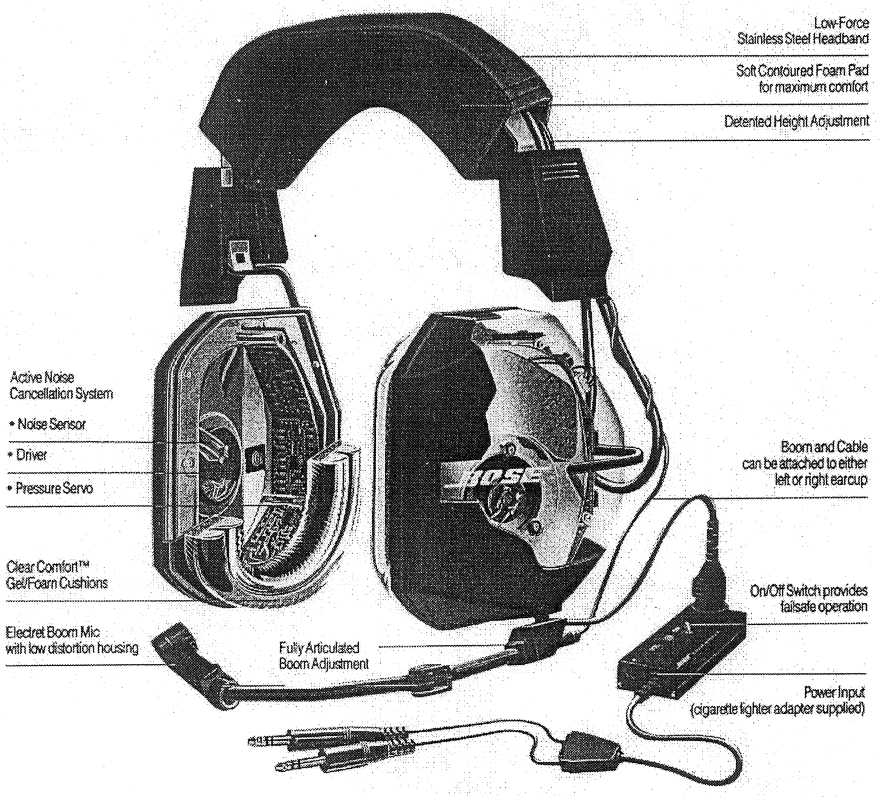

Figure 1.3. Active headset manufactured by Bose Corp. The tight seal around the ear attenuates high-frequency noise, low frequencies are actively cancelled. Desired audio, such as radio communications, are passed through which makes the headset useful for helicopter pilots etc. (Figure taken from [314]).

1.2 ACTIVE STRUCTURAL ACOUSTIC CONTROL (ASAC)

1.2.1 Application area

A separate class of control techniques, which are grouped under the name ASAC, are specifically developed to tackle the structure-borne noise problem. Structure-borne noise can be defined as noise for which a significant portion of the transmission path from source to receiver takes place in a solid structure rather than through a liquid or gas [27]. Structure-

borne noise generation thus involves three elements : a noise source (or the primary disturbance), a transfer path and a receiver system. Though it is often not possible to remove the noise source without changing the functionality of the system (mechanical vibration is often the by-product of mechanical power generation), the transfer path or the receiver system can be controlled actively. Other than in the case of ANC, ASAC makes use of the characteristics of the vibration field of the vibrating structure, and the generated sound field to reduce the sound pressure levels. Two main control approaches can be distinguished : controlling the transmission of vibration along the structural transfer paths, or controlling the vibro-acoustic response of the receiver system. Both approaches will be discussed in the next two paragraphs.

1.2.2 Control of a structural transfer path

It has been shown [28] that in propeller aircraft, the largest contribution to the interior propeller noise can be attributed to transmission via the frames (i.e. the longitudinal stiffeners) of the aircraft fuselage. Currently this problem is (only partly) solved by using dynamic absorbers, which are passive elements. Active isolation of these transfer paths could possibly further reduce interior propeller noise, but in this application that would imply a very large number of control actuators.
Actively blocking a structural vibration transfer path, which then results in acoustic control, may be applied when the primary disturbance is transmitted to the system via a limited number of transfer paths. E.g., this technique has been implemented with success to control noise transmission through a helicopter gearbox support strut [29]. In the considered helicopter, the main rotor drive and gearbox assembly were linked to the passenger cabin by four cylindrical steel load-bearing struts. These struts offer little vibration isolation, and provide an unwanted transmission path for low-frequency structural vibration, mainly at blade passing frequency, and also for much higher frequency due to gear meshing (the gear meshing tones contribute to high and disturbing interior noise levels). One of these struts has been set up in the laboratory. It was equipped with three magnetostrictive actuators to investigate the potential of controlling the longitudinal and lateral vibration transmission to a connected receiving structure. Attenuations in kinetic energy of the receiver in excess of 40 dB were measured at a number of frequencies over a range from 300 to 1250 Hz.

In [12] and [30], more general studies on active control of vibration transmission by means of active mounts are presented. In both studies, the transmission of vibration from a source (modelled as a rigid body) to a flexible support structure, the receiver, is considered. The analysis presented in [12] is threefold. Simple analytical models are first used to study the required control forces for active isolation of periodic machinery vibrations. Two methods of applying the "secondary" active actuator are suggested : *(i)* the "parallel cancellation" system, with the actuator mounted between the machine and the support structure ; and *(ii)* the "receiver cancellation" system in which the actuator is attached to the receiver directly opposite the point of attachment of the machine mount (e.g. by using an inertial actuator). In a first study, a single machine mount is used. The dynamics of the passive mount and the receiver are modelled by an equivalent mass, spring and damper. The secondary force that drives the displacement at the attachment point of the mount to zero is then calculated. Thus it is shown that at the resonance frequency of the passive mount, a secondary force in excess of the primary force is required in case of the "receiver" system. Using a "parallel" system, however, it is possible to remove the (conventional) necessity for the resonance frequency of the passive mount to be very much lower than the excitation frequency. By making the mount stiffer, the physical instability of conventionally mounted machines can be reduced. In a second stage, the receiver is modelled as a infinite flexible plate, such that the effect of a finite separation distance between the passive and secondary forces (both assumed to be point forces) could be studied. It is observed that, to obtain worthwhile reductions in total power output (to the receiver), the secondary force must be applied at a distance well within approximately 3/8 of a flexural wavelength from the primary force. This requirement defines an upper frequency limit to the effectiveness of active isolation when primary and secondary force are not perfectly aligned. The analysis is further extended to a more practical case of isolating a vibration source, mounted via 4 foam rubber cylinders on a finite plate. The rubber cylinders enclose an equal number of coil-in-magnets which provide the secondary forces (in parallel). This problem is studied both numerically (finite element simulation) and experimentally. The results illustrate that active control is primarily effective at low frequencies, as the effect of finite separation distance between primary and secondary force deteriorates the control performance at higher frequencies. Furthermore it was observed that more sensors must be distributed over the surface of the receiver in order to maintain the efficiency of the active/passive isolation system as frequency increases.

This study is further extended in [30], in which a detailed theoretical study of an active isolator is developed by modelling multi-distributed mounts and by considering a distributed receiver. The actuator is assumed to be in parallel with the passive mount and provides only an axial excitation. The motion and forces transmitted at each junction, however, are characterised by six complex arguments at each frequency of excitation. The effectiveness of minimising the total power transmitted to the receiver has then been compared with more practical control strategies defined at the junctions : the cancellation of force or velocity at the receiver junctions, the minimisation of axial power and the minimisation of the weighted sum of square value of velocity and force at the junctions. It is observed that the control of total power gives the best results under ideal conditions, but for realistic cases, characterised by measurement errors and flanking paths, the cancellation of velocity or force is more effective. This is primarily due to the fact that the strategy of minimising the total observed power can only be considered as being optimal if the power produced by all the sources acting on the receiver and related with all degrees-of-freedom of the system are accounted for in the measurement. Otherwise, flanking paths, if they are negligible before control, can become significant sources of power (transmitted to the receiver) when they interact with the control forces.
Also active engine mounts[3], used to reduce engine noise inside a car cabin, appear to be a straightforward application of the active reduction of vibration transmission through the engine mounts. However, it has been observed that minimising the vibration level at the engine mount location does not necessarily yield the largest interior noise reductions. Usually, an engine is fixed to a car chassis by three engine mounts. In [31], one of the passive mounts is replaced by an active engine mount which is used to drive to zero the output signal of *(i)* an accelerometer mounted on the chassis; and *(ii)* a microphone located at the driver's ear. In these experiments with configuration *(i)* it was observed that, while the vibration levels show a reduction of 17 dB at the second engine harmonic (2000 rpm), the second engine harmonic of the noise measured at the microphone was reduced by 3.3 dB only. Configuration *(ii)* yielded 15 dB engine noise reduction at the second engine harmonic ; however, the vibration level at that frequency was increased. The reduction in sound level was therefore accompanied by additional vibration induced in the vehicle chassis ("They use the engine mounts as shakers" [32]). Apart from the fact that mechanical fatigue of the chassis may be increased, these increased vibration levels lead to discomfort

[3] For an overview of active engine mount technology, refer to paragraph 5.1

for the passengers. This problem may be solved by actively controlling vibration transmission at all paths using three active mounts. An alternative solution, however, is suggested in [33], where the simple one mount control system was extended to include four interior microphones and two loudspeakers. With this control configuration, it was possible to realise significant reduction of interior noise while at the same time reducing the vibration levels at the steering column, the floor and the seat rail.

1.2.3 Control of vibro-acoustic system response

In cases where it is impossible or impractical to control all structural transfer paths to the receiver, the vibro-acoustic response of the receiver must be controlled in order to reduce the sound power radiated. At this point, it is interesting to consider the difference between two major approaches. On the one hand, one may control the radiated sound power by applying control forces to the vibrating structure, which approach is referred to as ASAC. On the other hand, an alternative approach is to locate a number of loudspeakers in the vicinity of the radiating structure and control the radiated sound field acoustically (which is rather an ANC approach), such as in the case of active control of transformer noise. In [34], both control approaches are applied to control harmonic sound radiated from a vibrating rectangular plate. Interestingly, the experimental results have shown that the ASAC approach appears to be more effective than the ANC approach. This was explained by the fact that the control mechanism of the second method tended to create an inverse pressure distribution at the panel surface and thus "unload" the panel by reducing the panel radiation impedance. The number of acoustic sources, required to achieve this, was seen to increase with panel modal order. The advantage of applying control directly to the structure lies in the fact that this configuration allows more efficient control by adjusting the structural response of the panel rather than totally minimising it (the ASAC control mechanisms will be further explained later-on).
In fact the authors of [26] feel that a wide enough variation in test conditions has been studied in order for their conclusions to be general conclusions. This section therefore concentrates on the various methods to achieve reduction of sound radiation by active control of vibration.

Active Vibration Control vs. reduction of the sound pressure level at a microphone

Perhaps the most straightforward control approach to control sound radiation is to reduce the vibration of the radiator and hence this approach is dealt with in numerous papers. The advantage of such a control configuration is that both the sensors and actuators are bound to the structure, resulting in a very compact configuration. It is, however, important to consider the potential problems associated with this approach. First of all, even if the structural vibration at a (limited number of) point(s) is reduced significantly, it is conceivable that this approach could result in structures that radiate higher sound levels. On the other hand, minimising the structural response at multiple points along the structure's surface (which would guarantee reduction of radiation) is considered to be an "overkill" in terms of efficiency [35].

This can be explained by the results achieved by Wang and Fuller [36]. In this work, the authors have considered the active control of harmonic radiated from a rectangular plate by means of one control force. The applied control force is determined by optimising four different cost functions as a function of the control force (in phase and amplitude). This allows to compare four different control approaches : control at distributed sound pressure sensors, control at one discrete pressure sensor, control at distributed acceleration sensor, and control at one discrete acceleration sensor. All approaches have been simulated numerically.

Using the accelerometer sensors results in more attenuation of plate vibration than using pressure sensors ; however, the corresponding sound pressure levels are not generally attenuated to the degree that the plate vibration is attenuated (This observation was also made in the case of more complex systems. E.g. in [37], it was concluded from numerical simulations that the reduction of the vibration of the frames of an aircraft fuselage would not significantly reduce the interior sound pressure levels of the aircraft).

The situation is more pronounced in the case of a discrete acceleration sensor. The discrete sensor generally performs worse than the distributed acceleration sensor and, moreover, increases the radiated sound power (with respect to the uncontrolled case) in certain frequency bands.

These results show that a pressure sensor (preferably distributed, or multiple discrete sensors) is superior to vibration sensors because it supplies the coupling information between sound radiation and mechanical vibration. This information is essential since the different structural modes couple differently to the surrounding acoustic medium. This is further explained by

the study presented in [34]. In this paper, it is investigated which control mechanisms appear when the sound pressure level at a microphone located above a vibrating panel is minimised by means of a single control force applied to the panel. Two mechanisms have been observed, which have been termed "modal suppression" and "modal restructuring". One mechanism may dominate the other, depending on the primary disturbance excitation (e.g. on-resonance or off-resonance). Modal suppression refers to the fact that the controller reduces the modal amplitudes of all modes which contribute significantly to the radiation sound field. In the case of modal restructuring, the controller will rather change the relative phases of the contributing modes, leading to a total vibration pattern that is more complex (i.e. has a lower radiation efficiency) and a corresponding reduction in the radiated sound level. In that case, the overall vibration response of the panel changes by only a relatively small amount.
In the case of AVC, on the other hand, the control mechanism which realises the overall reduction of vibration is modal suppression. Detailed studies of this control approach [38] [39] have shown that in that case the most important factors in successful control of sound radiation are the number of controlled (structural) modes and the choice of the controlled modes (and hence the number of control actuators used).
The previous observations suggest that the most simple, yet efficient, ASAC control configuration uses microphones located in the radiated sound field to determine the optimal control forces that must be applied to the structure in order to reduce the radiation of sound. A multitude of ASAC systems are indeed based on this principle (refer to proceedings of various active control conferences). The use of acoustic responses, however, is not in favour for feedback control (refer to paragraph 2.4.1) and moreover, it is not always practical to locate sensors in the radiated sound field, e.g. in cases where people are moving around in the same zone. Therefore, researchers have been exploring alternative methods to reduce structurally radiated sound while constraining the sensors to be located on the vibrating structure.

Wavenumber transform

It is common practice to describe a structural response in terms of structural modes and hence to express sound radiation in terms modal radiation efficiency and modal coupling. However, a mode can also be seen as a particular pattern of interference between travelling flexural waves. Hence, the radiation from the structure can also be expressed as a sum of the radiation of the component travelling waves. This formulation is particularly

interesting when noting that the radiation of sound energy from a planar structure can be associated with the presence in its normal vibration velocity distribution of supersonic wave-number components k_s, satisfying $k_s < k$ at the frequency concerned[4] ([40] p. 72 - 74). The wavenumber "content" of a vibration velocity distribution can be determined by means of the *wavenumber transform*, which is actually the spatial equivalent of the Fourier integral transform :

$$V(k_x, k_y) = \int_S \dot{w}(x, y) e^{-j(k_x x + k_y y)} \, dS \tag{1.1}$$

(w is the structural displacement).

Consequently, inspection of the wavenumber spectrum of the velocity distribution of a vibrating structure reveals whether it radiates significantly or not. Alternatively, the wavenumber transform may be used to verify whether a control action has been effective or not. This is again illustrated in [34] : when control is applied, all supersonic wavenumber components are seen to be reduced, which corresponds to global control of sound radiation. Furthermore the oscillations in the wavenumber spectrum at low wavenumbers appear to be smoothed. This indicates that the residual panel response is dominated by high wavenumber, i.e. short wavelength, components, which corresponds to higher order modal motion with a lower radiation efficiency in the considered frequency band. Note that the two control mechanisms, modal suppression and modal restructuring, are thus observed through the wavenumber transform.

As the radiated sound power can be shown to be related to the integration of the modulus-squared wavenumber spectrum, it can also be used to express the control objective. More specifically, an alternative approach to minimise the sound radiation from a planar structure can thus be specified by choosing the amplitudes of the wavenumber spectrum in the supersonic region as a cost function which is then optimised as a function of the applied control force(s). This approach was first proposed by Fuller and Burdisso [41].

Various ways to obtain the wavenumber spectrum from measurements directly on the system are reviewed by Wang [42]. A straightforward approach is to measure the acceleration in a number of locations on the structure and then to approximate the continuous acceleration wavenumber transform by a discrete acceleration wavenumber transform. The

---

[4] $k = \omega/c$ is the acoustic wavenumber ; c is the speed of sound in air. For planar structures, the structural wavenumber is calculated as $k_b = \sqrt{k_x^2 + k_y^2}$.

wavenumber transform can be implemented as a linear combination of the sensor signals which in fact realises a spatial filter which passes the radiating components of the vibration signal and rejects the non-radiating components [43]. An alternative approach is based on shaped PVDF sensors (PolyVinyliDeneFluoride). PVDF sensors are flat film piezopolymers which can be bonded to the surface of the structure and thus generate a voltage which is proportional to the structural displacement (for more details about PVDF and its implementation as a vibration sensor, refer to paragraph 5.1). A series of PVDF strip sensors is distributed, equally spaced, over the structure. By performing a discrete wavenumber transform on the PVDF sensor signals, the PVDF wavenumber transform is obtained. The sum of the mean square value of the PVDF voltage wavenumber transform in the supersonic region is then defined as the cost function. It is shown in [42] that this cost function is directly related to the radiated sound power.
Using the wavenumber transform provides the controller with input signals corresponding with surface velocity patterns that radiate well. By observing these more efficient acoustic radiators, control effort can be dedicated to reducing or rearranging the structural response contributing to the radiated sound, allowing spillover into the less efficient radiating modes. A similar approach is discussed below.

Location and shape of sensors

In important feature of the electrical response of a PVDF sensor is that the output voltage of a PVDF sensor is a function of its shape and location on the structure (the orientation with respect to the co-ordinate system of the structure). Hence, the sensor can be shaped and positioned to create any kind of "spatial window", e.g. to measure the response of individual modes (when the width is proportional to the second derivative of the mode shape [47]) or multiple modes. For the purpose of active control of sound radiation, the sensor may even be designed to weight each mode of the structure with a factor proportional to the sound radiation efficiency. Thus, significant levels of signal conditioning can be performed directly in the sensor design.
Snyder *et al.* [48] [49] present a methodology to consider active control of structural radiation using shaped piezo-electric polymer film sensors in a vibration source-based control strategy. The piezosensors are shaped such that they provide a measure of the modal displacement of *transformed* modes ; these are orthogonal collections of structural modes which radiate sound as a "single unit". Transformed modes are obtained from orthogonal

transformation of the transfer matrix describing the power radiated by a vibrating baffled panel. The approach takes benefit of formulating the problem in terms of transformed modes, because the number of transformed modes required to model the problem is low. The number of structural modes required to accurately construct the transformed mode is relatively high, but is done only once (off-line).
Some practical problems are associated with the approach in the sense that the transformation from structural modes to transformed modes is in principle frequency dependent ; the experimental work, however, considers the minimisation of *unweighted* (in frequency) transformed modal velocities. Minimising a measurement of transformed modes that have been determined neglecting the frequency dependency is strictly only correct at one single frequency and can seriously degrade results. Furthermore, precise measurement of the transformed modes would require a sensor which completely covers the plate with a film thickness varying as a function of the second derivative of the transformed mode of interest. Snyder *et al.* propose a simpler approach where only the principal varying direction of each of the transformed modes is allocated a shaped PVDF film sensor. A discussion of the errors resulting from these approximations, is presented in [48].
Another difficulty is that transformed modes are not modes in the traditional sense, with a resonance frequency and a single phase shift at this frequency ; their responses have numerous peaks and phase shifts (corresponding to the resonances of their structural modal constituents). Consequently, "simple" feedback of the transformed modal displacements and velocities, where the feedback control gains are fixed over the entire frequency band, did not produce optimal results. Moreover, it is not clear how the approach applies to structures that are more complex than a simple rectangular plate (how the shape of the piezosensors would have to be).

An explicit model for the fluid-structure interaction as a basis for controller synthesis

The approaches described above, essentially concentrate on defining appropriate measurable quantities which should be driven to zero by the controller in order to achieve a reduction of the radiated sound power. It was also shown that it is in general fundamentally wrong to consider the minimisation of structural modal velocities with a view to minimising radiated acoustic power ([48] p. 314). In order to be efficient, ASAC configurations which use the acceleration of the structure as an error signal,

need to include a data-processing stage which relates the structural response to the radiated acoustic power. The data-processing is based on a vibro-acoustic model of the structure.
Various formulations have been presented to realise this.
Naghshineh and Koopmann [35] write a quadratic expression for the total sound power radiated from a structure in terms of the discretised normal surface velocity vector of the structure. By writing the surface velocity in terms of a structural mobility matrix and the excitation forces, the quadratic expression can be expressed in terms of the primary excitation and the control forces. Using quadratic optimisation of that expression, a single control force vector is found that minimises the radiated sound power. The formulation which is presented is general for the single-frequency case. It is extended to the case of a structure subjected to a broadband excitation force ; the magnitude and phase of the excitation, however, are assumed to remain constant as the excitation frequency changes. The formulation has been implemented numerically (in which case the excitation force is known) and experimentally for a baffled beam controlled by forces and moments generated by piezoelectric actuators. In the experiments, the excitation force was applied by a shaker ; the effective shaker force was measured using a force gage placed between the shaker and the beam. The authors acknowledge that the driving voltages of the control actuators had to be fine tuned manually to achieve maximum control performance. This is said to be due to a combination of variations in actuator sensitivity and measurement errors.
Friot [50] represents the structural response of the vibrating structure (the structure under consideration is a rectangular plate controlled by piezoelectric actuators) by a linear state space model. This state-space model is identified from experimentally measured actuator-to-sensor Frequency Response Functions. The sound radiated from the structure is then modelled as a quadratic form of the state variables. To this aim, the acoustic pressure in an array of 9 microphones above the plate is measured and the quadratic sum of the acoustic pressures is expressed in terms of the vibration modes and modal participation factors (which account for the microphone sensitivity to sound radiated by each mode). A non-negative least-square fit of that function yields a state variable weighting index according to their contribution to the sound power radiated. An LQG controller (refer to chapter 2) is then synthesised which minimises a quadratic expression of the weighted vibration state variables. With this approach, no acoustic degrees of freedom are added to the state space model

to account for the structural radiation. For the identification phase, however, the cross terms between structural modes had to be omitted.
When expressing the velocity distribution on the surface of a structure in terms of the amplitudes of an infinite number of modes, the acoustic power radiated by the structure must rather be calculated as the sum of the squared modal amplitudes times their modal radiation efficiency, and the sum of a series of coupling terms between modes. Baumann *et al.* [51] [52] have calculated the modal radiation efficiencies and coupling factors by integrating the farfield sound intensity over a surface which encloses the radiating structure. These radiation efficiencies are used to synthesise so-called *radiation filters*. The total radiated sound power can thus be determined by summing the squared outputs of the radiation filters through which the time histories of the modal velocities have been passed. By realising the radiation filters in state space, and by combining that model with a state space model for the structural system response to external forces, an extended state space model was defined which yields an estimate of the radiated sound power as a function of the excitation forces. The state space model can then be used for the synthesis of a state feedback controller. This approach was also adopted by Thomas and Nelson [53 - 55], and Mørkholt [56].
The modal state space model which was developed by Faust *et al.* [57] relates the vibration of a sandwich cylinder and the acoustic pressure inside the cylinder to the external sound field which excites the cylinder (the sandwich cylinder represents the payload compartment of a satellite launcher such as the ARIANE 5). Other than in the work of Baumann, the vibration and interior sound pressure levels are assumed to be coupled (interior pressure fluctuation causes structural vibration and vice versa). The model is derived from a quasi closed-form solution for the motion of the shell and interior acoustic field. The approach works well as long as a low number of modes is involved ; for higher frequencies other approaches are suggested (e.g. finite element models).
An alternative approach, which is not based on a modal expansion of the structural response, is applied to control sound radiation from a cylinder (Maillard and Fuller [58]). The technique, which was demonstrated before on baffled plane radiators, is referred to as Discrete Structural Acoustic Sensing (DSAS). DSAS implements an array of N structural point sensors (accelerometers) whose outputs are passed through digital FIR filters to estimate in real time the far-field radiated pressure in a given direction (not total sound power) over a broad frequency range. The technique can also be shown to be equivalent to estimating wave-number components. In this

application, the FIR filters are determined using the Kirchhoff-Helmholtz integral expression ; for more complex geometries the problem must be solved numerically using the boundary element method. The FIR filter transfer functions represent the sound pressure radiated in the given direction from an elemental surface vibrating with unit acceleration. The procedure can thus be interpreted physically as summing up the radiation contribution, in the given direction, of N cylindrical pistons weighted by the measured acceleration amplitudes. As the technique basically comes down to spatial sampling, the accuracy of the sensor estimate is dictated by sampling requirements similar to those applying to the sampling of time domain signals. Good sensor accuracy is therefore only ensured over the entire radiating field as long as the number of measurement points is high enough relative to the dominant modes of response. Therefore some knowledge of the structural velocity distribution is necessary to determine the appropriate spatial discretisation level. On the other hand, the sensor transfer functions strictly depend on the geometry of the structure and the surrounding fluid properties. In that sense, the strategy has low modelling requirements because it does not require the knowledge of the structural mode shapes and moreover, it remains largely independent of the boundary conditions.

In [59], two formulations for calculating the total acoustic power radiated by a structure are compared (a similar comparison is used in [60]), in terms of the structural modes and in terms of the velocities of an array of elemental radiators on the surface of the structure. The publication is interesting in the sense that several inter-relations between the approaches summarised here can be deduced from the development presented in [59]. Furthermore, the paper introduces the concept of *radiation modes*. Radiation modes are a set of velocity distributions on the structure whose sound power radiation is independent (in contrast with structural modes) of the amplitudes of the other velocity distributions. The concept of radiation modes provides a means to quantify the contribution of the different vibration patterns to the acoustic power output. E.g., for the case of a baffled panel, the dominant radiation mode at low frequency has a uniform velocity distribution across the panel and an amplitude which is proportional to the volume velocity of the panel. This suggests that the sound radiation from the panel can be controlled by a control algorithm which minimises the output of a sensor which measures the volume velocity of the vibrating panel. A distributed volume velocity sensor which is based upon this concept, is presented in [61]. In fact, cancellation of this first radiation mode can be achieved by designing an actuator such that it couples into the first radiation mode only.

As shown in [62], such an actuator has the same shape as the volume velocity sensor and applies a uniform pressure to the panel. In the double-panel partition application of [62], however, it is shown that there is no advantage in controlling volume velocity alone in the high frequency range. In order to be effective up to higher frequency, sensors (actuators) would need to be developed which respond (excite) only to the velocity distributions of the different radiation modes.

1.3 MOTIVATION AND OVERVIEW OF THE THESIS

1.3.1 Motivation

High-level noise not only affects hearing, it can drive up blood pressure, disrupt sleep, and compromise the ability to work and learn. Vibration and noise nuisance is inevitably associated with transportation means (automobiles [63], high-speed trains, ...), manufacturing machines (metal-cutting and woodworking machines, stamping and forging presses, ... [64]), the generation of mechanical or electrical power, ventilation systems [65], or even agricultural activity [66]. Conventional methods of suppressing vibration and noise using passive measures generally do not work well at low frequencies. It has been shown in various applications that active control can be cope with low frequency noise and vibration problems. But active control will not solve any kind of large-scale, broadband, noise and vibration problem such as traffic noise along a highway -certainly not with the current technological state of the art. Furthermore, the development of an active control solution involves a considerable engineering effort, and the resulting system is not always directly portable to other applications. With respect to passive measures, active control systems are more complicated, they are (currently) more expensive, and consume energy.
Nevertheless, there are numerous low-frequency vibration and noise problems that have good potential for active control system because of its superior performance, or because it saves weight and/or energy. The observation that active control is more than an academic research topic is corroborated by the ever increasing number of active control applications which made it to cost-effective consumer products (a non-exhaustive overview is given in appendix).

This observation has motivated the research work performed in the framework of this thesis, which aims at the further development and improvement of active control systems.

Among the potential applications for active control, noise radiated by vibrating structures is an important problem area. This thesis contributes to the development of systems for Active Structural Acoustic Control. ASAC is a relatively new technique which offers interesting new research opportunities. First of all, ASAC was shown to be more effective than ANC [34] or AVC [67]. This is mainly due to the fact that in cases where a very large number of structural or acoustic modes are excited by the primary disturbance, it is impossible to achieve significant vibration or noise reductions using a realistic number of control sources. ASAC aims at observing and controlling the radiating components of the structural vibrations only. Thus, considerable reductions in radiated sound power can often be achieved with very few control forces ([67] p. 110). Furthermore, since ASAC deals with controlling the interaction between structural vibration and sound field, it presents a challenge in the domain of modelling, actuator and sensor design, signal processing and control synthesis.
This thesis is mainly motivated by the opportunities presented at the control side. Since ASAC of harmonic disturbances has been studied extensively, this thesis concentrates on the development of control algorithms and signal processing techniques which aim at the ASAC of broadband structure-borne noise.
To this aim, a profound overview of the control theory is presented -from the viewpoint of the design of active control systems. The aim of this overview is to provide a basic understanding of the fundamental properties of the control algorithms which are used most often in active control. On the one hand, the overview is the starting point for the subsequent chapters. On the other hand, however, the overview is organised and documented in a way that it can serve as a reference for the development of active control algorithms for applications other than ASAC, or for the evaluation of the control strategy used in similar research work, etc. In that sense, this overview is an essential contribution to realising the objectives of the thesis. It is by no means a continuation of the introduction to the thesis, it has a key role : to lead to a better design of controllers for active control of vibration and sound.
A first control strategy for ASAC which is developed in this thesis, aims at the design of a controller which uses vibration sensors located on the

structure to control the sound radiated by the structure due to a broadband disturbance for which no reference signal is available. This work is mainly motivated by the fact that it leads to a control strategy that can solve a very wide range of structure-borne noise problems. The proposed approach, which is based on earlier work [51], starts from a state space model for the radiation behaviour of the considered structure which is the used as a basis for the design of a feedback controller. The main contribution of this thesis is that it proposes a controller synthesis procedure which circumvents some practical limitations inherent to the approach presented in [51]. This generalises the approach and makes it applicable to more complex problems than the beam, which is dealt with in [51]. This control strategy is applied to reduce the sound radiated from a baffled, elastic, rectangular plate. The experiments which are presented, are believed to be the first of their kind.

In addition, an adaptive feedforward controller for the ASAC of structure-borne road noise in a passenger car is developed. This application serves as a practical example for the general problem of the reduction of structure-borne noise due to multiple uncorrelated sources. This thesis presents an new and innovative approach to this problem, viz. to use inertia shakers to control the car body vibration to driving over a coarse road surface. The main contribution of this part of the thesis is that it shows that this control approach can also be applied -with success- to complicated problems. The approach which is presented here, has recently been adopted by researchers dealing with structure-borne noise inside a high-speed passenger train [240]. Furthermore, this particular road noise application has motivated the development of a technique for the real-time enhancement of the reference signals for feedforward control. The new technique which is presented in this thesis, relies on a recursive algorithm which diagonalises the covariance matrix of the reference signals. It is shown that it is very effective for the considered application.

1.3.2 Chapter by chapter overview

Chapter 1, the introduction, describes the basic principles of active control of vibration and noise. An overview of techniques for Active Structural Acoustic Control (ASAC) is presented and the range of applications which are aimed at in this thesis is defined.

Chapter 2 gives an overview of the relevant topics in control theory. On the one hand, this provides a basis and for the discussion of the control approaches described in chapter 3 and 4. On the other hand, the presentation of the overview should result in a better understanding of the basic trade-offs which need to be considered in the synthesis of the appropriate controller for a given active control application.

Chapter 3 deals with the development of a model-based feedback control strategy to suppress broadband noise radiation from vibrating structures. The approach introduced by Baumann *et al.* [51] is used as a basis. An advanced system identification procedure is proposed. A proof-of-principle experiment on a baffled rectangular plate is presented.

Chapter 4 presents an active control solution for a specific practical problem : the reduction of structure-borne road noise in a passenger car. The development and optimisation of the control system is discussed in detail. Results of road tests are presented. A signal processing technique is developed in order to enhance the control performance. It is validated by means of numerical simulations.

Chapter 5 gives an overview of practical considerations related to the implementation of active control systems. Actuator and sensor technology for active control is presented, and electronics design, processor choice and programming issues are discussed.

Chapter 6 presents general conclusions of the work.

The *Appendix* gives a non-exhaustive overview of operational active control systems, consumer products using active control, and companies which are "active" in this field. The aim of this appendix is to illustrate how relevant active control is in the domain of vibration and noise control ; and which are typical active control applications.

CHAPTER 2

CONTROL THEORY

2.1 INTRODUCTION

The design of an appropriate controller is central in the development of systems for active control of vibration and sound. The controller is the "brain" of the control system : it takes in sensor signals, calculates the appropriate control action, and drives control sources in order to realise the control objective. Eventually, the controller may also be programmed to "learn" from its actions and to update its control parameters iteratively.
The literature volume on system identification theory and control theory providing methodologies for controller design is enormous and the application of advanced control theory in the field of active control appears to be straightforward at first glance -the only prerequisite being the availability of a set of "Toolboxes" in Matlab®. Early work on active control (mid 1960s) has often been constrained due to the inability to implement the

high-order controllers which result from applying advanced control techniques. This is because these techniques are basically developed for finite-order, lumped-parameter systems and hence lead to high-order controllers when used to control distributed-parameter systems of, at least in theory, infinite order. With the advent of Digital Signal Processors (DSPs) at affordable price in the mid 80s, control processing complexity has rapidly grown from low order Single Input/Single Output (SISO) systems -often realised in analog filters- to high-order, adaptive, Multiple Input/Multiple Output (MIMO) digital controllers driving a multitude of control sources based on information carried within a multitude of sensor signals.
Literature overviews presenting all possible control techniques relevant for active control, together with the algorithms, C- and assembly code implementations, is published on a regular base (see, e.g. [68]). Though the compilation work associated with these publications is impressive, the link with classical control theory is often vague as a result of which it appears as if active control is a control theory on its own where control inputs are exclusively loudspeaker signals and sensors are limited to be microphones. Furthermore, the way the control algorithms are presented often leads to the misleading impression that designing an active control system requires nothing more than to select a tailored algorithm from a list, to copy and download the software to a DSP board, after which the application can be run. For most applications, however, it is necessary to innovate important enhancements to existing algorithms, or to synergise control, applied mathematics and digital signal processing methods in order to attain the targets. This work can obviously only be performed if one is thoroughly aware of the physical mechanisms that lie behind the control algorithm employed and as a result of which control performance may or may not be constrained.
This chapter is therefore conceived as an introduction, to highlight the basic principles of control theory in order to provide a basis to allow interpretation of the results achieved in the subsequent chapters dealing with practical applications. Feedback and feedforward control theory are first dealt with in separate paragraphs (2.2 and 2.3). A practical application concludes each paragraph. Though active control systems are often categorised based on the observation whether the control algorithm is basically feedback or feedforward, it is actually more correct to distinguish LTI (Linear Time Invariant) from adaptive control designs. This classification is motivated in paragraph 2.4, where the strong equivalence relation between the feedback and feedforward control paradigms is pointed out.

2.2 FEEDBACK

2.2.1 A general feedback control configuration

The block diagram of a general feedback control configuration is depicted in figure 2.1. The *controller* is described by its complex transfer function matrix[1] $\mathbf{K}(s)$, $s \in \mathbb{C}$, which can be evaluated as a function of frequency by setting the Laplace variable $s = j\omega$. The system to be controlled, or *plant*, described by its complex transfer function matrix $\mathbf{G}(s)$, is subject to the exogenous input(s) $\mathbf{u}_w$, representing external disturbances acting on the system, and control inputs $\mathbf{u}_c$, with which the system response is controlled. The block diagram defines two different system outputs. The *performance* output vector $\mathbf{z}$, is the variable which is used to specify control performance. In *regulator* problems, the performance output is used to formulate a performance specification which aims at reducing the vibration or acoustical energy in the system. *Servocontrol* problems are aiming at optimising the tracking of a prespecified (temperature, displacement, or other) trajectory. The performance output is then used to represent the error between the desired and actual trajectory in the controller performance specification. Active control problems are obviously regulator problems, therefore all control configurations that are presented in this text are representing regulator problems. Interpretation of any configuration in either sense, however, is straightforward[2]. The *feedback* output vector $\mathbf{y}$ represents the physically measured system outputs that are fed back to the controller. Outputs $\mathbf{y}$ and $\mathbf{z}$ may eventually be collocated. Separating the system outputs into $\mathbf{y}$ and $\mathbf{z}$ allows to specify the control objective as a function of a variable which is not directly measurable but which is observed through $\mathbf{y}$ (a straightforward example is to control system velocity based upon measurement of the acceleration). $\mathbf{G}_{zw}(s)$ denotes the open loop transfer function (matrix) between $\mathbf{u}_w$ and $\mathbf{z}$, etc., whereas $\tilde{\mathbf{G}}_{zw}(s)$ denotes the same

[1] Throughout this text, bold-faced symbols denote matrix variables as well as column and row vector variables. Symbols in italics denote 1-dimensional variables or functions, e.g. a complex number, or a complex number as a function of frequency (frequency response function), respectively.

[2] A regulator may also be regarded as a servocontroller for which the desired trajectory is specified as zero (vibration or acoustic) energy ; or, inversely, a servocontroller is a regulator which minimises the (energy in) the error between desired and actual trajectory.

transfer function but with the control loop between $\mathbf{y}$ and $\mathbf{u}_c$ closed ($\tilde{\mathbf{G}}_{zw} = \mathbf{G}_{zw} + \mathbf{G}_{zc}\mathbf{K}\left(\mathbf{I} - \mathbf{G}_{yc}\mathbf{K}\right)^{-1}\mathbf{G}_{yw}$).

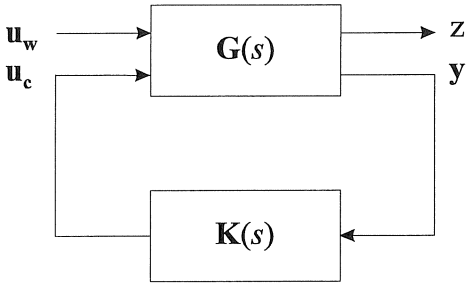

Figure 2.1. Block diagram of a general feedback control configuration. Input $\mathbf{u}_w$ represents the exogenous input vector ; input $\mathbf{u}_c$ represents the control input vector. Output z is the *performance* output vector, its value(s) appears in the objective function that is optimised by the controller. Output y is the *feedback* output vector, these are the sensor signals that are measured by the controller and from which the control signals are calculated.

Figure 2.2 presents a simplified feedback scheme where a single disturbance and a single control input are supposed to be additive (negative feedback) and where $\mathbf{y}$ and $\mathbf{z}$ are 1-dimensional and collocated. Assuming that disturbance and control input "enter" the system at the same point is a condition which is encountered, for example, in active isolation systems where an actuator is used to minimise the transmission of vibration from the work floor (*d*) to a fragile piece of equipment (the response, or vibration of the equipment, is represented by *e*). A possible configuration is then to mount the actuator in parallel with the existing mount which configuration allows to apply counteracting forces to the same transfer path (figure 2.3). Such a SISO control configuration is widely used in practice and will be used here to shortly illustrate some basic principles of feedback control.

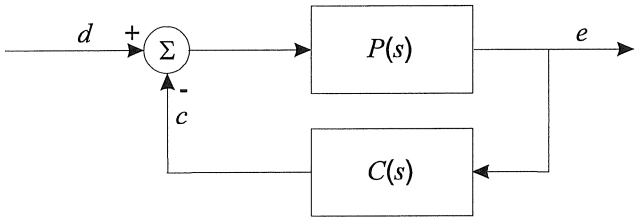

Figure 2.2. SISO feedback control system ; $P(s)$, the *plant*, is the system to be controlled by the controller $C(s)$.

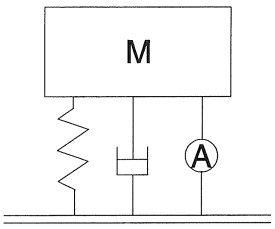

Figure 2.3. Active isolation problem. The equipment M is to be isolated from the work floor by means of control forces generated by the actuator A. The spring-damper combination represent the passive mount on which M is mounted.

The symbols used in figure 2.2 and in the following discussion differ from the symbols used in figure 2.1 to stress the fact that the relations obtained are not necessarily valid for the general MIMO case. $P(s)$ is the complex transfer function representing the plant subject to the disturbance d and control action c, $C(s) \in \mathbb{C}$ represents the controller which transforms the residual signal e at the output directly into a control action. The dynamic properties of the control actuator (including power amplification) are supposed to be included in the controller. For SISO controllers, $C(s)$ may be regarded as a filter (the *control filter*) without loss of generality.
The change in the response due to closing the feedback control loop is given by the transfer function :

$$H(s) = \frac{E(s)}{D(s)} = \frac{P(s)}{1 + P(s)C(s)} . \tag{2.1}$$

Obviously, to make the controlled response small compared to the uncontrolled response it is necessary to make :

$$|PC| >> 1 , \tag{2.2}$$

i.e., the *loop gain* must be made large. In control theory, this condition is mostly formulated as a condition on the *sensitivity function*, $S(s) = \frac{1}{1 + P(s)C(s)}$ which needs to be made small. We will get back to this formulation in paragraph 2.2.2.

It is important to note :

- In the regulation band where $|PC| >> 1$, the phase of PC is immaterial to performance and small deviations of C from design goals result in only comparably small deviations of closed loop performance.
- The closed-loop response will be reduced relative to open loop response at each frequency according to equation (2.1) - that is, regardless of whether the disturbance is deterministic or random, narrowband or broadband, continuous or transient. By closing the feedback loop, the disturbance "sees" a different system at the input.

To this point feedback control seems to be very simple, ensuring any desired reduction as a function of loop gain. The complexity, however, enters in the fact that the gain must eventually become small at high frequency (physical power limitation) which must be realised without causing the system to become unstable. Indeed, as variation of amplitude of the control filter necessarily implies corresponding phase changes, the stability of the closed loop system (2.1) can only be ensured by imposing particular conditions between amplitude and phase of the loop gain. From equation (2.1) it is clear that, in order to maintain stability, as the magnitude of $P(s)C(s)$ is reduced, the phase of $P(s)C(s)$ should not exceed 180° until the magnitude of $P(s)C(s)$ is below unity, i.e. :

$$\angle\{P(s)C(s)\} \leq 180^\circ \quad \text{for} \quad |P(s)C(s)| > 1. \tag{2.3}$$

A second constraint which is imposed to $C(s)$ pertains to avoiding out-of-regulation band noise amplification. If measurement noise adds to the feedback signal as shown in figure 2.4, it is coupled to the system output through the controller. Considering the corresponding transfer function $R(s) = \frac{E(s)}{V(s)} = \frac{P(s)C(s)}{1+P(s)C(s)}$, it is clear that optimising the closed loop gain may cause measurement noise to be reproduced or even amplified at the output[3]. The avoidance of noise amplification is usually a more severe constraint than simply maintaining stability.

Apart from these considerations, it is equally important to take *robustness* of the controller into account before implementation. This is basically because a controller's characteristics are determined based on the dynamic

[3] A typical example of this being the complete set-up resonating at harmonics of 50 Hz (60 Hz in the US) outside the regulation band when the control loop is closed...

characteristics of the plant under nominal conditions, i.e. the controller is designed for a given *nominal* plant. Due to various effects such as ageing or wear of mechanical components, drift in electronic circuitry, etc., time variation of the actual plant with respect to the nominal plant is very likely to occur in practice. Robust control design techniques [69] have been developed to cope with that problem. Robustness can be considered in two ways : robust stability and robust performance. Robust stability implies that the controller stabilises all plants in a given set around the nominal plant. Robust performance implies that certain performance bounds (e.g. 20 dB vibration reduction in a given frequency band) are guaranteed for all plants in a given set around the nominal plant.

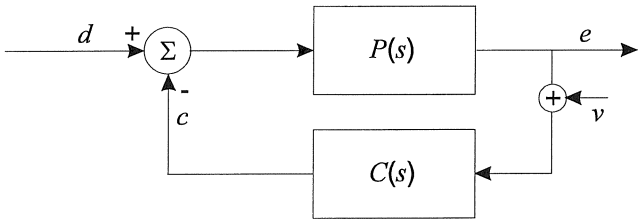

Figure 2.4. SISO feedback control system for the case where measurement noise v adds to the feedback signals.

For this simple example, robust stability can be guaranteed by creating large enough a phase margin (typically 45°, but often application-dependent) at the cross-over, i.e. where $|P(s)C(s)|=1$, and/or an amplitude margin (typically >6 dB) at the point where $\angle\{P(s)C(s)\}\approx 180^\circ$. The design and analysis of robust controllers is a research domain on its own and it is well beyond the scope of this thesis to deal with that specific theory in detail. However, the techniques will be introduced in the following paragraphs in order to show that the work on robust control techniques is particularly relevant for the active control of vibration and sound. For further details, reference is given to tutorials and/or text books.

Designing a controller basically comes down to realising the control objectives under the boundary conditions pointed out above. Feedback control theory provides a wide range of methods to do this, ranging from PID-control design for (simple) SISO systems, to advanced, model-based control techniques that allow design of controllers with which the various cross-couplings of a range of inputs with a range of outputs can be

controlled [70]. The period 1930 - 1960, labelled "Classical Control," produced the standard frequency domain concepts which make up the bulk of industrial control practice to this day. Though these techniques are not completely irrelevant, this thesis concentrates on advanced control approaches. The Modern Control period (1960 - 1980) saw the introduction of state-space matrix equations and LQG synthesis. These tools are usually thought of as time-domain concepts. The Robust Control period (1980 - present) has seen a return to frequency-domain thinking in H_∞ synthesis, μ and singular value robustness analysis, and LQG with loop transfer recovery (LQG/LTR). The following paragraphs will shortly introduce the model-based control techniques that have been considered in this work. The discussion starts with explaining some basic concepts of state feedback. The observations made above will thus be put in a more general framework.

2.2.2 State feedback

State feedback has emerged in the 1960s as a linear, model-based control theory. The purpose of a system model is to represent the dynamic properties of the system as a function of frequency or time. Frequency domain linear system models can in general be expressed as a rational expression of two polynomials in s with constant and real coefficients as in (2.4) for the SISO case :

$$G(s) = \frac{Num(s)}{Den(s)} = \frac{\sum_{k=1}^{m} b_k s^{k-1}}{\sum_{l=1}^{n} a_l s^{l-1}}. \tag{2.4}$$

The extension to a MIMO transfer function matrix is straightforward. The response, in the time domain, of $G(s)$ to an input can then be determined, for example, by convolution of the inverse Laplace transform of (2.4) with the time series of the input signal.
A system model which describes the dynamic response directly in the time domain, is the so-called *state space model* representation (2.5)

$$\begin{aligned} \dot{\mathbf{x}} &= \mathbf{A} \cdot \mathbf{x} + \mathbf{B} \cdot \mathbf{u} \\ \mathbf{y} &= \mathbf{C} \cdot \mathbf{x} + \mathbf{D} \cdot \mathbf{u} \end{aligned} \tag{2.5}$$

where **A**, **B**, **C**, and **D** are constant real matrices, vector **x** comprises the system *states*, **u** and **y** are the inputs and outputs, as defined before. The

relation between (2.4) and (2.5) is simple and straightforward as $G(s) = \mathbf{D} + \mathbf{C}(s\mathbf{I} - \mathbf{A})^{-1}\mathbf{B}$. If $G(s)$ would be the transfer function describing the acceleration response of the equipment in figure 2.3 to a force input at the base, logical system states would be velocity and displacement. A state space model has the inherent ability to describe, not only what happens at the outputs of the system, but also to reflect how the system behaves "internally". For the given example (figure 2.3) it may actually be so that the system displacement is beyond all safety margins even at an acceptable acceleration level (which is monitored).

A *state feedback* controller will feed back a linear combination of the system states in order to generate the control signals $\mathbf{u}_c$, thus the feedback law takes the following form :

$$\mathbf{u}_c = -\mathbf{K} \cdot \mathbf{x}, \tag{2.6}$$

in which $\mathbf{K}$ is a feedback matrix (in which the minus sign may be absorbed) which is determined such that a predefined control objective is realised.
If we now write down the state space equations of the closed loop system, we see that the controlled system exhibits a different behaviour :

$$\begin{aligned} \dot{\mathbf{x}} &= (\mathbf{A} - \mathbf{B}_2\mathbf{K}) \cdot \mathbf{x} + \mathbf{B}_1 \cdot \mathbf{u}_w \\ \mathbf{y} &= (\mathbf{C} - \mathbf{D}_2\mathbf{K}) \cdot \mathbf{x} + \mathbf{D}_1 \cdot \mathbf{u}_w \end{aligned} \tag{2.7}$$

(the columns corresponding to $\mathbf{u}_c$ and $\mathbf{u}_w$ have been assembled in $\mathbf{B}_2$ and $\mathbf{B}_1$, respectively; $\mathbf{D}_2$ and $\mathbf{D}_1$ are obtained in a similar manner). Expression (2.7) explicitly shows that feeding back the system states actually allows to change the system poles. *Pole placement* is therefore one of the most straightforward model-based control techniques with which the control designer basically determines the desired closed-loop poles and then imposes them via the feedback matrix $\mathbf{K}$ [71]. A specific technique, *eigenstructure assignment*, has been developed which, in addition, allows to impose prespecified eigenvectors together with the eigenvalues [72].
Though it is conceivable that SISO systems for active control can be designed by means of pole placement, it is much less evident how poles would have to be placed if one is aiming at reducing a specific output response of a high order MIMO system where all possible interactions with other outputs -which should not be affected by the control action- come into play. To solve this problem, advanced controller synthesis techniques have been developed that provide a formal mathematical synthesis procedure to determine $\mathbf{K}$ to simultaneously satisfy all controller requirements. As

pointed out before, the basic requirements of a closed-loop feedback system are :

1. *Stability* : bounded outputs $\mathbf{y}(t)$ and $\mathbf{z}(t)$ for all bounded disturbances $\mathbf{u}_w(t)$
2. *Performance* : small outputs $\mathbf{z}(t)$ in the presence of $\mathbf{u}_w(t)$, and
3. *Robustness* : stability and performance maintained in the presence of model uncertainties

The stability requirement has already been expressed mathematically for a simplified case (2.3). More in general, this requirement imposes structural constraints on certain transfer functions of the closed-loop system, e.g. a Nyquist encirclement count for the function $det\left(\mathbf{I}+\mathbf{G}_{zc}\mathbf{K}\right)$ [73].

Likewise, the second requirement imposes magnitude constraints on certain transfer functions. This is summarised in a fundamental frequency domain prescription which can be stated as : "make $\tilde{\mathbf{G}}_{zw}(s)$ small whenever $\mathbf{u}_w(s)$ is large". Complex vectors are taken as small or large according to the size of their 2-norm (Euclidean norm). Complex matrices $\tilde{\mathbf{G}}_{zw}(s)$ are taken as small if their largest singular value $\bar{\sigma}\left\{\tilde{\mathbf{G}}_{zw}(s)\right\}$ is small, they are taken large if their smallest singular value $\underline{\sigma}\left\{\tilde{\mathbf{G}}_{zw}(s)\right\}$ is large[4].

The third feedback requirement is also expressed in terms of magnitude constraints which, however, depend on how model uncertainty is characterised. The traditional approach described before dictates gain margins and phase margins be used to characterise tolerable uncertainty. This characterisation can also be generalised to MIMO problems where it leads to constraints on the so-called *complementary sensitivity function* $T(s)$ on the frequency axis [75].

In the simple example of 2.2.1, requirements (2) and (3) lead to the constraint that two functions, $S(s)$ and $T(s)=\dfrac{PC}{1+PC}$, need to be small on the $j\omega$ - axis (refer to 2.2.1 for S and to [76] for T). Since $S(s)+T(s)=1$ it is clear that both cannot be made small simultaneously. Feedback design can thus be seen as a game of essential trade-offs between transfer functions. A modern (LQ-control) and a robust (H_∞-control) approach to this dilemma, which are also two of the techniques that are most often encountered in active control literature, are now discussed from this point of view.

---

[4] For a detailed overview of vector and matrix norms and their relevance in control theory, refer to [74].

2.2.3 Linear Quadratic (LQ) control

Linear Quadratic Regulator and Linear Quadratic Gaussian Control

Perhaps the best known example of formal mathematical controller synthesis procedure is the Linear Quadratic optimal control problem. This problem formalises the construction of feedback controllers for finite-dimensional linear plant models with a least-squares performance specification (*cost function*) as design objective. The synthesised controller is optimal in the sense that the cost function specification allows to weight the control effort that is required to realise the control objective.
The *Linear Quadratic Regulator* optimises the following cost function (2.8) :

$$J = \int_{t_o}^{t} \left(\mathbf{x}^T \mathbf{Q}_{ctr} \mathbf{x} + \mathbf{u}_c^T \mathbf{R}_{ctr} \mathbf{u}_c \right) d\tau \ . \tag{2.8}$$

$\mathbf{Q}_{ctr}$ and $\mathbf{R}_{ctr}$ are positive semi-definite, resp. positive definite *weighting* matrices which allow to balance the necessary control energy against the energy in the system states. When $\mathbf{Q}_{ctr}$ is made considerably larger than $\mathbf{R}_{ctr}$, the optimal controller will reduce the system states considerably, eventually at the expense of a large control effort.
Under the assumption that $\mathbf{z}$ and $\mathbf{u}_c$ decay to zero at $t \rightarrow \infty$ (this will be the case for transient, or impulsive, excitation), J will converge to a finite value. If the system is subject to persistent exogenous inputs which can assumed to be Gaussian white noise, expression (2.8) is substituted by (2.9)

$$J = \lim_{T \to \infty} \frac{1}{T} E\left\{ \int_{0}^{T} \left(\mathbf{x}^T \mathbf{Q}_{ctr} \mathbf{x} + \mathbf{u}_c^T \mathbf{R}_{ctr} \mathbf{u}_c \right) d\tau \right\} \tag{2.9}$$

where $E\{ \cdot \}$ is the expectation operator, i.e. the average value of the cost function over all possible realisations of the disturbances. The *LQG* (*G* for *Gaussian*) controller that optimises the above quadratic performance criterion (2.9) is found by solving the Algebraic Riccati Equation (ARE) [77] [78],

$$\mathbf{SA} + \mathbf{A}^T\mathbf{S} - \mathbf{SB}_2\mathbf{R}_{ctr}^{-1}\mathbf{B}_2^T\mathbf{S} + \mathbf{Q}_{ctr} = 0 \tag{2.10}$$

for $\mathbf{S}$, after which the feedback matrix $\mathbf{K} = \mathbf{R}_{ctr}^{-1}\mathbf{B}_2^T\,\mathbf{S}$ is determined.

If the system is subject to coloured noise, the system model must be augmented with a shaping filter such that the augmented system can be assumed to be subject to white noise, which implies that the LQG control theory remains valid.

The performance specification is not limited to be expressed as a function of the system states but can also be formulated in terms of linear combinations of the system states. To this aim, a set of *performance* outputs **z** is defined with which (2.9) is then expressed as

$$J = \lim_{T\to\infty} \frac{1}{T} E\left\{ \int_0^T \left(\mathbf{z}^T \mathbf{Q}_{ctr}\, \mathbf{z} + \mathbf{u}_c^T \mathbf{R}_{ctr}\, \mathbf{u}_c \right) d\tau \right\}. \tag{2.11}$$

The associated ARE changes to

$$\mathbf{SA} + \mathbf{A}^T\mathbf{S} - \mathbf{S}\mathbf{B}_2\tilde{\mathbf{R}}_{ctr}^{-1}\mathbf{B}_2^T\mathbf{S} + \tilde{\mathbf{Q}}_{ctr} = 0\,, \tag{2.12}$$

where $\tilde{\mathbf{Q}}_{ctr} = \mathbf{C}_1^T\mathbf{Q}_{ctr}\,\mathbf{C}_1$ and $\tilde{\mathbf{R}}_{ctr} = \mathbf{R}_{ctr} + \mathbf{D}_{12}^T\mathbf{R}_{ctr}\,\mathbf{D}_{12}$; and is again solved for $\mathbf{S} = \mathbf{S}^T$ after which $\mathbf{K} = \tilde{\mathbf{R}}_{ctr}^{-1}\mathbf{B}_2^T\,\mathbf{S}$ is solved. System matrices $\mathbf{C}_1$ etc. are defined by the following relations :

$$\begin{aligned} \dot{\mathbf{x}} &= \mathbf{A}\cdot\mathbf{x} + \mathbf{B}_1\cdot\mathbf{u}_w + \mathbf{B}_2\cdot\mathbf{u}_c \\ \mathbf{z} &= \mathbf{C}_1\cdot\mathbf{x} + \mathbf{D}_{11}\cdot\mathbf{u}_w + \mathbf{D}_{12}\cdot\mathbf{u}_c \\ \mathbf{y} &= \mathbf{C}_2\cdot\mathbf{x} + \mathbf{D}_{21}\cdot\mathbf{u}_w + \mathbf{D}_{22}\cdot\mathbf{u}_c \end{aligned}\,. \tag{2.13}$$

Linear quadratic control theory is particularly interesting for active control applications in that it provides a performance specification which is directly related to what the aim of active control is. Returning to the simple control problem of figure 2.3, where obvious choices for system states have been shown to be velocity and displacement, it immediately follows that a LQG controller will minimise the total vibration energy of the system, which is exactly what we want to achieve.

Three important remarks must be made :

- Although LQG controllers are often referred to as optimal controllers, it is important to be aware of the fact that they are only "optimal" with respect to the specified cost function. The solution of the ARE, and hence the control performance, is determined by the system characteristics on the one hand and by the specified weighting matrices on the other hand. This implies that the extent to which the LQG controller is really optimal is to a large part determined by how the control system is configured (number and location of actuators and sensors) and which weighting matrices are used. Needless to say that both aspects are the responsibility of the control engineer.

- Until now, all formulations have been expressed in the continuous time domain. Modern controllers, however, are most often implemented on digital processors and thus all system equations must be transformed to the discrete time domain using the techniques[5] described in [80] [81]. Discrete time system equations for $\mathbf{G}(z)$ are presented in (2.14) :

$$\begin{aligned}\mathbf{x}(k+1) &= \mathbf{A}\cdot\mathbf{x}(k)+\mathbf{B}_1\cdot\mathbf{u}_w(k)+\mathbf{B}_2\cdot\mathbf{u}_c(k)\\ \mathbf{z}(k) &= \mathbf{C}_1\cdot\mathbf{x}(k)+\mathbf{D}_{11}\cdot\mathbf{u}_w(k)+\mathbf{D}_{12}\cdot\mathbf{u}_c(k)\\ \mathbf{y}(k) &= \mathbf{C}_2\cdot\mathbf{x}(k)+\mathbf{D}_{21}\cdot\mathbf{u}_w(k)+\mathbf{D}_{22}\cdot\mathbf{u}_c(k)\end{aligned} \quad . \tag{2.14}$$

  Note that, though the same symbols have been used for clarity, discrete time system matrices are basically different from continuous time matrices.
- The feedback controller (2.6) is called the *full-state* feedback controller. Full state feedback controllers, however, are not always realistic as their construction assumes access to all system states. For applications where this is not possible, the controller is complemented with a state observer (also *estimator*) as explained below. Two basic estimator configurations, the *prediction* and *current* estimator, are discussed in [81] (pp. 145-148). The prediction estimator predicts the estimate $\hat{\mathbf{x}}(k)$ of the system state, based upon an output measurement, made on time step k-1. The current estimator predicts an initial guess, $\bar{\mathbf{x}}(k)$, but updates $\hat{\mathbf{x}}(k)$ based upon measurement at the current time step.

The dynamics of a current estimator are governed by the time update equation (2.15)

$$\bar{\mathbf{x}}(k+1) = \mathbf{A}\hat{\mathbf{x}}(k)+\mathbf{B}_2\mathbf{u}_c(k) \tag{2.15}$$

and the observation update equation (2.16)

$$\hat{\mathbf{x}}(k) = \bar{\mathbf{x}}(k)+\mathbf{L}\left(\mathbf{y}(k)-\hat{\mathbf{y}}(k)\right) \tag{2.16}$$

where $\mathbf{L}$ is the estimator gain matrix. An *LQG* optimal estimate of the state is produced by a stationary *Kalman filter*. The Kalman filter is determined based upon knowledge of the process and measurement noise variances, i.e.

---

[5] Though the design of controllers in discrete time seems to involve no more than applying the appropriate transformation technique, it may lead to various problems associated with the introduction or shift of system zeros etc. Refer to e.g. [79] for further detail.

$E\{\mathbf{u}_w\mathbf{u}_w^T\} = \mathbf{Q}_{est}$ and $E\{\mathbf{v}\mathbf{v}^T\} = \mathbf{R}_{est}$ respectively (measurement noise $\mathbf{v}$ adds to the feedback outputs $\mathbf{y}$, refer to figure 2.5). An estimate for the system output, $\hat{\mathbf{y}}(k)$, is given by (2.17)

$$\hat{\mathbf{y}}(k) = \mathbf{C}_2\bar{\mathbf{x}}(k) + \mathbf{D}_{22}\mathbf{u}_c(k) \tag{2.17}$$

where the control signal is determined based on the estimated state as in (2.18)

$$\mathbf{u}_c(k) = -\mathbf{K}\hat{\mathbf{x}}(k)\,. \tag{2.18}$$

The dynamic equations of the controller-estimator $\mathbf{K}(z)$ (figure 2.5) are obtained from (2.16), (2.17) and (2.18) :

$$\begin{aligned}
\bar{\mathbf{x}}(k+1) &= \left[\mathbf{A} - \mathbf{ALC}_2 - (\mathbf{B}_2 - \mathbf{ALD}_{22})\mathbf{E}(\mathbf{K} - \mathbf{KLC}_2)\right]\bar{\mathbf{x}}(k) \\
&\quad + \left[\mathbf{AL} - (\mathbf{B}_2 - \mathbf{ALD}_{22})\mathbf{EKL}\right]\mathbf{y}(k) \\
\mathbf{u}_c(k) &= \left[\mathbf{K} - \mathbf{KLC}_2 + \mathbf{KLD}_{22}\mathbf{E}(\mathbf{K} - \mathbf{KLC}_2)\right]\bar{\mathbf{x}}(k) \\
&\quad + \left[\mathbf{KL} + \mathbf{KLD}_{22}\mathbf{EKL}\right]\mathbf{y}(k)
\end{aligned} \tag{2.19}$$

where $\mathbf{E} = (\mathbf{I} - \mathbf{KLD}_{22})^{-1}$.

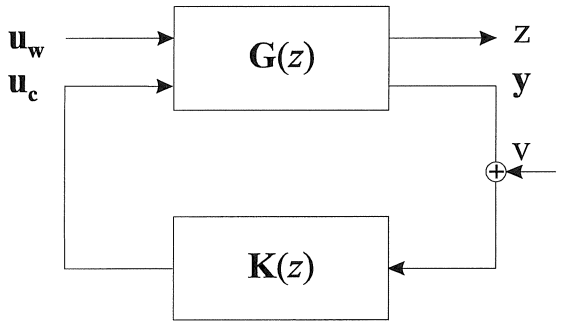

Figure 2.5. Controller block diagram for the case where measurement noise adds to the feedback signals.

In contrast with a *full-state feedback* configuration (2.6), the controller-estimator (2.19) is a dynamic system with inputs $\mathbf{y}(k)$ and outputs $\mathbf{u}_c(k)$ and thus it is fundamental to properly tune the dynamics of the controller-

estimator in order to achieve the control performance aimed at. The poles of the closed-loop system $\tilde{\mathbf{G}}(z)$ can be shown to be equal to sum of the observer poles and the controller poles which are unchanged from those obtained assuming actual state feedback [81]. This effect is referred to as the *separation principle* and it implies that the control and estimation can be designed separately.
The estimator dynamics are basically determined by the operational conditions in which the system needs to be controlled : if measurement noise is very low compared to process noise, the estimator can be made extremely fast because the estimator can rely completely upon $\mathbf{y}(k)$ for the update of the system state estimate. The bandwidth of the estimator can then be increased beyond the bandwidth necessary for control such that the effect of estimation on the control performance will be rather limited. In case of considerable measurement noise, the estimator needs to be slowed down which may limit the achievable control performance.

The LQG/LTR procedure

The full-state feedback *optimal* controller enjoys guaranteed robust stability margins (60 degrees phase margin, [+∞, -6 dB[gain margin) in each control channel [74]. These margins were however found to disappear when Kalman state estimators are employed [82] as a result of which the performance and stability of LQG estimated-state feedback controllers, supposedly "optimal", were often found to be very sensitive to modelling errors. The LQG/LTR (Loop Transfer Recovery) method has been developed [76] [82] with which the full-state feedback closed-loop system properties can be recovered asymptotically by speeding up the observer dynamics in a "controlled way" by adding fictitious process noise of a very specific kind (It is also shown that arbitrary increases of $\mathbf{Q}_{est}$ will not in general produce the desired effect). Though this method is constrained in the sense that perfect recovery will only be achieved if the plant is minimum phase and under the boundary conditions of extremely low measurement noise, it strongly suggests that the matrices $\mathbf{Q}_{est}$ and $\mathbf{R}_{est}$, which represent noise intensities in the Kalman filter design, should instead be treated more freely as design parameters which can be selected to suit broader purposes such as robustness and control performance.
A very interesting observation, to a large part inspired by the LQG\LTR approach, is that time-domain LQG problem can, by Parseval's theorem, be shown to be equivalent to what is described mathematically as a so-called

H_2 optimisation problem in the frequency domain. H_2 optimisation in the frequency domain yields a mathematical expression for the control design trade-offs pointed out in paragraph 2.2.2. Indeed, given the sensitivity $\mathbf{S}(s)$ and complementary sensitivity function $\mathbf{T}(s)$, and weights $\mathbf{W}(s)$ to trade one against the other, the three basic requirements for feedback control can be satisfied by determining a stabilising $\mathbf{K}(s)$ which minimises

$$J_{H_2} = \int_0^\infty \left(\mathrm{Tr}\left[\mathbf{SWW}^H\mathbf{S}^H\right] + \mathrm{Tr}\left[\mathbf{TT}^H\right]\right) d\omega. \tag{2.20}$$

($\mathrm{Tr}(\cdot)$ is the trace of the matrix, superscript ^{H} denotes Hermitian, i.e. complex conjugate, transpose). This optimisation problem is a so-called H_2 optimisation problem Stein and Athans [76] have determined how to manipulate the free parameters of the LQG problem in order for the standard LQG problem to accomplish the H_2-trade-offs between sensitivity and complementary sensitivity. Moreover, they show that these manipulations are equivalent to LQG\LTR.
The reinterpretation of LQG as a frequency domain optimisation approach provides an interesting comparison with H_∞ optimisation as it implies that LQG may also be regarded as a loop shaping tool in the frequency domain.

2.2.4 H_∞ control

The main problem with LQG is that it cannot cope directly with model uncertainty. Successful application of LQG is therefore only achieved through careful attention to robustness margins. Though it is not impossible to formally address a robustification procedure for LQ regulators [84] it was only in the early 1980s that a new control design procedure was presented which explicitly addresses model uncertainty in the early design stage. These developments centered on H_∞ optimisation and originated from the influential work of Zames [85] (emphasis on SISO).

The basic idea of H_∞ control is to minimise the H_∞ norm of stable, proper transfer function matrices. The H_∞ norm of a system $\mathbf{G}$ is defined as [74] :

$$\|\mathbf{G}\|_\infty = \sup_\omega \bar{\sigma}\{\mathbf{G}(j\omega)\}. \tag{2.21}$$

An important interpretation of the H_∞-norm is that it is the maximum transfer function *gain* on the $j\omega$ axis :

$$\|\mathbf{G}\|_\infty = \sup_{\mathbf{u}\neq 0} \frac{\|\mathbf{Gu}\|_2}{\|\mathbf{u}\|_2}. \tag{2.22}$$

Therefore, $\|\mathbf{G}\|_\infty$ gives the maximum possible gain in signal energy for sinusoidal inputs.
This is in contrast with the transfer function H_2-norm, defined as

$$\|\mathbf{G}\|_2 = \frac{1}{2\pi}\sqrt{\int_{-\infty}^{\infty} \mathrm{Tr}\left[\mathbf{G}^H(j\omega)\mathbf{G}(j\omega)\right]d\omega}\,, \tag{2.23}$$

which can be interpreted as the RMS output power of $\mathbf{y}$ ($\sqrt{E\{\mathbf{y}^T\mathbf{y}\}}$) where $\mathbf{y}$ is the response to a white noise input $\mathbf{u}$ with autocovariance matrix $E\{\mathbf{u}\mathbf{u}^T\} = \mathbf{I}$. The H_2-norm therefore measures RMS response to white noise.

The interpretation of the H_∞-norm as a maximum energy gain is particularly useful when one is interested in reducing the effects of uncertain disturbance signals $\mathbf{u}_w$. If $\mathbf{W}(s)$ is a weighting function (matrix) which is large over the frequency band to which $\mathbf{u}_w$ is known to be restricted to, then minimising $\|\mathbf{W}\mathbf{G}_{zw}\|_\infty$ is equivalent to minimising the maximum possible energy in the performance output over the set of all possible disturbances. In contrast to LQG-control, disturbances may be narrowband signals as well, which does away with the criticism that the representation of uncertain disturbances by white noise processes is unrealistic [84].
The true advantage of the H_∞ norm is that it is also significant when one is interested in reducing the effects of model uncertainty on closed-loop stability. To that aim, a general perturbation model is defined (figure 2.6) which represents model uncertainties as additional disturbance inputs. These additional disturbance inputs are determined by feeding back the outputs of $\tilde{\mathbf{G}}(s)$ through a Δ-block which satisfies $\|\Delta\|_\infty \leq 1$ (this may require to scale some of the out/inputs of the system model). This perturbation model is simple yet very general [86]. A necessary and sufficient condition for the closed-loop system $\tilde{\mathbf{G}} - \Delta$ to be stable with respect to all possible perturbations such that $\|\Delta\|_\infty \leq 1$ is that $\left\|\tilde{\mathbf{G}}\right\|_\infty \leq 1$. This conditions applies to SISO as well as MIMO systems.

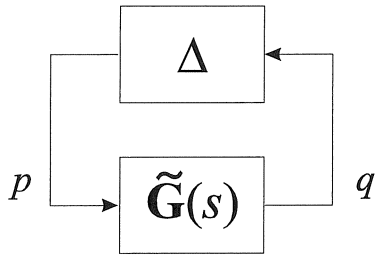

Figure 2.6. General perturbation model.

Though the first book on H_∞ control was published in 1987 [87], a real breakthrough was realised in 1988, with a publication which presented state space solutions for the synthesis of H_∞ controllers (first presented on American Control Conf., June 1988; IEEE paper in 1989 [88]). The H_∞ controller synthesis procedure has been reduced to solving two Riccati equations. Not only has this procedure been proven to be more computationally efficient, it also explicitly described how closely related H_∞ and LQG approaches are.

Despite its usefulness in view of the design of robust controllers, H_∞ control also has a few apparent disadvantages. First of all, the choice of weighting functions, with which performance and robustness bounds are specified, is crucial to the control performance achieved. Unfortunately, there are few general rules on how to select these and as a result optimal weightings are often only found after a lot of practice. Secondly, although it looks very convenient to characterise all possible plant perturbations by the perturbation model (figure 2.6), this formulation often allows far more perturbations than may actually occur. If, for example, the perturbations are caused by the variation of a single parameter which variation has an important effect on the loop gain, then it may be possible that these perturbations specify quite a large bound which allows many other perturbations. Including these bounds into the controller synthesis may easily render the controller to be very conservative. Specific tools, called μ-analysis, have therefore been developed which allow to specify *structured* uncertainty (such as the variation of one single parameter). For further detail, refer to [89] (an extensive tutorial introduction -90 references- to this subject).

As a matter of conclusion, it is important to stress the relevance of these modern robust control techniques in view of active control. As active

control is often aiming at controlling the response of high-order systems, model uncertainty is always an important issue, mainly because system models are constrained to be finite order. But also because the closed loop transfer functions may exhibit multiple cross-over points due to the presence of a large number of poles and zeros in the model, it is virtually impossible to deal with robustness using classical methods of control theory (e.g. based on ensuring phase and gain margin).
Furthermore, robust control design is a frequency domain technique. This is important from a practical point of view since the performance specifications can more directly be expressed as a function of the frequency content of the actual disturbance when the controller is designed in the frequency domain (as pointed out in the previous section, this also applies to LQG control).

2.2.5 Example : active control of duct noise

Introduction

In this section, an active control system for the reduction of duct noise is developed. The set-up, used in the experiments, is presented in figure 2.7. The duct noise is simulated by bandlimited white noise in the range 0 to 500 Hz, injected by a loudspeaker (the disturbance speaker) into the duct. The control source is a secondary loudspeaker, located near the end of the duct.
So far, this corresponds to the classical active control configurations set up for the control of duct noise [90] employing a reference sensor (a microphone mounted "upstream" with respect to the control source) and a feedforward control strategy to determine the control signal. In this example, however, a feedback controller is developed to control the sound field in the duct. Two control configurations are tested. In both cases the performance output $\mathbf{z}$ and the feedback output $\mathbf{y}$ of the system are not co-located. In each case, one of the microphones serves as a feedback microphone, and the other as a monitor microphone to measure the control performance. With this example it is illustrated that, when properly configured, feedback control may yield satisfying control performance even in systems where responses are subject to acoustic delays. Secondly, the example allows to clearly illustrate the design trade-offs that must be considered in the design of a controller with a state observer.

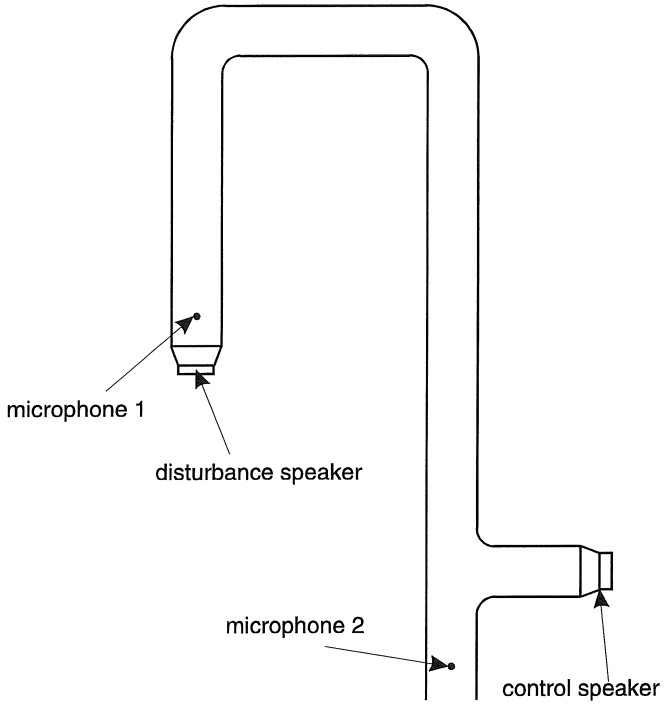

Figure 2.7. Experimental set-up for the active control of duct noise.

The results achieved in this application are put in a broader perspective in paragraph 2.4.2 where the apparent equivalence between feedback and feedforward controllers is pointed out.
Extensive treatment of this application can be found in [91].

Problem statement and short literature survey

Active control of duct noise has been the subject of much attention, since successful duct silencing has a commercial potential [92]. The application area ranges from automobile exhaust systems, HVAC systems (Heat, Ventilation and Air Conditioning) to large industrial systems such as chemical scrubbers to clean process air before exhausting to the outside atmosphere. Hence, the serach for successful noise control systems is well motivated. Moreover, duct systems can mostly be described by relatively simple one-dimensional models which presents an opportunity for low order -and thus cost effective- active control systems.

A state space feedback controller, designed by means of pole placement, for the reduction of duct noise has been presented by Hull *et al.* [93]. The dynamic behaviour of the duct is described by a state space model which is based on a modal decomposition of the acoustic response of the duct. By carefully placing the poles of the closed-loop systems, the authors show they have control over the modes of the system. As a result, overall noise reduction is achieved in the duct. This result contrasts with the often applied strategy of reducing the noise level at the duct outlet only, an approach which may easily increase the noise levels elsewhere in the duct.
State feedback is also employed by Bai *et al.* [94], who have used LQ control theory for the design of the controller. The controller is in essence an *Independent Modal Space Controller.* In order to satisfy the controllability and observability requirements associated with the latter approach, the authors used 4 loudspeakers and 4 feedback microphones in their numerical simulations.
Nonami *et al.* [95] used H_∞ control theory in the development of their feedback controller for the reduction of duct noise. The choice of the appropriate weighting functions for the design of the H_∞ controller is discussed. Experimental results are presented showing significant reduction of the noise levels at the error microphone. It should be noted that the control results achieved here do not guarantee overall noise reduction in the duct (this is not analysed in [95]).
H_∞ control theory is also the basis of the hybrid feedforward/feedback controller presented in [96]. The authors recognise that H_∞ design tools may easily produce a controller which is too conservative (refer to paragraph 2.2.4). They resolve this problem by using Quantitative Feedback Theory to further improve the control performance by sequential tuning of the feedback and feedforward control filters based on experimental data.
In this work, an LQG controller with estimator (referred to as the observer/controller) is designed and implemented on a duct. The experiments highlight the importance of an appropriate hard- and software configuration in order to recover the properties of the full-state feedback controller.

State space model for a lightly damped cavity

A state space model (eq. 2.5) for the standard control configuration (figure 2.5) can be obtained in different ways. As will be shown in the following sections, it is important to optimise the location of the feedback sensor in

order to maximise the control performance. This involves the generation of a range of different system models for each new sensor configuration. When the system model is obtained from identification of experimentally acquired input/output transfer functions, this is a very time consuming work. From that perspective, it might be useful to first generate an acoustic finite element model of the system, which characterises the sound field as a whole (simple systems such as a duct do not need FEM, but can be modelled analytically). Each finite element node provides a possible input or output location. After truncation into its low frequency modes the finite element model can be turned into a state space model, the time inputs and outputs being physical quantities such as flows or pressures.
However, when it comes to implementing the controller in real-time, the operational acoustical modes need to be identified experimentally as it is virtually impossible to properly model the boundary conditions in FE code (not to the accuracy necessary for control synthesis). This is particularly true for a lightly damped cavity, such as the duct considered here, which acoustic response exhibits sharp resonances such that the associated resonance frequency should be determined exactly in order to avoid large errors. Furthermore, it is important to take into account the dynamics of the control loudspeaker (i.e. complement the acoustic model with a loudspeaker model). Hence, there is an interplay between the two modelling techniques. Finite element models are useful to roughly optimise the control source and sensor locations, while an identification phase is essential to guarantee model accuracy for controller synthesis.

Optimisation of the control parameters in the presence of acoustic time delays

For the experiments, an LQG controller with Kalman state observer (refer to paragraph 2.2.3) will be designed. A "benchmark" will be set by designing a full-state feedback controller using identical weighting matrices in the LQG objective function. Thus, the performance of the observer/controller can be compared -at least on simulations- with the ideal situation.
The performance of the observer/controller is largely determined by the dynamics of the observer. The state observer should be able to track state changes caused by disturbances, this within the frequency range of the state feedback control operation. The speed at which the system states respond to changes in the disturbance is given by the controller eigenvalues of the matrix $\mathbf{A}-\mathbf{B}_2 \cdot \mathbf{K}$. The estimation process should at least be as fast as the controller eigenvalues. Eigenvalues added by the estimator should not

interfere with the dynamics of the state feedback. This is not easily realised in the case of high bandwidth digital control systems. When talking about low frequency acoustic control, bandwidth may reach up to several hundred Hertz. With the observer eigenvalues conventionally chosen five times faster than the controller bandwidth, the required sampling rate becomes often too high. Furthermore, a very fast observer will be very sensitive to measurement noise (in fact, the observer will "see" measurement noise as actual state changes). An alternative to reducing control bandwidth, is to allow observer poles to interfere with state feedback dynamics, adding a small phase lag to the estimation process.

There is however another important effect showing up when closing the feedback loop by means of a state estimator. The physical phase lag due to acoustic wave propagation between the disturbance entering the duct and the feedback microphone measurement also causes reduced performance. Remark that this phase lag is not a pure time delay which affects the states of the system (if that would be the case, the system would be non-linear). The system states respond immediately to acoustic excitations. The phase lag between these state changes and the system response measured at the output is determined by the specific pole-zero combinations which correspond to the transfer function of the considered input-output configuration. When the output (the feedback microphone) of the system is located near the input (disturbance source), the acoustic delay will be virtually non-existent. While the poles of the transfer function corresponding to a remote microphone location (remote with respect to the disturbance source) will be exactly the same, the phase lag perceived at the remote location will be larger due to the fact that the pole-zero combination is different.

The acoustic time delay forms a physical limitation of the input/output configuration of the control system, which cannot be influenced by the control design itself. No matter the location of controller-observer poles, the physical delay will always remain. In [91], a numerical simulation is presented showing the influence of both effects on the performance of an LQG controller reducing the sound pressure in a specific zone (the **z**-output of the system) of a rectangular cavity ($5 \times 7 \times 3$ m). The disturbance source was located in a corner. In a first instance, the feedback sensor, which was not co-located with **z**, was located in the opposite corner. In this configuration, the control performance of the full-state feedback controller could not be realised with the observer/controller, even if the observer dynamics were speed up to unrealistic levels. However, when moving the feedback sensor closer to the disturbance source, the full-state feedback

control performance could be approximated. Thus it was shown that the performance loss due to the acoustical delay can be minimised by locating the feedback sensor as close as possible to the disturbance source. Note that the separation between control source and the target zone (where sound pressure must be reduced) has an influence on control performance as well. However, the observation that the the performance can partly be optimised by locating the feedback sensor such that it serves as a noise observer, can be put in a larger perspective (refer to paragraph 2.4.2)

Experiments

Figure 2.8 plots the measured (solid) and identified (dashed) frequency response functions between the microphone output voltages and loudspeaker input voltages of the test set-up presented in figure 2.7.

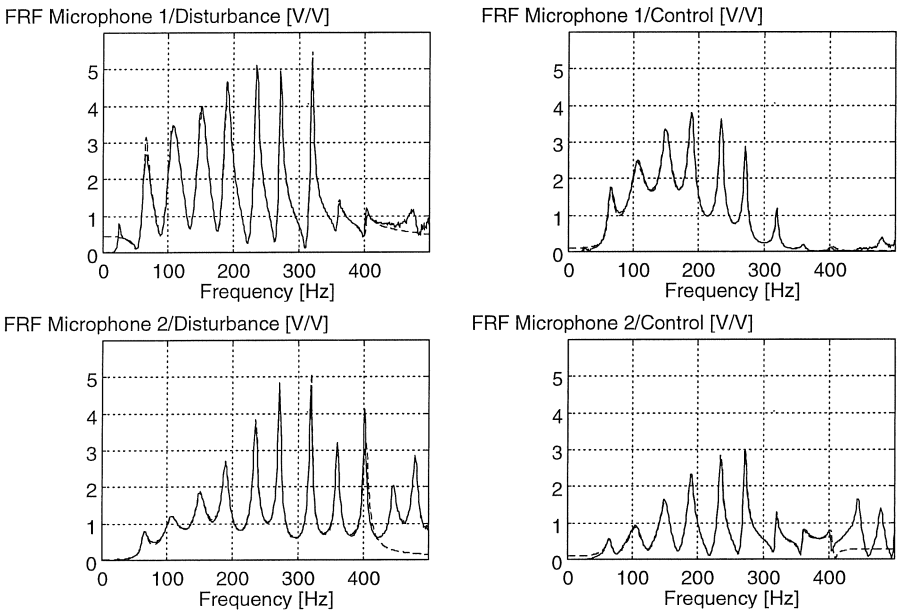

Figure 2.8. Identification results of the acoustic response of the duct.

The controller was synthesised based upon the identified model and implemented on a TMS320C40 DSP board which was hosted in a PC. The sample frequency was 2500 Hz. Even when the system model has been identified accurately in the frequency band of interest, two problems arise when a reduced order controller is used to control a system with, in theory, an infinite number of modes, namely : *control spillover* and *observation*

spillover. Control spillover refers to the phenomenon where control energy spills over into the residual (higher-order) modes which were not considered in the model which was used for the design of the controller. This occurs when the control input is not orthogonal with the residual modes. Observer spillover occurs when the measured system response contains contributions of residual modes. The important difference between control spillover and observation spillover is that control spillover cannot destabilise the controlled system, although it may degrade control performance, whereas observation spillover can produce instability in the residual modes ([97], pp. 327 - 328).
Control methods to avoid spillover have been presented (*Independent Modal Space Control*, IMSC, [98]) but these imply the use of a number of control actuators equal to the number of modes to be controlled -to avoid control spillover- and a large set of measurement sensors so that the modelled modes can be estimated without much error -to avoid observer spillover. In this application, a more pragmatic approach is presented. From the observer point of view, unmodelled modes appear as an additional noise component. The measures to be taken for avoiding spillover can therefore be similar to those for avoiding measurement noise. An anti-spillover filter added to the control loop reduces the spillover effect. The anti-spillover filter can be implemented either at the measurement or at the control side. Implementation at the measurement side is preferable, since the filter can then serve as anti-aliasing filter too. In the experiments a fourth order Butterworth anti-spillover filter is used, implemented at the measurement side. The anti-spillover filter adds frequency dependent phase lag to the control loop. In order for this phase lag not to interfere with the state feedback control action, the cut-off frequency of the anti-spillover filter as well as its order should be chosen carefully in order to establish a compromise between spillover reduction and added phase lag to the control loop. This is illustrated by the experiments described below.

Two control configurations have been compared. In the first configuration, microphone 2 serves as the feedback sensor, while microphone 1 monitors the target zone (where sound pressure should be reduced). In the second configuration, microphone 1 is the feedback sensor, while microphone 2 is the monitor microphone at the target zone. Although duct noise should primarily be reduced at the outlet, the first control configuration is treated here because it is relevant from a control point of view.
Control design for the first configuration is based on a reduced order model taking into account the five acoustic modes in the range 50-250 Hz. The

design of the controller is basically a two-stage process. In the first stage the weighting matrices $\mathbf{Q}_{ctr}$ and $\mathbf{R}_{ctr}$ of (2.9) are determined. Diagonal weighting matrices were chosen, such that they could be represented by $\mathbf{Q}_{ctr} = q \cdot \mathbf{I}$ and $\mathbf{R}_{ctr} = r \cdot \mathbf{I}$, where q and r are scalars. By increasing the ratio q/r, the performance of the controller can be increased until the limit of maximum allowable control energy is exceeded. This limit was determined based on a simplified model for the control loudspeaker and its amplifier, as explained in [91]. The control energy used by the controller and the corresponding control performance was simulated for the full-state feedback case. Secondly, $\mathbf{Q}_{est}$ and $\mathbf{R}_{est}$ of the observer (a Kalman filter, refer to paragraph 2.2.3) are determined in a similar way. By increasing the ratio of process noise variance $\mathbf{Q}_{est}$ over measurement noise $\mathbf{R}_{est}$, the observer is made faster. The limation which is encountered here is the occurrence of observer spillover. As shown in figure 2.9, only very limited noise reduction could be achieved at the modelled modes. This is explained by the fact that this configuration is subject to a large acoustic time delay, which seriously reduces the control performance of the controller with observer with respect to the full-state feedback controller. Furthermore, due to the effect of observation spillover, the sixth and seventh modes, which lie outside the frequency range of the design model, are amplified.

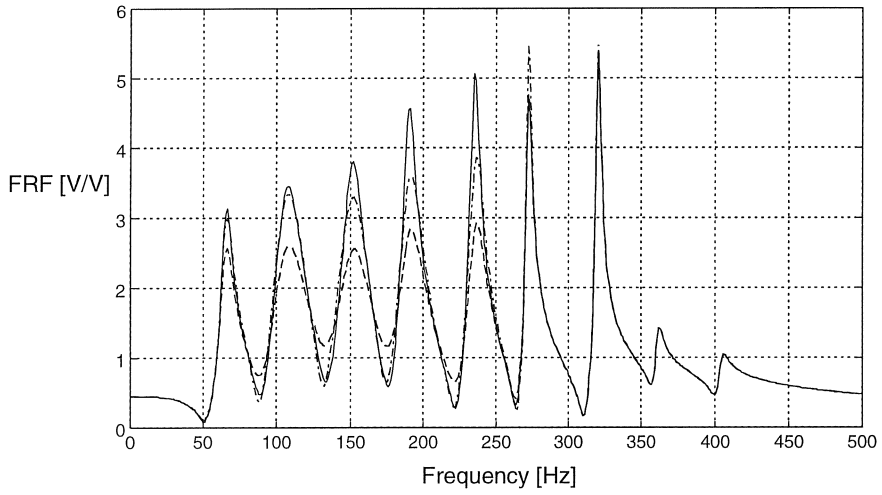

Figure 2.9 : Simulation results at the target location for the first configuration. (open loop response in solid line, full-state feedback in dashed line, and observer/controller in dash-dotted line)

The latter effect could have been predicted when looking at the responses from figure 2.8, which shows that the unmodelled sixth and seventh mode contribute significantly to the acoustic response at microphone 2. In order to reduce the effect of observer spillover, the cut-off frequency from the anti-spillover filter had to be set to approximately 60 Hz for the experiments. This adds a substantial phase lag to the model in the control bandwidth aimed at. Due to this phase lag, performance is very limited. The acoustic time delay together with the sensitivity to spillover yields poor results for the first configuration both on simulation and in the experiments (figure 2.10) which yield exactly the same result (compare figure 2.10 to figure 2.9).

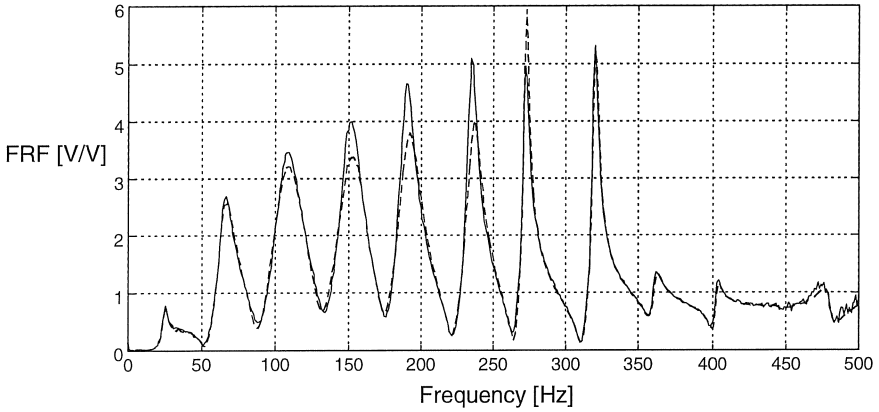

Figure 2.10 : Experimental results at the target location for the first configuration. (open loop response in solid line, closed loop response of observer/controller in dashed)

In the second control configuration, microphone 1 is used as feedback microphone. The responses presented in figure 2.8, show that beyond the seventh mode, a few modes have a node which is located close to the feedback sensor location. Thus, by including modes six and seven in the design model, a configuration can be obtained which is relatively insensitive to observation spillover. The acoustic system itself physically acts as an anti-spillover filter. Figure 2.11 shows the simulation results obtained for the second control configuration, with modes six and seven included in the design model. Because of the small contribution of higher order modes in the measurement, the cut-off frequency of the anti-spillover filter could be chosen near 300 Hz.

Moreover, there is almost no acoustic time delay between disturbance source and feedback location such that using an observer did not

significantly reduce control performance with respect to state feedback (compare figure 2.9 to figure 2.11).

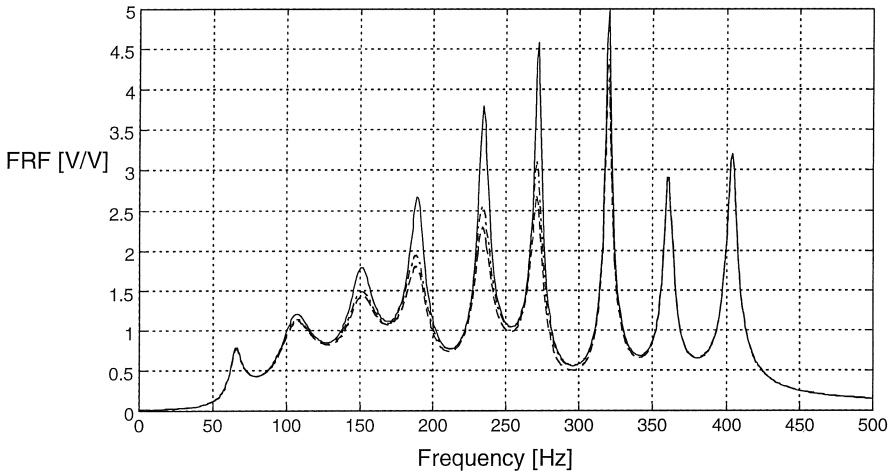

Figure 2.11 : Simulation results at the target location for the second configuration. (open loop response in solid line, full-state feedback in dashed line, and observer/controller in dash-dotted line)

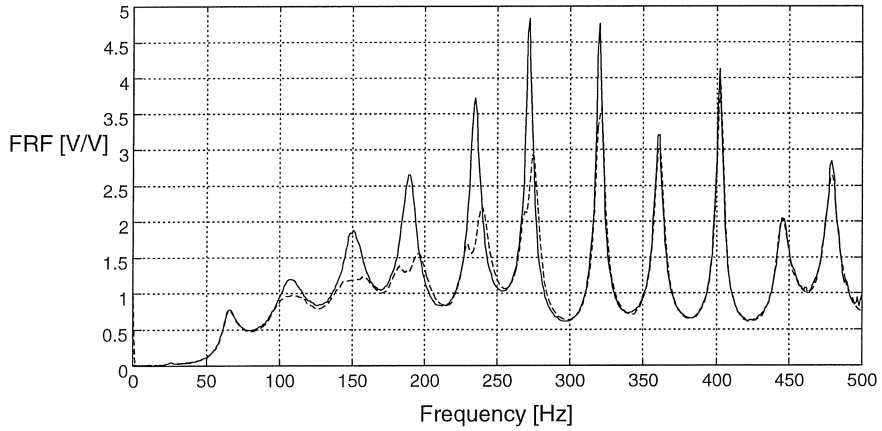

Figure 2.12 : Experimental results at the target location for the second configuration. (open loop response in solid line, closed loop response of observer/controller in dashed)

In simulation, it was possible to approximate the state feedback control performance by speeding up the estimator. However, it was impossible to implement this observer/controller in practice as the estimator speed is

limited by a measurement noise constraint (the controller saturated even without a primary disturbance). Therefore, in the experiments, the observer was tuned to be as fast as possible without amplifying measurement noise. Figure 2.12 shows the corresponding experimental results (they differ from the simulation results of figure 2.11).

Conclusions

This section discusses the design of a state feedback controller to actively control the sound field in a duct. The simulation results and the experimental results reveal some interesting issues that must be taken into account in the design of the control configuration and the state observer. The results achieved in this application will be put in a broader perspective in paragraph 2.4.2.

2.3 FEEDFORWARD

2.3.1 A general feedforward control configuration

The block diagram of a general feedforward control regulator (figure 2.13) is straightforward[6]. The vector $\mathbf{d}(k)$ denotes the *disturbances*, i.e. the system responses that we want to suppress. In feedforward control, it is explicitely assumed that a set of *reference signals* $\mathbf{x}(k)$ can be measured which are correlated with the disturbances (it will be shown later-on that the assumption of correlation is essential). The references are thus assumed to describe the *disturbance sources* which cause the disturbances $\mathbf{d}(k)$. The feedforward control approach then consists of processing the references, in order to generate a *control signal* $\mathbf{y}(k)$ with which the response of the system is controlled.
In linear control theory, the control action comes down to adding the control signal to the disturbances $\mathbf{d}(k)$. The role of the reference signal is to provide a measure of the spectral content of the disturbances. The exact phase and

[6]Note that this development is presented in the discrete time immediately, for reasons explained later-on.

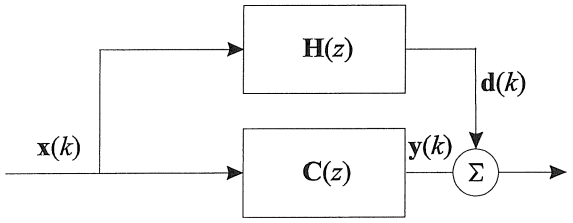

Figure 2.13. Block diagram of a general feedforward control configuration. The *reference* $\mathbf{x}(k)$ is processed by the controller $\mathbf{C}(z)$ which yields the *control signal* $\mathbf{y}(k)$. Interference of $\mathbf{y}(k)$ with the *disturbances* $\mathbf{d}(k)$ is aimed at suppression of the latter.

magnitude information of $\mathbf{d}(k)$, however, is determined by the dynamic properties of the system which is subjected to the disturbance sources. In linear control theory, this relation is expressed as $\mathbf{d}(k)$ being the response of the system, represented by its transfer function $\mathbf{H}(z)$, to the reference signal (which was assumed to describe the disturbance sources). The feedforward controller $\mathbf{C}(z)$ is then determined such that it realises the appropriate phase and magnitude relation between the reference and the control signal which yields maximum suppression.

Applying this to the active isolation problem (figure 2.3), the variable that we want to suppress is the force applied by the passive mount to the equipment. An evident reference signal is the acceleration measured at the work floor. The controller $\mathbf{C}(z)$, which comprises the dynamics of the actuator used, is then supposed to realise the right counteracting force which cancels out the disturbance force.

An obvious choice for the controller transfer function $\mathbf{C}(z)$ is to be exactly equal to the system transfer function $\mathbf{H}(z)$ as $\mathbf{y}(k)$ would then be exactly equal to $\mathbf{d}(k)$ at any time instance (perfect cancellation is then achieved by inversion of the sign). This transfer function could be determined off-line. This controller will be referred to as the LTI (linear time invariant) feedforward controller.

There are a lot of very good reasons why this will often not work in practice. For example, as $\mathbf{C}(z)$ comprises the actuator dynamics, these dynamics will need to be exactly compensated internally if $\mathbf{C}(z)$ needs to perfectly match $\mathbf{H}(z)$. This is often not possible. Furthermore, in practice, variation of $\mathbf{H}(z)$ is very likely to happen : not only will this occur when some of the system parameters are subject to ageing phenomena, it is also possible that the coupling of the disturbance sources to the actual disturbances $\mathbf{d}(k)$ changes with time. In the simple active isolation problem, for example, the latter would occur when due to some reason an additional transfer path is created

between the work floor and the equipment. $\mathbf{H}(z)$ would then change from a SISO to a single input-two output system ; which is a substantial difference. In contrast to feedback control, the performance of a feedforward controller which is designed off-line, will be very sensitive to the slightest changes in $\mathbf{H}(z)$ as these changes require identical changes to be applied to $\mathbf{C}(z)$ (even if we suppose that the actuator dynamics can exactly be compensated). As these changes in $\mathbf{H}(z)$ would not be measured through the reference, it is necessary to augment the control configuration with a measure of the system response.
A general *adaptive* feedforward control configuration is depicted in figure 2.14. The error sensor signal $\mathbf{e}(k)$ is used to update the controller to cope with variation of the disturbance sources. The controller update process is performed iteratively. Since this process is most easily implemented on DSPs, this section is focusing on discrete-time realisations of feedforward controllers. The following paragraph gives an overview of different approaches to the iterative optimisation of the feedforward control parameters.

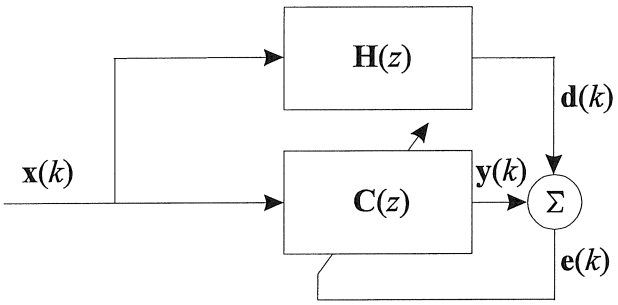

Figure 2.14. Block diagram of an adaptive feedforward controller. The *error* $\mathbf{e}(k)$ is used to iteratively optimise the parameters of the controller.

2.3.2 Adaptive optimisation of feedforward control parameters

The basic configuration which is considered for the discussion of the adaptive algorithms is depicted in figure 2.15. The aim of the adaptive process is to find the most optimal controller transfer function $\mathbf{C}(z)$. This transfer function is, in its most general form, described by a rational expression, for the SISO case given by (2.24)

$$C(z) = \frac{\sum_{k=0}^{n} b_k z^{-k}}{1 + \sum_{l=1}^{m} a_l z^{-l}}. \qquad (2.24)$$

The feedforward control parameters can thus be comprised within one parameter vector θ, defined as $\theta = [-a_1, \ldots, -a_m, b_1, \ldots, b_n]^T$. Defining a vector $\varphi(k) = [y(k-1), \ldots, y(k-m), x(k), \ldots, x(k-n)]^T$, which denotes the generalised reference signal of the feedforward controller, then the control output is determined as $y(k) = \varphi^T(k) \cdot \theta$. For multiple, say P, references, there is one control filter per reference, such that $y(k) = \varphi_1^T(k) \cdot \theta_1 + \varphi_2^T(k) \cdot \theta_2 + \ldots + \varphi_P^T(k) \cdot \theta_P = \varphi^T(k) \cdot \theta$. If the controller has multiple, say M outputs, θ and $\varphi(k)$ are matrices with M columns and the controller output relation is obtained as a matrix product : $\mathbf{y}(k) = \varphi^T(k) \cdot \theta$.

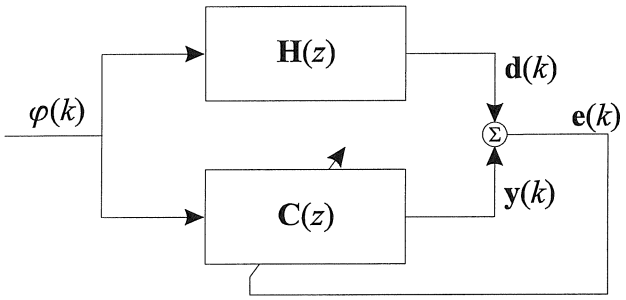

Figure 2.15. Basic scheme used for the development of the theory of adaptive feedforward controllers. A generalised reference signal is used.

The optimal controller is then determined as the parameter vector which optimises the following cost function in a least squares sense (the so-called Wiener-Hopf optimal filter) :

$$J(\theta) = E\{\mathbf{e}^T(k)\mathbf{e}(k)\} = E\{(\mathbf{d}(k) - \varphi^T(k) \cdot \theta)^T (\mathbf{d}(k) - \varphi^T(k) \cdot \theta)\}. \qquad (2.25)$$

The optimum of the cost function is determined by

$$\theta^{opt} = \mathbf{R}^{-1} \cdot \mathbf{P}, \qquad (2.26)$$

where $\mathbf{R} = E\{\varphi(k)\varphi^T(k)\}$ is the so-called input auto-correlation matrix, and

$\mathbf{P} = E\{\varphi(k)\mathbf{d}^T(k)\}$ is the cross-correlation matrix.

The optimum is defined if $\mathbf{R}$ is non-singular. If $\mathbf{R}$ is positive definite, then the optimum is a global and unique minimum.

This least squares approach assumes perfect knowledge of the correlation matrices and non-singularity of $\mathbf{R}$ to assure invertibility. The latter condition is referred to in signal theory as the *persistent excitation* requirement [99] [100]. Expression (2.26) does not directly lend itself to implementation in real-time such that recursive algorithms have been developed to iteratively determine the optimal control filter.

Recursive Least Squares (RLS) algorithms

A simple approach is to recursively determine $\mathbf{R}$ and $\mathbf{P}$ as in (2.27)

$$\begin{aligned}\mathbf{R}(k) &= \lambda(k)\mathbf{R}(k-1) + \varphi(k)\varphi^T(k),\\ \mathbf{P}(k) &= \lambda(k)\mathbf{P}(k-1) + \varphi(k)\mathbf{y}(k)\end{aligned} \tag{2.27}$$

after which a new estimate of the parameter vector, $\hat{\theta}(k)$, is determined by :

$$\hat{\theta}(k) = \hat{\theta}(k-1) + \mathbf{R}^{-1}(k)\varphi(k)\left(\mathbf{y}(k) - \varphi^T(k)\hat{\theta}(k-1)\right). \tag{2.28}$$

The weighting factor $\lambda(k)$ allows to weight the incoming information as a function of time. In case of non-stationary processes, this allows to track a time-varying optimal parameter vector (use small weighting) ; for stationary processes $\lambda(k) = 1$.

As the matrix inversion implies $O(N^3)$ calculations (N is the control filter order), real-time implementation of (2.28) is still not very realistic. The Sherman-Morrison identity is therefore used to recursively calculate the inverse of $\mathbf{R}$ [99] [100], such that the least squares optimal control filter is then recursively calculated as :

$$\kappa(k) = \frac{\mathbf{R}^{-1}(k-1)\varphi(k)}{\lambda(k) + \varphi^T(k)\mathbf{R}^{-1}(k-1)\varphi(k)} \tag{2.29a}$$

$$\mathbf{R}^{-1}(k) = \frac{1}{\lambda(k)}\left(\mathbf{R}^{-1}(k-1) - \kappa(k)\varphi^T(k)\mathbf{R}^{-1}(k-1)\right) \tag{2.29b}$$

$$\hat{\theta}(k) = \hat{\theta}(k-1) + \kappa(k)\left(\mathbf{y}(k) - \varphi^T(k)\hat{\theta}(k-1)\right). \tag{2.29c}$$

Expression (2.29) is generally denoted as the *Recursive Least Squares* (*RLS*) algorithm. Note that the algorithm requires an initial estimate for $\mathbf{R}^{-1}$ at the start of the recursion.

Though the number of calculations has been reduced to $O(N^2)$ by invoking the Sherman-Morrison identity, *Fast Recursive Least Squares* (*FRLS*) algorithms have been developed which further reduce the computational burden. (Note that the attribute "fast" denotes the computational efficiency of the algorithm, rather than the convergence speed). Ljung, Morf and Falconer have presented an algorithm [101] which makes use of the symmetry of the input auto-correlation matrix which yields an algorithm with a complexity $O(8N)$. This algorithm was one of the first efficient parameter estimator schemes and is, due to its analogy with the Kalman filter [102] generally denoted as the *Fast Kalman Filter* algorithm. Other versions of the FRLS algorithm have been developed since then. Among the fastest are : the *Fast A priori Error Sequential Technique* (*FEAST*) algorithm [103] with a complexity $O(5N)$, the *Fast Transversal Filter* (*FTF*) [104] which was presented shortly after and which has a complexity $O(6N)$. The *normalised FTF* with a complexity $O(5N)$ can be proven to be equivalent to the FEAST algorithm [100].

The iterative algorithms described above have one key feature in common, namely they are all aiming to recursively calculate $\mathbf{R}^{-1}$. As knowledge of this inverse matrix allows to calculate the exact Wiener-Hopf optimum, these algorithms are referred to as "exact" algorithms [105]. There is, unfortunately, another common characteristic in the behaviour of these algorithms, namely, they are very susceptible to divergence due to numerical instability [100] [105] [106, app. E]. This is basically due to the fact that these algorithms try to determine the inverse of a matrix, which obviously does not exist when that matrix is singular. Therefore the stability of these algorithms is largely determined by the nature of the input signals. As mentioned before, RLS-like algorithms will suffer from instability as when the process is not *persistently exciting*. (A related problem is the fact that even for persistent excitations, the correlation matrix is not always

guaranteed to be positive definite). Another important source of divergence is numerical instability due to round-off errors. This is certainly true for the FRLS algorithms, of which the vast reductions in complexity are often connected with many inner recursions yielding a great risk of numerical instability due to finite precision effects (a relation between the occurrence of instability and the round-off error has been proven for the FTF-algorithm in [107]). Measures which are necessary to cope with this problem increase the complexity again. E.g., the most advanced method, SFEAST (*stabilized FEAST*) has a complexity of $O(8N)$.

Gradient search algorithms

One way to avoid the computationally "expensive" matrix inversion is to iteratively search the optimum of the cost function by moving over the cost function surface in the inverse direction of the gradient. This yields a so-called *steepest descent* algorithm. The exact gradient can easily be determined by taking the first derivative with respect to the parameter vector of (2.25). This leads to an iterative expression for the estimate of the parameter vector, $\hat{\theta}(k)$:

$$\hat{\theta}(k) = \hat{\theta}(k-1) + 2\mu\left(\mathbf{P} - \mathbf{R}\hat{\theta}(k-1)\right), \tag{2.30}$$

in which μ is the convergence coefficient, with which the step size along the gradient can be set. As will be shown later-on, the choice of μ is very important as it has implications both on the convergence speed and the stability of the update process.

A simpler approach is to approximate the exact gradient with the instantaneous instead of the exact gradient, which does not require knowledge of the correlation matrices and thus can easily be determined at each time instance. The instantaneous gradient is determined by taking the first derivative of (2.25) where the expectation operator is omitted. After some simple algebra this yields an update rule :

$$\hat{\theta}(k) = \hat{\theta}(k-1) + \mu\mathbf{e}(k)\varphi(k)\,. \tag{2.31}$$

This algorithm, which was presented first by Widrow and Hoff in 1960, is called the *Least Mean Square* (*LMS*) algorithm [108]. The behaviour of the algorithm has been analysed extensively in literature. The topic which has attracted most attention are the convergence properties of the algorithm.

This is an important issue as the main difference between LMS and RLS algorithms lies in the fact that as soon as convergence of the RLS algorithm is assured, it converges to the optimum (2.26) because this solution is recursively calculated. This is not necessarily true for gradient-search algorithms like the LMS algorithm. However, it was proved that if the convergence coefficient was chosen such that $0 < \mu < \frac{1}{tr(\mathbf{R})}$, then the adaptive filter coefficients will relax from their initial condition to the Wiener-Hopf solution (this was proved for convergence of the mean as well as for convergence of the variance [109]). Proving convergence with certain correlated and non-stationarity inputs is intricate. A rigorous mathematical treatment is provided for the LMS algorithm in [110].

The LMS algorithm is very computationally efficient with a complexity of $O(2N)$ but is often associated with slow convergence rates when the inputs are strongly correlated (in space and time), a problem which will be discussed later-on. Other gradient-based algorithms have been developed which aim at improving the convergence rate of the LMS-algorithm. Boucher *et al.* [111], present an extension of the multiple error LMS algorithm which provides range of algorithms ranging from Newton's algorithm [108] at one extreme (fastest convergence) to the LMS algorithm at the other. Also the *Fast Quasi Newton* (*FQN*) algorithm [112], is aiming at reducing the influence of the input signal statistics on the convergence rate.

Remarks

- A more general expression for a cost function that is to be optimised by the controller is a cost function which takes into account the control energy used to achieve the control objective. Expression (2.25) then extends to

$$J(\boldsymbol{\theta}) = E\left\{\mathbf{e}^T(k)\mathbf{e}(k) + \beta\mathbf{y}^T(k)\mathbf{y}(k)\right\}, \tag{2.32}$$

  in which β is the control effort weighting factor.
  The use of this type of cost function for the gradient-based LMS algorithm leads to the *Leaky LMS* algorithm [108] which is in fact equal to the LMS algorithm except for the fact that a leakage factor is introduced in the update formula such that the control filter coefficients tend to decay ("leak") to zero if the errors were to go to zero. As long as the errors are not zero, the leakage factor will partly compensate the

continuous increase of the control filter coefficients due to the second term of the update equation (2.31) and hence prevents saturation of the control signal.

- An important remark pertains to the control configuration which has been used as a basis in this paragraph (figure 2.15). This configuration assumes that the output of the adaptive controller is directly added to the disturbance $\mathbf{d}(k)$. In practice, this is rarely the case. A more realistic configuration is presented in figure 2.16. In this configuration, the output of the controller is applied to a system $\mathbf{S}(z)$ (the so-called *secondary path*) of which the output, $\mathbf{z}(k)$ is then added to the disturbances. This represents the more realistic case where $\mathbf{y}(k)$ is the output (voltage) of a digital controller, and where $\mathbf{S}(z)$ represents the dynamics of the control source (including power amplifier) and the way it couples to the system to be controlled. This configuration has the consequence that the cost function surface, and hence the optimum and the gradient to the cost function, are substantially different from the previous case. Thus the characteristics of $\mathbf{S}(z)$ need to be taken into account in the update rule. In [108], it is shown that this can be achieved by filtering the reference signal with a model of the secondary path before using it in the update rule (2.31), which yields the well-known *Filtered-X LMS* algorithm. It is important, however, to note that the development of the Filtered-X LMS algorithm is based on the assumption of system linearity and time invariance. Though adaptive controllers are not linear [108] and per definition varying with time, it has been shown (see, e.g. [68] p. 66) that bounds can be determined for the convergence coefficient which assure convergence to the optimal solution. These bounds are determined by *(i)* the power in the input signals and *(ii)* the delays occurring in the secondary paths.

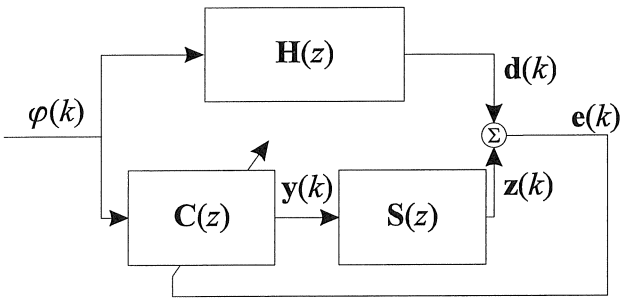

Figure 2.16. Adaptive feedforward controller with secondary path S(*z*).

- In this overview, it has been stressed that the application of RLS or FRLS algorithms is not always straightforward due to numerical instabilities which are likely to occur. The RLS algorithm has the additional disadvantage that its tracking performance in non-stationary circumstances is often very poor [100] [113]. Another disadvantage associated with the RLS or FRLS algorithms, apart from their inherent computational complexity, is the complexity of the mathematical expressions describing the algorithms. Due to the fact that the Filtered-X LMS algorithm is simple, efficient, and yet often offers very satisfying performance, it is not surprising that this algorithm is most widely used for adaptive feedforward control of vibration and sound, or even for active control in general (refer to proceedings of *First and Second Conference on Recent Advances in Active Control of Sound and Vibration, ACTIVE 95, ACTIVE 97,...*). Therefore, this algorithm is discussed in somewhat more detail in the following paragraph.

2.3.3 The Filtered-X LMS adaptive feedforward control algorithm

General form

The term Filtered-X LMS is in general limited to applications where the controller is represented by *Finite Impulse Response* (*FIR*) filters. In contrast to *IIR* (*Infinite Impulse Response*) filters, FIR filters are system transfer functions with no poles and only zeros. The FIR filter is represented by a transfer function (2.24) which has no numerator. IIR filters have both poles and zeros which allows to exactly match poles as well as zeros of physical systems whereas FIR filters can only give a rough approximation of the poles. An adaptive algorithm for IIR filters was developed by Eriksson [114] which adapts the filter coefficients in a similar way as the LMS algorithm. This algorithm is known as the *Recursive Least Mean Squares* (*RLMS*) algorithm. This algorithm has been extended to compensate for the effect of the secondary path to form the *Filtered-U RLMS* algorithm [115]. This type of algorithm is especially useful in the presence of feedback paths between the control output and the reference signals. Compensation of these feedback paths is essential as these may easily destabilise the control system. The ability of IIR filters to represent poles is particularly suitable for the compensation of these feedback effects since the feedback effects can be shown to introduce poles into the optimal controller transfer function [116].

Though they have been shown to yield better performance in some applications, IIR filters are not so common as FIR filters in active control applications because of *(i)* the higher computational complexity, *(ii)* the fact that the cost function for IIR filters is not guaranteed to have a unique and global minimum, and *(iii)* stability considerations. The latter relates to the fact that the adaptive process, when it is not closely monitored, may evolve to (or through) a parameter set which represent an IIR control filter with poles outside the unit circle. Measures have been developed to avoid this (e.g. the Schur-Cohn algorithm, [117] p. 214), but result in a strong increase of the computational complexity because they require to monitor and eventually stabilise the poles of the IIR filter at each update. Another problem associated with the use of IIR filters lies in the convergence properties of the Filtered-U RLMS algorithm. First of all, IIR adaptive algorithms can have a relatively slow convergence rate in comparison with FIR filters. The optimal solution can be extremely ill-conditioned if a large number of control coefficients are used, in which case there is a very large set of nearly optimal solutions around which the adaptation algorithm will drift. Secondly it is often claimed that the theoretical background (e.g. concerning the convergence properties) for adaptive IIR filters is not yet well established such that their successful application is strongly dependent on knowing the right "tricks" to make them work. The truth is that rigorous mathematical treatment of the behaviour of adaptive IIR filters requires a strong theoretical background (although in [118], an attempt is made to present a comprehensive theory of adaptive IIR filters).
The additional complications associated with using IIR filters therefore imply that their use is only justified in applications where the optimal controller transfer function is very lightly damped which would require too large a FIR filter order to correctly model its impulse response. This paragraph therefore concentrates on the Filtered-X LMS algorithm using FIR secondary path filters and FIR control filters. Figure 2.17 presents a block diagram of the Filtered-X adaptive feedforward control scheme.

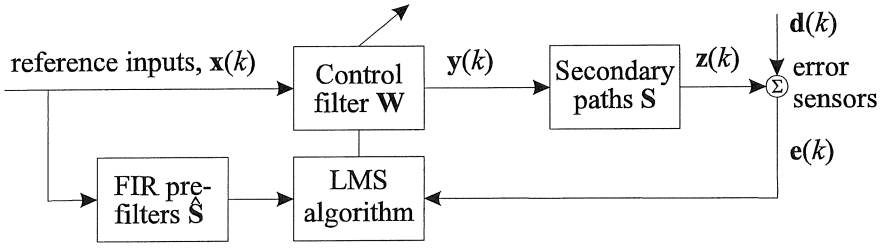

Figure 2.17. Filtered-X LMS adaptive feedforward control scheme.

Assuming a control system with N control sources, M error sensors and P reference sensors, the sound pressure measured at M error sensors can be expressed as :

$$\mathbf{e}(k) = \mathbf{d}(k) - \mathbf{z}(k) = \mathbf{d}(k) - \mathbf{X}^{\mathbf{f}}(k)^T \mathbf{w}(k) \tag{2.33}$$

where $\mathbf{e}(k) = \left[e_1(k)\, e_2(k) \ldots e_M(k)\right]^T$,

$\mathbf{d}(k) = \left[d_1(k)\, d_2(k) \ldots d_M(k)\right]^T$, the disturbances,

$\mathbf{X}^{\mathbf{f}}(k) = \left[\mathbf{x}^{\mathbf{f}1}(k)\, \mathbf{x}^{\mathbf{f}2}(k) \ldots \mathbf{x}^{\mathbf{f}M}(k)\right]$,

with $\mathbf{x}^{\mathbf{f}m}(k) = \left[\mathbf{x}^{\mathbf{f}m1}(k)^T\ \mathbf{x}^{\mathbf{f}m2}(k)^T \ldots \mathbf{x}^{\mathbf{f}mN}(k)^T\right]^T$,

$\mathbf{x}^{\mathbf{f}mn}(k) = \left[\mathbf{x}_1^{\mathbf{f}mn}(k)^T \quad \mathbf{x}_2^{\mathbf{f}mn}(k)^T \quad \ldots \quad \mathbf{x}_P^{\mathbf{f}mn}(k)^T\right]^T$, in which

$\mathbf{x}_p^{\mathbf{f}mn}(k) = \left[x_p^{\mathbf{f}mn}(k) \quad x_p^{\mathbf{f}mn}(k-1) \quad \ldots \quad x_p^{\mathbf{f}mn}\left(k - L_{cf} + 1\right)\right]^T$, and

$$x_p^{\mathbf{f}mn}(\kappa) = \sum_{i=0}^{L_{sp}-1} h_{mni}\, x_p(\kappa - l - i) \quad \text{for } \kappa = k, k-1, \ldots, k - L_{cf} + 1$$

$\mathbf{w}(k) = \left[\mathbf{w}_1(k)^T\ \mathbf{w}_2(k)^T \ldots \mathbf{w}_N(k)^T\right]^T$ is the adaptive FIR control filter, with $\mathbf{w}_n(k) = \left[\mathbf{w}_{n1}(k)^T \quad \mathbf{w}_{n2}(k)^T \quad \ldots \quad \mathbf{w}_{nP}(k)^T\right]^T$.

The FIR control filter $\mathbf{w}_{np}(k)$ and the time vector $\mathbf{x}_p^{\mathbf{f}mn}(k)$ have length L_{cf}. $\mathbf{X}^{\mathbf{f}}(k)$ is the *filtered-x* reference signal matrix, $x_p(k)$ is the p-th reference signal and h_{mni} is the i-th coefficient of the FIR filter $\hat{\mathbf{S}}$ (length L_{sp}) that models the secondary path $\mathbf{S}$ between the n-th control actuator and the m-th error sensor. Secondary path modeling is performed in parallel with control and can be implemented both off-line or on-line. Algorithms for combining active control and secondary path identification have been developed and studied by Bao [119]. On-line identification is useful in applications where the system characteristics are time varying in the case of non-linearities (e.g. the dynamics of rubber mounts are dependent on mechanical (pre)load, temperature, time, etc.).

The Wiener optimum of the cost function (2.25),

$$\mathbf{w}^{opt} = \left(E\left\{\mathbf{X}^{\mathbf{f}}(k)\mathbf{X}^{\mathbf{f}}(k)^T\right\}\right)^{-1} E\left\{\mathbf{X}^{\mathbf{f}}(k)\mathbf{d}(k)\right\} \tag{2.34}$$

is now expressed as a function of the matrices

$$\mathbf{R} = E\left\{\mathbf{X}^{\mathbf{f}}(k)\mathbf{X}^{\mathbf{f}}(k)^T\right\}, \tag{2.35}$$

the so-called input auto-correlation matrix, and

$$\mathbf{P} = E\left\{\mathbf{X}^{\mathbf{f}}(k)\mathbf{d}(k)\right\}, \tag{2.36}$$

the cross-correlation matrix.

Updating the control filters in the inverse direction of the instantaneous gradient of the error surface defined by $E\{\mathbf{e}(k)^T\mathbf{e}(k)\}$ results in the Filtered-X LMS update rule:

$$\mathbf{w}(k+1) = \mathbf{w}(k) + \mu\,\mathbf{X}^{\mathbf{f}}(k)\mathbf{e}(k) \tag{2.37}$$

where a factor 2 is absorbed in μ.

The behaviour of the Filtered-X LMS algorithm has been analysed extensively in literature. For the Filtered-X LMS algorithm it is shown in [106] that bounds can be determined for the convergence coefficient such that the adaptive control filter converges to the Wiener optimal solution. The practical implication of this result is that any convergence coefficient that ensures stable convergence, also assures convergence to the Wiener optimal solution (2.34). The single-channel Filtered-X LMS algorithm was independently derived by Widrow [120] in the context of adaptive control and Burgess [121] for ANC applications. The Multiple Error Filtered-X LMS algorithm for ANC applications was introduced by Elliott *et al.* [122]. In contrast to the LMS algorithm, it is acknowledged [123] that "The theoretical analysis of the behaviour of the Multiple Error LMS algorithm is not well developed".

However, some aspects of the convergence of the algorithm have been analysed. The convergence time of the algorithm was shown to be dependent on the eigenvalues of the input auto-correlation matrix (2.35). This leads to the conclusion that the convergence speed depends not only on the spectral properties of the reference signals, but also on the dynamics of the system to be controlled. The effect of time delays in the secondary paths have been accounted for in the time domain in [119] and [124]. Also the spatial distribution of control sources and error sensors has an influence on the convergence speed of the algorithm. This was clearly demonstrated in a frequency domain analysis [125 -126] for the specific case of a harmonic reference signal. The study presented in [126] also shows which is the effect of errors in the secondary path models used to obtain the filtered references (also refer to [127 -130]). For the single channel case the effects of phase errors are well known [122] : provided they are within approximately ±90° and the convergence coefficient is sufficiently small, then the control

system will be stable. In the multichannel case, a common practice is to provide some form of effort weighting in the cost function (i.e. use the *Leaky Filtered-X LMS algorithm*, [38] p. 77). In [128] it is shown that this effort weighting, which avoids excessive power demands, can also be used to stabilise an otherwise unstable control system. The value of the leakage factor is in general determined on an experimental basis, as a compromise between robustness and loss of performance of the adaptive filter.

The practical relevance of these studies is that in most applications, the Filtered-X LMS algorithm can be robustified with a few simple measures (reduction of convergence coefficient, introduction of leak factor) which can be optimised "in situ" such that this algorithm suits almost all control purposes. Nevertheless, a wide range of alternative adaptive algorithms have been developed, based on the Filtered-X LMS algorithm with the aim to enhance its robustness, performance, convergence speed, computational efficiency, etc. Some examples are given in the next section.

Alternative forms of the (Filtered-X) LMS algorithm

Time varying convergence coefficient.

The selection of μ is very critical for the LMS algorithm. The convergence coefficient should be determined to offer the best compromise between robustness and stability : a small μ will ensure small residual errors in steady state, but the algorithm will converge slowly and may not track non-stationary disturbances very well. A large μ will in general provide faster convergence (better tracking) but yields limited robustness margins and larger residual errors in steady state. As it has been shown [108], the maximum μ is inversely proportional to the power of the reference signal. One important technique to optimise the speed of convergence while maintaining the desired steady-state performance, independent of the reference signal power, is to normalise the reference as in (2.38) :

$$\mathbf{w}(k+1) = \mathbf{w}(k) + \mu \sum_{m=1}^{M} \left(e_m(k) \frac{\mathbf{x}^{fm}(k)}{\mathbf{x}^{fm}(k)^T \mathbf{x}^{fm}(k)} \right). \qquad (2.38)$$

This algorithm is referred to as the *Normalised Filtered-X LMS* algorithm [131]. Note that this algorithm in effect comes down to introducing a time varying convergence coefficient. Algorithms using a time varying μ have been studied intensively [132] [133] because they offer the possibility to eliminate the "guess work" involved in the selection of the appropriate

convergence coefficient. Algorithms with adaptive μ aim at optimising μ at every time instance to satisfy the following requirements : 1. high convergence speed ; 2. small residual error in steady-state small in stationary conditions ; and 3. optimal tracking in non-stationary conditions. In [132], μ is adapted using a gradient descent algorithm (which is controlled by a constant ρ). In [133], a scheme is presented by using an estimate of the cross-correlation of the reference and the error signal. As the cross correlation reduces when the controller converges [134], it can be used as a criterion to reduce μ accordingly.

The estimate for the cross correlation $\rho_m(k)$ between the m-th error signal and P references is given by (2.39) :

$$\hat{\rho}_m(k) = \lambda \hat{\rho}_m(k-1) + (1-\lambda)\bar{x}_m(k)e_m(k) \tag{2.39}$$

where $\bar{x}_m(k)$ is the "average" of the filtered reference signals, calculated according to :

$$\bar{x}_m(k) = \frac{1}{NP}\sum_{n=1}^{N}\left(\sum_{p=1}^{P}\left(\mathbf{x}_p^{\mathbf{f}mn}(k)\right)\right) \tag{2.40}$$

(λ is the forgetting factor to deal with the non-stationary character of the adaptation error process). The convergence coefficient is then adjusted according to changes in the estimate in the cross correlation as follows :

$$\mu_m(k) = \alpha \hat{\rho}(k) \tag{2.41}$$

(α is a scale factor). Note that there is a different convergence coefficient for each error signal.

The update equation becomes :

$$\mathbf{w}(k+1) = \mathbf{w}(k) + \sum_{m=1}^{M}\left(\mu_m(k)e_m(k)\frac{\mathbf{x}^{\mathbf{f}m}(k)}{\mathbf{x}^{\mathbf{f}m}(k)^T\mathbf{x}^{\mathbf{f}m}(k)}\right). \tag{2.42}$$

Introduction of the time variant step size makes the adaptive algorithm very stable. Once the adaptive algorithm converges, the cross correlation between the error and the reference signal is close to zero, and so is the convergence coefficient (the adaptive system is in an "asleep" state). A short disturbance, will not destabilise the system due to the very low adaptive gain. On the other hand, the algorithm still has tracking capability. The adaptive algorithm can be awakened automatically whenever the system parameters start to change, i.e. when the actual control filter is getting suboptimal. In that case, the cross correlation will start to rise and the adaptive algorithm enters the "active" state.

Though the algorithms presented in [132 - 133] with adaptive convergence coefficient are aimed at reducing the "guess work" to determine the optimal μ, they introduce new control parameters (ρ in [132] and the forgetting factor λ and the scale factor α in [133]) which again require optimisation. Furthermore, the computational complexity of these algorithms is increased significantly with respect to Filtered-X LMS. Normalised Filtered-X LMS can therefore be regarded as the best compromise among the algorithms with variable convergence coefficient [135].

Frequency domain algorithms.

Stothers et al. [136] have presented a hybrid algorithm (for the cancellation of road noise) which is more computationally efficient than the Filtered-X LMS algorithm. The algorithm is hybrid in the sense that it performs the control filtering in the time domain while performing the update of the control filters in the frequency domain. Though the DFT involves a number of additional calculations[7], the computational complexity of the frequency domain algorithms can be potentially reduced for high order control filter implementations. This is because the time domain convolutions (involving multiplications and additions) can be performed more efficiently in the frequency domain (comparison of computational complexity in [136] p. 731). Additional time saving follows from the fact that secondary path compensation is performed in the frequency domain by multiplication of the Fourier transform of the error signals with the complex conjugate of the frequency domain model of the secondary path. This way the number of operations does not increase if the number of references increases. Furthermore the proposed approach allows to perform the update as often as computational limits allow. On the other hand, frequency domain algorithms in general require more address space in the DSP.

The algorithm has been found to have comparable convergence properties to that of the Filtered-X LMS algorithm and converges to the same control filters. Application of the algorithm can also be found in [137].

In fact, an even more computationally efficient algorithm was presented by Shen and Spanias (single channel in [138], extension to multi-channel in [139]) who propose to implement both the control "filtering" and the control filter update in the frequency domain (analysis of the computational complexity in [139] p. 762). It is important to note that this frequency domain algorithm has a total delay (between measurement of the reference

[7] This can be optimised by transforming signal blocks of which the length is a power of 2 (allows FFT).

and output of the control signal) which is equal to the block length of the DFT. This makes them unsuitable for broadband control applications. This problem can be overcome using a block overlap. If the overlap is equal to the block length minus one time sample, the delay of the frequency domain algorithm is equal to a time domain algorithm which runs at the same sample frequency. The introduction of block overlap, however, significantly increases the computational complexity of the algorithm. Furthermore, as all update is performed in the frequency domain, the procedure is not guaranteed to converge to a causal control filter (the issue of causally-constrained updating the control filters is explained in [137]).

The true advantage of frequency domain implementations lies in the fact that they enable to control individual frequency components of the error signal by specifying a frequency dependent convergence coefficient which controls the convergence speed of the different frequency components. This is particularly useful in circumstances where the input auto-correlation matrix has a large eigenvalue spread (which lead to slow convergence in the time domain).

Extended Filtered-X LMS and RLS.

As mentioned before, the development of the Filtered-X LMS algorithm is, at least theoretically, only correct for linear and time invariant systems. This is actually due to the fact that in the development, it is assumed that $\mathbf{S}(z)$ and $\mathbf{C}(z)$ can be switched for the calculation of $\mathbf{z}(k)$. Obviously, this is only mathematically correct under the aforementioned conditions. In practice, this restriction is relaxed to the well-known constraint on the adaptation speed of the control filter coefficients which should not change significantly on a timescale associated with the dynamic response of the secondary path[8] [122]. However, as the implementation of the Filtered-X LMS algorithm requires the availability of a secondary path model, it is possible to calculate and compensate for the error, $\Delta\mathbf{e}(k)$ which occurs due to switching $\mathbf{S}(z)$ and $\mathbf{C}(z)$.

Figure 2.18 presents the configuration in which this is realised. In this configuration, the LMS update is based on $\varepsilon(k) = \mathbf{e}(k) + \Delta\mathbf{e}(k)$ rather than on $\mathbf{e}(k)$. This construction has been developed by Bronzel and who called it the *Extended Filtered-X LMS* algorithm ([100] p. 45). The performance of a

[8] This constraints may raise the question how relevant the fast converging adaptive algorithms are if their convergence speeds should almost always be limited in the presence of secondary paths.

SISO extended Filtered-X LMS algorithm has been simulated and compared to a SISO RLS-based algorithm (FTF) which was extended in a similar way ([100] p. 55 - 57).

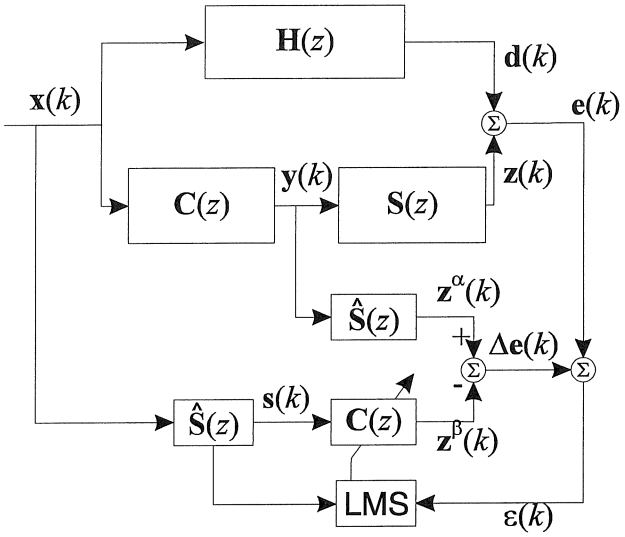

Figure 2.18. Extended Filtered-X adaptive feedforward control scheme.

Two important conclusions can be drawn from the results obtained in this work. First of all, in the case of high convergence speed, it was observed that the compensation term, $\Delta\mathbf{e}(k)$, reached the same order of magnitude as the error $\mathbf{e}(k)$. As a result a significant error is introduced in the adaptive process. This was illustrated by the fact that, in this specific example, the FTF algorithm diverged repeatedly as long as the compensation term was not included. Secondly, it was observed that the convergence properties (stability and convergence speed) of the extended Filtered-X LMS algorithm were not improved with respect to the Filtered-X LMS algorithm.

This numerical example illustrates that the RLS-based algorithms, which were already known to be very susceptible to numerical instabilities, need extra care in the presence of secondary paths. The addition of the compensation term $\Delta\mathbf{e}(k)$ in the update procedure, however, further increases the computational complexity of these algorithms. This demonstrates once more the superiority of the LMS-based algorithms with respect to the RLS-based algorithms.

2.3.4 Why adaptive - Performance limits of an adaptive control filter

Another good reason to apply adaptive feedforward control

The arguments why feedforward controllers should ideally be configured with an adaptive scheme have already been raised before. Though time variation of system dynamics is a problem which is common to feedback as well as to feedforward controllers, it is important to stress that feedforward controller performance is much more influenced by these effects than in the case of feedback. This does not mean that LTI feedforward controllers are totally irrelevant for the control of dynamic systems. On the contrary, LTI feedforward control has been applied successfully, e.g. to servo-control of machine tool axes and in robotics [140 - 142]. These control configurations are, however, complemented with a feedback loop which, under certain circumstances, allows to compensate for the error introduced by the "misadjusted" feedforward controller and thus robustifies the complete controller [142]. The situation in active control of vibration and sound is slightly different in the sense that the need for a time varying control filter is not only due to time variation of the dynamics of system components, but also due to potential time variation of the disturbances. If the spectral content of the disturbances would significantly change (e.g. a frequency shift of a harmonic disturbance), the optimal control coefficients will need to be changed accordingly. Due to the ability of the adaptive feedforward controllers which enables them to adapt to changing circumstances, they are applied in a majority of active control applications.
There is, however, another interesting feature common to the adaptive Filtered-X LMS algorithm. To explain this, let's turn our attention to the feedforward control configuration depicted in figure 2.16. Assuming a SISO configuration, the transfer function of the optimal feedforward controller, which perfectly cancels the error, can easily be determined off-line, namely

$$C^{opt} = \frac{-H}{S}. \tag{2.43}$$

The same result would be obtained from (2.34) if the disturbance source would be perfect white noise.
Apart from a magnitude relation, (2.43) specifies a phase relation in the z-domain. Depending on the pole-zero location of the two transfer functions involved (H and S), the specified phase relation may eventually involve poles outside the unit circle. These occur when S has unstable zeros. As the

latter is very likely to occur due to the inherent delays of acoustic systems[9], (2.43) might specify an optimal control filter which is not realisable. The optimal controller becomes realisable when the unstable zeros of S are cancelled by zeros in H. Referring to the footnote, this is often physically interpreted in the sense that the delays in the secondary path should not exceed the delays occurring in the primary path. In other words, the control system should be *causal*. Causality implies that no prior information is necessary to calculate the optimal control signal at each time instance. For simple SISO systems, such as the active control of duct noise, this physical interpretation is mostly valid and suggests that the optimal controller is realisable as soon as a sensor and actuator configuration is found which satisfies the timing conditions imposed by the causality constraint.

Though most studies of feedforward controllers are restricted to this interpretation of the causality constraint (also in [68], app. B), it is important to note that this physical interpretation is not always valid. For MIMO configurations, the phase relation imposed by (2.34) can often not be made causal by moving around sensors and actuators until a certain threshold delay time is exceeded. Moreover, a system with poles outside the unit circle may as well be interpreted as a causal, but unstable, system. This means the system can only be controlled with an unstable controller. In these cases, the theoretical optimal controller may never be realisable and the best (suboptimal [143] but causal and stable) alternative must be determined. At this point the Filtered-X LMS algorithm turns out to be a very practical tool to realise this because it will search the cost function surface until an optimum is reached. As the algorithm is implemented in real-time using FIR filters, it is always guaranteed to yield the optimal causal and stable controller.

Apart from the causality constraint, which is also discussed in detail in [144 - 147], there are two other reasons why the performance of the adaptive controller may be constrained in practice. This is explained in the next two sections.

---

[9] As a matter of example, note that a (continuous time domain) first order approximation of a pure delay t_d is $\frac{1-\frac{t_d}{2}s}{1+\frac{t_d}{2}s}$, which has one Right Half Plane zero. Inversion of the transfer function yields an unstable pole.

Convergence speed of the algorithm

Due to the fact that the control filter update relies on an estimate of the instantaneous gradient to the cost function, the LMS algorithm converges only in a statistical sense to the optimum. Therefore the LMS algorithm is often referred to as a *stochastic gradient search* algorithm. The convergence speed of the LMS algorithm was said to be determined by the eigenvalue spread of the input auto-correlation matrix. In practice this means that fast convergence is only assured in the case of white noise inputs. A geometric interpretation for this fact is given in [108] where that the eigenvalues of the input auto-correlation are shown to be related with the curvature of the cost function surface along its main axes. For white noise, the cost function surface is a perfect error "bowl" with a uniform slope along its main axes. For highly correlated input signals, however, the cost function surface may exhibit a steep slope along one axis but a relatively flat slope along another [148]. Depending on the initial value of the parameters, this may result in a very slow convergence towards the optimum. The basic problem of the LMS algorithm for that type of inputs lies in the fact that the gradient of a function does not necessarily point in the direction of the optimum. This is in contrast with RLS-based algorithms, which are always assured to converge in the direction of the optimum (this can also be understood by noting that the influence of ill-conditioned input signals is cancelled because the inverse of the input auto-correlation matrix is determined recursively for the RLS).

Though this geometrical interpretation does not directly carry over to the multiple error Filtered-X LMS algorithm (in which case the input auto-correlation matrix is a complex combination of different references, filtered with different secondary paths), the same observation is made that the algorithm converges only fast for (quasi) white noise excitations. Some measures to cope with this problem, which have resulted in alternative forms of the adaptive algorithm, have been mentioned before. A more detailed study of this issue is presented in chapter 4 (paragraph 4.4) where an alternative approach is presented to enhance the reference signals for the control of structure-borne road noise in a car cabin.

Coherence between reference(s) and error signal

An expression, in dB, for the maximum reduction achievable with the Wiener optimal control filter in the case of a random sound field, generated by a number of independent noise sources, has been derived in [149] (an earlier reference is [150]) :

$$\Delta_{max} = -10\,log\left(1-\gamma^2_{d,\{x\}}\right) \tag{2.44}$$

where $\gamma^2_{d,\{x\}}$ is the multiple coherence of all reference signals with respect to the error signal under consideration. This is easily understood when noting that both the Wiener optimum and the coherence are determined from auto- and cross-correlation functions. At this point it is important to stress the fact that this expression is only exact for control filters that are not constrained to be causal and therefore it determines a theoretical upper bound which predicts a control performance which is typically better than that which could be achieved in practice. Other constraints to the control performance are : limited control power, limited control filter order, the convergence process, etc. Furthermore, it should be clear that (2.44) is based on a quantity which is obtained by time averaging and therefore it yields an estimate for stationary conditions only. In non-stationary conditions, the actual control performance may even be better than what is predicted by (2.44) [151].

2.3.5 Example : adaptive control of power flow in a finite plate

Introduction

This section illustrates how an adaptive feedforward controller is designed and optimised to actively control flexural vibrations in plates. The proposed strategy consists of minimising the power flow across a closed path encircling the perturbation force location and the control actuators on a finite plate. the perturbation force is assumed to be harmonic, and it is assumed that a reference for can be measured. This makes the considered problem perfectly suitable for feedforward control. In order to highlight the fact that adaptive feedforward controllers need not necessarily be designed in the time domain, an adaptive frequency domain feedforward control strategy is applied. The main difference with the frequency domain algorithms discussed in 2.3.3, lies in the fact that the problem which is considered here, is formulated in the frequency domain, which implies that the transformation from time to frequency domain (and back) can be omitted.

The proposed strategy is investigated using a numerically simulated example consisting of a rectangular plate excited by a perturbation force. The expression of the gradient of the power flowing in or out of a region encircling the perturbation force and the control actuators is derived. The convergence properties of the adaptive scheme are investigated using an off-

line simulation in the frequency domain. It is shown that the power flow control can result in significant overall vibration reduction, which is the ultimate goal.
The work which is presented in this section was performed in the framework of a collaboration between Departamento de Mecânica Computacional, FEM, Universidade Estadual de Campinas and PMA with the financial support of the Brazilian research funding agency CNPq (Proc. No. 200028/86-3) and the KULeuven. This section highlights the issues related to the design of the controller. Extensive treatment of this control application can be found in [152].

Problem statement and short literature survey

An alternative approach to structural vibration analysis, which is increasingly attracting researchers in the field of active control is the use of the *structural power flow* or *vibration intensity* concept [153 - 154]. With this approach, vibrations are not regarded as standing waves within an elastic body, where energy dissipation is taken into account via a global parametric model (viscous or structural damping), but, instead, as a wave propagation phenomenon, where the structural power flow within the elastic medium and through its boundaries is investigated. The standing waves account for the reactive part of the vibration power while the propagating waves account for the active part. Active vibration control is thus carried out using models and measurements directly associated with propagating waves rather than models and measurements which are more closely related to standing waves.
There are different approaches to the idea of active control of power flow. The simplest one would be to try to absorb as much active power as possible with the control actuators. In general, however, this does not work, as increasing the overall vibration level is also likely to increase the active power dissipated by the control actuators. A more elaborate approach is to try to alter the power flow in such a way that the vibration energy is driven away from where it annoys and direct it to where it can be dissipated. Using the latter approach, Miller *et al.* [155] have developed methods aiming at the active control of structures consisting of assembled one-dimensional waveguides, such as large truss structures.
Tanaka *et al.* proposed two different schemes for the active control of flexural wave propagation in plates. One of them consists of using *active sinks* to create non-reflective boundary conditions, which would avoid the establishment of standing waves and, thus, the excitation of structural

modes. The other [156] consists in actively creating *power flow vortices* to control flexural vibrations in plates.
Gibbs *et al.* [157] proposed the use of especially tailored *wave vector sensors* made of PVDF patches properly laid on a beam such that their combined electrical signals generate signals proportional to the flexural and extensional propagating-wave amplitudes. These signals are then used in an adaptive control scheme. An alternative technique for measuring flexural wave intensity in the far field is proposed by Pan *et al.* [158]. The technique is based on the property that structural intensity (in one direction) is proportional to the product of the outputs of two closely spaced accelerometers.
In this work, a strategy is proposed consisting of minimising the power flow across a closed path encircling the perturbation and the control actuators. This approach is equivalent to the active noise control based on the far-field power over a closed volume, where the disturbance source location is assumed known [159]. As real structures always present some internal damping, any vibration will produce power flow. Thus, measuring and controlling power flow ultimately results in vibration reduction. The basic principle behind the proposed strategy is that the active control forces dissipate the input power due to the perturbing force, thus preventing the structure from having to vibrate in order to dissipate the incoming energy. Hence, the overall vibration level can be minimised.
A frequency-domain adaptive control scheme is developed aiming at the attenuation of steady-state, periodic vibrations. It is assumed that the location of the perturbation is known (the source localisation problem using power flow methods was treated by Arruda and Mas in [160]).

Adaptive control of flexural power flow in plates

Tanaka *et al.* [161], express the power flow in a beam as a function of the square of the flexural and extensional propagating-wave amplitudes. With the application of special wave vector filters, these wave amplitudes can be indirectly measured and fed to the filtered-X LMS algorithm as the error signals that are minimised, resulting in the control of power flow in the beam. In this section, the power flow (the objective function) is expressed as a function of directly measured quantities. A frequency-domain gradient descent algorithm is then used to find the optimal parameters of the feedforward controller which minimise this objective function.
The control strategy proposed here is the following : given the region of the plate where the energy source is located, one or more control actuators are

placed as close as possible to the source. A closed path encircling the energy source and the control actuators is then defined so that the total power flowing through it can be measured (computed). The simplest way to define a closed path encircling the energy source and the control actuators is a rectangular area of width L_x and length L_y, in which case the total power flowing into or out of the enclosed part of the structure can be approximated by

$$P_c(\omega) = (P_{x+} - P_{x-})L_y + (P_{y+} - P_{y-})L_x \tag{2.45}$$

where P_{x+} is the power flow at the side parallel to the y axis corresponding to the larger value of x and so forth, as illustrated in figure 2.19. The objective function to be minimised by the controller is then the absolute value of $P_c(\omega)$.

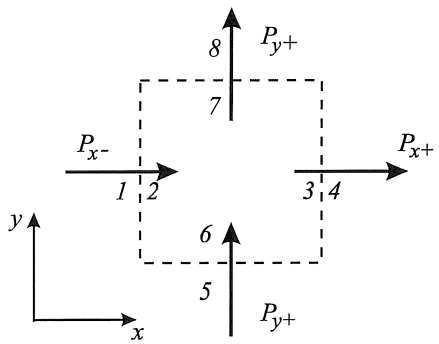

Figure 2.19. Measurement cell and location of the accelerometers (numbers 1 ... 8) for calculation of total power flow across a rectangular path

Each of the power flow terms in Eq. (3) can be approximated by a finite difference expression, as explained in [152]. The spatial derivative which appears is known to be very sensitive to measurement noise (see, for instance, [162]). Therefore it is proposed using a minimum of 8 measurements (2 accelerometers located at each side of the rectangle) or preferably more. This reduces the sensitivity to measurement noise because of the filtering effect of the averaging, which is implicitly associated with the measurements to compute the power balance in a closed region.

In a feedforward control system, the control input (here : control force $\mathbf{F}_c$) applied to the system is generated by feeding the reference signal x through a feedforward control filter w. In the frequency domain this reduces to, per

frequency line, multiplying the complex scalar X (frequency domain reference) with a vector $\mathbf{W}$ of complex scalars ($\mathbf{F}_c = \mathbf{WX}$). For each frequency line, each of the elements of $\mathbf{W}$ is a control gain which realises the appropriate amplitude and phase of the control signal that is sent to the corresponding actuator. The weights $\mathbf{W}$ are updated using a frequency-domain gradient descent scheme as follows :

$$\mathbf{W}_{k+1} = \mathbf{W}_k - \mu\nabla_k \tag{2.46}$$

where $\mathbf{W}_k$ is the weighting vector at iteration step k and ∇_k is the gradient to the cost function which is optimised.
In [152] it is shown how the power flow crossing the rectangular path (the cost function under consideration) can be expressed as a function of the perturbation and control forces, and the transfer functions between the control forces and the plate velocity at the accelerometer locations. Substituting $\mathbf{F}_c = \mathbf{WX}$ in this expression and differentiating with respect to $\mathbf{W}$ yields an expression for the gradient to that function :

$$\frac{\partial}{\partial \mathbf{W}}\left|P_c(\omega)\right| = \frac{P_c(\omega)}{\left|P_c(\omega)\right|}\left[\left(\frac{\partial P_{x+}}{\partial \mathbf{W}} - \frac{\partial P_{x-}}{\partial \mathbf{W}}\right)Ly + \left(\frac{\partial P_{y+}}{\partial \mathbf{W}} - \frac{\partial P_{y-}}{\partial \mathbf{W}}\right)Lx\right] \tag{2.47}$$

Determination of the optimal convergence coefficient

The μ constant (convergence coefficient) in (2.46) determines the iteration step size, and its choice depends on the properties of the reference signal and of the system that is controlled. It is determined as a compromise between stability (maximum specification) and tracking (minimum specification). A mathematical expression for the upper limit is derived here. The development starts with determining the theoretical optimum of the objective function. A harmonic perturbation is assumed. Recalling eq. (7) from [152]

$$\frac{\partial P}{\partial \mathbf{W}} \cong \frac{\sqrt{D\rho}}{\Delta} X^*\left[iH_{kp}F_pH_{lc}^H - iH_{lp}F_pH_{kc}^H - i\left(H_{kc}^H H_{lc} - H_{lc}^H H_{kc}\right)F_c\right], \tag{2.48}$$

where X^* is a complex scalar, F_p is the perturbation force, H_{kp} is the frequency response function (FRF) between the perturbation force and the velocity at location k, and H_{kc} is the FRF between a control force and the velocity at location k. D is the flexural stiffness of the plate and Δ is the

spacing between the measurement points in one orthogonal direction. The terms involving the perturbation force can be determined through measurement of the velocity at locations 1, 2, ... 8, as indicated in [152] (eq. (5)).

An expression for $\mathbf{W}^{opt}$ is determined by setting (2.47) to zero :

$$\begin{aligned}\mathbf{W}^{opt} = &\left\{-iX\left[\left[\left(H_{1C}^{H}H_{2C} - H_{2C}^{H}H_{1C}\right) - \left(H_{3C}^{H}H_{4C} - H_{4C}^{H}H_{3C}\right)\right]\frac{L_y}{\Delta_x} + \cdots\right.\right. \\ &\left.\left. + \left[\left(H_{5C}^{H}H_{6C} - H_{6C}^{H}H_{5C}\right) - \left(H_{7C}^{H}H_{8C} - H_{8C}^{H}H_{7C}\right)\right]\frac{L_x}{\Delta_y}\right]\right\}^{-1} \times \cdots \\ \times &\left\{-i\left[\left(\left(H_{2P}F_PH_{1C}^{H} - H_{1P}F_PH_{2C}^{H}\right) - \left(H_{4P}F_PH_{3C}^{H} - H_{3P}F_PH_{4C}^{H}\right)\right)\frac{L_y}{\Delta_x} + \cdots\right.\right. \\ &\left.\left.\left(\left(H_{6P}F_PH_{5C}^{H} - H_{5P}F_PH_{6C}^{H}\right) - \left(H_{8P}F_PH_{7C}^{H} - H_{7P}F_PH_{8C}^{H}\right)\right)\frac{L_x}{\Delta_y}\right]\right\}\end{aligned} \tag{2.49}$$

The update equation (2.46) can then be written as

$$\mathbf{W}_{k+1} - \mathbf{W}^{opt} = \mathbf{W}_k - \mu\nabla_k - \mathbf{W}^{opt}. \tag{2.50}$$

Using (2.49) and the expression for the gradient, this may also be written as

$$\begin{aligned}&\mathbf{W}_{k+1} - \mathbf{W}^{opt} = \\ &\left\{\mathbf{I} - \mu\left(i\sqrt{D\rho}\,X^{*}X\right)\left(\left[\left(H_{1C}^{H}H_{2C} - H_{2C}^{H}H_{1C}\right) - \left(H_{3C}^{H}H_{4C} - H_{4C}^{H}H_{3C}\right)\right]\frac{L_y}{\Delta_x} + \cdots\right.\right. \\ &\left.\left.\left[\left(H_{5C}^{H}H_{6C} - H_{6C}^{H}H_{5C}\right) - \left(H_{7C}^{H}H_{8C} - H_{8C}^{H}H_{7C}\right)\right]\frac{L_x}{\Delta_y}\right)\right\}\cdot\left(\mathbf{W}_k - \mathbf{W}^{opt}\right)\end{aligned} \tag{2.51}$$

in which $\mathbf{I}$ is a unitary matrix.

Replacing $\mathbf{W}_{k+1} - \mathbf{W}^{opt}$ by $\mathbf{V}_{k+1}$, and decomposing the matrix

$$\begin{aligned}\mathbf{R} = i\sqrt{D\rho}X^{*}X\left\{\left[\left(H_{1C}^{H}H_{2C} - H_{2C}^{H}H_{1C}\right) - \left(H_{3C}^{H}H_{4C} - H_{4C}^{H}H_{3C}\right)\right]\frac{L_y}{\Delta_x} + \cdots\right. \\ \left. + \left[\left(H_{5C}^{H}H_{6C} - H_{6C}^{H}H_{5C}\right) - \left(H_{7C}^{H}H_{8C} - H_{8C}^{H}H_{7C}\right)\right]\frac{L_x}{\Delta_y}\right\}\end{aligned}$$

using its eigenvalue decomposition $\mathbf{Q}\Lambda\mathbf{Q}^{-1}$, in which $\mathbf{Q}^{-1} = \mathbf{Q}^{H}$ because the matrix $\mathbf{R}$ is Hermitian, (2.51) reduces to

$$\mathbf{V}_{k+1} = \left(\mathbf{I} - \mu\mathbf{Q}\Lambda\mathbf{Q}^{H}\right)\mathbf{V}_{k}. \tag{2.52}$$

With $\mathbf{V}_k^{\sim} = \mathbf{Q}^{H}\mathbf{V}_k$, assuming $\mathbf{W}_0 = [0 \quad 0 \quad \cdots \quad 0]^T$, and reasoning inductively from $k = 0$,

$$\mathbf{V}_k^{\sim} = \left(\mathbf{I} - \mu\Lambda\right)^{k}\mathbf{V}_0^{\sim}. \tag{2.53}$$

Equation (2.53) is actually a set of decoupled equations that may be written as

$$\begin{bmatrix} V_{1,k}^{\sim} \\ V_{2,k}^{\sim} \\ \vdots \\ V_{nact,k}^{\sim} \end{bmatrix} = \begin{bmatrix} \left(1-\mu\lambda_1\right)^{k} & 0 & \cdots & 0 \\ 0 & \left(1-\mu\lambda_2\right)^{k} & \cdots & 0 \\ \vdots & \vdots & \ddots & \vdots \\ 0 & 0 & \cdots & \left(1-\mu\lambda_{nact}\right)^{k} \end{bmatrix} \cdot \begin{bmatrix} V_{1,0}^{\sim} \\ V_{2,0}^{\sim} \\ \vdots \\ V_{nact,0}^{\sim} \end{bmatrix}. \tag{2.54}$$

Expression (2.54) shows that the rate of convergence process is determined by the eigenvalues of $\mathbf{R}$, i.e. the larger the eigenvalue, the faster the convergence. For reasons of stability, the convergence coefficient is limited to be chosen $0 < \mu < 2 / \lambda_{\max}$ (usually $\lambda_{\max}$ is λ_1). Though $2 / \lambda_{\max}$ is the theoretical upper limit, a practical rule of thumb is to choose half of this value in order to account for variation in the transfer functions that constitute $\mathbf{R}$. Also, to reduce the steady state misadjustment, it is advised to use smaller values for μ (basically this depends on what is the aim, namely if tracking is more important than steady state accuracy, large values for μ will be necessary). Note that with this choice of μ it is clear that, for k → ∞, the adaptive scheme converges to the optimal solution $\mathbf{W}^{opt}$.

In the multi-sine case, a similar expression to (2.48) can be written for each frequency line, resulting in boundary conditions on μ per frequency line. In fact, this illustrates the true advantage of a frequency domain adaptive scheme, as different convergence coefficients may be chosen per frequency line, possibly favouring some frequency lines with respect to others.

Also note that this derivation has been conducted in the purely deterministic case. In the more general case, the expected value of the gradient must be used to yield an expression for the expected value of $\mathbf{W}_k$. Under these conditions the analysis tends to be a tedious task. For stationary input

processes and under the assumptions of decorrelation of the inputs, however, similar conclusions can be drawn.

Numerical example

Model description

In order to investigate the structural power flow in thin plates exposed in the previous sections, the responses of a rectangular plate were simulated using a finite element model. FE modelling was performed by R. Arruda (see [152] for all relevant details).

The simulated plate is a 0.45 m × 0.40 m, 1 mm thick aluminium plate. The plate was simulated to be free at all four sides, and connected to a rigid foundation in four locations (figure 2.20) by means of flexible mounts. The perturbation force (unity force excitation) and control forces are simulated by point force excitation. The plate was modelled without internal damping, such that all the energy dissipation occurs at the rubber mounts, which is a reasonably realistic assumption for an aluminium plate mounted on rubber isolators.

The FRFs, necessary for the numerical simulation, were computed by modal superposition using the first 60 modes. The contribution of the residual flexibility of the higher order modes was included. The objective function based on the power flow was computed using the measurement cell of figure 2.19 centred at $x = 22.56\,\text{cm}$, $y = 25\,\text{cm}$ (distance with respect to node 1) with $L_x = 14.36$ cm and $L_y = 14\,\text{cm}$. The spacing between measurements was $\Delta x = 1.03\,\text{cm}$ and $\Delta y = 1\,\text{cm}$. The illustrative results presented in this section refer to 128 Hz except where otherwise indicated.

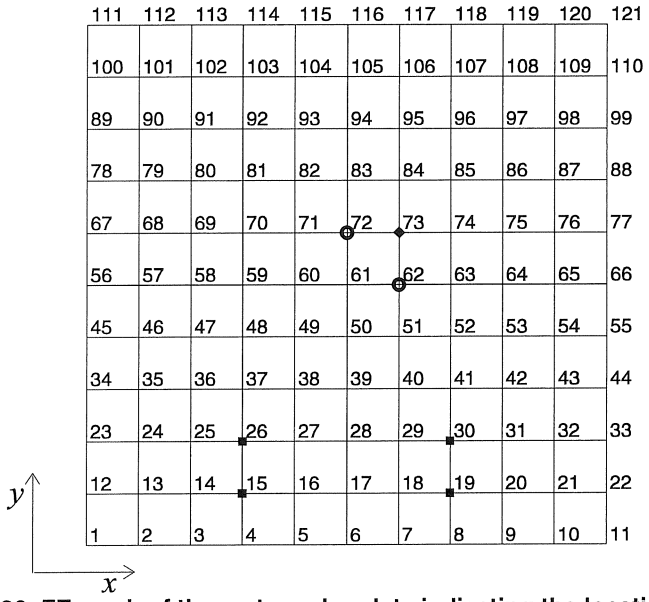

Figure 2.20. FE mesh of the rectangular plate indicating the location of the rubber mounts (squares), perturbation exciter (diamond), and control actuators (circles).

Control results

Assuming the perturbation forces are known, the exact optimal control forces can be calculated for this numerically simulated example. The overall vibration reduction of the plate has been calculated in [152] for the optimal control forces corresponding to 3 types of objective function : *(i)* vibration reduction at actuator positions, *(ii)* vibration reduction at all DOFs of the FE model, and *(iii)* reduction of power flow. Approach *(ii)*, which is actually the "best achievable" result, but which is not realisable in practice as it implies an enormous amount of accelerometers, yields 18.49 dB overall vibration (RMS velocity) reduction. Approach *(iii)* was shown to yield 15.25 dB overall vibration reduction, while approach *(i)* actually increased the overall vibration level. These results illustrate that the proposed control strategy (control of power flow) realises the objective and outperforms the often applied collocated control strategy *(i)* for the considered location of the actuators.

Figure 2.21 illustrates the convergence of the gradient method using (2.46) with $\mu = 50$ and initial weight values of $\mathbf{W}_k = \{1.9, 1.9\}^T$. From the eigenvalue decomposition of $\mathbf{R}$, the maximum value for μ was determined

to be 1738. In order to satisfy stability conditions, a practical value for μ would therefore be 850. However, stability is not the only issue which is relevant to the choice of μ as its value also severely affects the "accuracy" with which the theoretical optimum of the objective function is attained (this effect is referred to as *total misadjustment* [108]). Obviously, the larger μ is, the larger the total misadjustment will be. Therefore, if fast tracking is not a major requirement, μ may be chosen to be significantly smaller than 850. Total misadjustment may be compromised by using larger μ values in cases where the perturbation is significantly varying with time (e.g. an accelerating or decelerating engine).

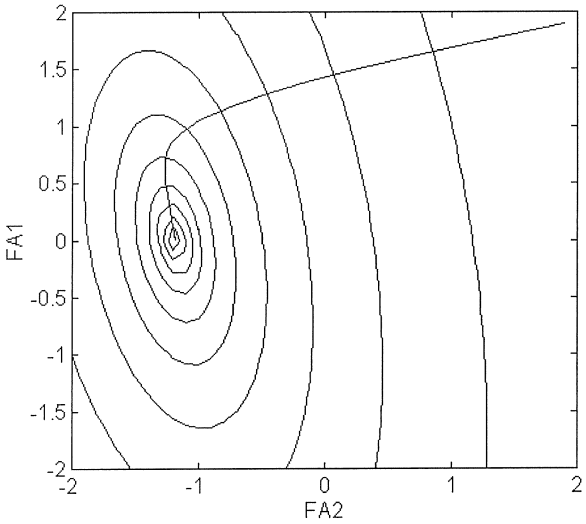

Figure 2.21. Steepest descent search of the minimum of the power flow objective function for the control parameters FA1 and FA2 (the active control forces).

With $\mu = 50$, the controller converged after 200 iterations to control weights 0.0096 and -1.1841. The objective function optimum was reached with a negligible total misadjustment (refer to [67], Table 1). This yields an attenuation of almost 80 dB relative to the approximate power flow with the initial control weights or 60 dB relative to the uncontrolled plate. With these control force amplitudes the attenuation of the mean RMS velocity in the plate was of 14.85 dB. Figures 2.22(a) and 2.22(b) show the reduction in the objective function and the overall vibration attenuation (with respect to the uncontrolled structure) as a function of the iteration number.

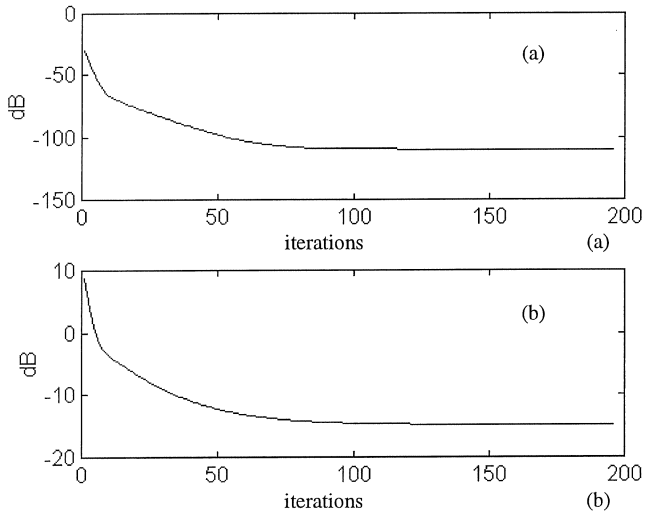

Figure 2.22. Iterative minimisation of : (a) the power flow objective function and (b) the resulting attenuation of the overall RMS velocity level. Reduction, with respect to situation without control, plotted in dB.

Concluding remarks

- The estimation of the power flow across the measurement cell is far from being exact. The approximations involved are the free-field, finite-difference approximation of the power flow and the assumption of constant power flow across each side of the measurement cell. To improve estimation of the power flow across a path encircling the perturbation and control actuators, the number of measurement locations can be increased and more sophisticated power flow measurement schemes using spatial approximations can be used [163]. It should be stressed that the precision of the estimated power flow was not observed to be a critical issue in this study. The important issue is rather to detect if there is power flow across the closed path in order to be able to minimise it.

- In this simulation, the weighting factors of the controller were limited to real numbers. It was observed that, when allowing the weighting factors to be complex, the objective function had no single optimum anymore and thus the (sub)optimum at which the adaptive process arrived was dependent on the initial values of the weights. Therefore, the weights were set to real, thus decreasing the number of parameters to be

optimised and yielding an objective function with only one global optimum which was always "found" by the adaptive procedure, regardless of the initial control weight values.

- Using a numerically simulated example consisting of a rectangular plate supported by four rubber mounts, it was shown that the power flow control can result in significant overall vibration reduction, which is the ultimate goal. The numerical simulation also illustrated the fact that a collocated feedback control scheme using two actuators placed close to the perturbation force location can fail to minimise the overall vibration, even though they minimise the vibrations at the control actuator locations.

- The next step is the actual experimental implementation of the proposed controller. A limited experimental study has already been realised and is presented in [179]. Future research will include the investigation of power flow sensors that might replace the 8 closely-spaced measurements, real-time and block-time implementations of the adaptive controller, and investigations on the optimal location and number of control actuators.

2.4 DIFFERENCES AND EQUIVALENCE BETWEEN FEEDBACK AND FEEDFORWARD

2.4.1 Different application areas for feedback and feedforward control

When considering the design of a control system in general, the question is often raised which of both control approaches, feedback or feedforward, is the "best" alternative. Apart from the classical remark that feedforward is more suited for stationary disturbances, whereas feedback is more suited for controlling transients [45], a comparison of different control applications, to answer this question, is very likely to fail because the control objective which is realised is mostly different. Nevertheless, at least one argument can be raised which is entirely in favour of feedforward control. Theoretically speaking, feedforward allows to realise perfect cancellation. A feedback control configuration, on the other hand, will only give rise to a control action as long as an error is measured. The existence of a remaining error is an implicit feature common to feedback controllers, which will vanish only

in the theoretical case of infinite feedback loop gain. Therefore, if the control application allows to determine a reference signal based upon which the control action can be determined (in a causal and stable way), feedforward control seems the best choice. Indeed, in these circumstances, it would be injudicious to discard the valuable information which is carried in the reference.
On the other hand, however, it is often argued that "the design procedure of the feedforward control system is basically non-existent, in contrast to feedback control where pole allocation etc. is extensively used" [15]. This remark seems to be in sharp contradiction with the observation that a substantial amount of work has been dedicated to the development of design procedures for LTI feedforward controllers for, e.g. motion control applications [140 - 141]. However, it is a fact that little of this work has been carried over to the domain of active control of sound and vibration although feedforward controllers make up the major part of the applications (refer to proceedings of active control conferences). This is due to the fact that mainly adaptive feedforward controllers are employed which are non-linear and difficult to analyse. Only recently, attempts have been made to resolve this problem by Burdisso and Fuller, who dedicated a series of papers [15] [16] [164] to develop a formal design procedure similar to that employed in feedback techniques.
Therefore, though the Filtered-X LMS algorithm will, in most circumstances, yield satisfying control performance and can be made to work by taking into account a few simple heuristic rules, it may be instructive to consider the origin of the following advantages and disadvantages of either control approach.

Feedback is inherently more robust against model error

As pointed out in paragraph 2.3.1 and 2.2.1, the performance of LTI feedforward controllers is inherently more sensitive to deviations of the control filters from the ideal control filters. The obvious answer to that problem is to complement the feedforward controller with an adaptive loop (this is also motivated in [123] p. 14). Compared to the LTI invariant implementation (feedforward or feedback), however, this results in a considerable increase of the computational complexity of the controller. Adaptive feedforward implementations for broadband control typically require filter orders in a range between 50 and 500 ([100] p. 22), whereas a 500th order feedback controller is only rarely encountered in practice.

On the other hand, it must be said that in the design process of feedback controllers, great care must be taken to avoid noise amplification out of the regulation band. System stability of feedforward controllers can be readily ensured and out-of-band noise amplification is not usually a significant problem ([165] p. 85). When the available computing power allows the additional complexity associated with adaptivity, this favourable condition can be complemented with robustness against model errors.

Feedforward is more compatible with controlling acoustic targets

The most straightforward control configuration with which control of a (radiated) sound field can be realised is a configuration in which the sound pressure levels at a number of microphones is reduced. Obviously, this configuration is not in favour of feedback control due to the delays associated with measuring acoustic responses. These delays will considerably limit the maximum control gain, and hence controller bandwidth and performance. In paragraph 2.2.1, this is shown for a simple SISO feedback controller but this observation is valid in general as the poles of a closed-loop feedback system are known to evolve towards the zeros of the open-loop system for increasing closed-loop gain. As acoustic delays give rise to RHP zeros (in the continuous time domain), loop gain will need to be limited to preserve stability. In the framework of ASAC, this dilemma has led to the development of feedback control strategies where the acoustic field is controlled using information of sensors located on the vibrating structure (refer to paragraph 1.2).
Feedback control using microphones as feedback sensors will therefore involve specific measures. A first obvious choice is to co-locate control source and feedback sensor, a configuration which was proposed already in 1953 by Olson and May [166], and which is also applied in active headsets [167], to create a "zone of quiet" around the microphone. Such a configuration is not always realisable in practice because it implies that the control source must be placed at, or very close to, the location where the sound level must be reduced.
A second option which has been chosen by other authors, is to apply the wide variety of model-based feedback control design tools (pole placement in [93], LQG [94] [168], H_∞ [95], H_∞ combined with Quantitative Feedback Theory [96], and others [169]) in order to overcome the problem. These tools basically allow designing a feedback control system in which the feedback signal does not necessarily need to be the response which is

controlled. Thus a collocated feedback sensor may be used to yield noise suppression at a remote target location.

Model-based feedback control is more closely related to modal control approach

The ability of model-based feedback control to separate the controlled response from the observed response (which is fed back), enables to express control objectives in the modal domain and thus to guarantee global control instead of local control. This has been illustrated in the example (paragraph 2.2.5) where the system states of the state space model are associated with the modal amplitudes. Specifying the LQ control objective as a function of these system states realises modal control. The apparent prerequisites for this approach to be successful are total controllability and observability of all system states. The latter may eventually be realised with one error sensor only (though this is not recommended).
On the other hand, filtered-X LMS feedforward control using one error sensor will in general not guarantee reductions at locations other than error sensor location and may even result in amplification of the total acoustic power in the sound field (refer, e.g. to [134], pp. 234 - 235, for the case of the interference of a control loudspeaker with a disturbance speaker in the free field and aiming at perfect cancellation at one location). Global reduction will instead be achieved if a large number of error sensors is used. Indeed, with the latter configuration, the filtered-X LMS algorithm will converge to a control filter which minimises the total acoustic energy in the sound field as it uses a sum of squared error signals as objective function[10]. Hence, if the application allows a modal expansion of the control problem, model-based feedback control may achieve global control with a smaller set of error sensors than in the case of filtered-X LMS.

In general, however, it is important to realise that the success of the feedback approach heavily depends on how good the (modal) model is. Though the implementation of filtered-X LMS is also subjected to

[10] From this point of view, it may sound irrelevant to use filtered-X LMS for applications where only one error sensor is used as reducing the amplitude or the amplitude squared of that signal is in essence the same thing. However, note that the expression for the gradient to the cost function takes a very elegant form in the case of a quadratic cost function, which is the reason why the same algorithm is used in single-channel applications.

requirements with respect to (secondary path) modelling, these constraints are in general not so restrictive. For problems involving systems with a low modal density in the frequency band of interest, such as the duct noise problem which is dealt with in e.g. [93 - 95], feedback may be applied with success. Very complex problems, such as controlling the sound field inside a car interior, which cannot be modeled to the required accuracy, will be solved more efficiently using an adaptive feedforward approach.

2.4.2 Equivalence relations between feedback and feedforward

In contrast to the above arguments that illustrate some of the basic differences between feedback and feedforward control, there are some apparent similarities between both control configurations. Traditionally, the distinction between feedback and feedforward is made on the basis of whether the input to the controller is the system state (e.g. the response to be controlled) or some other measurement, respectively. The observed feedback signals are in general affected by the control action, which distinguishes them from "other" measurements. Consequently, a feedforward control problem with physical coupling of the control action back to the reference is not actually a feedforward but, rather, a feedback control problem (this will be shown explicitly later on). Moreover, feedback controllers where the observed and controlled response do not coincide may as well be configured such that the feedback signal describes the disturbance rather than the system response to the control action. Thus the observed response acts as a feedforward rather than as a feedback signal, as we observed in the example in paragraph 2.2.5 (also refer to [169]). Not surprisingly, a substantial number of studies suggest there is a strong equivalence between the two control paradigms [168] [170 - 173].

Equivalent Linear System Approach

An equivalent LTI system representation of the LMS algorithm in the case of periodic disturbance was developed by Widrow and Stearns [108]. This method of analysing adaptive filters using an equivalent LTI feedback system was applied to the multiple error filtered-X LMS algorithm by Elliott *et al.* in [122]. The equivalent system approach used in their work allows to exactly describe the behaviour of the adaptive algorithm for the case of a single channel active control system by an LTI transfer function between the error signal and the controller output. The controller transfer

function is derived for the case of a synchronously sampled tonal reference signal. This formulation has been used to study the stability boundary of the filtered-X LMS algorithm by analysing the variation of the upper limit on the convergence coefficient with delay in the secondary path.
The studies in [108] and [122] remain in the frequency domain. Burke [170] derives a state space (time domain) representation for the equivalent model of a SISO filtered-X LMS feedforward controller (model again limited to tonal disturbances). The state space model is derived from the transfer function using standard methods. The formulation also allows extension to MIMO systems. The state space model of the controller is combined with a state space model of a physical plant to provide the state equations of the closed-loop system, which makes it possible to compare this control strategy with others. The stability boundary, given by the state space model, is compared to the stability boundary given by the frequency domain approach in [126].

The equivalent system representation is also used by Berkman *et al.* [172] to specify trade-offs between using the filtered-X LMS algorithm and a compensator/regulator feedback controller for narrowband control. They present their study from the feedback viewpoint in order to obtain simple criteria for the selection of control parameters to achieve a specific control performance while maintaining stability and avoiding noise amplification out of the regulation band. Their feedback representation leads to the observation that the filtered-X LMS feedforward control algorithm with a narrowband reference signal has several attributes that make it less desirable than alternate forms such as the feedback compensator/regulator which is proposed in [172]. The primary drawback of the filtered-X LMS algorithm with a tonal reference is said to be the loss of design control over the effective loop gain and consequent inability to *(i)* design to performance specifications independent of the system to be controlled and *(ii)* provide reasonable guarantees of system stability or avoidance of significant noise amplification outside the regulation band in the case of a system with a rapidly varying transfer function over the regulation band.
In order to prove these statements, the authors derive an expression for the loop gain[11] of the equivalent feedback form of the filtered-X LMS algorithm, which is shown to be equal to

[11] The *loop gain* of the feedback controller depicted in figure 2.2 is defined as $L(s)=P(s)C(s)$.

$$L(j\omega) \approx |P_o|^2 \cdot K_{lms} \cdot H(j\omega), \tag{2.55}$$

at and around the disturbance frequency ω_0. In this expression, P_o is the system transfer function at ω_0, $H(s)$ is a narrowband filter, defined as

$$H(s) = \frac{\frac{s}{\omega_o}}{1+\left(\frac{s}{\omega_o}\right)^2}. \tag{2.56}$$

The feedback gain factor, K_{lms} is shown to be $K_{lms} = \frac{\mu}{\omega_o \Delta}$ and hence it is determined by the LMS convergence coefficient μ and LMS update time interval Δ.

It can readily be observed that the filtered-X LMS algorithm enjoys favourable stability properties in comparison to a general feedback controller ([172], observations 1 and 2 p. 1157-1158) when the phase of $P(s)$ does not vary significantly over the regulation band. However, to the extent that $P(s)$ does not vary in magnitude over that regulation band, the filtered-X LMS algorithm is equivalent to a feedback controller with effective loop gain factor $K_{eff} = |P_o|^2 K_{lms}$. In contrast to a narrowband feedback controller, which control performance is determined by selecting the appropriate loop gain through a gain factor K, the control performance of the filtered-X LMS algorithm is cannot be ensured or predetermined as it is determined by the system transfer function amplitude. Large values of noise or vibration reduction are typically required in frequency ranges where either the uncontrolled system response is large or where there is particular operational concern ; neither of which necessarily corresponds to the frequency bands where the amplitude of the system transfer function is large.

Furthermore, when $P(s)$ does vary significantly in magnitude and phase, the filtered-X LMS control system may have limited stability margins ([172], observation 4, p. 1158).

The authors therefore suggest to employ a feedback configuration in which the system transfer function is compensated by a compensation filter $\hat{P}^{-1}(s)$. Of course, the effectiveness and stability of such a compensator/regulator configuration depends on the degree to which $P^{-1}(s)$ is causal and well approximated.

Bode integral constraints on achievable performance of feedback controllers

Hong and Bernstein have investigated the relationship between feedforward and feedback control by means of the classical Bode integral constraints on achievable performance [168]. The Bode integral in essence constrains the integrated log-magnitude of the sensitivity **S** to be zero. It is then shown that if the observed response (feedback signal) and controlled response are non-collocated, and the disturbance and the control source are non-collocated, the feedback controller which satisfies the Bode integral constraint coincides with the feedforward controller which optimises the controlled response. To show this, we write down the system equations of the general feedback control configuration for the case of 1 observed response (y), 1 controlled response (z), 1 disturbance source (w) and 1 control source (u) :

$$\begin{aligned} y &= G_{yw}w + G_{yu}u \\ z &= G_{zw}w + G_{zu}u \end{aligned} \quad . \tag{2.57}$$

The control input u is given by

$$u = K(s)y \tag{2.58}$$

($K(s)$ comprises both observer dynamics and state feedback control).
The closed-loop transfer function from w to z can then be written as

$$\tilde{G}_{zw}(s) = \left[G_{zw}(s) - \left(G_{zw}(s)G_{yu}(s) - G_{zu}(s)G_{yw}(s)\right)\right]K(s)\cdot S(s) = F(K(s))S(s) \tag{2.59}$$

where $S(s)$ is the sensitivity defined as

$$S(s) = \frac{1}{1 - L(s)}, \qquad L(s) = G_{yu}(s)K(s) \tag{2.60}$$

(the sensitivity defined in paragraph 2.2.1 satisfies this general definition).
From (2.59) and (2.60) it is clear that $\tilde{G}_{zw}(s)$ is determined by a spatial component $F(K(s))$ that depends on the arrangement of actuators and sensors, and the sensitivity $S(s)$ which depends on the loop gain $L(s)$.

The Bode sensitivity integral constraint states that, for stable open-loop transfer functions with greater than one pole roll-off,

$$\int_0^\infty log\left|S(j\omega)\right| d\omega = 0\,, \tag{2.61}$$

which constraint is often referred to as the *waterbed effect*[12] : it is impossible to simultaneously reduce S (i.e. attenuate disturbances) over all frequencies. Indeed, (2.61) imposes a hard constraint on the integral of the log amplitude of $\tilde{G}_{zw}(s)$:

$$\begin{aligned}\int_0^\infty log\left|\tilde{G}_{zw}(j\omega)\right|d\omega &= \int_0^\infty log\left|F(K(s))\right|d\omega + \int_0^\infty log\left|S(j\omega)\right|d\omega \\ &= \int_0^\infty log\left|F(K(s))\right|d\omega\end{aligned} \tag{2.62}$$

If the observed and controlled response are collocated, $G_{zw}(s) = G_{yw}(s)$ and $G_{zu}(s) = G_{yu}(s)$, then $F(K(s)) = G_{zw}(s)$, and thus

$$\int_0^\infty log\left|\tilde{G}_{zw}(j\omega)\right|d\omega = \int_0^\infty log\left|G_{zw}(j\omega)\right|d\omega . \tag{2.63}$$

The same result is obtained when disturbance and control source are collocated.

Thus, in both cases, requiring the closed-loop magnitude to be less than the open-loop magnitude over some frequency interval implies that $\left|\tilde{G}_{zw}(j\omega)\right|$ must be greater than $\left|G_{zw}(j\omega)\right|$ elsewhere. This phenomenon is referred to as *spillover* in [168].

However, in a non-collocated control configuration, it is possible to specify the so-called *zero spillover controller* given by

$$K(s) = \frac{G_{zw}(s)}{G_{zw}(s)G_{yu}(s) - G_{zu}(s)G_{yw}(s)}, \tag{2.64}$$

as it yields $\tilde{G}_{zw}(s) = 0$ and thus yields perfect cancellation of the disturbance at every frequency. Note that (2.64) is not realisable in the case of a

---

[12] The term *waterbed effect* is also used to denote feedback bandwidth limitations imposed by the presence of right half plane poles and zeros. Indeed, it has been shown that if the plant is non-minimum phase, then requiring $\left|S(j\omega)\right|$ to be arbitrarily small over some frequency interval forces $\left|S(j\omega)\right|$ to be arbitrarily large elsewhere ([292] p. 97). In [293] it is shown that equivalent statements of these constraints can also be formulated in terms of integral relations which must be satisfied by $\left|S(j\omega)\right|$.

collocated sensor configuration or collocated disturbance and control source.
More importantly, this zero spillover controller was shown in [89] to be identical to the feedforward controller $C(s)$ which uses the observed response as reference and which minimises the controlled response as :

$$C = \frac{H_0}{H_1 H_0 - H_2} \tag{2.65}$$

([168], p. 932). In (2.65), H_1 is the transfer function from the control source to reference sensor (which coincides with the feedback sensor of the *zero spillover* feedback controller), H_2 is the transfer function from the control source to the error sensor (which coincides with the controlled response of the *zero spillover* feedback controller), and H_0 is the transfer function from the reference to the error sensor. Note that (2.65) reduces to (2.43) for the case with no with physical coupling of the control action back to the reference.
The important contribution of [168] is that the paper specifies a state space realisation of the *zero spillover controller* that is useful for implementation. To that aim, the paper starts with specifying a realisation of the *approximate Zero Spillover Controller* from which the *ZSC* can be recovered asymptotically if the *ZSC* would not be realisable. Furthermore the paper determines the conditions under which the *AZSC* stabilises the closed-loop transfer function. The authors come to the interesting conclusion that a generalisation of the *AZSC* for the general MIMO case can be found by using standard LQG theory.

It is interesting to note that the results obtained in paragraph 2.2.5 lead to a similar conclusion. Also in that application, it was found that maximum performance was achieved by locating the feedback sensor as close as possible to the disturbance source. This suggests that, though a feedback sensor in feedback controllers is conceived to provide information about the system response to the control action, the feedback sensor rather acts as a reference sensor (as in feedforward control) and the state observer rather acts as a disturbance observer. This assumption implies that system response to the control action can be derived accurately from the system model (The relatively poor control results that have been achieved in the experiments of paragraph 2.2.5 are very probably also due to the latter constraint). It is important to note that this latter conclusion is confirmed by the work of Elliott *et al.* [173], who showed that a general feedback control system can be written as a feedforward controller if one disposes of an

internal model of the plant which is exactly equal to the plant transfer function. In fact, this feedforward representation goes back to the *Youla parameterisation* technique, which is a formulation to parameterise all stable controllers, and which has been used extensively in the design of H_∞ controllers (refer, e.g. to [87], pp. 36 - 42; and [74], pp. 94 - 98) until state space solutions have been proposed which solve the H_∞ control problem by solving two Riccati equations [88].

Another equivalence relation between feedback and feedforward control was derived from LQG control theory by Doelman [171]. His paper basically addresses the problem that the optimal broadband feedforward control filter is not always realisable because of causality and stability constraints, as explained in paragraph 2.3.4. The paper first shows that the more reverberant the primary sound field is, the less the deterioration of the control performance due to these constraints is. The paper then presents a fundamental approach to deal with these problems by deriving the feedforward case from the theory of LQG control. Furthermore, a strategy is proposed to reach the LQG solution using a recursive estimator. From that perspective, the RLMS algorithm is discussed and it is shown that the RLMS algorithm actually converges to the LQG solution only under a strict condition. It must be noted -this is acknowledged in the paper- that the formulation results in a very severe condition for acoustic systems.

2.4.3 An alternative classification of active control systems

The previous paragraph illustrates that, for time-invariant systems subject to stationary disturbances, the difference to LQ-type controllers and a fully converged filtered-X LMS controller is irrelevant provided the optimal feedforward control filter can be described by a causal and stable transfer function. The reason why the one is preferred over the other often depends on the background of the actual control engineer who is responsible for the implementation. This has resulted in a number of studies where the performance and stability features of filtered-X LMS have been explained from a feedback point of view [172] on the one hand, and studies where feedback controllers are designed using a feedforward approach [173] on the other hand.
There is, however, a clear distinction to be made between the control approaches to the various active control applications. Rather than to

distinguish feedback from feedforward control, it seems to be more relevant to distinguish LTI control designs from adaptive control algorithms. In contrast to LTI controllers, adaptive controllers have the ability to track time variation in system transfer functions and disturbance sources, or to cope with non-linearities (to a certain extent). Adaptive controllers may alternatively be used to adaptively find a realisable to optimum a quadratic cost function in cases where the design of an LTI controller is constrained by the degree to which the system transfer function can be described (and hence by the complexity of the system transfer function).
Probably the single most used adaptive control algorithm in active control of vibration and sound is the filtered-X LMS algorithm. It must, however, be stressed that adaptive feedback controllers have been developed and applied in active control as well (a fully adaptive SISO feedback controller in [165], pp. 86 - 88; a self tuning LQG algorithm in [55]). They have not been discussed in this chapter because they appear relatively rarely in active control. In general, it is not so straightforward to derive bounds which guarantee unconditional robust performance of the adaptive feeback controller. When comparing adaptive feedback controllers with the filtered-X LMS algorithm, it is not so evident to make them work in practice.

2.5 CONCLUSIONS

This chapter presents and discusses the control theory and control techniques which are relevant to active control of vibration and sound. The aim of presenting this overview is twofold. Firstly, the current state of the art is outlined and standard formulae are given which allow the implementation of either of the algorithms presented. Secondly, it is shown how these most currently applied active control techniques relate to the vast background constituted by the "traditional" control theory (this includes modern and robust control). To this aim, the overview is not presented as a inventory of heuristic rules which would make active control look more like a black art rather than a control theory. This way it is stressed that active control should not be considered as a completely separate class of control techniques. In the end, this should lead to a better understanding of the basic mechanisms behind these techniques.

Two practical examples, the active control of duct noise and the active control of power flow in a finite plate, have been presented as an illustration of the theoretical issues.
Some of the equivalences between feedback and feedforward control have been touched upon and a new classification, distinguishing LTI and adaptive control systems, has been motivated.

This chapter has not dealt with control approaches such as Artificial Neural Networks (ANNs) and Fuzzy Logic. These approaches are said to be more suited to control problems where the model of the process is ill-defined, incomplete, or too non-linear to deal with it by conventional means. Applications of ANNs and fuzzy logic to active control have been presented in a few papers (e.g. [174 - 176]). It must, however, be acknowledged that the application of ANNs is not anticipated in the near future [177] : the technique is backed by a complicated theoretical basis (literature survey presented in [178], 29 pages and 177 references) and the computational burden associated with the implementation is substantial.

CHAPTER 3

A FEEDBACK CONTROL STRATEGY FOR ACTIVE STRUCTURAL ACOUSTIC CONTROL

3.1 INTRODUCTION

This chapter presents a general method for the active suppression of radiated sound power by means of active control of the vibration of the radiator. The method is general in the sense that it is applicable for any kind of disturbance (harmonic, transient, or broadband random) for which it is not assumed that there is a coherent reference available, and that it guarantees reduction of the total radiated sound power for any configuration of the control actuators and error sensors. The first requirement is satisfied by realising the control objective with a feedback controller. The second requirement is satisfied by designing a controller that minimises a cost function that is an exact expression for the total sound power radiated.
In order to determine the forces that control the vibro-acoustic response of the radiator, the controller measures vibration levels on the structure, rather

than acoustic responses. A model for the fluid-structure interaction is integrated into the design of the controller which allows to optimally control a cost function which expresses the sound power radiated from the radiator into the free field or the acoustic energy in an enclosure due to sound radiated into the enclosure. As shown before in paragraph 1.2.3 this approach is essentially different from other strategies such as minimising the sound pressure at a specified set of locations which strategy is conceivably dependent on the directivity pattern of the radiating structure and hence the control performance is heavily dependent on the choice of these locations. Moreover, as the control configuration as it is presented here does not require a set of error microphones located in the sound field generated by the radiator, it results in a more practical configuration for applications where the sound field is controlled in an environment where people may be expected to move around.

The feedback controller is synthesised in the state space. The control approach is based on the technique which has first been presented by Baumann *et al.* in [51] where the technique is applied to controlling the sound power radiated by an impulsively excited beam (simulations only). Simulation results for control of a beam subjected to broadband disturbances have been presented shortly after [52]. The same approach is also used as a starting point in the work performed by Thomas *et al.* [53 - 55]. In [53] the basic concepts are reiterated from [51] after which preliminary simulation results are presented for a simply supported rectangular plate. Experimental results obtained with applying the technique to a panel representing the interior trim panel of an aircraft are presented in [54] and [55] (in [55] a self-tuning feedback controller is described and tested). The test set-up used in these publications, however, is a stiff and light panel which acts as a rigid panel up to relatively high frequencies (500 Hz) as a result of which only one rigid body mode of the panel is significant in the radiation behaviour. The control objective in [54] and [55] is, therefore, the minimisation of the velocity measured by a centrally placed accelerometer. The control configuration consists of one control actuator and one error sensor and hence the system model reduces to a relatively low order filter. Other authors dealing with design of state space controllers for control of sound radiation from a rectangular panel (e.g. [199] have reduced the problem to controlling the vibration response of the plate which has been shown to be an inferior approach (refer to paragraph 1.2).

In the work presented here, the control technique introduced by Baumann [51] has been generalised and complemented with a new identification procedure which greatly enhances the applicability of the control approach to systems other than beams or rectangular plates acting as a rigid body. Furthermore, the control approach has successfully been implemented to control the sound radiated from a rectangular plate.

This chapter starts with deriving state space models that describe *(i)* the structural response of a structure to a point force excitation, and *(ii)* the sound power that is radiated due to that structural response. Both radiation into the free field as well as radiation into an enclosure are considered. Next, the design of the controller is discussed, after which a series of experiments is described in which the technique is applied to controlling the sound radiated from an elastic rectangular baffled plate.

3.2 STRUCTURALLY RADIATED SOUND

Structurally radiated sound originates at the surface of a vibrating structure. Derivation of the equations describing the motion of a distributed parameter system has been undertaken many times before but is re-iterated for completeness. The control problem can be described as controlling the structural response (or displacement) of a distributed structure whose behaviour is governed by a partial differential equation :

$$\mathscr{L}w(x,t)+\mathscr{C}\dot{w}(x,t)+m(x)\ddot{w}(x,t)=\sum_{j=1}^{L}f_j(x,t)\,, \tag{3.1}$$

where $w(x,t)$ is the normal structure displacement, at time t, at any point with generalised co-ordinate x, which is located inside the domain of the structure. $\mathscr{L}$ is a homogeneous spatial differential stiffness operator of order $2p$, $\mathscr{C}$ is a homogeneous spatial differential damping operator, $m(x)$ is the mass density and $f_j(x,t)$ (j = 1, 2, …, L) are L distributed forces applied to the structure. The solution $w(x,t)$ of eq. (3.1) is subject to p boundary conditions

$$B_i w(x,t)=0, \quad x=\Gamma\,, \tag{3.2}$$

where B_i is a differential operator of maximum order $2p$-1, and Γ defines the boundary of the structure.
Invoking the expansion theorem [97] assumes a solution in the form :

$$w(x,t) = \sum_{i=1}^{\infty} W_i(x)\eta_i(t), \tag{3.3}$$

where $\eta_i(t)$ are the *modal amplitudes* or *modal participation factors*. Modal expansion is achieved by solving the differential eigenvalues problem

$$\mathscr{L}W(x) = \lambda m(x)W(x) \tag{3.4}$$

for the eigenvalues $\lambda_i = \omega_i^2$ (where ω_i is the *eigenfrequency* of mode *i*) and eigenfunctions $W_i(x)$ (the *modeshape* of mode *i*). The eigenfunctions are orthogonal and can be normalised as to satisfy the orthonormality conditions

$$\int_{\Omega} mW_iW_k dx = \delta_{ik}, \quad \text{for } i,k = 1,2,... \tag{3.5a}$$

$$\int_{\Omega} W_i \mathscr{L} W_k dx = \omega_i^2 \delta_{ik}, \quad \text{for } i,k = 1,2,... \tag{3.5b}$$

$$\int_{\Omega} W_i \mathscr{C} W_k dx = 2\zeta_i \omega_i \delta_{ik}, \quad \text{for } i,\ k = 1,2,... \tag{3.5c}$$

where Ω is the domain of the structure.
Introducing (3.3) in (3.1), multiplying with W_k, integrating over the domain Ω and considering the orthonormality relations (3.5 a - c), an infinite set of independent second-order ordinary differential equations, *modal equations*, is obtained :

$$\ddot{\eta}_i(t) + 2\zeta_i\omega_i\dot{\eta}_i(t) + \omega_i^2\eta_i(t) = F_i(t), \quad i = 1,2,... \tag{3.6}$$

where $$F_i(t) = \sum_{j=1}^{L} \int_{\Omega} W_i(x) f_j(x,t) dx \tag{3.7}$$

are *modal forces*.
In general, a reduced set of *N* eigenfunctions will be used to describe the structural response in order to reduce the *order* of the model, i.e. the number of decoupled equations in (3.6).

Closed-form eigensolutions only exist in a limited number of cases. E.g. in the case in which the damping operator does not satisfy orthonormality condition (3.5c), no closed-form solution of (3.1) is possible (condition (3.5c) will only be satisfied in the case of *proportional damping* [97]) as a result of which the system will not lend itself to the decoupling procedure described here.
In those cases an approximate solution is expressed using a set of *comparison functions*[1] ϕ_k ($k = 1, 2, \ldots, n$) in the form :

$$w(x,t) = \sum_{k=1}^{n} \phi_k(x) q_k(t) \,. \tag{3.8}$$

Inserting (3.8) into (3.1), multiplying by ϕ_j ($j = 1, 2, \ldots, n$), and integrating over the domain Ω, a set of n second-order ordinary differential equations is obtained which can be written in the matrix form

$$\mathbf{M}\ddot{\mathbf{q}}(t) + \mathbf{C}\dot{\mathbf{q}}(t) + \mathbf{K}\mathbf{q}(t) = \sum_{j=1}^{L} \mathbf{Q}_j(t) \,, \tag{3.9}$$

in which $\mathbf{q}(t) = \left[q_1(t) \;\; q_2(t) \;\; \ldots \;\; q_n(t)\right]^T$ is a vector of generalised participation factors. The definition of the vector of generalised forces $\mathbf{Q}_j(t) = \left[Q_{1j}(t) \;\; Q_{2j}(t) \;\; \ldots \;\; Q_{nj}(t)\right]^T$ and of **M**, **C**, and **K** (resp. mass, damping, and stiffness matrices) is given in appendix 3A. The solution of equation (3.9) can again be obtained by the modal approach, resulting in a finite set of decoupled equations as in (3.6). The modes, obtained from the eigenvalue problem, are eigenvectors instead of eigenfunctions ; the number of modes, is finite and equal to n.
In the remainder of this chapter, it will be assumed that the structural response is expressed as a reduced series of N modes.

State space description of the dynamic behaviour of the structure can then be obtained from (3.6) :

---

[1] *Comparison functions* are functions that are $2p$ times differentiable and satisfy all boundary conditions (3.2), but not necessarily the differential equation (3.4). An approximate solution in the form (3.8) can be realised in finite element code.

$$\begin{aligned} \dot{\mathbf{x}}(t) &= \mathbf{A}\mathbf{x}(t) + \mathbf{B}\mathbf{u}(t) \\ \mathbf{y}(t) &= \mathbf{C}\mathbf{x}(t) + \mathbf{D}\mathbf{u}(t) \end{aligned} \tag{3.10}$$

where $\mathbf{x}(t) = \left[\eta_1(t) \;\; \dot{\eta}_1(t) \;\; \eta_2(t) \;\; \dot{\eta}_2(t) \;\; \ldots \;\; \eta_N(t) \;\; \dot{\eta}_N(t)\right]^T$ is a $2N \times 1$ dimensional state space vector, the $2N \times L$ input vector $\mathbf{u}(t)$ comprises the input forces ($\mathbf{B}\mathbf{u}(t)$ are the inputs transformed into the modal domain) ; $\mathbf{y}(t)$ is a $K \times 1$ output vector of which any element can be any linear combination of the system states and the inputs.

With this state space model (3.10), the velocity distribution over the structure can be calculated as a function of any kind of input. From the velocity distribution, a measure of the radiated acoustic energy can be calculated. At this point, it is important to note that the acoustic radiation from a vibrating structure is not only determined by the velocity distribution over its surface, but also by the acoustic impedance that at the surface of the structure (the acoustic impedance is the ratio of sound pressure over particle velocity). The sound energy passing through a surface in the vicinity of the vibrating structure can be expressed by means of the acoustic intensity $\mathbf{I}(t)$. The intensity is a time-dependent, vector-valued quantity, defined as the sound power per unit area [180] :

$$\mathbf{I}(t) = p(t)\mathbf{v}(t)\,, \tag{3.11}$$

where $p(t)$ and $\mathbf{v}(t)$ are sound pressure and vector-valued particle velocity, respectively.
Assuming a simple harmonic plane wave, where $p(t)$ and $\mathbf{v}(t)$ pulsate at the same frequency but with a phase difference equal to ψ, then the instantaneous value of the intensity can be calculated from (3.11) as

$$\mathbf{I}(t) = p\mathbf{v}\sin(\omega t)\sin(\omega t + \Psi) = \frac{1}{2}p\mathbf{v}(1-\cos 2\omega t)\cos\Psi + \frac{1}{2}p\mathbf{v}\,\sin 2\omega t\,\sin\Psi\,. \tag{3.12}$$

Two specific cases can be distinguished. Assuming phase angle $\psi = 0$, the second term in (3.12) vanishes and acoustic energy propagates through the unit surface with a pulsation twice as high as the frequency of the acoustic wave. The time-averaged intensity, obtained by integrating (3.12) over one period, is constant (and equal to $\frac{1}{2}p\mathbf{v}$). If, on the other hand, the phase angle $\Psi = \frac{\pi}{2}$ or $\frac{-\pi}{2}$, the time-averaged intensity is zero, which means that

energy oscillates through the surface resulting in zero net energy transport. This is the case in pure standing wave fields.
For any other phase angle which follows from the acoustic impedance, none of the terms in (3.12) vanishes and thus a part of the energy propagates, whereas another part oscillates in the wave without contributing to the energy transport.
Based upon these observations it is clear that, in order to adequately express the nuisance due to the sound radiated from a vibrating structure, it is necessary to distinguish acoustic radiation to the free field on the first hand, and acoustic radiation into a cavity on the second hand.
In the first case, the vibrating structure will generate a flow of acoustic energy that flows from the structure to the free field. One can look at this case as if the free field *absorbs* all the acoustic energy that is generated by the radiator. Reduction of the acoustic energy in the free field due to the radiation from the vibrating structure can thus be re-formulated as the reduction of active acoustic power flow from the structure. In the second case, however, active acoustic power flow will only exist if absorbers are located in the cavity (in which case energy will flow from the radiator towards the absorbers, in which the energy is dissipated). In the case where the cavity is undamped, all acoustic power will be reactive and there will be no active acoustic power flow. The acoustic excitation due to a vibrating structure will give rise to a standing wave field in which the energy oscillates, but does not propagate. Therefore the reduction of the sound radiation into the cavity needs to be formulated as the reduction of total acoustic energy in the cavity.

Radiation into the free field

An expression will be derived for the sound power that is radiated to the far field. The *far field* is a distance R from the structure where $kR >> 1$ (k is the acoustic wavenumber defined by $k = \omega/c$ where ω is the pulsation and c is the speed of sound). The sound waves, originating at the surface of the vibrating structure, can be assumed to be plane waves in the far field. The total acoustic energy E_{tot} that is radiated by a vibrating structure can be calculated as the time-integral of the sound power transmitted through a surface enclosing the radiator. Thus

$$E_{tot} = E(\infty) = \int_0^\infty \int_S \mathbf{I}(t)\, dS\, dt\,, \tag{3.13}$$

where S is a surface enclosing the radiator (e.g. a sphere).

Applying Parseval's theorem, the time-integral expression (3.11) is transformed to the frequency domain under the assumption of system causality (i.e. $\mathbf{I}(t) = 0$ for $t < 0$) :

$$E_{tot} = \frac{1}{\pi} \int_0^\infty \int_S \mathbf{I}(\omega)\, dS\, d\omega \,. \tag{3.14}$$

With this transformation, the development can be pursued in the frequency domain which means that all physical quantities can be treated as complex-valued functions of frequency. For clarity, the same symbols will be used to denote the complex amplitude of the same physical quantities either in the frequency and the time domain. Time or frequency dependence will be explicitly mentioned whenever this would not be clear from the context.

A frequency domain expression for the acoustic intensity is determined from the definition of acoustic intensity in the time domain (3.12). In the frequency domain, particle velocity and sound pressure are complex quantities, as a result of which it is easy to show that their complex product

$$\frac{1}{2} p(\omega)\mathbf{v}^*(\omega) = \frac{1}{2} \Re\{p(\omega)\mathbf{v}^*(\omega)\} + \frac{1}{2} j\Im\{p(\omega)\mathbf{v}^*(\omega)\} \tag{3.15}$$

corresponds to equation (3.12) but in the complex (frequency) domain.

Particle velocity and sound pressure are related by the *acoustic impedance* of the medium through which the sound waves propagate. By virtue of the wave equation for free propagating plane waves, and the momentum equation that relates time derivative of sound pressure with spatial derivative of particle velocity, the acoustic impedance in the far field is real and constant as a function of frequency : $v = \frac{p}{\rho c}$ (where ρ is the mass density of air). In that case, expression (3.15) will be strictly real. Furthermore, knowledge of the sound pressure in the far field suffices to calculate the total acoustic energy that is radiated by the structure. Expression (3.14) is then solved by determining the sound pressure at each point of S. The surface S will be described in a spherical co-ordinate system (R, ϕ, θ).

If no fluid loading on the structure is taken into account, the sound pressure at a point (R, ϕ, θ) due to the vibration of the structure, can be expanded as a function of the structural modes only

$$p(R,\phi,\theta,\omega)=\sum_{i=1}^{N} H_i(R,\phi,\theta,\omega)\dot{\eta}_i(\omega)=\sum_{j=1}^{N} H_j(R,\phi,\theta,\omega)\, x_{2j}(\omega)\,, \qquad (3.16)$$

where $H_i(R,\phi,\theta)$ is the transfer function determining the contribution of mode i to the radiated sound pressure. Therefore these transfer functions are determined by the vibration patterns (*mode shapes*) of the structure. An expression for $H_i(R,\phi,\theta)$ can be obtained after numerical integration of the *Rayleigh integral* (cfr. example in paragraph 3.4) or using the acoustical *BEM* (boundary element method) or *FEM* (finite element method) [181].

With $\mathbf{H}=[H_1 \;\; H_2 \;\; \ldots \;\; H_N]$ and $\mathbf{n}=[\dot{\eta}_1 \;\; \dot{\eta}_2 \;\; \ldots \;\; \dot{\eta}_N]^T$, where $\mathbf{n}$ is the frequency-dependent vector comprising the complex amplitudes of the modal velocities (in which the pulsation has been omitted for clarity), exp. (3.16) reduces to the vector form :

$$p(R,\phi,\theta,\omega)=\mathbf{H}\cdot\mathbf{n}\,. \qquad (3.17)$$

Combination of (3.14), (3.15) and (3.17) yields an expression for the total radiated acoustic energy as a function of the structural mode shapes :

$$E_{tot}=\frac{1}{2\pi\rho c}\int_0^{\infty}\int_S \mathbf{n}^H\mathbf{H}^H\mathbf{H}\,\mathbf{n}\,dS\,d\omega \qquad (3.18)$$

where $(\cdot)^H$ denotes *Hermitian* (complex conjugate) transpose.

Since $\mathbf{n}$ is independent of the position (R,ϕ,θ) in the free field, the surface integral over S is evaluated as follows :

$$\int_S \mathbf{H}^H\mathbf{H}\;dS=\mathbf{M}(\omega)\,. \qquad (3.19)$$

$\mathbf{M}(\omega)$ is a symmetric, positive semi-definite, frequency-dependent $N \times N$ matrix of which each element $\mathbf{M}[i,j]$ determines the contribution to E_{tot} of structural mode i if the structural response would be a combination of modes i and j only (so it resembles a modal radiation efficiency). Assuming existence of a spectral factor $\mathbf{G}(\omega)$ (the conditions for existence as well as a procedure to obtain the spectral factor are given in the next section) such that $\mathbf{M}(\omega)=\mathbf{G}^H(\omega)\mathbf{G}(\omega)$, expression (3.15) reduces to

$$E_{tot} = \frac{1}{2\pi\rho c}\int_0^\infty \mathbf{n}^H \mathbf{G}^H \mathbf{G}\,\mathbf{n}\, d\omega = \frac{1}{2\pi\rho c}\int_0^\infty \mathbf{z}^H \mathbf{z}\, d\omega\,, \tag{3.20}$$

where $\mathbf{z}$ is a $N \times 1$ vector resulting from passing the vector of modal velocities, $\mathbf{n}$, through the system $\mathbf{G}$. A time-domain expression can be obtained by applying Parseval's theorem :

$$E_{tot} = \frac{1}{2\pi\rho c}\int_0^\infty \mathbf{z}(t)^T \mathbf{z}(t)\, dt\,, \tag{3.21}$$

where $\mathbf{z}(t)$ is obtained by inverse Laplace transform of $\mathbf{z}(s)$, with $s = j\omega$ (recall that the same symbols have been used for frequency and time domain).

Following the terminology introduced by Baumann *et al.* [51], $\mathbf{G}(\omega)$ can be referred to as a *radiation filter*, to which the modal velocities are input and of which the 2-norm of the output vector is a measure for the acoustic energy that is radiated by the given vibration pattern. Once the frequency domain model representation for $\mathbf{G}$ has been determined applying techniques described in paragraph 3.3, the system can be described in its state space form :

$$\begin{aligned} \dot{\mathbf{r}} &= \mathbf{A}_G \mathbf{r} + \mathbf{B}_G \mathbf{n} \\ \mathbf{z} &= \mathbf{C}_G \mathbf{r} + \mathbf{D}_G \mathbf{n} \end{aligned} \tag{3.22}$$

in which $\mathbf{r}$ is a $N_G \times 1$ state vector, where N_G is the order of the model of the spectral factor $\mathbf{G}$.
Combining expressions (3.10) and (3.22) yields a state space description for the acoustic energy that is radiated by the vibrating structure as a function of the input forces :

$$\begin{aligned} \begin{bmatrix} \dot{\mathbf{x}} \\ \dot{\mathbf{r}} \end{bmatrix} &= \begin{bmatrix} \mathbf{A} & \mathbf{O}_{N_G \times N_G} \\ \tilde{\mathbf{B}}_G & \mathbf{A}_G \end{bmatrix} \begin{bmatrix} \mathbf{x} \\ \mathbf{r} \end{bmatrix} + \begin{bmatrix} \mathbf{B} \\ \mathbf{O}_{N_G \times L} \end{bmatrix} \mathbf{u} = \mathbf{A}_e \begin{bmatrix} \mathbf{x} \\ \mathbf{r} \end{bmatrix} + \mathbf{B}_e \mathbf{u} \\ \mathbf{z} &= \begin{bmatrix} \tilde{\mathbf{D}}_G & \mathbf{C}_G \end{bmatrix} \begin{bmatrix} \mathbf{x} \\ \mathbf{r} \end{bmatrix} + \mathbf{O}_{N \times L} \mathbf{u} = \mathbf{C}_1 \begin{bmatrix} \mathbf{x} \\ \mathbf{r} \end{bmatrix} + \mathbf{D}_1 \mathbf{u} \\ \mathbf{y} &= \begin{bmatrix} \mathbf{C} & \mathbf{O}_{K \times N_G} \end{bmatrix} \begin{bmatrix} \mathbf{x} \\ \mathbf{r} \end{bmatrix} + \mathbf{D}\mathbf{u} = \mathbf{C}_2 \begin{bmatrix} \mathbf{x} \\ \mathbf{r} \end{bmatrix} + \mathbf{D}_2 \mathbf{u} \end{aligned} \tag{3.23}$$

where $\mathbf{O}_{r\times s}$ is a $r \times s$ null matrix, $\tilde{\mathbf{B}}_G(i,2j) = \mathbf{B}_G(i,j)$, $i = 1,\ldots,N_G$, $j = 1,\ldots,N$; and $\tilde{\mathbf{B}}_G(i,2j-1) = 0$, $i = 1,\ldots,N_G$, $j = 1,\ldots,N$ (similar definition applies to $\tilde{\mathbf{D}}_G$). Subscript *e* refers to "extended system matrices".

Having obtained the state space description of the control problem, a feedback controller will be designed that reduces the total acoustic energy that is radiated by the vibrating structure. The controller will drive a subset of the system inputs, **u**, in order to control the system response. This *M*-dimensional subset, *the control inputs*, will be referred to as $\mathbf{u}_c$. Referring to figure 2.1, the corresponding input matrices will be referred to as $\mathbf{B}_2$, and $\mathbf{D}_{12}$ (coupling to output **z**) and $\mathbf{D}_{22}$ (coupling to output **y**). These matrices are obtained by selecting corresponding columns from $\mathbf{B}_e$, $\mathbf{D}_1$ and $\mathbf{D}_2$. The *L* - *M* remaining system inputs represent external (exogenous) disturbances that excite the system (*process noise*, joined in the vector $\mathbf{u}_w$), corresponding input matrices are referred to as $\mathbf{B}_1$, and $\mathbf{D}_{11}$ (coupling to output **z**) and $\mathbf{D}_{21}$ (coupling to output **y**).

Identification of equation (3.21) with (2.9) shows that the $M \times (2N + N_G)$ feedback matrix **K,** which optimises a balance between the reduction of radiated sound power and associated control energy, can be determined using LQG-control theory (from equation 2.10). In the general expression (2.11) for the cost function that is optimised by the controller, $\mathbf{Q}_{ctr}$ needs to be chosen as the identity matrix ; $\mathbf{R}_{ctr}$ may be any positive definite matrix. The ARE is then solved using the extended system matrices described in (3.23).

Note that an alternative control objective exists in the sense that one could design a controller that reduces the vibration of the structure without taking the radiation behaviour (the radiation filter) into account. Recalling that the state vector of the structural model comprises amplitudes of modal displacements and modal velocities, this is realised by optimising a cost which is function of states **x** of the structural model (a subset of the extended state vector $\mathbf{x}_e$) as in (3.24) :

$$J_{vib} = \lim_{T\to\infty} \frac{1}{T} E\left\{\int_0^T \left(\mathbf{x}^T \mathbf{Q}_v \mathbf{x} + \mathbf{u}_c^T \mathbf{R}_v \mathbf{u}_c\right) d\tau\right\}. \qquad (3.24)$$

The associated feedback matrix, referred to as $\mathbf{K}_v$, is now found solving the ARE

$$\mathbf{S}_v\mathbf{A} + \mathbf{A}^T\mathbf{S}_v - \mathbf{S}_v\tilde{\mathbf{B}}_2\mathbf{R}_v^{-1}\tilde{\mathbf{B}}_2^T\mathbf{S}_v + \mathbf{Q}_v = 0 \tag{3.25}$$

for $\mathbf{S}_v = \mathbf{S}_v{}^T$, where $\tilde{\mathbf{B}}_2(i,j) = \mathbf{B}_2(i,j)$ for $i = 1,\ldots,2N$, and $j = 1,\ldots,M$; after which $\mathbf{K}_v = \mathbf{R}_v{}^{-1}\tilde{\mathbf{B}}_2^T\mathbf{S}_v$ is solved.

Though sound radiation will indeed be reduced when structural vibration is reduced, this approach leads to a larger control effort to achieve the same control performance. This is easily understood by noting that $\mathbf{M}(\omega)$ is, in general, not diagonal because structural modes do not radiate independently from each other. This issue will be treated more into detail in paragraph (3.4).

Radiation into a cavity

In the case of an undamped cavity, the sound pressure and particle velocity field as a function of time and location can completely be expressed by means of standing waves. Sound pressure and particle velocity oscillate at the same pulsation but with a 90 degrees phase shift and thus all acoustic power is reactive. The total acoustic energy, which is the sum of potential and kinetic energy, is constant because potential and kinetic acoustic energy will oscillate with the same amplitude and pulsation (twice the pulsation of the standing wave field), but with a 180 degrees phase shift : potential energy reaches its maximum when the kinetic energy vanishes and vice versa. Therefore the total acoustic energy can be expressed as the time average of the potential energy only. Sound reduction in a cavity due to persistent exogenous excitation is thus expressed as the reduction of the following cost function :

$$\lim_{T\to\infty}\frac{1}{T}E\left\{\int_0^T\int_V p^2(x,y,z,t)\,dV\,dt\right\}, \tag{3.26}$$

where V is the volume of the cavity.

Expressing the sound pressure as a function of the structural modal co-ordinates and vibro-acoustic transfer functions H_i, as in (3.16), it is clear that

this case leads to a similar expression as (2.11) and thus a controller is found in the same way. The nature of the vibro-acoustic transfer functions H_i is somewhat different from the free field case in the sense that H_i will not only be determined by the modal behaviour of the structure but also by the acoustic modal behaviour of the cavity. For simple cavity geometries, such as a cylinder or a rectangular cavity, these acoustic modes can be determined analytically [67].

In the case where damping occurs within the cavity, a certain amount of active power will flow due to the fact that sound pressure and particle velocity will no longer be 90 degrees phase shifted (with an exception for resonance frequencies). The acoustic intensity will not be purely real nor purely imaginary, indicating that a part of the energy propagates, whereas another part oscillates in the wave without contributing to the energy transport. The amount of energy that is transported from the source(s) to the absorber(s) depends on the amount of damping that is present. Note that in case there would be substantial damping, all acoustic energy produced by the radiator, would be absorbed by the damper which reduces the problem to the case of free-field radiation. The case where the cavity is very lightly damped, which actually is more likely to lead to a noise problem, would be treated as the undamped case for which an active control solution is designed as described above.

Vibro-acoustic coupling

A general remark pertains to the assumption that fluid loading will not affect the vibration behaviour of the structure. Though this assumption will generally hold for free radiating structures, substantial error may be introduced in the case of sound radiation into cavities of which the walls have a low dynamic stiffness (such as the cavity between the trim and the skin panel of an aeroplane). In the latter case, the behaviour of the structural system will be influenced by the acoustic system and vice versa (which phenomenon is referred to as vibro-acoustic *coupling*). As a consequence, the sound pressure needs to be expressed as a function of the *coupled modes*, these are the eigenfunctions (or eigenvectors) of the coupled system. The coupled system is described by a coupled set of differential equations, which are derived from the differential equation describing the structural response under structural as well as acoustic loading (3.27) and the

Helmholtz equation describing the response of the acoustic medium subject to simultaneous acoustic and structural excitation (3.28) :

$$\mathscr{D}w(x,t)+\mathscr{C}\dot{w}(x,t)+m(x)\ddot{w}(x,t)=\sum_{j=1}^{L}f_j(x,t)+l_p(x,t)\,, \tag{3.27}$$

where $l_p(x,t)=\int_{\Gamma_c} p(x,t)\,d\Gamma_c$ is loading on the boundary surface Γ_c of the cavity due to the acoustical pressure $p(x,t)$;

$$\nabla^2 p(x,t)-\frac{1}{c^2}\cdot\frac{\partial^2 p(x,t)}{\partial t^2}=-\rho\cdot\dot{q}_v(x,t)+\frac{\partial}{\partial t}l_f(x,t)\,, \tag{3.28}$$

where $l_f(x,t)=\int_{\Gamma_c}\rho\,\dot{w}(x,t)\,d\Gamma_c$ is the excitation of the acoustic medium due to the normal vibration of boundary surface Γ_c of the cavity.

A coupled set of equations is obtained by substituting an expression for sound pressure, obtained from (3.28), in (3.27); and an expression for the normal vibration of the cavity surface, obtained from (3.27), in (3.28). Rewriting the problem in a generalised eigenvalue problem, yields the coupled modes and resonance frequencies.

3.3 SPECTRAL FACTORISATION OF POSITIVE DEFINITE SPECTRA

The radiation behaviour of the structure is determined by numerical integration of expression (3.19), which yields a matrix $\mathbf{M}(\omega)$ which is a symmetric, positive semi-definite, frequency-dependent $N\times N$ matrix ; or in other words, $N\times N$ series of real-valued numbers as a function frequency. The aim is to find a state space model for $\mathbf{G}(\omega)$ such that $\mathbf{M}(\omega)=\mathbf{G}^H(\omega)\mathbf{G}(\omega)$.

Some methods to obtain a state space model for $\mathbf{G}(\omega)$ from $\mathbf{M}(\omega)$-data have been suggested in [51]. A first way to compute the spectral factorisation is to perform a Cholesky (or other, such as SVD) decomposition of the $\mathbf{M}(\omega)$ matrices, which yields the spectral factors $\mathbf{T}(\omega)$ at the given frequencies. A state space model that describes the radiation behaviour of the structure can then be obtained by fitting a frequency function to the curves obtained from $\mathbf{T}(\omega)$, which is essentially a *system identification* procedure. A typical

parametric approach to this identification problem would consist of using a non-linear least squares criterion, that is then optimised using a non-linear search in the parameter space. However, due to the positive-definiteness of the spectral factors $\mathbf{T}(\omega)$, an a-priori parameterisation will be hard to find, and numerical and convergence problems are very likely to occur.
A second way, also suggested in [51], is to find a state space realisation for $\mathbf{M}(\omega)$ directly (through non-linear least squares), and then apply state space factorisation methods described by Francis [182] (chapter 7, Factorisation Theory). Again, due to the positive-definiteness of $\mathbf{M}(\omega)$, the identification part of this procedure will tend to be very involving. Furthermore the application of the factorisation methods described in [182] is not straightforward and requires considerable effort for each new case.

As the spectral factorisation step is a fundamental phase in the design of the controller, a more profound approach to this problem is suggested here. The procedure described in the sequel essentially stems from the domain of system identification and consists basically in the application of a new subspace algorithm for the identification of multi-input multi-output linear discrete time systems from a given set of power spectrum data. The development of the identification algorithm is the result of the joint work of both the department ESAT (development of the algorithm in its basic form) and PMA as described in a number of joint papers (e.g. [183 - 184]). The developed identification algorithm is briefly outlined below.

Given : $N_M + 1$ matrices $\mathbf{S}_k \in \mathbb{C}^{N \times N}$ representing the spectrum of $\mathbf{M}(z)$ evaluated in $N_M + 1$ equidistant points over the unit circle :

$$\mathbf{S}_k = \mathbf{M}\left(e^{j\frac{2\pi k}{N_M}}\right) \quad , \quad k = 0, \ldots, N_M \tag{3.29}$$

A state space realisation $\mathbf{A}_G$, $\mathbf{B}_G$, $\mathbf{C}_G$, $\mathbf{D}_G$ of the discrete-time system $\mathbf{G}(z)$ is determined with the following procedure :

- Expand the $N_M + 1$ given points $\mathbf{S}_k$ to a signal of length $2N_M$: $\mathbf{S}_{N_M+k} = \mathbf{S}^*_{N_M-k}$ for $k = 1, \ldots, N_M - 1$.
- Compute the $2N_M$ points inverse discrete Fourier transform s_k of the signal $\mathbf{S}_k$.
- Form the block-Hankel matrix $\mathbb{S} \in \mathbb{R}^{Nq \times Nr}$ as in (3.30) :

$$\mathbb{S} \overset{\text{def}}{=} \begin{pmatrix} s_1 & s_2 & s_3 & \cdots & s_r \\ s_2 & s_3 & s_4 & \cdots & s_{r+1} \\ s_3 & s_4 & s_5 & \cdots & s_{r+2} \\ \cdots & \cdots & \cdots & \cdots & \cdots \\ s_q & s_{q+1} & s_{q+2} & \cdots & s_{r+q-1} \end{pmatrix} \tag{3.30}$$

with the number of block rows $q \geq 2n$ and the number of block columns $r \geq 2n$, and $r+q \geq 2N_M$.

- Compute the Singular Value Decomposition :

$$\mathbb{S} = \begin{pmatrix} \mathbf{U}_1 & \mathbf{U}_2 \end{pmatrix} \begin{pmatrix} \mathbf{S}_1 & 0 \\ 0 & 0 \end{pmatrix} \begin{pmatrix} \mathbf{V}_1^T \\ \mathbf{V}_2^T \end{pmatrix}. \tag{3.31}$$

- The number of singular values $\mathbf{S}_1$ different from zero is equal to two times the system order (n).
- Determine $\mathcal{U}$ and $\mathcal{V}$ as : $\mathcal{U} = \mathbf{U}_1 \cdot \mathbf{S}_1^{\frac{1}{2}}$ and $\mathcal{V} = \mathbf{S}_1^{\frac{1}{2}} \cdot \mathbf{V}_1^T$.
- Determine the eigenvalue spectrum of $\underline{\mathcal{U}}^{+} \cdot \overline{\mathcal{U}}$ where $\underline{\mathbf{X}}$ and $\overline{\mathbf{X}}$ denote the matrix $\mathbf{X}$ with the N last respectively first rows deleted[2]. The stable eigenvalues of this spectrum are denoted $\alpha_1, \ldots, \alpha_{n_r}$ and $\beta_1 \pm \mathrm{j}\gamma_1, \ldots, \beta_{n_c} \pm \mathrm{j}\gamma_{n_c}$.

  Determine the system matrix $\mathbf{A}_G$ as $\mathbf{A}_G = \Omega(\alpha, \beta, \gamma)$, where

$$\Omega(a,b,c) \overset{\text{def}}{=} \begin{pmatrix} a_1 & \cdots & 0 & 0 & 0 & \cdots & \cdots & 0 & 0 \\ \cdots & \cdots & \cdots & \cdots & \cdots & \cdots & \cdots & \cdots & \cdots \\ 0 & \cdots & a_{n_r} & 0 & 0 & \cdots & \cdots & 0 & 0 \\ 0 & \cdots & 0 & b_1 & c_1 & \cdots & \cdots & 0 & 0 \\ 0 & \cdots & 0 & -c_1 & b_1 & \cdots & \cdots & 0 & 0 \\ \cdots & \cdots & \cdots & \cdots & \cdots & \cdots & \cdots & \cdots & \cdots \\ 0 & \cdots & 0 & 0 & 0 & \cdots & \cdots & b_{n_c} & c_{n_c} \\ 0 & \cdots & 0 & 0 & 0 & \cdots & \cdots & -c_{n_c} & b_{n_c} \end{pmatrix} \tag{3.32}$$

[2] In practice, when data are perturbed by noise, this simple solution is not guaranteed to have N stable and N unstable eigenvalues. An alternative solution, is to solve the symmetric characteristic polynomial which parametrises the null space of $\mathcal{U}$ which for each root r_k also has a root $1/r_k$. [183].

- Determine the matrix $\mathbf{Q} = \left(\mathbf{I}_n - \mathbf{A}_G{}^{2N_M}\right)^{-1}$. Determine the real matrix $\mathbf{T}^0 = \left(\mathbf{T}_1^0 \quad \mathbf{T}_2^0\right)$ from the eigenvectors of $\underline{\mathcal{U}^+} \cdot \overline{\mathcal{U}}$.
- Solve the following linear equation for the elements $\delta_k, \lambda_k, \rho_k$:

$$\mathcal{U}^+ . \Pi . \mathcal{V}^T = \mathbf{T}_1^0 . \mathbf{Q} . \Omega^T(\delta, \lambda, \rho) . \left(\mathbf{T}_2^0\right)^T + \mathbf{T}_2^0 . \Omega(\delta, \lambda, \rho) . \mathbf{Q}^T . \left(\mathbf{T}_1^0\right)^T \qquad (3.33)$$

where $\Pi \in \mathbb{R}^{N.N_M \times N.N_M}$ is the permutation matrix given by :

$$\Pi \overset{\text{def}}{=} \begin{pmatrix} 0 & 0 & \cdots & \mathbf{I}_N \\ \cdots & \cdots & \cdots & \cdots \\ 0 & \mathbf{I}_N & \cdots & 0 \\ \mathbf{I}_N & 0 & \cdots & 0 \end{pmatrix} \qquad (3.34)$$

- Determine the matrix $\mathbf{H}^T$ and the system matrix $\mathbf{C}_G$ as the $N \times N_M$ bottom right respectively top left sub-matrices of :

$$\left(\mathcal{U} . \mathbf{T}_1^0 \quad \mathcal{U} . \mathbf{T}_2^0 . \Omega(\delta, \lambda, \rho)\right) \qquad (3.35)$$

- Determine $\Lambda_0 = s_0 - \mathbf{C}_G \mathbf{A}_G^{2N_M - 1} \mathbf{Q} \mathbf{H} - \mathbf{H}^T \left(\mathbf{A}_G^T\right)^{2N_M - 1} \mathbf{Q}^T \mathbf{C}_G$.
- Find $\mathbf{P}$ through the solution of the Riccati equation (3.36)

$$\mathbf{P} = \mathbf{A}_G \mathbf{P} \mathbf{A}_G^T + \left(\mathbf{H} - \mathbf{A}_G \mathbf{P} \mathbf{C}_G^T\right)\left(\Lambda_0 - \mathbf{C}_G \mathbf{P} \mathbf{C}_G^T\right)^{-1} \left(\mathbf{H} - \mathbf{A}_G \mathbf{P} \mathbf{C}_G^T\right)^T \qquad (3.36)$$

and determine $\mathbf{B}_G$ and $\mathbf{D}_G$ as :

$$\mathbf{B}_G = \left(\mathbf{H} - \mathbf{A}_G \mathbf{P} \mathbf{C}_G^T\right) . \left(\Lambda_0 - \mathbf{C}_G \mathbf{P} \mathbf{C}_G^T\right)^{-1/2} \quad , \quad \mathbf{D}_G = \left(\Lambda_0 - \mathbf{C}_G \mathbf{P} \mathbf{C}_G^T\right)^{1/2} \qquad (3.37)$$

Note that the procedure is performed iteratively ; in a first iteration, r and q are determined based on an initial guess for the system order n (i.e. large enough).

An important remark is that this procedure requires that each of the given data matrices $\mathbf{S}_k$ has to be positive definite. In practice, when the data are corrupted by noise, this property is not always guaranteed as a result of which the Riccati equation (3.36) has no positive definite solution and the spectral factor cannot be computed. Two possible solutions to this problem are suggested in [183].

An important feature of the algorithm is that the model order of the spectral factor can be balanced against precision of the fit. With the control application in mind, model order is an important aspect in the implementation phase as it has a direct impact on the order of the controller order and thus on the computational burden associated with implementing the controller in real-time on a digital signal processor.

3.4 A MODEL FOR THE SOUND POWER RADIATED BY A RECTANGULAR PLATE

In this paragraph, it is shown how the proposed control approach applies to a practical problem. The structure under consideration is a rectangular baffled aluminium plate, with dimensions 500 × 720 x 5 mm (width L_x × length L_y × thickness h); the corresponding coincidence frequency is approximately 2400 Hz. As there is no exact analytical solution for the vibration problem of rectangular plates unless at least two opposite edges of the plate are simply supported [185], the plate is assumed to be simply supported at all boundaries. The disturbance input is assumed to be a single point force, applied to the plate. The best choice of control input is to match the spatial variation of the primary forces [186]. Even with a distributed elastic system, primary point forces (disturbances) may not effectively be controlled by distributed control forces. Therefore the plate response is controlled using a single point force.

Following the procedure outlined in paragraph 3.2, a partial differential equation of motion for the rectangular plate is first derived (from Kirchhoff's law) :

$$D\left(\frac{\partial^4}{\partial x^4}+2\frac{\partial^4}{\partial x^2\partial y^2}+\frac{\partial^4}{\partial y^4}\right)w(x,y,t)+\rho_p h\frac{\partial^2 w(x,y,t)}{\partial t^2}=p_p(x,y,t)\,, \qquad (3.38)$$

where $w(x,y,t)$ is the motion of the plate in a direction perpendicular to the plate, at location (x,y), $p_p(x,y,t)$ is the force per unit area, ρ_p is the mass density of the plate material, D is the *bending stiffness* of the plate ($D=\frac{Eh^3}{12(1-\nu^2)}$ for linear isotropic plates; in which E is *Young's* modulus and ν is *Poisson's* coefficient).

Solving the differential eigenvalues problem (3.4) for the eigenvalues and eigenfunctions yields the structure's modeshapes :

$$W_{mn}(x,y)=\sin\frac{m\pi x}{L_x}\sin\frac{n\pi y}{L_y}, \tag{3.39}$$

in which m and n are the number of 1/2 structural wavelengths of the modeshape along the X-axis and Y-axis, respectively. The corresponding eigenvalues λ_{mn} determine the associated eigenpulsations :

$$\lambda_{mn}=\omega_{mn}^2=\frac{D}{\rho_p h}\left[\left(\frac{m\pi}{L_x}\right)^4+2\left(\frac{m\pi}{L_x}\right)^2\left(\frac{n\pi}{L_y}\right)^2+\left(\frac{n\pi}{L_y}\right)^4\right]. \tag{3.40}$$

Supposing the plate is excited by L point forces $f_l(t)$, the force per unit area is expressed as

$$p_p(x,y,t)=\sum_{l=1}^{L}\delta(x-x_l,y-y_l)f_l(t), \tag{3.41}$$

where $\delta(x-x_l,y-y_l)$ is a Dirac impulse at location (x_l,y_l).

This yields an expression for the modal forces $F_{mn}(t)$

$$F_{mn}=\frac{4}{\rho_p h L_x L_y}\sum_{l=1}^{L}\sin\left(\frac{m\pi x_l}{L_x}\right)\sin\left(\frac{n\pi y_l}{L_y}\right)f_l(t). \tag{3.42}$$

Combination of (3.42) and (3.6) yields a state space representation of the vibration behaviour of the rectangular plate (restricting the modes in the expansion to N)

$$\begin{bmatrix}\dot\eta_1\\ \ddot\eta_1\\ \vdots\\ \dot\eta_N\\ \ddot\eta_N\end{bmatrix}=\begin{bmatrix}0 & 1 & .. & 0 & 0\\ -\omega_1^2 & -2\zeta_1\omega_1 & .. & 0 & 0\\ \vdots & \vdots & \ddots & \vdots & \vdots\\ 0 & 0 & .. & 0 & 1\\ 0 & 0 & .. & -\omega_N^2 & -2\zeta_N\omega_N\end{bmatrix}\begin{bmatrix}\eta_1\\ \dot\eta_1\\ \vdots\\ \eta_N\\ \dot\eta_N\end{bmatrix}+$$

$$\frac{4}{\rho_p h L_x L_y}\begin{bmatrix}0 & .. & 0\\ \sin\frac{m_1\pi x_1}{L_x}\sin\frac{n_1\pi y_1}{L_y} & .. & \sin\frac{m_1\pi x_L}{L_x}\sin\frac{n_1\pi y_L}{L_y}\\ \vdots & \ddots & \vdots\\ 0 & .. & 0\\ \sin\frac{m_N\pi x_1}{L_x}\sin\frac{n_N\pi y_1}{L_y} & .. & \sin\frac{m_N\pi x_L}{L_x}\sin\frac{n_N\pi y_L}{L_y}\end{bmatrix}\begin{bmatrix}f_1\\ \vdots\\ f_L\end{bmatrix} \tag{3.43}$$

An expression that relates the sound pressure at a point $\vec{r}(R,\varphi,\theta)$ in the far field of the spherical co-ordinate system of figure 3.1 due to the vibration of the plate, can be obtained from Rayleigh's integral expression

$$p(R,\varphi,\theta,\omega)=\frac{j\omega\rho}{2\pi}\int_{\Omega}\frac{v(\vec{r}_s)\,e^{-jk|\vec{r}-\vec{r}_s|}}{|\vec{r}-\vec{r}_s|}\,d\Omega\,, \tag{3.44}$$

where $\vec{r}(R,\varphi,\theta)$ is a spatial vector, $\vec{r}_s(x,y,0)$ an integration point on the panel, $v(x,y)$ is the surface velocity distribution on the panel, i.e. $v(x,y)=\dot{w}(x,y)$. $|\vec{r}-\vec{r}_s|$ is the distance from the integration point on the panel to $\vec{r}(R,\varphi,\theta)$.

The total acoustic energy that is radiated is calculated considering a half sphere that encloses the rectangular plate. In appendix 3B it is shown how the integral expressions (3.44) and (3.19) have been evaluated. The first 7 analytical plate modes (modes listed in appendix 3B) have been taken into account for the calculation of the corresponding **M**(ω) data in a frequency band from 0 to 500 Hz. Based upon the data generated by numerical integration, the radiation model has been identified. The calculated matrices are used as the input for the identification algorithm of paragraph 3.3. A spectral factor **G**(ω) with a system order equal to 5 has been identified, the result of the identification is shown in figure 3.2. A very good agreement has been achieved between the model and the numerically generated data.

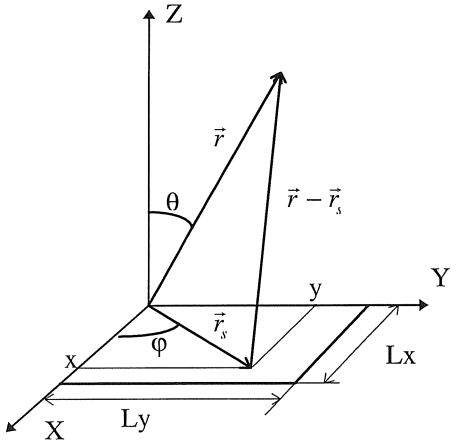

Figure 3.1. Location and orientiation the spherical co-ordinate system with respect to the panel.

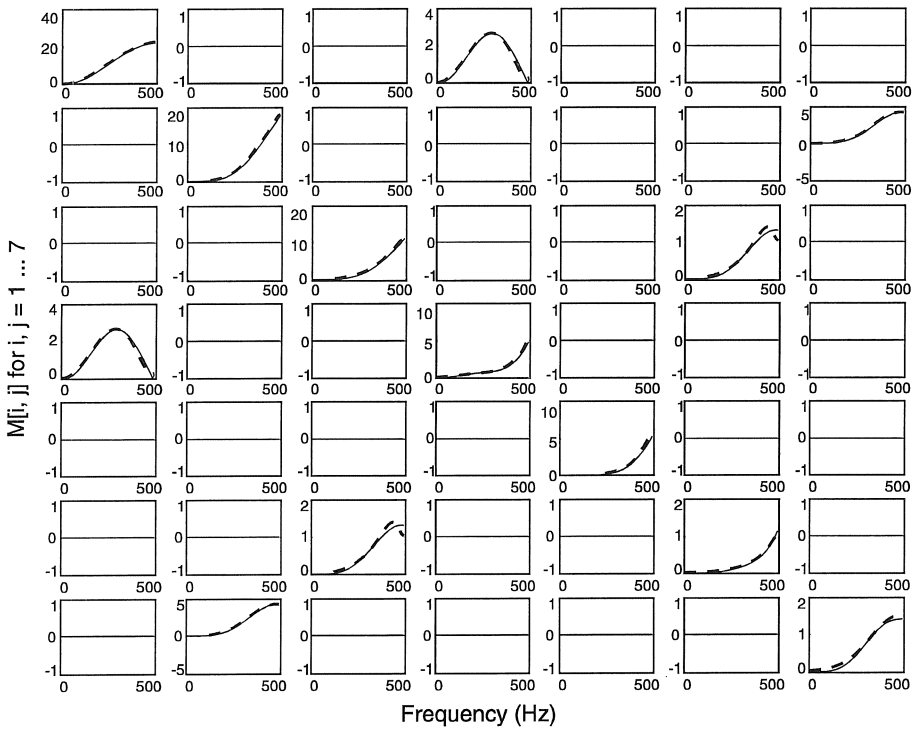

Figure 3.2. M[i, j] for i, j = 1, ..., 7 from 0 to 500 Hz based on analytical mode shapes. Solid line is original data set obtained after numerical integration of (3.19), the dashed line is synthesised using the spectral factor $\mathbf{G}(\omega)$ which has been identified with system order $n = 5$.

Control mechanisms

A closer look at the numerically generated data provides additional insight in how the controller can most optimally achieve its control objective. The diagonal elements of $\mathbf{M}(\omega)$ have been plotted as a function of frequency in figure 3.3. This result indicates that the [odd, odd] structural modes radiate most efficiently. Though this effect has been reported many times before [187] it is important to stress this fact in view of the design of an appropriate controller : it is clear that, in order to save control energy, the controller needs to concentrate on controlling the [odd, odd] modes first. Furthermore, the figure shows that the radiation efficiencies of all modes increase as a function of frequency and reach approximately the same value at high frequency (when the flexural wavenumber exceeds the acoustic wavenumber), which effect is explained in [40]. This indicates that only at higher frequency efficient control of sound radiation can be achieved by

merely controlling the vibration of the plate, without taking into account the radiation behaviour of the different modes before control. At these frequencies, however, passive measures may be effective as well.

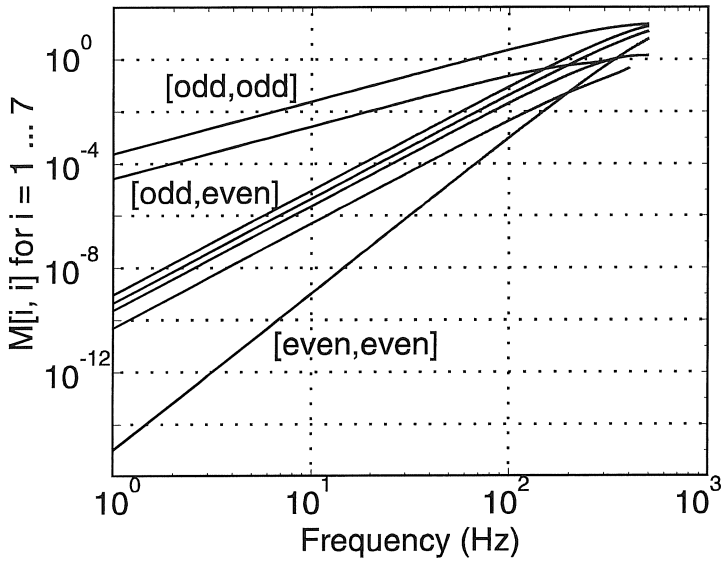

Figure 3.3. Diagonal elements of $\mathbf{M}(\omega)$, describing the modal radiation efficiencies as a function of frequency. Modes are identified by mode numbers [*m*, *n*] and fall apart in 3 classes.

This work concentrates on the lower frequency range such that knowledge of the radiation efficiency of the different modes is essential for the controller to achieve reduction of sound radiation. The controller basically uses two mechanisms to achieve this goal. In literature, these mechanisms are generally called *modal control* and *modal restructuring*. A physical interpretation is obtained by close inspection of the expression for the acoustic radiation from a plate which vibration response is dominated by two modes i and j (3.45) :

$$\overline{\Pi}(\omega) = M_{ii}(\omega).\left|\dot{\eta}_i\right|^2 + M_{jj}(\omega).\left|\dot{\eta}_j\right|^2 + 2.M_{ij}.\Re(\dot{\eta}_i.\dot{\eta}_j^{\,*}) . \qquad (3.45)$$

It is obvious that the controller can decide either to reduce the modal velocity of mode i or j (*modal suppression*) or alternatively to rearrange the phasing of the modes such that the third term cancels out the first two terms

as much as possible (*modal restructuring*). The selection of the appropriate mechanism is highly determined by the structure of matrix **M**. Recalling the definition of the matrix **M** from paragraph 3.2 and recalling figure 3.2, it is observed that all diagonal elements are non-zero, but some off-diagonal elements may be zero. Zero entries in $\mathbf{M}(\omega)$ occur for combinations of modes of which the modenumbers [*m*, *n*] are of a different *group*. There are basically 4 groups : [odd, odd] modes, [odd, even] modes, [even, even] modes, and [even, odd] modes. This effect is often referred to as *coupling* between structural modes : coupling only occurs between structural modes of the same group. The physical reason is that the radiation pattern of e.g. the [odd, odd] modes have significant monopole components and hence the acoustic power output of, say, the [1, 1] mode can be altered by the presence of the [3, 1] mode. The radiation pattern of the [2, 1] mode, however, has no monopole component but it is a pure dipole and therefore its presence can not alter the acoustic power output of the [1, 1] mode (or any other [odd, odd] mode). Mode [2, 1] can only couple to other modes which have dipole components as well. In the case where all modes which contribute to the structural response belong to a different group, only modal suppression will reduce the acoustic radiation. The same applies to the case where the off-diagonal elements of **M** are of a smaller order of magnitude than the diagonal elements.
The next paragraph discusses how these control mechanisms are realised for this application.

3.5 ACTIVE CONTROL OF SOUND POWER RADIATED BY A RECTANGULAR PLATE

3.5.1 The test set-up and control hardware

Implementing the aforementioned control strategy in real-time brings with it a number of problems which are all related to how the control approach is realised in practice. Figures 3.4 and 3.5 present the test set-up that has been built to experimentally verify and validate the control approach developed in the previous sections. The test set-up was installed in a semi-anechoic chamber. The rectangular plate has been fit to a stiff frame which was mounted above a reverberant cellar. With this construction, it was impossible to realise simply supported boundary conditions for the plate. The plate was clamped at all sides instead. Electrodynamic proof-mass

shakers (Gearing & Watson IV40) have been used to apply the disturbing force and the control force. The shakers have been mounted directly on the plate and add a mass of 1.25 kg each. The disturbance and control shaker were located at [142, 115] and [358, 605] respectively (dimensions in mm, refer to figure 3.1 for x- and y-direction), which implies symmetry with respect to the centre of the rectangular plate. With this configuration, the shaker location was not a parameter in the control performance achieved as both shakers can excite exactly the same modes. Six accelerometers have been put on the plate to measure the plate response.
The control algorithm was implemented on a Texas Instruments TMS320C40 DSP. The DSP was installed on a Loughborough Sound Images carrier board (DPC40B), which was hosted in a 486DX2 PC. The C40 DSP is a 32 bits floating point digital signal processor capable of executing 40MFLOPS. A daughter module was plugged on the carrier board, providing 2 ADC (16 bit) and 2 DAC (16 bit) with a maximum sampling speed of 200 kHz. Additional input channels were provided by a parallel 4-input, 2-output board (12 bits, maximum sampling speed 200 kHz), hosted in the PC and connected to the carrier board via DSPLINK. The control program runs at a sampling frequency of 1000 Hz. Working with a digital controller implies that the control law needs to be designed in the discrete time domain. Furthermore, an anti-aliasing filter must be used in order to cut off all signal content above the Nyquist frequency (half the sampling frequency).

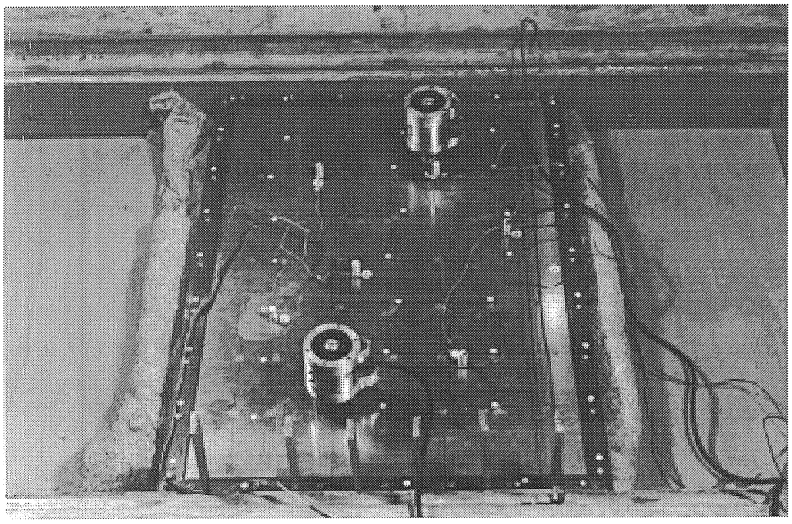

Figure 3.4. View on the test set-up.

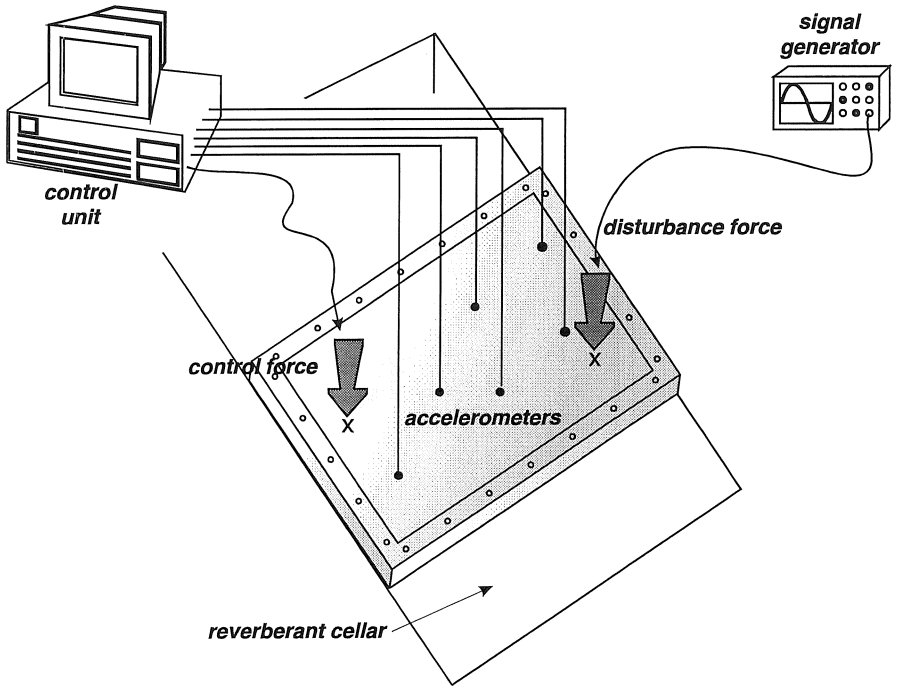

Figure 3.5. Lay-out of the test set-up.

3.5.2 Experimental system model

An experimental modal analysis was performed in order to come to an accurate system model. The resonance frequencies, modal damping factors and mode shapes were identified experimentally using Cada-X® software. The measurement grid was determined such that it coincides with a Gaussian point distribution in order to allow using the data for integration by numerical quadrature as described in appendix 3B. The resonance frequencies of the first 4 theoretical modes are compared to the resonance frequencies of the corresponding experimental modes in table 3.1.

From these results, and comparing these with the analytical results presented in [9], it is clear that the actual boundary conditions were closer to clamped at all sides instead of simply supported. The fact that the [2, 1] mode is shifted down (in contrast with all others which shift up in

frequency) is due to the first bending mode of the frame on which the plate was mounted. Furthermore it was observed from the experimental modal analysis that 3 additional modes appear at 202.0 Hz, 226.9 Hz, and 276.9 Hz, respectively. These modes do not resemble analytical modes and are likely to be introduced due to the construction of the set-up and the loading due to the presence of the inertia shakers (the mass of the plate is approximately 5 kg).

Mode	analytical (simply supported)	experimental
[1, 1]	72.8 Hz	107.2 Hz
[1, 2]	143.8 Hz	186.3 Hz
[2, 1]	220.1 Hz	213.0 Hz
[1, 3]	262.2 Hz	315.2 Hz

Table 3.1. Analytical and experimental resonance frequencies

The knowledge of the measured modeshapes allows to determine the modal forces. This is done by replacing the analytical modeshapes in (3.42) by the measured values at the relevant locations. With these modal forces, and the values of the experimental modal damping and resonance frequencies, the experimental system model can be synthesised as in (3.43). The frequency range of interest for this application was limited to a frequency band from 80 to 400 Hz. The controller is synthesised based on a system model which is valid in this range. The first 7 experimental modes have been taken into account in order to synthesise a model for the plate dynamics and for the radiation model. A discrete time model for the plate dynamics has been obtained using *Zero Order Hold* transformation [80], which accounts for the effect induced by the process of sampling and digitising in- and outputsignals. The procedure for calculating the $\mathbf{M}(\omega)$ matrix was modified in order to be compatible with experimentally measured modeshapes (explained in appendix 3B). A model for the spectral factor $\mathbf{G}(z)$ has been identified in the discrete time domain directly. Figure 3.6 shows the result.
It is important to note that none of the experimental modeshapes were found to be exactly orthogonal with respect to each other. This is easily controlled by calculating the MAC-matrix (Modal Assurance Criterion). As a result, none of the coupling terms in $\mathbf{M}(\omega)$ is equal to zero, though some are relatively small. The smaller contributions have not been identified to the same accuracy in order to limit the system order (figure 3.6, e.g. $\mathbf{M}[6,3]$).

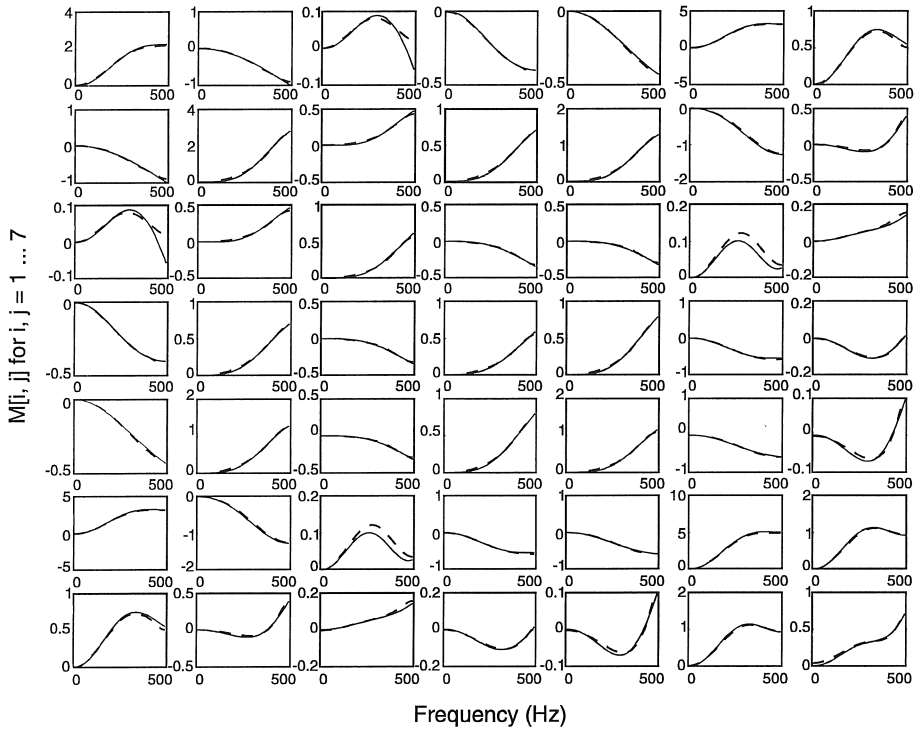

Figure 3.6. M[i, j] for i, j = 1, ..., 7 from 0 to 500 Hz based on experimental mode shapes. Solid line is original data set obtained after numerical integration of (3.19), the dashed line is synthesised using the spectral factor $G(\omega)$ which has been identified with system order $n = 5$.

A corollary of using electrodynamic shakers to apply forces to the rectangular plate is that the shaker dynamics need to be taken into account by the controller. In practice it means that the controller should not calculate the control force that should be applied to the rectangular plate, but rather the control voltage that should be sent to the shaker. This is achieved by including the transfer function from input voltage to the power amplifier driving the shaker to the force applied by the shaker to the plate in the system model. This transfer function has been acquired experimentally. An 8^{th} order discrete time state space model has been identified using non-linear least squares identification techniques (figure 3.7).

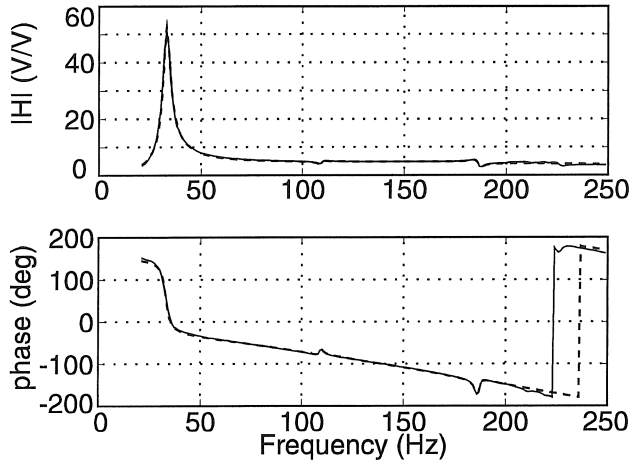

Figure 3.7. Measured (solid) and identified (dashed) transfer function between voltage applied to the power amplifier and voltage measured at the force cell mounted between the shaker and the panel.

The dynamic equations combining the model for the shaker, structural response, and radiation behaviour of the plate are presented in the discrete time domain in (3.46) :

$$\begin{bmatrix} \mathbf{x} \\ \mathbf{x}_s \\ \mathbf{r} \end{bmatrix}_{k+1} = \begin{bmatrix} \mathbf{A} & \mathbf{B}\cdot\mathbf{C}_s & \mathbf{O}_{N_G\times N_G} \\ \mathbf{O}_{N_s\times 2N} & \mathbf{A}_s & \mathbf{O}_{N_s\times N_G} \\ \tilde{\mathbf{B}}_G & \mathbf{O}_{N_G\times N_s} & \mathbf{A}_G \end{bmatrix} \begin{bmatrix} \mathbf{x} \\ \mathbf{x}_s \\ \mathbf{r} \end{bmatrix}_k + \begin{bmatrix} \mathbf{B}\cdot\mathbf{D}_s \\ \mathbf{B}_s \\ \mathbf{O}_{N_G\times L} \end{bmatrix} \mathbf{u}_k = \mathbf{A}_e \begin{bmatrix} \mathbf{x} \\ \mathbf{x}_s \\ \mathbf{r} \end{bmatrix}_k + \mathbf{B}_e \mathbf{u}_k$$

$$\mathbf{z}_k = \begin{bmatrix} \tilde{\mathbf{D}}_G & \mathbf{O}_{N\times N_s} & \mathbf{C}_G \end{bmatrix} \begin{bmatrix} \mathbf{x} \\ \mathbf{x}_s \\ \mathbf{r} \end{bmatrix}_k + \mathbf{O}_{N\times L}\mathbf{u}_k = \mathbf{C}_1 \begin{bmatrix} \mathbf{x} \\ \mathbf{x}_s \\ \mathbf{r} \end{bmatrix}_k + \mathbf{D}_1\mathbf{u}_k \qquad (3.46)$$

$$\mathbf{y}_k = \begin{bmatrix} \mathbf{C} & \mathbf{O}_{K\times(N_s+N_G)} \end{bmatrix} \begin{bmatrix} \mathbf{x} \\ \mathbf{x}_s \\ \mathbf{r} \end{bmatrix}_k + \mathbf{D}\mathbf{u}_k + \mathbf{v}_k = \mathbf{C}_2 \begin{bmatrix} \mathbf{x} \\ \mathbf{x}_s \\ \mathbf{r} \end{bmatrix}_k + \mathbf{D}_2\mathbf{u}_k + \mathbf{v}_k$$

Note that all matrices in this equation refer to the discrete time equivalent system matrices obtained from the continuous time models such as (3.10). For clarity, the same symbols have been used though not all of the matrices are identical (refer to paragraph 2.2) The subscript "s" refers to the system matrices corresponding to the shaker model, N_s is the order of this model. Note that all inputs to the model (3.46) have to be specified as input voltage

(instead of input force). The measurement of the system outputs is subject to measurement noise, which directly adds to the measured signals. Measurement noise is introduced via the vector **v** (figure 2.5). The extended system state comprises the state variables describing the plate dynamics (3.43), the state variables associated with the "radiation filter" (3.22), and the state variables associated with the shaker model. The system outputs are defined as accelerations at specific locations on the plate.

3.5.3 Control results - simulation

The controller has first been implemented on simulation, which allows feeding back all system states (disregarding the fact whether or not they can be directly measured), i.e. the *full-state feedback* controller (2.6). Two different types of active control configurations are first compared : *vibration control* (*AVC*) and *structural acoustic control* (*ASAC*). Both controllers have been designed such that the overall reduction of acoustic radiation in the frequency band from 80 to 400 Hz is equal. This is achieved by varying **R** in the expression for the LQG cost function (2.11). The overall reduction is calculated as the integral of the difference between radiated sound power with and without control over the frequency band of interest. The results of the simulations are presented in figures 3.8 and 3.9. Most important observation is the fact that, though total reduction in this frequency band is equal (4.55 dB overall reduction), AVC consumes more than two times the control energy (integral of control signal squared) consumed by ASAC in the same frequency band (figure 3.9). This is explained by the results presented in table 3.2.

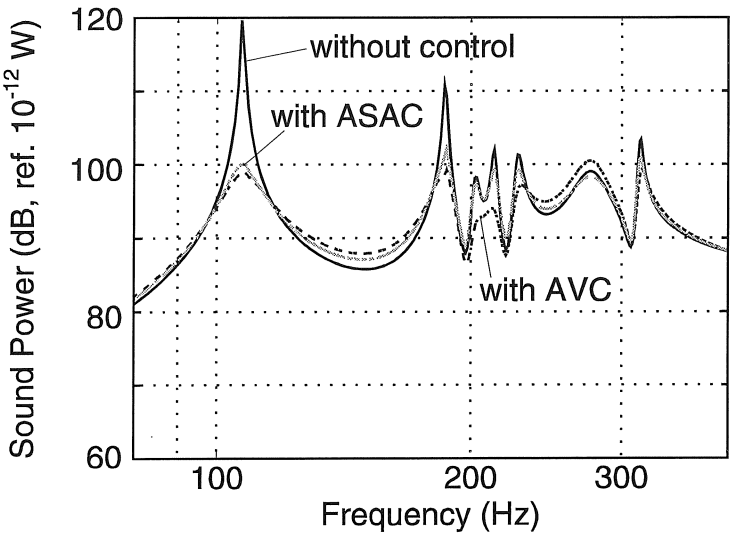

Figure 3.8. Comparison of the control result achieved with AVC and ASAC.

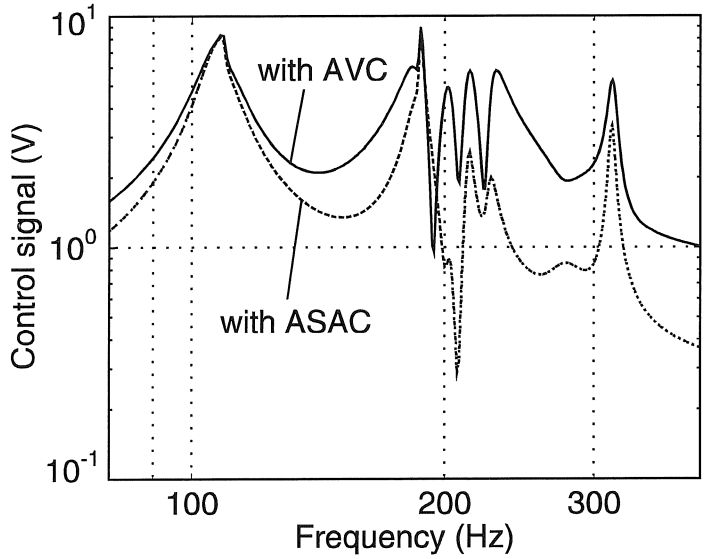

Figure 3.9. Control signal corresponding to AVC and ASAC.

Mode	reduction (dB) AVC	reduction (dB) ASAC
1	10.4	9.8
2	6.1	4.8
3	3.4	0.4
4	4.1	1.3
5	1.0	2.5
6	-0.7	0.4
7	2.3	1.1

Table 3.2. Reduction of modal displacement at resonance frequency of each mode.

Table 3.2 shows that AVC is reducing some modes considerably more than ASAC. Actually these are the modes which have the largest amplitude. However, AVC is reducing these modal amplitudes regardless of the fact whether they contribute to the acoustic radiation, whereas ASAC aims at controlling only those modes that radiate efficiently. This is also shown in figure 3.8. These observations have not come as a total surprise as similar results have been reported in several related studies (refer to paragraph 1.2). The experiment has only been re-iterated here as a matter of example. The remainder of this chapter concentrates on implementing the ASAC configuration.

The full-state feedback controller is not directly realisable since it is not possible to directly measure all system states. Therefore the controller needs to be complemented with an observer which provides an estimate of the extended system state $\mathbf{x}_e(k)$ based upon measurement(s) of the system output(s). The six accelerometers provide these as an input to the observer.

In order to optimise the computational burden (which is closely related to the order of the controller) with respect to the controller bandwidth aimed at, a *reduced-order* controller has been synthesised. As a matter of example, the reduced-order controller was designed for a bandwidth up to 200 Hz. As a comparison, an *extended-order* controller has been designed to achieve control bandwidth up to 400 Hz, taking into account the first 7 (experimental) modes of the system.

In a first instance, the first 3 experimental modes have been taken into account for the design of the reduced-order controller. First, a reduced-order and extended order full-state feedback controller was designed, the result of which is shown in figure 3.10. Apparently, control spillover did not seem to be a major problem.

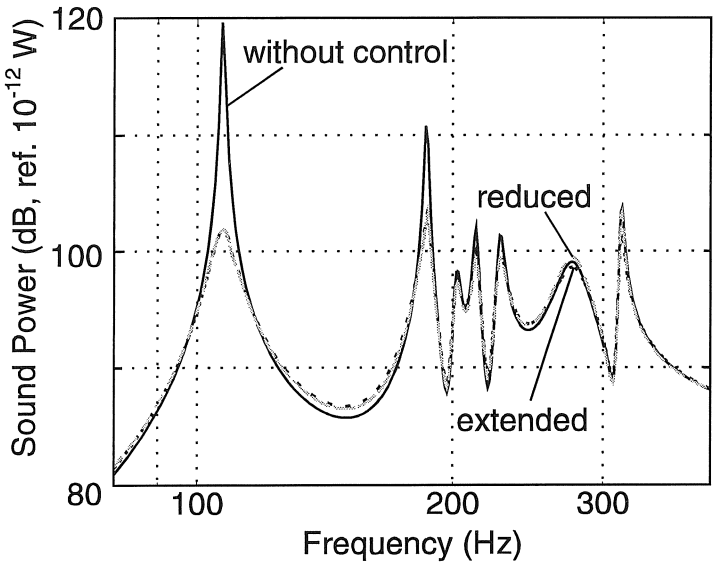

Figure 3.10. Control result achieved with reduced and extended order full-state feedback controller.

Secondly, a controller with state observer was designed. It was readily observed that the control performance had to be reduced drastically in order to avoid observer spillover causing the 6th and 7th mode go unstable. One can also look at this problem as an observer design problem : the residual modes present themselves basically as measurement noise in the measured system output. Since measurement noise is generally considered as high-frequency, low-amplitude noise (otherwise something is seriously wrong with the signal to noise ratio of the set-up), this is rarely a signal component that limits the maximum achievable observer bandwidth. However, as the dynamics of the residual modes lie well within in the observer bandwidth, they affect the stability of the closed-loop system.

The controller has been adjusted in two ways. First of all, due to the presence of 3 modes with relatively high modal damping in the frequency range 200 - 250 Hz, the first 5 experimental modes had to be taken into account for the design of the reduced-order controller in order to obtain an accurate plate model up to 200 Hz. Secondly, a 4th order Butterworth filter with cut-off at 250 Hz was put at the controller output such that excitation of the residual modes could be avoided. The model for this filter was incorporated in the model for the shaker, which explains the increasing phase lag observed in figure 3.7. These measures have resulted in a stable reduced-order controller of which achieves the same performance as the

extended-order controller and which only mildly excites the 6th mode (figure 3.11).

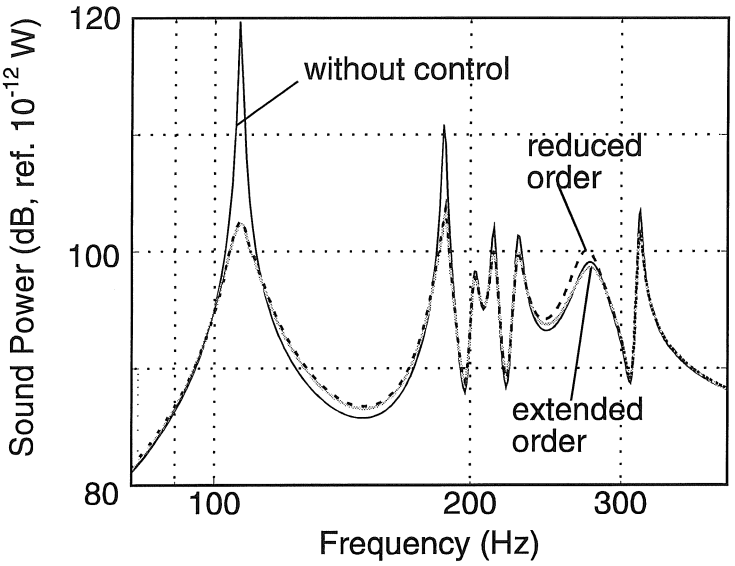

Figure 3.11. Control result achieved with reduced and extended order controller-estimator.

3.5.4 Control results - experiments

An extended-order controller (27 system states) has been implemented on the digital controller and has been tested on the experimental set-up. Two series of experiments have been performed. A broadband excitation was applied by the disturbance shaker. In a first instance, a controller with a limited closed-loop gain has been tested. Next, a controller with large closed-loop gain has been designed and tested. The average acoustic intensity through a surface parallel with the plate has been measured by scanning with an intensity probe (ONO SOKKI MI 6410, microphone pre-amp CF 0610) perpendicular to and close to the plate. The result before and after control is presented in figure 3.12. The difference between the experimental Frequency Response Functions (figure 3.12) and the numerically obtained results (figures 3.8 to 3.11) are largely due to the interaction of the plate with the reverberant cellar under the plate as shown in figure 3.5. This interaction gives rise to, for example, the small peak at 123 Hz, which is in effect due to the first acoustic mode of the reverberant

cellar. As this mode has not been taken into account in the model, it is not controlled and gives rise to spillover if the control gain is increased substantially (figure 3.12). The extended-order model for the design of the controller comprised all modes up to 315 Hz. Therefore the mode at 350 Hz is not controlled. Due to the fact that the cut-off frequency of the anti-aliasing filter was set to 250 Hz, spillover in modes above 315 Hz is well under control.

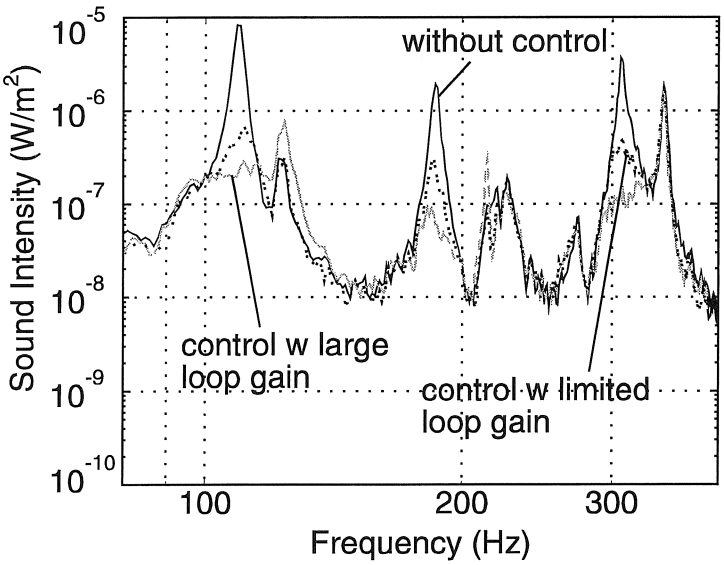

Figure 3.12. Results of control experiments on test set-up for a controller with limited (dotted) and large (grey) controller loop gain.

3.6 CONCLUSIONS

3.6.1 General conclusions

This chapter presents a control technique, based on the approach first introduced by Baumann *et al.* [51]. The contribution of this chapter is threefold. First of all, the control approach has been generalised and formulated as a general control strategy for feedback control of vibro-acoustic systems. The domain of application includes controlling the sound

radiated from vibrating structures to the free field as well as radiation of into a cavity due to vibration of the cavity shell.
Secondly, the research in this framework has triggered the of a development new subspace algorithm for the identification of multi-input multi-output linear discrete time systems from a given set of power spectrum data. Complementing the control approach with a this identification procedure, greatly enhances the applicability of the control approach to more complex systems other than beams, as in [51].
Thirdly, the control approach has been successfully implemented to control the sound radiated from a rectangular plate. To our knowledge, it is the first time this theory has been illustrated with experimental results.
The applicability of the control approach is in theory limitless, and the experimental results achieved in this work suggest nothing else. However, its application to other practical examples is yet to be performed. A number of suggestions for further work in this direction are given in the remainder of this paragraph.

3.6.2 Suggestions for further work

An opportunity for modal updating

Fitting a numerical prediction model to experimental results is a common problem encountered in the field of modelling and control. In this specific application the actual problem is to accurately predict the radiated acoustic energy as a function of frequency. This is accomplished by means of a so-called radiation filter. Taking into account that the data for the radiation filter are generated by numerical evaluation of the Rayleigh integral over the structure's surface, assuring the accuracy of the vibro-acoustic model is primarily a function of how accurate the structure's resonance frequencies, mode shapes, and modal damping factors are identified. The ad-hoc procedure with which the experimental model has been synthesised in this work has several shortcomings in this sense.
The analytical model description used here assumes proportional damping which implies the experimentally determined modes must be restricted to be real instead of complex. However, for set-ups where the boundary conditions are the main source for the introduction of damping in the system, complex modes are the only correct modal base [50]. The main disadvantage of using a complex modal base is that the modal equations no longer form a decoupled set of equations as in (3.6) [91], which complicates the synthesis procedure. However, "forcing" the experimental modal

analysis to real (normal) modes may introduce errors that have to be compensated heuristically by tuning other model parameters such as modal damping factors.
For more complex applications it is therefore suggested that the model description starts from a FEM-model, and that advanced tools of *Modal model updating* ([188], Chapter A.6. Model Updating) are used to fine-tune the model. State space description of the system can then be obtained using the procedures provided in software such as the "Structural Dynamics" Toolbox of Matlab®.

Optimisation of number and location of actuators and feedback sensors

For this application, the control actuator and feedback sensors have been located on the panel based on common engineering sense, i.e. not too close to the borders, not on the nodal lines of the participating modes, etc. The number of error sensors was set equal to the maximum available input channels of the DSP Board as to maximise the observability of all participating modes. The effect of reducing this number on controller performance and robustness has not been studied. Since it is, at least in theory (if all observability conditions are met), possible to observe all participating modes with just one error sensor, using 6 may look as a major overkill and it would be interesting to further study what the potential improvement in this sense may be.[3]
Selecting an optimal number of optimally located actuators and sensors affects both maximum achievable reduction [189] and the control energy associated with achieving a predefined control performance [190]. In addition, the sensitivity to observation and control spillover can directly be affected by the arrangement of sensors and actuators [191 - 192]. Hence it is an important aspect in determining the optimal controller and should therefore be included in the iterative loop of designing and testing the controller. The optimisation of the number and location of actuators and feedback sensors has not been dealt with explicitly and the gap between this work and the intensive research in the field of optimisation (refer to special sessions on conferences such as ACTIVE 95, ACTIVE 97 etc.) remains to

[3] This is a relevant question in the sense that it may easily be argued that, by reducing the sound pressure at a set of 6 microphones, one could very probably guarantee control of the total sound power radiated too, questioning the relevance of the complexity of the control approach presented here. If the number of error sensors could be reduced to 1, however, this would be very unlikely.

be bridged and leaves open a research opportunity towards developing a so-called "mechatronic compiler".

Control design for robustness

There is a trend among control engineers to say that LQG controllers, in general, "do not work in practice" (i.e. outside laboratory) [193]. Indeed, despite of its relevance in the formulation of performance requirements, LQ optimal control was shown to possess no guaranteed robustness margins if applied in conjunction with an observer or Kalman filter [194]. This problem is particularly important for this application as the performance variable (the total sound power) and feedback variables (accelerometers) are not collocated such that the system states of the radiation filter are estimated *indirectly,* through an estimate of modal amplitudes. Thus it would be an important asset to be able to consider the robust performance issue in the design stage of the controller. The robustification procedure used in the current work was based on LQG/LTR control theory (refer to paragraph 2.2.3 and to [56]).

H_∞ and μ control theory has specifically been developed to be provide a powerful set of tools which aim at the design of robust controllers (refer to paragraph 2.2.4). The main disadvantage of these tools is that the H_∞ framework does not lend itself very much to the specification of control performance. As shown in this chapter, physical objectives for control performance is more easily expressed using H_2 norms, which allows to express the "cost" associated with the frequency-integrated energy in the system states (in this case the states associated with the radiation filter). In H_∞, one is constrained to express control design objectives as a bound on the maximum value over the frequency of the largest singular value of a specified transfer function.

The design problem of stating performance and robustness objectives in both the H_2 and H_∞ framework has recently been formulated as the "Mixed H_2/H_∞ Control Problem" [195 - 196] [69] (Chapter 4, pp. 97 - 122). In this framework, the input variables $\mathbf{w}$ and output variables $\mathbf{z}$ are split in two sets ($\mathbf{w}_1$, $\mathbf{z}_1$) , which are related to H_2 or LQ type of performance criteria, and ($\mathbf{w}_2$, $\mathbf{z}_2$) which are related to H_∞ norm requirements. The general mixed H_2/H_∞ problem minimising the transfer function in the H_2 sense from $\mathbf{w}_1$ to $\mathbf{z}_1$, while constraining the H_∞ norm of the transfer function from $\mathbf{w}_2$ to $\mathbf{z}_2$ to some bound, is in fact unsolved [69]. However, in [195], it is shown that this formulation does not address *robust* H_2 performance in a practical sense.

Steinbuch and Bosgra suggest therefore a new formulation, minimising the H_2 norm of the transfer function from $\mathbf{w}_1$ to $\mathbf{z}_1$ using the feedback $\mathbf{K}(s)$, while maximising the H_2 norm of the same transfer function over the H_∞ norm bounded allowable system uncertainties [195].
The application of a mixed H_2/H_∞ approach to design feedback controllers for active control is not new. In [197], the performance and robustness requirements for the feedback control of sound in a headrest are expressed using H_2 and H_∞ norms, after which the controller synthesis is shown to be a convex optimisation problem which can be solved using standard optimisation tools. This work, and related work, give an interesting starting point for the further development of the controller presented here.

Appendix 3A

Generalized forces are defined as

$$Q_{ij}(t) = \int_{\Omega} \phi_i(x) f_j(x,t) dx\,, \quad i = 1,\ldots,n \quad j = 1,\ldots,L \tag{3.A1}$$

The mass matrix is defined as $\mathbf{M} = [m_{ik}]$ where

$$m_{ik} = \int_{\Omega} m\phi_i\phi_k dx = m_{ki}\,, \quad i,k = 1,2,\ldots,n \tag{3.A2}$$

the damping matrix $\mathbf{C} = [c_{ik}]$, where

$$c_{ik} = \int_{\Omega} \phi_i \mathscr{C} \phi_k dx\,, \quad i,k = 1,2,\ldots,n \tag{3.A3}$$

the stiffness matrix $\mathbf{K} = [k_{ik}]$, where

$$k_{ik} = \int_{\Omega} \phi_i \mathscr{L} \phi_k dx = k_{ki}, \quad i,k = 1,2,\ldots,n \tag{3.A4}$$

Appendix 3B

The surface integral over the rectangular plate can be determined analytically.
For the specific example of a baffled plate, (3.35) can be solved as

$$p = jk\rho c \frac{e^{-jkR}}{2\pi R} \int_0^{L_x}\int_0^{L_y} \dot{w}(x,y) e^{j\frac{\alpha x}{L_x}} e^{j\frac{\beta y}{L_y}}\, dy\, dx \tag{3.B1}$$

where $\alpha = kL_x \sin\theta\cos\varphi$ and $\beta = kL_y \sin\theta\sin\varphi$.

Expanding the surface velocity in the structural modes (3.30) and solving the surface integral leads to an expression in the form of the general expression (3.17) :

$$p = jk\rho c \frac{e^{-jkR}}{2\pi R} \frac{L_x L_y}{\pi^2} \sum_{i=1}^{N} \frac{\dot{\eta}_i}{m_i n_i} \left[\frac{\left(e^{j\alpha}(-1)^{m_i} - 1\right)\left(e^{j\beta}(-1)^{n_i} - 1\right)}{\left(\left(\frac{\alpha}{m_i \pi}\right)^2 - 1\right)\left(\left(\frac{\beta}{n_i \pi}\right)^2 - 1\right)} \right] \tag{3.B2}$$

The integral expression (3.19) is numerically evaluated using numerical quadrature [198]. Note that the value for R vanishes in the expression as

$$\int_S f(R,\theta,\phi)\, dS = \int_\phi \int_\theta f(R,\theta,\phi)\, R^2 \sin\theta \, d\theta \, d\phi \tag{3.B3}$$

when integrating over a constant radius in a spherical co-ordinate system. The integral is evaluated using 32 abscissa points for $\phi \in [0, 2\pi[$ and $\theta \in \left[0, \frac{\pi}{2}\right[$; which has proved to yield sufficient accuracy. In order to generate data for the extended system model, the matrix $\mathbf{M}(\omega)$ is calculated at 500 equidistant frequency points from 1 to 500 Hz. The first 7 plate modes have been taken into account in the extended system model. The mode numbers and corresponding resonance frequencies have been listed below (table 3.B1).

Mode number	$[m, n]$	natural frequency (Hz)
1	[1, 1]	72.8
2	[1, 2]	143.8
3	[2, 1]	220.1
4	[1, 3]	262.2
5	[2, 2]	291.1
6	[2, 3]	409.5
7	[1, 4]	428.0

Table 3.B1. Modes and natural frequencies of the baffled plate (analytical).

The procedure is programmed in Matlab®. The algorithm has been speed up by skipping combinations of modes for which the surface integral equals zero.

The procedure is modified in the case that experimentally measured modeshapes are used (paragraph 3.5). Also the surface integral over the plate (3.35) must then be calculated by numerical quadrature. Furthermore, as none of the experimental modes is perfectly symmetric as the theoretical modes, none of the coupling terms of $\mathbf{M}(\omega)$ can be assumed to be zero and hence these must all be calculated as well. Taking into account the first 7 experimental modes of the plate, the calculation took approximately 27 hours on a Hewlett-Packard 712/80 PA-RISC workstation (82 10^9 flops).

CHAPTER 4

A FEEDFORWARD CONTROL APPROACH TO REDUCE STRUCTURE-BORNE ROAD NOISE IN A PASSENGER CAR

4.1 INTRODUCTION

4.1.1 Acoustic comfort as a new design criterion in car design

Acoustic comfort has recently become an important design criterion in the development of new automobiles and measures to deal with this problem in all design stages are discussed intensively in literature [200 - 202] (also refer to the table of contents of the *SAE Noise and Vibration Conference*, Traverse City, MI, 1991, 1993, 1995). Apart from "evident" criteria, such as road handling and fuel efficiency, the acoustic comfort (which is not solely described by the sound pressure level [202]) inside a car cabin is considered as an important aspect in the subjective evaluation of a car.
The sound spectrum, measured inside a car cabin in operating conditions, consists of three major components : powertrain noise, aerodynamic noise,

and road noise (another contributor, which will not be considered here, is the so-called squeak-and-rattle noise).
Powertrain noise refers to all noise components which are related to, or caused by, the operation of the engine, gearbox, etc. The powertrain noise has a structure-borne as well as an air-borne component. Structure-borne noise has been defined as noise for which a significant portion of the transmission path from source to receiver takes place in a solid structure rather than through a liquid or gas (paragraph 1.2.1). Air-borne noise is thus mainly transmitted through a liquid or gas (air). The airborne powertrain noise component is caused by sound waves which are radiated from the surfaces of the engine block, after which they are transmitted through the air in the engine bay, and excite the car body panels, which, in turn, radiate sound into the car cabin [203]. Structure-borne powertrain noise is caused by the transmission of engine and gearbox vibration through engine mounts ("silent-blocks"), gearbox mounts, drive shafts, etc., to the car body.
Automobile aerodynamic noise is defined as the noise generated by the flow of air around the exterior of the car. Reducing aerodynamic noise does not only come down to reducing automobile aerodynamic drag [204] but also requires wind-noise related design features to be added to the car, such as auxiliary door seals etc. Aerodynamic noise testing implies full-scale wind tunnel testing [204 - 205], as there is no similarity law for aerodynamic noise as there is for drag. These experiments are often complicated by the fact that most wind tunnels are not designed with that kind of experiments in mind and produce relatively high levels of background noise.

This chapter presents the development of an active control system to reduce the road noise level inside a car cabin. The research work has been performed in the framework of a Brite-Euram project, called "ANRAVA". The test car under consideration is a mid-size station wagon (Volkswagen Passat Variant) with a VR6 petrol engine. Tests have shown [206] that engine noise and aerodynamic noise are relatively well under control in this type of car. Especially at higher speeds or on rough road surfaces the contribution of the structure borne road noise is dominant and determinant for the comfort of the passengers. The project was focused on further reducing the interior noise level by reducing the road noise component with active control methods.

4.1.2 Road noise

Automobile interior noise due to tire-road interaction has an air-borne and a structure-borne component as road noise is either radiated from the tire into the passenger compartment or transmitted via the vehicle's structure. An experimentally based structural/acoustic automobile tire noise model, which accounts for both transmission media, is presented in [207].
A traditional measure, which copes with exterior as well as interior road noise, is to design "silent" tire tread patterns and to apply a porous asphalt road surface. This type of tire-road contact situation has been studied extensively in order to quantify the influence of road surface and tire tread characteristics on the airborne noise level [208 - 211]. These studies mainly show that these measures only provide a temporary solution. First of all, while smooth tires are very quiet on smooth roads, it has been shown that when tires which are worn smooth are running on coarse road surfaces, they can be noisier than treaded tires [208]. The damping effect of the porous asphalt, on the other hand, is decreasing with time as the porosity decreases because porous asphalt is often too ductile to withstand the load due to heavy traffic and due to clogging [212] (2 dB(A) less noise reduction after 1 year has been reported). Furthermore, while it may be possible to minimise the noise level produced by a specific combination of a certain tire and a certain road surface, this very combination will not always be encountered in practice. Therefore, car manufacturers are highly interested in finding a solution which is independent of the road surface encountered or the tire used.
Structure-borne road noise is generated by road induced excitation forces which excite the car body through a number of transfer paths. Physically, these transfer paths are connections of the wheel suspension with the car body. Studies of the transmission of road noise through the suspension are presented in [214 - 217]. Structure-borne road noise dominates the airborne noise in the lower frequency range (below 400 Hz) [218 - 219]. The frequency band below 400 Hz is critical in car acoustics due to the presence of pronounced acoustic cavity resonances in the range 100 to 200 Hz and below.
The basic problem is that a car suspension is actually designed to filter out road undulations. The necessary bandwidth of a suspension system to realise that is 10 to 15 Hz. Above that frequency, the shock absorber, for example, transmits all vibrations to the car body. Current techniques for structure borne road noise reduction rely mainly on the use of rubber bushings at the connection of the wheel suspensions with the car body. The isolation

capabilities of these connections are however compromised because of the need for high stiffness at lower frequencies, as required for road handling purposes [220]. Neither passive noise reduction techniques using absorbing or damping material give full satisfaction since they are only effective in the higher frequency range (above 400 Hz).
These observations show that the structure-borne road noise problem present an opportunity for active control. An efficient active control system that reduces the road noise level would at the same time allow to reduce the car weight and to enhance the dynamic characteristics of the car in terms of road handling. The latter would result from the fact that the suspension design would no longer be a compromise between vibration transmission to the car body and road handling (the ideal bushing from the latter perspective is a very stiff bushing). In the event of a commercial success, and taking into account a penetration of 3 % into the world-wide care productions of 30 million units/year, a control system rated at 100 - 200 ECU [221] would yield 90 - 180 MECU per year. Due to this perspective, 8 partners (Elesa, KULeuven - PMA, LMS International, MONROE Belgium, Univ. Manchester, Metzeler Gimetall, Univ. Patras, Volkswagen AG) and the EC have expressed their interest in the development of an active road noise control system by participating in the ANRAVA project. The complete development of the innovative control approach, and the implementation of the control algorithm has been the responsability of KULeuven. This chapter gives an overview of the work performed in the project (paragraphs 4.2 and 4.3) after which an innovative approach is presented which is aimed at enhancing the performance of the controller developed in the ANRAVA project (paragraph 4.4). Various aspects of this work have been presented in [222 - 226].

4.2 DESIGN OF THE CONTROL SYSTEM

4.2.1 Literature overview

Active control of road noise using acoustic control sources has been the topic of intensive research. A study of the maximum achievable control performance for linear and causal feedforward controllers has been presented by Sutton *et al.* [227]. In this paper, the potential of non-linear controllers (ANNs) as an alternative control algorithm is also investigated by means of numerical simulations. An overview paper covering the work

on active control of road noise, performed by Sutton *et al.*, presents a detailed study of the road noise problem, the design of the controller and the results that have been achieved during road tests [228]. Reductions of around 7 dB(A) in the range 100-200 Hz were measured using a two-loudspeaker system in a Citroen AX driving at 60 km/h over a coarse road surface.

The active control of road noise using loudspeakers was also studied extensively at Purdue University. A lot of attention was paid to choosing the appropriate set of reference signals for feedforward control. The coherence problem was addressed by Ferren and Bernhard in [229]. Heatwole *et al.* have further worked on optimisation the reference set in view of choosing the appropriate number and locations for the reference transducers [230 - 232]. For these studies, a condition number analysis is combined with a multiple coherence analysis to determine which combinations of the references monitor the source the best. Experimental data are generated by exciting a tire of a test vehicle with using a shaker [231] or by putting one tire on a roller test bench [230]. The prediction of the control performance is discussed in [232]. An overview paper, which summarises the work performed on active control of road noise at Purdue, was presented by Bernhard as a keynote speech on the ACTIVE 95 Conference [233]. No road tests have been performed.

Active adaptive noise control in cars is discussed by Guicking *et al.* [234]. The paper presents active control strategies to reduce engine noise and road noise. In this paper, the trade-off between using FIR or IIR control filters is discussed by means of simulations. The application of adaptive filtering techniques to the active control of road noise is discussed by Bronzel in his PhD. thesis [235]. No road tests have been performed in this work.

An RLS controller is suggested Sano *et al.* in [236] to improve the convergence speed of the adaptive feedforward controller. His studies include numerical simulations but no road tests. In [237], Sano *et al.* propose another alternative algorithm, the single channel filtered-X Least Squares Lattice (LSL) algorithm, to improve the convergence speed with respect to the filtered-X LMS controller. The algorithm is tested in a single-channel (1 reference, 1 control source, 1 error sensor) laboratory experiment where one rear spindle of a test car was excited by an electrodynamic shaker. An alternative approach to enhance the convergence speed of the adaptive feedforward controller is dealt with by Freymann *et al.* [238] (refer to paragraph 4.4.3 for more detail). Yet another control algorithm is proposed by Sano *et al.* in [239]. In this paper, a 2DOF-ANC system is proposed, which consists of a conventional filtered-X LMS adaptive

feedforward part and a feedback part which is based on the Internal Model Control theory. The paper concentrates on a subspace identification method which is used to synthesise the feedback controller and to reduce the number of arithmetic operations in feedforward control. The effectiveness of that method is demonstrated through computer simulations.
Stothers *et al.* [236] presented a computationally-efficient hybrid control algorithm which performs the control filters update in the frequency domain. The algorithm has been discussed in paragraph 2.3.3. As adaptation need only be performed on a time scale which allows reasonable tracking of changes in the disturbance, it was found in practice that the total computational requirements are only marginally higher than the control filtering alone. Simulations are presented, predicting the control performance based upon data corresponding to a medium sized car (12 references, 4 error microphones, 4 control loudspeakers).
Berkman and Bender present an active system (the *QuietChip* controller) designed to reduce both road noise and engine noise in a 1995 Chevrolet Cavalier [165]. The system uses four OEM speakers, four error microphones, and 6 reference accelerometers mounted on the car suspension. The system was tested with the auto travelling at 65 mph on an interstate highway. The interior noise power spectral density shows a prominent series of harmonics of the wheel rotation frequency and a broadband component. The harmonic components were reduced by 5 to 10 dB. The broadband component that underlies the narrowband noise components was reduced by about 3 dB.

4.2.2 The control strategy

The active control systems for the reduction of road noise, which appear in literature, all rely on using loudspeakers mounted in the car cabin to control the interior sound field. This thesis presents a completely new and innovative control strategy, namely to control the structural-acoustic response of the car body such that the structure-borne road noise level inside the car cabin is reduced. Inertia shakers, located at the main transfer paths of the car suspension are used as control sources. This approach has been taken over in [240] to control the transmission of noise and vibration from the bogie to the passenger compartment of a high speed railcar. This control configuration will be referred to as the ASAC system. Figure 4.1 presents the ASAC control configuration. The optimisation of the number and location of the inertia shakers will be discussed in paragraph 4.2.3.

A loudspeaker system has been developed in parallel to the ASAC system in order to critically compare the major implications of either control strategy. The loudspeaker system will be referred to as the ANC system ; it is presented in figure 4.2. The ANC system uses four loudspeakers which are located in each car door. The number and location of these loudspeakers has not been optimised because they were supposed to coincide with the speakers of the car hi-fi system.
The control sources are driven by an adaptive feedforward controller. The controller configuration (algorithms, references, error sensors) is discussed in paragraph 4.2.4.

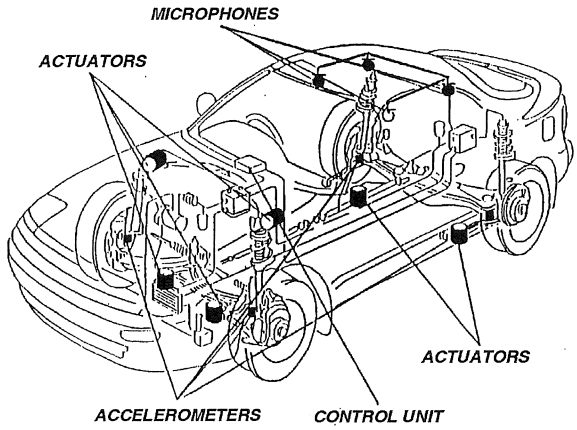

Figure 4.1. ASAC system.

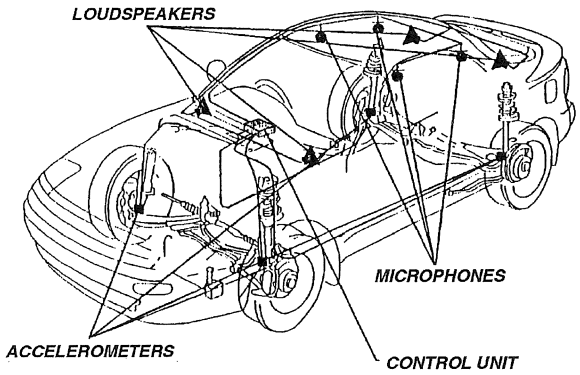

Figure 4.2. ANC system.

4.2.3 Determination of the optimal control actuator locations by TPA

In the particular case of structure-borne noise, the optimal location of the control actuators is suggested by the nature of the problem.
Actively blocking a structural vibration transfer path, which then results in acoustic control, as the primary disturbance is transmitted to the system via a number of identifiable transfer paths. The number of controlled transfer paths must be minimised (due to weight and controller design constraints), but a maximal possible noise reduction must be envisaged. Therefore it is important to understand which energy transmission paths from the suspension elements to the car interior acoustics are the most important with respect to the total noise level in the cabin. This study was done based upon the transmission path analysis technique [241]. The transmission path analysis technique is based upon combining estimates of the operational forces in each of the transmission paths with in laboratory measured frequency response functions (pressure or acceleration to force applied in each of the transmission paths). The determination of the operational forces can be based upon the complex dynamic stiffness method, which combines measurements of the complex dynamic stiffness of the bushings, with relative operational displacements over the mounts. An alternative but less well established methodology is based upon the inversion of a matrix of frequency response functions between acceleration responses on the car body and force applied at the different transmission paths. This matrix is combined with operational accelerations on the car body, in order to obtain estimates of the operational forces on the body.
For structure-borne road noise, the transfer paths are locations in which the suspension elements are connected to the car body by means of "bushings". Some practical considerations come into play at this point. Ideally, to reduce the vibration level at the main transfer paths by means of active control, the control actuators should be located in the main transfer paths and supplement the original -passive- bushings. This would imply that the actuator would have to be designed such that it is able to withstand superimposed forces of low frequency (e.g. static loads, such as car weight), and such that the original road handling characteristics (which are significantly determined by the bushings) are preserved. This is very hard to realise.
An alternative approach is to mount the actuator in parallel with the bushing, but only connected to the car body, and working against an inertia mass. In this case, however, the control and disturbance forces applied to the car body will inevitably be separated by a finite distance. Jenkins *et al.* [12]

show that, for the case of an infinite plate excited by a point force disturbance, the control force must be applied at a distance well within approximately three-eighths of a flexural wavelength from the disturbance force in order to achieve a significant reduction of the vibrational energy of the plate. In many circumstances, any value for this distance will be not realisable.

Furthermore, for practical reasons, the number of transfer paths to be controlled will be limited and therefore some flanking paths will always remain. Consequently, it may be very difficult, if not impossible, to obtain worthwhile noise reductions using this control approach (this has been confirmed by simulations and laboratory experiments of a vibration control system, refer to paragraph 4.2.6).

Because of these considerations, the control objective used in the research work presented here was focused on controlling the vibration behaviour of the receiver system such that the sound pressure level at a number of error microphones inside the car cabin is reduced (instead reducing the vibration level at a number of transfer paths). The control actuators need then to be located such that controllability is maximised. Since the main transfer paths, identified by TPA, are locations where the operational forces (road noise sources) couple very well into the acoustic car cavity modes, also the control actuator locations were chosen as close as possible to these locations.

For the transmission path analysis, a total of 30 transmission paths have been considered from the suspension into the car body : 10 connection points (rear axle, rear shock absorbers, 2 front suspension connection locations, front shock absorbers), in 3 translational directions (rotational degrees of freedom have not been considered). An important intermediate result of the analysis were the estimates of the operational forces in the transmission paths. The analysis in [242] showed that, in the frequency range of interest, the operational forces do not exceed 40 N (35 N peak force at 35 Hz). This implies that vibration levels at the transmission paths can be controlled with compact actuators. Note that the force levels are considerably higher at frequencies below 20 Hz, where the dynamic forces appear which are associated with the movement of the car body (the compenation of these forces is actually the scope of active car suspensions). Eight main transmission paths have been retained after the analysis. The optimisation of the optimal number and location (selected from the 8 main transmission paths) is discussed in paragraph 4.2.6.

4.2.4 The control algorithm

An adaptive feedforward controller has been chosen as the control strategy for this application. This choice is motivated, firstly, by the fact that there is a reference available for the primary disturbance (this is explained later-on). Secondly, the vibro-acoustic behaviour of the car body is very complex and cannot be modelled to the accuracy which is required in the design of a model-based feedback controller.
The multiple error filtered-X LMS feedforward control algorithm has been used in the laboratory tests and the road tests. The vibro-acoustic response of the car cabin was found to be relatively well damped and hence the control and secondary path filters were implemented using FIR filters. This corresponds with the findings of Bernhard [233] and Bronzel [235], who compared the potential of using IIR filters instead of FIR filters for the active control of road noise. They concluded that FIR filters were the best compromise (performance vs. computational complexity).
An alternative control algorithm, the RLS algorithm, has been suggested by Sano *et al.* [236]. Based on numerical simulations, this algorithm is supposed to enjoy higher convergence speeds than the filtered-X LMS algorithm in the application considered here. Referring to the practical problems associated with implementing the RLS algorithm in real-time (refer to paragraph 2.3.2), this algorithm was not considered in the research work presented here. An alternative approach to enhance the convergence speed of the filtered-X LMS algorithm has been developed instead, which is presented in paragraph 4.4.

The selection of the appropriate error signals is discussed in paragraph 4.2.6. The reference signals for the feedforward controller have been obtained from accelerometers which were mounted on the car suspension. Referring to paragraph 2.3.4, it is obvious that the selection of the appropriate reference set is essential in order to maximise the control performance. From the abundant number of reference sensor configurations which appropriately describe the road excitation, a reference set must be selected which *(i)* maximises the multiple coherence with respect to the error signal, *(ii)* meets the causality constraints, and *(iii)* yields maximum convergence speed.
While it is perfectly possible to determine the multiple coherence between any reference set and the error signal, and hence, through expression (2.44), the maximum achievable reduction, it is extremely complicated for this type of problem to quantify whether the causality constraints are met. This is due

to the fact that it is virtually impossible to exactly express the phase and amplitude relation imposed by the optimal control filter for a problem which involves a multitude of reference signals, control inputs, error signals, and secondary path transfer functions because the correlation matrices **R** and **P** take a very complicated form (refer to paragraph 2.3.4). However, an obvious requirement for the reference set to yield a causal controller, is to maximise the time advance available for the controller to calculate and apply the control action. This has been demonstrated by Sutton *et al.* [227], who simulated the effect of adding fictitious delays in the control loop on the control performance.
Heatwhole has further shown that it is important to consider the convergence properties of a given reference set [231] in the case of road noise. Because road noise is caused by multiple uncorrelated sources, relatively large reference sets are often employed to describe the primary disturbance (e.g. 12 references, in [228]). As a consequence, different reference sets which yield comparable multiple coherence with respect to the error signal, may yield a convergence speed which is an order of magnitude larger (or smaller) [233].
Due to the above considerations, the reference set for the ASAC system which is discussed here was a set of 6 signals, selected from the 12 accelerations, measured in 3 directions at the 4 wheel centres. The number of references was mainly determined by the available computing power. The 6 references were selected such that the multiple coherence was maximised (y- and z-direction acceleration at the front wheels, y-direction acceleration at the rear wheels). Furthermore, using wheel centre accelerations provides a maximum time advance. For the ANC system, 6 accelerometers have been placed along the 6 main vibration transmission paths. The potential loss of control performance is thus compensated by an increase of the multiple coherence. This configuration is not relevant for the ASAC system as it would lead to feedback of the control action to the references. Ways to optimise the convergence speed of the algorithm are discussed later-on (i.e. this issue has not been considered for the selection of the references).

4.2.5 Control hardware

A specific actuator, based on the moving coil inertial mass principle, has been designed by Metzeler in order to satisfy the determined requirements of force, bandwidth and size. The inertia shakers generate 40 N peak force (weight 1.1 kg, dimensions : Ø 80 × 76 mm). Figure 4.3 shows how the

inertia shakers were mounted to the car body. The loudspeakers utilised in the ANC system have been selected considering the power spectra of the error microphones during road measurements.
At the time of the definition of the controller hardware, it was understood that the extendibility of the digital controller would be a key factor in the optimisation of the control performance. Therefore, a state of the art DSP-processor was used for the implementation of the control algorithm. Control and identification programs have been implemented in C-code and run on a QPC40 DSP Board (Loughborough Sound Images) which was hosted in an industrial PC. The DSP board hosts 4 Texas Instruments TIM TMS320C40 DSP modules. Three DSPs run in parallel for the execution of the control routines, the fourth communicates with the PC, e.g. for data exchange purposes. Additionally an I/O board, able to manage up to 16 inputs and 8 outputs, is linked to the DSP board. The controller runs at a sample frequency of 1024 Hz.
A classic configuration of anti-aliasing filters at the inputs (cut-off frequency smaller than Nyquist frequency) and reconstruction filters at the outputs (control signals sent to shakers or loudspeakers), to avoid high frequency quantisation noise, is used. These low pass filters have been set at 320 Hz directly on the I/O board.
The installation of the controller hardware in the test car is shown in figure 4.4.

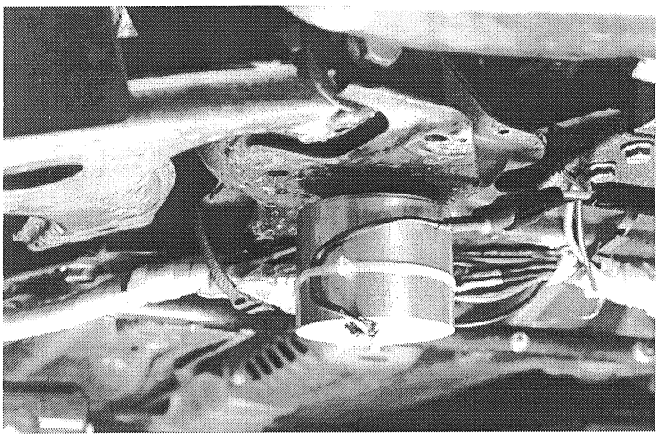

Figure 4.3. Control actuator mounted at the car body.

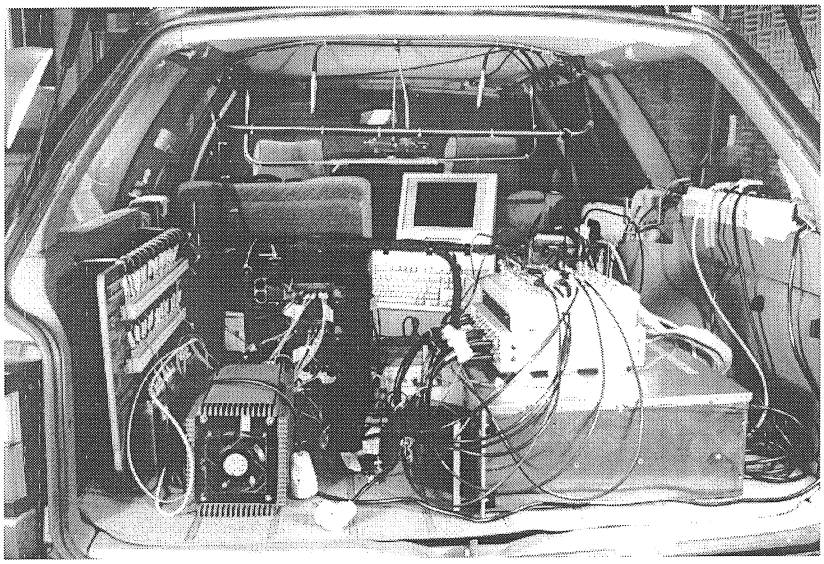

Figure 4.4. Installation of the controller hardware in the test car.

4.2.6 Optimisation of the control parameters by means of numerical simulations

The control performance of different control configurations for a car driven on rough asphalt has been simulated with numerical models in order to determine the optimal control configuration and corresponding controller parameters to be implemented for the road tests.
Simulations have been performed in the frequency domain, as well as in the time domain. The main difference between the time and the frequency domain lies in the fact that in the frequency domain, only steady state behaviour can be analysed. In the time domain, on the other hand, transient effects can be simulated as well. Thus, in the time domain, it is possible to take into account the behaviour of the adaptive control algorithm. The frequency domain simulations have been used to determine the optimal control configuration in terms of the optimal number and location of control actuators and feedback sensors.

Frequency domain simulations

The frequency domain simulations in the framework of the ANRAVA project have been performed by LMS International in co-operation with

PMA and are fully documented in [243]. The most important conclusions are summarised here.

The achievable performance of various ASAC configurations has been compared in simulations, using experimentally acquired data (operational data taken on the road, i.e. acoustical and vibrational measurements), as well as in-laboratory acquired frequency response functions. These FRFs were the transfer functions between a force applied at all possible control actuator locations and the response measured at all possible error sensor locations. The set of control forces, per frequency line, was calculated such that the superposition. Once the optimal control forces are determined, the residual sound field (and thus the achieved reduction) can be determined by superposition of the primary sound field and the secondary sound field obtained by applying the optimal control forces to the FRF matrix.

By these simulations it was understood that using microphones as feedback sensors is more efficient in terms of interior noise reduction compared to feedback of the vibration levels at the actuator locations, even if the controller would be able to significantly suppress these vibration levels (refer to figures 4.5 and 4.6). This was also confirmed by laboratory experiments, as explained in [224] (and by the results achieved in related work dealing with noise in a high speed railcar [240]). As a consequence, collocated feedback sensors were not considered in the remainder of the work. The error microphones were constrained to be located at the ceiling of the car cabin ; the most reasonable choice was to locate them above each passenger's head.

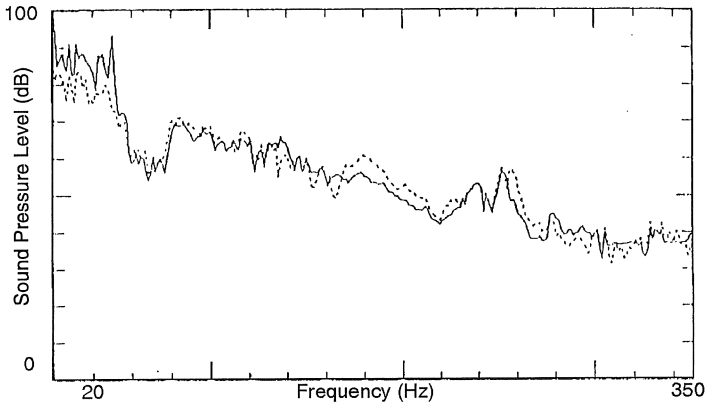

Figure 4.5. Frequency domain simulation. Synthesised Sound pressure level at the error microphone using vibration at actuator locations as feedback signal (dotted : with control, solid : without control).

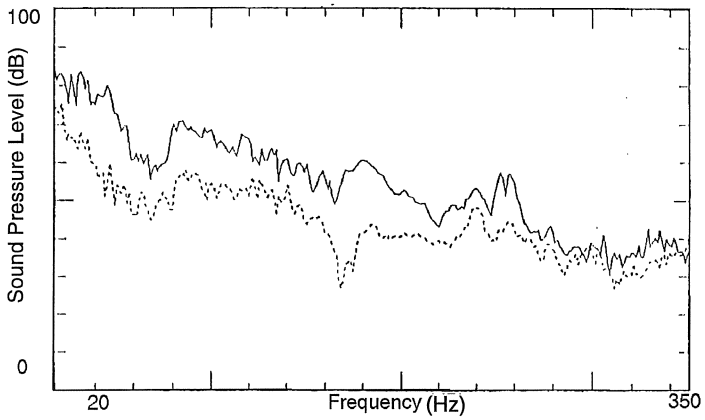

Figure 4.6. Frequency domain simulation. Synthesised sound pressure level at the error microphone using microphones as feedback sensors (dotted : with control, solid : without control).

The frequency domain simulations have been used to determine the optimal number and location of the control actuators. An optimal compromise (hardware cost and weight vs. control performance) was found for a configuration using 6 control actuators, located at the front shock absorber top mount, the triangle mount of the front suspension, and the lower mount of the rear suspension (left/right symmetric configuration). Figure 4.7 shows the location of the control actuators on the car suspension.

Frequency domain simulations lack the constraint of causality and assume stationarity. Furthermore, the effect of coherence between references and error signals is not included, such that the selection of the appropriate reference signals is not taken into account. Frequency domain simulations may indicate limits of performance for various control actuator configurations but they do not exactly predict the control performance nor do they yield information on the transient behaviour of the controller. For these reasons, a time domain simulation tool has been developed, which is discussed below.

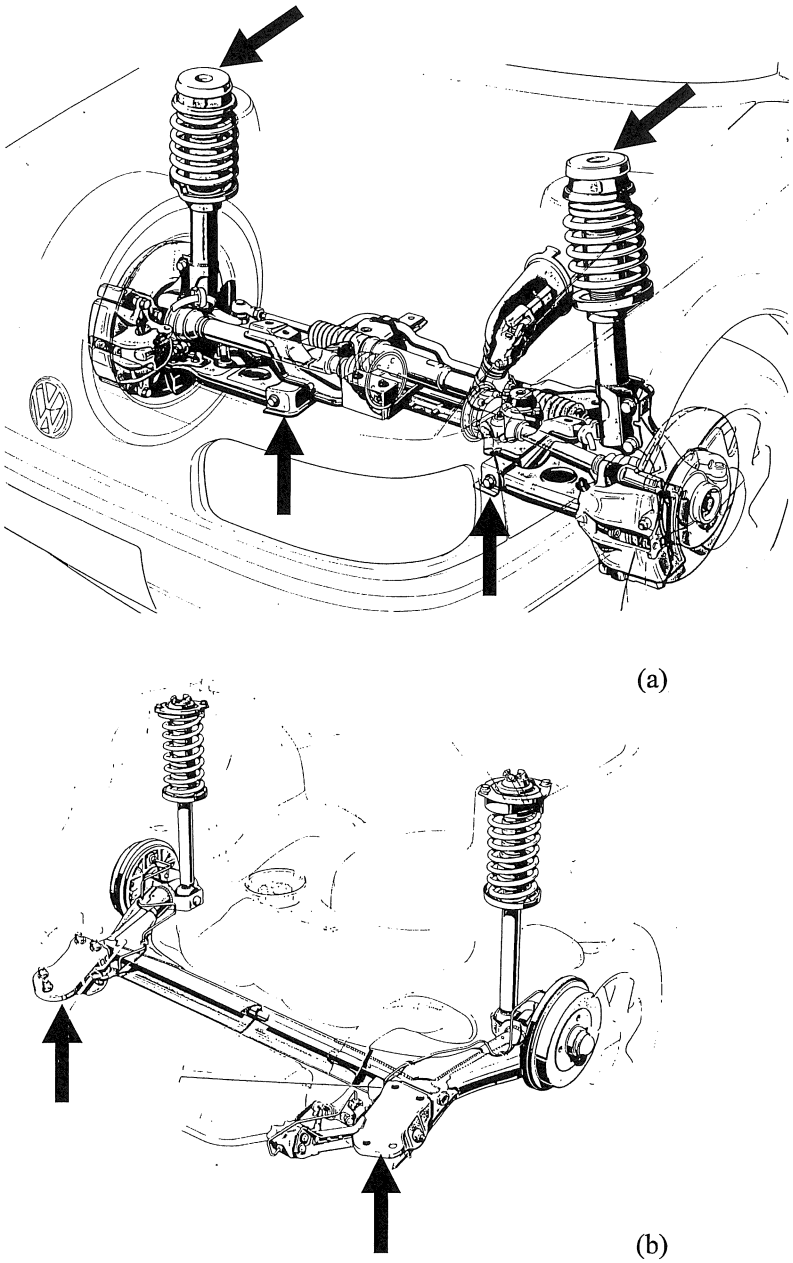

Figure 4.7. Location and actuation direction (direction of the arrow) of the optimal set of control actuators mounted at the front (a) and rear (b) suspension.

Time domain simulations

The time domain simulation tool integrates FRFs acquired in laboratory, operational data measured during road tests, and the multi-channel Filtered-X LMS adaptive feedforward controller. Figure 4.8 presents a schematic overview of the time domain simulation tool.

The FRFs are vibro-acoustic transfer functions that represent the physical secondary paths. An FRF model of the complete car (a 30 by 4 FRF matrix for 30 possible actuator positions and 4 possible error microphone positions) has been composed. The control actuators can thus be "connected" to any of the excitation points by selecting the appropriate FRF in the simulations. The operational data are the wheel centre vibrations and the sound pressure levels inside the car cabin, measured during road tests performed on rough asphalt. A selection of the wheel centre vibrations is used as a reference set for the feedforward controller, which in turn drives models of the secondary paths (impulse response functions, derived from the FRFs) instead of physical secondary paths. The output of the secondary path models (synthesised secondary sound pressures) is delayed one sample period, to account for computational delay introduced by the DSP, after which it is added to the primary sound pressure measured at the error microphones during road tests. This provides the error signal to be used in the adaptive loop of the control algorithm. The simulation tool was validated by simulating a single channel control configuration of the laboratory tests, as explained in [223].

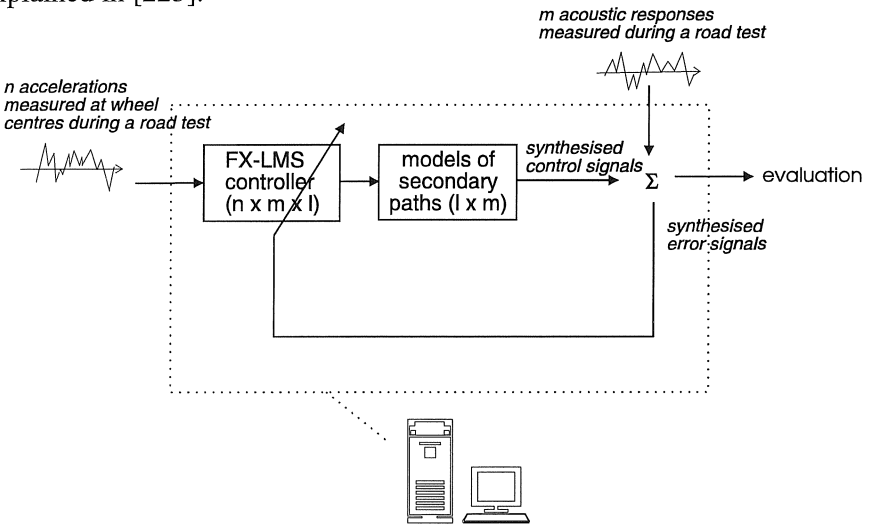

Figure 4.8. Basic scheme for the time domain simulations.

The time domain simulations have focused on optimising the control system using 6 control actuators and 4 error microphones which locations have been determined by frequency domain analysis as explained before. The control configuration is further analysed by simulating the effect of the reference set on the achievable reduction. Figure 4.9 compares the multiple coherence between 12 reference sensors, located at the wheel centres (x-, y-, and z-direction per wheel) to the multiple coherence between a set of six references (y- and z-direction in front, y-direction in the rear). Clearly the coherence is far from equal to one and it drops drastically above 350 Hz. Limiting the number of references to 6[1] seems to be appropriate because *(i)* the coherence does not drop too significantly in the main frequency bands of interest (ref. figure 4.10), *(ii)* it is less computationally intensive and *(iii)* the convergence properties of the controller are enhanced (refer to paragraph 4.4).
Using the simulation tool and the operational data, the controller parameters were optimised. The length of the control filters was set to 140 coefficients whereas the secondary path model filter length was set to 80 coefficients. Furthermore, measures have been taken to constrain the control voltages (which can also be monitored during simulation) within the output range of the DSP. The latter was achieved by high-pass filtering (8th order Butterworth filters with cut-off at 60 Hz) reference and error signals. Thus it was avoided to spend too much control energy into lower frequency cavity modes that are hardly perceived by the human ear.

[1] It may seem strange that the road excitation cannot be described appropriately by 4 accelerometers (a car has 4 wheels). In this particular project, however, it was found that the muliple coherence of 4 references was considerably worse than in the case of 6 references. This seems to be confirmed by other studies, which also suggest a larger number of references (larger than 4) [228]. A larger number of reference sensors is motivated by that fact that the car suspension is in essence a non-linear system.

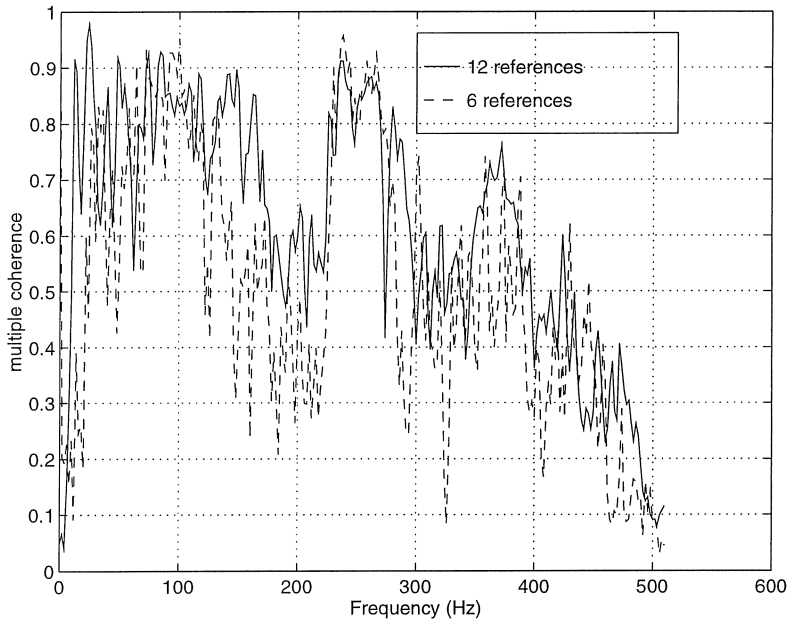

Figure 4.9. Multiple coherence between 12 and 6 references and the error microphone.

Figure 4.10 presents the synthesised sound pressure level[2] of the rear left error microphone after 87.000 simulation steps. The sound spectrum in the car cabin is dominated by two major effects, namely the second longitudinal mode of the acoustic cavity (78 Hz), and a tire resonance (250 Hz). The controller is primarily concerned with reducing the noise level at these frequencies because this primarily affects the reduction of the cost function that is to be optimised (sum of the squared error signals). In the frequency range from 75 to 105 Hz, an average noise reduction of 7.3 dB has been achieved in the rear left error microphone. In the frequency range from 225 to 275 Hz, an average noise reduction of 5.2 dB has been achieved in the rear left error microphone. Comparable reduction is achieved in the rear right microphone. Somewhat smaller reductions are achieved in the front, this is because the sound level in the rear is larger over the whole frequency band.

[2] For reasons of confidentiality, no calibrated sound pressure levels are presented in this text. Sound pressure levels, presented in all figures in dB, are actually dBV values (voltage measured at the microphone) without mentioning the calibration factor.

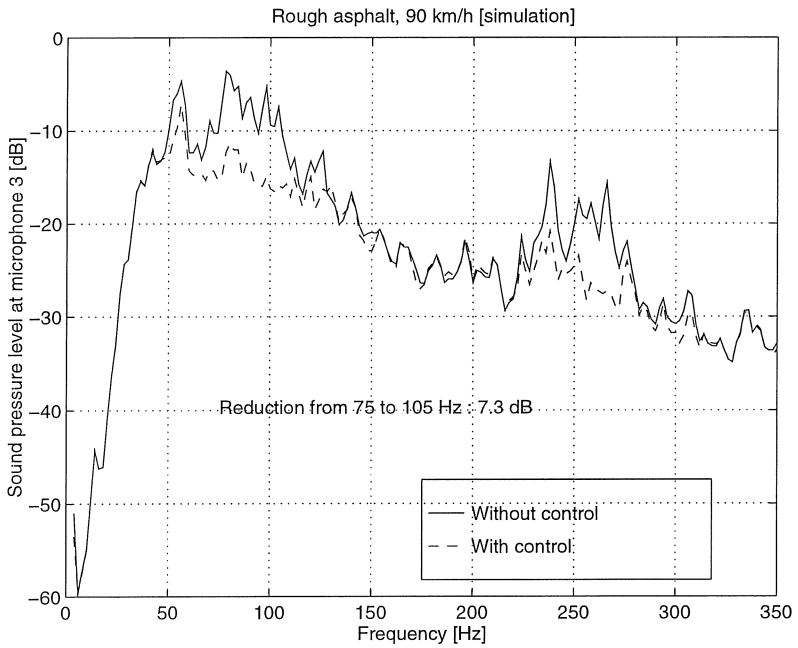

Figure 4.10. Synthesised sound pressure level at the rear left error microphone without/with control. Results achieved on simulation.

Figure 4.11 presents the synthesised control voltage sent to one of the control actuators during the last 100 ms of the simulation for the case without, and for the case with high-pass filtering of the references and errors. The control voltage has been reduced by a factor of 10.

4.3 Experimental results

4.3.1 Laboratory tests

To experimentally validate the control approach, tests have been performed on the demonstrator car. An LDS 2200 N shaker (Model V650) excites one rear wheel of the demonstrator car to reproduce the wheel centre vibrations for normal operating conditions (measured during road tests) in terms of frequency content and amplitude (figure 4.12). Bruel & Kjær ½-inch

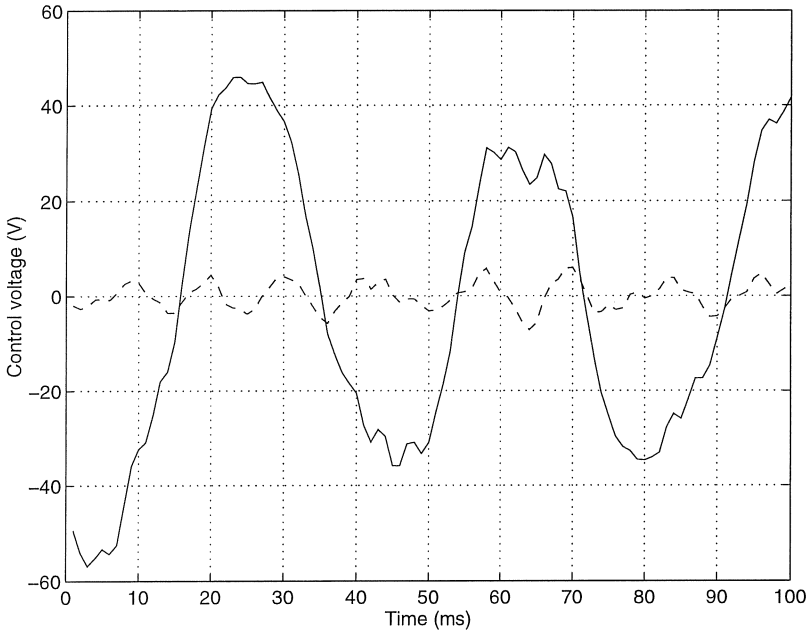

Figure 4.11. Synthesised control signal sent to the same actuator before (solid) and after (dashed) high-pass filtering the error and reference signals.

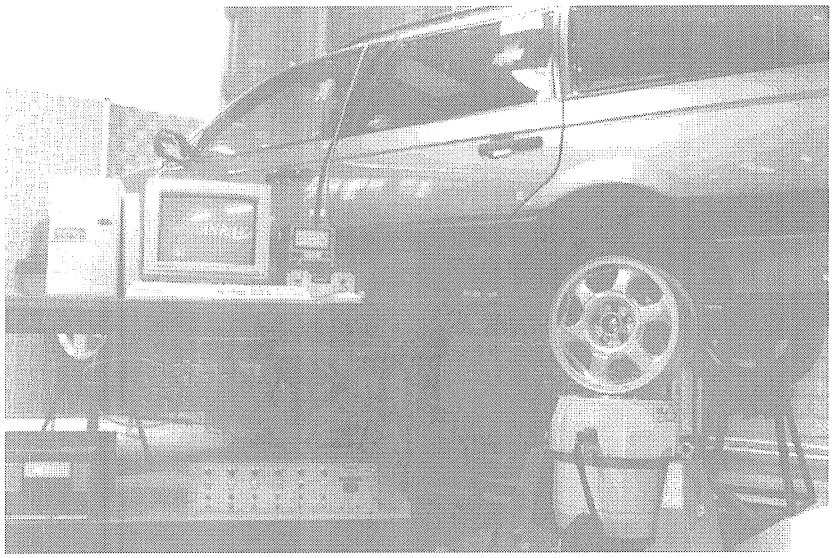

Figure 4.12. Laboratory set-up.

condenser microphones (type 4188) serve as error microphones, the output of which is fed to the controller as well as to an Ono Sokki CF-350 frequency analyser for control performance evaluation. Data records have been transferred to Matlab®, overall reductions have been calculated by averaging sound pressure level^2 differences (without control - with control) in dB at the error microphone over the frequency band of interest.

Single channel control

A single channel controller (one control actuator and one error microphone) was used in a first series of experiments to demonstrate the effect of causality. Figure 4.13 presents the coherence for three different reference sensor positions (position (a) corresponds to the wheel hub, (b), and (c) are locations on the suspension and closer to the car body). The overall values indicate that the coherence increases for position (b) and (c), although this effect is very limited because the measurements have been performed in laboratory conditions and thus the effect of non-linearities and other non-coherent noise sources is well under control.

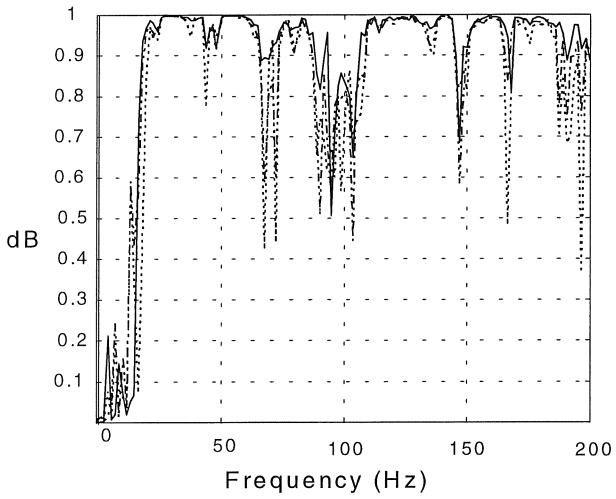

Figure 4.13. Coherence between the reference signal and the error sensor signal for three different reference sensor positions. Overall values : position (a) : 0.91, position (b) : 0.92, position (c) : 0.94.

Figure 4.14 presents the noise levels inside the car cabin when one error microphone and one control actuator are used to control the structure-borne noise level, for each of the reference sensor positions. Although the

coherence is slightly better, the overall reduction decreases for positions (b) and (c), indicating that the corresponding control configuration does not meet the time constraints any more. The best performance is achieved when the reference sensor is located at the wheel hub : 7.13 dB overall noise reduction from 50 to 200 Hz, and over 10 dB in the frequency range from 110 to 160 Hz.

Multiple references

In order to simulate road excitation by multiple uncorrelated forces, an additional primary disturbance shaker was connected to the second rear wheel of the demonstrator car. The primary disturbance shakers were driven with uncorrelated white noise signals.
The maximum achievable reduction drops drastically when only one reference signal is used under these circumstances. This is mainly due to the fact that an individual reference sensor does not pick up all necessary information to control both uncorrelated sources. This is clearly indicated by the ordinary coherence of a single reference sensor with respect to the sound

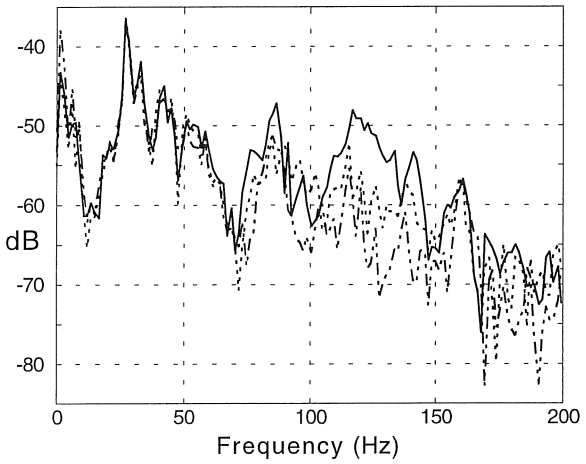

Figure 4.14. Controlled noise level in the error microphone using one control actuator and three different reference sensor positions. Overall reduction for reference sensor in pos. (a) : 7.13 dB, pos. (b) : 5.44 dB, pos. (c) : 2.6 dB.

pressure at the error microphone, in the case where two uncorrelated primary sources are exciting the demonstrator car (figure 4.15). The reference sensors were located on the left and right rear wheel hub (figure 4.15a and 4.15b, respectively). Note that both reference signals are

complementary, which indicates the need for two references to detect both primary disturbances.

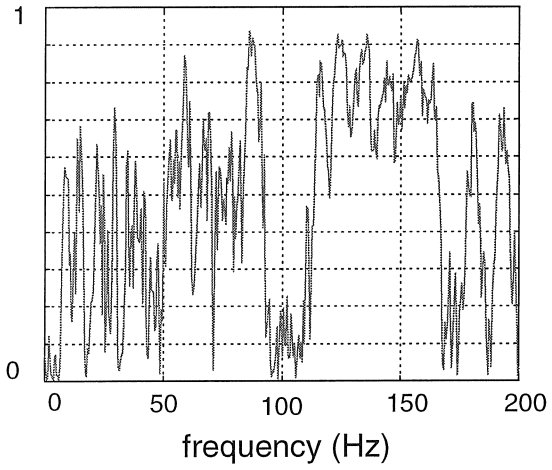

(a)

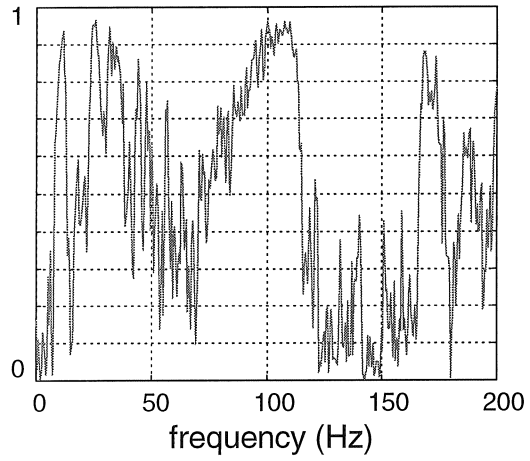

(b)

Figure 4.15.Ordinary coherence between the error signal and each of the reference signals in the case of two uncorrelated primary sources.

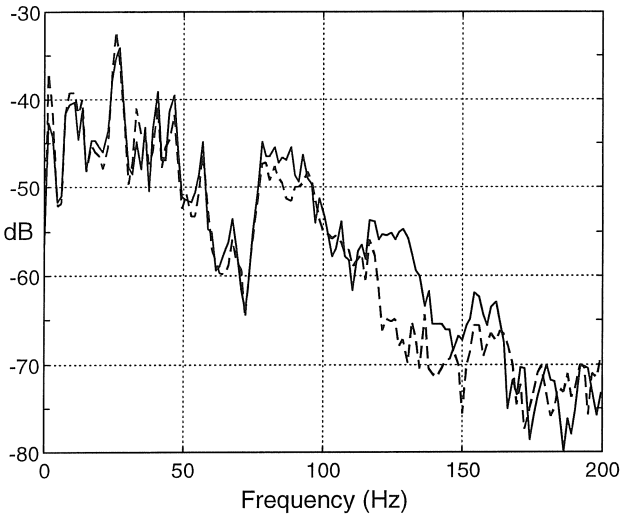

Figure 4.16. Sound power spectrum of the error microphone for two uncorrelated primary disturbances when only one reference signal is used (solid : without control, dashed : with control). Overall reduction in the band from 70-150 Hz is 3.8 dB.

The control result for the case where only one reference signal (corresponding to figure 4.15a) is used in the presence of two primary disturbances, is shown in figure 4.16. Two control actuators have been used to reduce the sound pressure at two error microphones inside the car cabin. The sound pressure at the error microphone is only effectively reduced in the range where the ordinary coherence is considerably high (cf. figure 4.15a). The maximum achievable reduction is 3.8 dB in the frequency range from 70 to 150 Hz.

Using both reference signals (located on the left and right rear wheel hub), two control actuators and two error microphones, the overall reduction in the frequency range from 50 to 160 Hz has been increased to 7.8 dB (Figure 4.17).

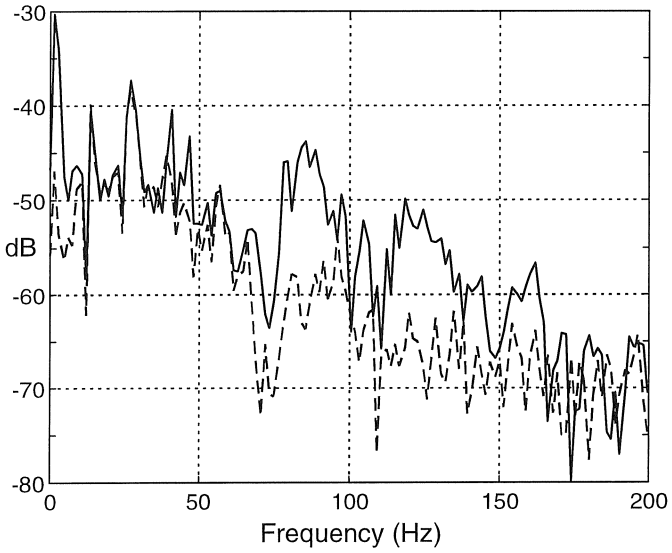

Figure 4.17. Sound power spectrum of the error microphone for two uncorrelated primary disturbances (solid : no control, dashed : with control). Overall reduction in the frequency band from 50-160 Hz is 7.8 dB.

4.3.2 Road tests

ASAC system

Road tests with the full system (6 references, 6 actuators, 4 error microphones) have been performed at a constant speed of 90 km/h. The background noise generated by the control and measurement equipment (PC, amplifiers, etc.) was evaluated and was found to be negligible. Also the physical feedback of the control action to the references was found to be negligible (this implies that the bushings are actually relatively efficient, because they isolate that actuators from the reference sensors - at the same time this means that the active control system is actually reducing a residual component of the road excitation, namely the part which is not reduced by the bushings). Special care was taken to prevent output saturation during the road tests. This easily occurs in overdetermined control systems (more control actuators than error sensors). Figure 4.18 presents the attenuation obtained with the ASAC system.

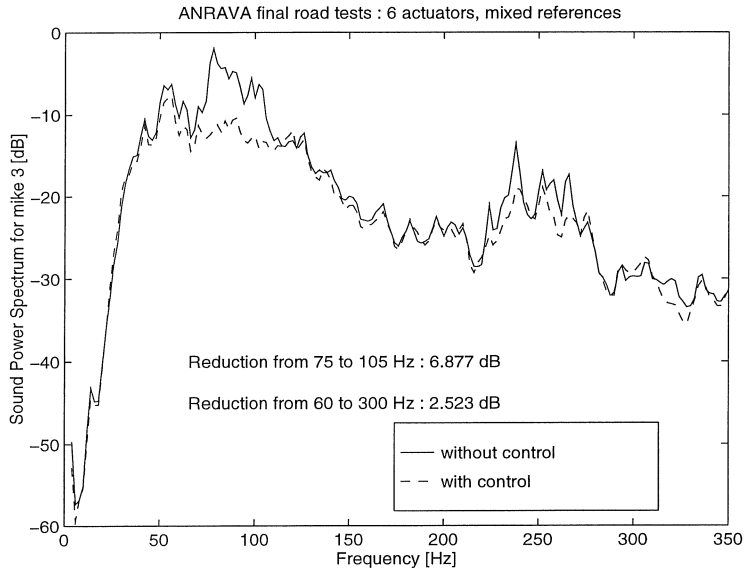

(a) Reduction at rear left error microphone

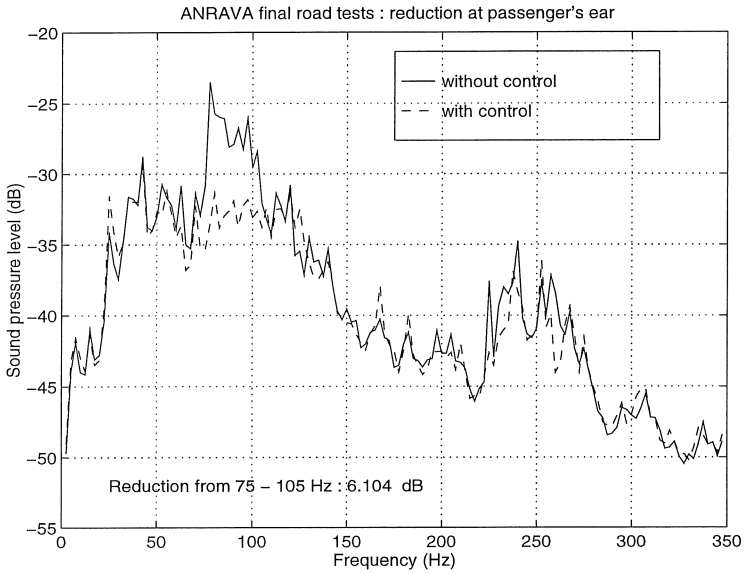

(b) Reduction at the passenger's ear at rear left seat

Figure 4.18. Results of the road tests with the ASAC system.

The reduction is sensible in particular frequency ranges (60-120, 225-280 Hz) that correspond to booms of the car cavity and to the tire resonance respectively. An average noise reduction of 6.9 dB reduction has been achieved in the range from 75 - 105 Hz at the error microphone. This yields 6.1 dB reduction at the passenger's ear in the same frequency range.

ANC system

Comparative road tests with the ANC system have been carried out. The number of loudspeakers used for this control system was limited to 4 for practical reasons. The results presented in figure 4.19 have been achieved using car body references. As in the case of ASAC, the noise reduction is sensible in particular frequency ranges (60-120, 225-280 Hz). A maximum reduction of 10.2 dB was achieved in the range from 75 - 105 Hz at the error microphone. At the passenger's ear, this yields 8.8 dB reduction.

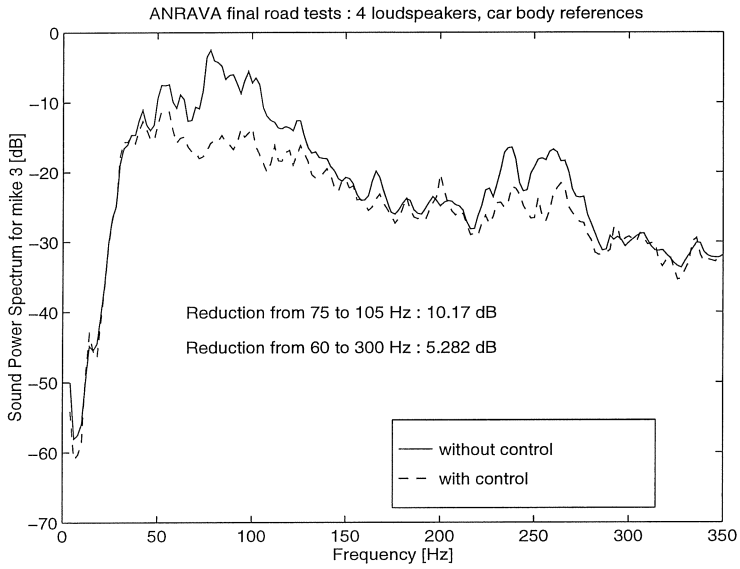

(a) Reduction at rear left error microphone

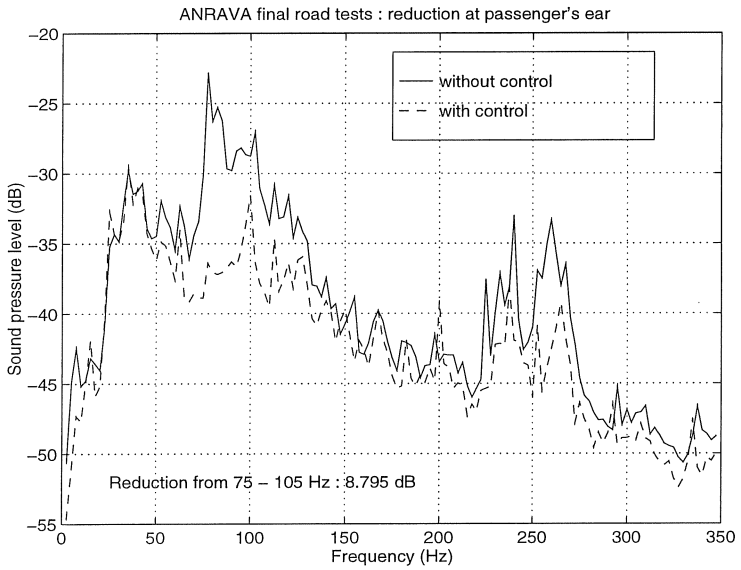

(b) Reduction at the passenger's ear at rear left seat

Figure 4.19. Results of the road tests with the ANC system.

Evaluation and conclusions

As the ASAC configuration is inherently more expensive than the ANC system (the ANC system uses the original loudspeakers whereas the ASAC system adds -relatively expensive- inertia shakers to the system) it is certainly relevant to critically compare the performance of both systems.
The reason why the loudspeaker system achieves better performance than the actuator system is twofold. First of all, when using loudspeakers instead of actuators, it is possible to locate the reference sensors on the main transfer paths and thus to achieve relatively high multiple coherence. Secondly, it was observed that the sound levels that are to be generated to control the sound field inside the car cabin are within the dynamic range of the loudspeakers while the control forces that are to be generated by the vibration actuators are very close to the maximum force that can be generated by the vibration actuators.
However, although the absolute reduction at the error microphones as well as at the monitor microphone are larger than with the ASAC system, the sound field outside the error microphones gets relatively heavily distorted. Because the loudspeakers act much more as point sources, this effect is

easily recognisable when the observer is moving closer to the loudspeakers (although the reduction measured at the passenger's ear, presented in Fig. 14, is considerable). Therefore, there is less sensation of acoustic comfort with the ANC system, compared to the ASAC system which achieves a more uniform reduction in the entire car cabin.

It should be stressed that it is difficult to quantify the acoustic comfort which is achieved by installing an active control system. General noise assessment is carried out using equivalent noise level criteria such as L_{Aeq}. This may lead to an underestimation when using this criterion for active control applications since the largest reductions are generally achieved in a low frequency range. Therefore, in order to evaluate the acoustic comfort which is provided by the active control systems, it is necessary to subjectively evaluate the results [244]. Other than objective measurements, subjective evaluation will reveal the influence of psycho-acoustic effects such as masking [245] (p. 7) and phenomena associated with the perception of (relatively) low-frequency noise [245 - 246].
These effects are particularly important in this research work, since most apparent reductions are achieved in a frequency region (75 - 105 Hz) where the human ear is less sensitive to reduction of sound levels than in higher frequency regions. Furthermore, reducing the sound level at low frequencies takes away the masking effect associated with those low frequency components, which yields the subjective evaluation that higher frequency sound is increased (not that low frequency sound is reduced) when the control system is switched on.
These observations should not mean that reducing low frequency noise components is irrelevant. First of all, the standard deviation of human hearing in the low frequency region is relatively large : 1 out of 6 test persons will have a 5 dB larger sensitivity to low frequency sound than the average. Secondly, though the "audible" sound pressure level threshold increases as the frequency decreases, it has been observed that in particular for low frequency sound, the "annoyance" threshold level is exceeded very soon [246]. As a result, the subjective effect of active control on annoyance is often much clearer than indicated by L_{Aeq} [244]. Reducing low frequency sound, which is achieved by both control systems presented, may thus reduce the effect of interior noise on, e.g., fatigue due to long journeys ([8], p. 58), which justifies the development of such systems.

4.4 REAL-TIME ENHANCEMENT OF THE REFERENCE SIGNALS FOR FEEDFORWARD CONTROL OF RANDOM NOISE DUE TO MULTIPLE UNCORRELATED SOURCES

4.4.1 Introduction

A reference signal for feedforward control needs to be determined such that it characterises the noise source as well as possible. In the particular case of multiple uncorrelated sources one is faced with locating reference sensors that are most likely to sense the multiplicity of all noise sources. As the maximum reduction that can be achieved with a Filtered-X LMS adaptive feedforward controller is determined by the multiple coherence between the set of references and the error signal, it is suggested that it is of prime importance to select a set of references that yields maximum multiple coherence. In the case of a control problem involving multiple uncorrelated sources, it is common practice to use a set of references that is, say, "overdetermined" to realise this. This is mainly done because it is often impossible to know what is the exact number of noise sources and, even if it were possible, it is hard to imagine that each of the noise sources could be measured directly. As a consequence, each of the references will, to some extent, carry information on each of the uncorrelated noise sources.
With a set of references being overdetermined one may expect to "cover" the ensemble of uncorrelated noise sources and thus maximise the multiple coherence between the reference set and the error signal which in turn maximises the maximum achievable reduction at the error sensor. At the same time such an extended set of references seriously increases the computational burden for the DSP executing the Filtered-X control algorithm as well as it deteriorates the convergence speed of the control algorithm.
For a control configuration involving P reference sensors, M control sources, N error sensors, L_{sp} secondary path filter taps and L_{cf} control filter taps, the execution of the control action together with the control filter update according to (2.37), involves

$\left[(P\times N)+(M\times N\times P)\right]\times L_{cf}+(M\times N\times P)\times L_{sp}$ multiplications,

$(P\times N)\left(L_{cf}-1\right)+(P\times N\times M)\left(L_{sp}-1\right)+(M\times N\times P)\times L_{cf}$ additions, and

$P+N+M$ I/O-conversions.

Hence the computational burden is directly proportional to the number of references used. Furthermore, the memory requirements for the implementation of the Filtered-X algorithm are also directly related to the number of references used ($M \times N$ arrays of filtered reference signals and $M \times N$ control filters per reference signal, ...).

In this section, a new technique is introduced that aims at the enhancement of the information that is carried within the references such that the number of references that is used by the control algorithm can be reduced significantly. The basic idea is to generate a reduced set of *virtual references* out of an extended set of references such that duplication of information in the references is avoided. The algorithm which accomplishes this task in real-time is first presented in paragraph 4.4.2. In paragraph 4.4.3, it is then shown that compressing information into a smaller set of references also enhances the convergence speed of the algorithm. In paragraph 4.4.4, the technique of virtual references is applied to the practical problem of reducing structure-borne road noise level inside a car cabin by means of active control. The virtual reference technique presented here, is also discussed extensively in [247].

4.4.2 The virtual reference technique

The idea of virtual references is not entirely new as it relates to similar techniques applied in signal analysis, namely Principal Component Analysis [248]. The application of principal component analysis techniques to the active control of road noise inside automobiles has been presented in [231], where the Number of Independent Sources (NIS) technique is presented which is used to determine how many of the eight reference transducers under consideration are required to achieve significant noise reduction. Road noise was simulated by exciting a tire of a test vehicle using a shaker driven with broadband random noise. The number of independent sources occurring at the source, which directly relates to the minimal number of reference transducers, is determined by computation of the condition number (the ratio of the largest to the smallest singular value) of the matrix composed of the auto- and cross-spectra of the references. The best combination of references was determined using a condition number analysis and multiple coherence analysis for all possible sets of references. A fixed set of references was retained after the procedure.

However, due to the inherent non-linear nature of the vibration energy propagation through a car's suspension, the optimal set of reference transducers will depend on the operating conditions (pavement, smooth asphalt,...). As a result, though some upper limit to the number of independent sources -hence to the number of transducers- may be assumed, the physical transducers which best describe these sources may vary as a function of the operating conditions. The on-line estimation scheme proposed here, uses a fixed, extensive, set of reference transducers which responses are processed to a limited number of virtual reference signals. These virtual references may thus be different as a function of the operating conditions.

Frequency domain data enhancement

In [249] a frequency domain technique for enhancement of references is proposed, based on the diagonalisation of the cross spectral density matrix $[\mathbf{S_{xx}}]$ of the reference signals :

$$[\mathbf{S_{xx}}(\omega)] = \mathbf{E}\left\{[\mathbf{X}(\omega)][\mathbf{X}(\omega)]^H\right\} = \mathbf{E}\left\{\begin{bmatrix} \mathbf{X_1}(\omega)\mathbf{X_1}(\omega)^H & \cdots & \mathbf{X_1}(\omega)\mathbf{X_P}(\omega)^H \\ \vdots & \ddots & \vdots \\ \mathbf{X_P}(\omega)\mathbf{X_1}(\omega)^H & \cdots & \mathbf{X_P}(\omega)\mathbf{X_P}(\omega)^H \end{bmatrix}\right\}. \quad (4.1)$$

With : $[\mathbf{X}(\omega)]_{P\times 1} = \mathcal{F}\left\{[\mathbf{x}(k)]_{P\times 1}\right\} = [\mathbf{X_1}(\omega) \ \cdots \ \mathbf{X_P}(\omega)]^T$ the spectra of the references ($\mathcal{F}\{\cdot\}$ denotes discrete Fourier transform).

The cross spectral density matrix $[\mathbf{S_{xx}}]$ has the (real) power spectral densities of the references as diagonal elements and the (complex) cross spectral densities of the references as off-diagonal elements. Cross-diagonal elements are complex conjugate.
Calculating the singular value decomposition of the cross spectral density matrix yields :

$$[\mathbf{S_{xx}}(\omega)]_{P\times P} = [\mathbf{U}(\omega)]_{P\times P}[\Sigma(\omega)]_{P\times P}[\mathbf{V}(\omega)]^H_{P\times P}. \quad (4.2)$$

This expression holds for every frequency line. For readability the explicit frequency dependence is omitted in the next equations.
Since the power spectral density matrix is a complex conjugate matrix $\left([\mathbf{S_{xx}}] = [\mathbf{S_{xx}}]^H\right)$, left and right singular vectors are identical, or :

$$[\mathbf{S_{xx}}]_{P\times P} = [\mathbf{U}]_{P\times P}[\Sigma]_{P\times P}[\mathbf{U}]^H_{P\times P}. \quad (4.3)$$

With : $[\Sigma]_{P\times P}$ the diagonal matrix with the singular values (in descending order, i.e. $\sigma_1 \geq \cdots \geq \sigma_P \geq 0$),

$[\mathbf{U}]_{P\times P}$ the orthonormal matrix $\left([\mathbf{U}][\mathbf{U}]^H = [\mathbf{I}]\right)$ with the singular vectors as columns,

the cross spectral density matrix can be written as a sum of independent terms, each corresponding to a singular value :

$$[\mathbf{S_{xx}}]_{P\times P} = \sum_{i=1}^{P}\left(\sigma_i [\mathbf{U_i}]_{P\times 1}[\mathbf{U_i}]^H_{1\times P}\right). \tag{4.4}$$

With N_S singular values which are supposed to be significantly larger than zero, $\sigma_1 \geq \cdots \geq \sigma_{N_S} > 0$, $\sigma_{N_S+1}\cdots\sigma_P \approx 0$, the sum can be truncated and the cross spectral density matrix can be approximated by :

$$[\mathbf{S_{xx}}]_{P\times P} \approx \sum_{i=1}^{N_S}\left(\sigma_i [\mathbf{U_i}]_{P\times 1}[\mathbf{U_i}]^H_{1\times P}\right) = [\mathbf{U}]_{P\times N_S}[\Sigma]_{N_S\times N_S}[\mathbf{U}]^H_{N_S\times P} \tag{4.5}$$

With : $[\Sigma]_{N_S\times N_S}$ the matrix with the N_S largest singular values

$[\mathbf{U}]_{P\times N_S}$ the matrix with the N_S first singular vectors

Thus, truncation is equivalent to keeping the N_S largest singular values and the corresponding N_S singular vectors. Hence, the rank of $[\mathbf{S_{xx}}]$ is reduced from P to N_S.
Thus, after some manipulations :

$$[\Sigma]_{N_S\times N_S} \approx [\mathbf{U}]^H_{N_S\times P}[\mathbf{S_{xx}}]_{P\times P}[\mathbf{U}]_{P\times N_S}. \tag{4.6}$$

A set of N_S independent virtual reference signals $[\mathbf{X}^\circ]$ can now be obtained by defining :

$$[\mathbf{X}^\circ]_{N_S\times 1} = [\mathbf{U}]^H_{N_S\times P}[\mathbf{X}]_{P\times 1}. \tag{4.7}$$

The cross spectral density matrix of these virtual reference signals yields:

$$[\mathbf{S_{X^\circ X^\circ}}]_{N_S\times N_S} = \mathbf{E}\left\{[\mathbf{X}^\circ]_{N_S\times 1}[\mathbf{X}^\circ]^H_{1\times N_S}\right\} = [\mathbf{U}]^H_{N_S\times P}[\mathbf{S_{xx}}]_{P\times P}[\mathbf{U}]_{P\times N_S} \approx [\Sigma]_{N_S\times N_S}. \tag{4.8}$$

Some physical considerations can be made at this point:

- The virtual reference signals obtained by (4.7) are independent, since the cross spectral density function between every pair of virtual reference signals equals zero.
- The total power present in the original set of reference signals is conserved since the transformation matrix [**U**] is unitary.
- The number of significant singular values N_s is equal to the number of independent sources that adequately describe the set of original reference signals, at a particular frequency line.

The development presented above shows that it is possible to obtain a set of independent virtual reference signals that consists of only N_s signals (instead of P). The required computation time for the control algorithm will thus decrease. At the same time, the set of virtual reference signals contains all the significant information that is present in the original reference signals. The theoretical maximum achievable reduction is thus unaffected.
However, the virtual reference signals are defined in the frequency domain and cannot be used for real-time control. Time-domain virtual references are obtained by inverse discrete Fourier transformation of (4.7) :

$$\begin{aligned}\left[\mathbf{x}^{\circ}(k)\right]_{N_S\times 1} &= \mathcal{F}^{-1}\left\{\left[\mathbf{X}^{\circ}(\omega)\right]_{N_S\times 1}\right\} \\ &= \mathcal{F}^{-1}\left\{\left[\mathbf{U}(\omega)\right]^{H}_{N_S\times P}\left[\mathbf{X}(\omega)\right]_{P\times 1}\right\} \\ &= \left[\mathbf{u}(k)\right]^{H}_{N_S\times P} * \left[\mathbf{x}(k)\right]_{P\times 1}.\end{aligned} \tag{4.9}$$

(* denotes the convolution operator)

The matrix $\left[\mathbf{U}(\omega)\right]$ can thus be interpreted as the matrix of frequency response functions (FRFs) between the original and the virtual references. The matrix $\left[\mathbf{u}(k)\right]$ contains the corresponding impulse response functions (IRFs). For computational reasons, these IRFs are implemented as finite impulse response filters (FIR-filters), which are truncated impulse response functions.
Thus, each time domain virtual reference signal is obtained as a sum of convolutions of every time domain original reference signal and the corresponding FIR-filters:

$$x_i^{\circ}(k) = \sum_{j=1}^{P}\left(u_{ij}(k) \otimes x_j(k)\right) \quad i = 1\cdots N_S. \tag{4.10}$$

When applying the frequency domain data enhancement technique to the operational data sets, acquired during road tests (paragraph 4.3), it was observed that this approach leads to severe problems in practice. First of all, since the singular value decomposition is computationally involving, it is calculated off-line. The obtained transformation matrix is then transformed to the time domain and implemented as FIR-filters. The off-line generated FIR-filters are then used for the on-line control algorithm. This approach assumes stationary conditions which are not necessarily valid, specially not in the case of active control of road noise in vehicles. Furthermore, as the transformation matrix is obtained in the frequency domain, it is not constrained to be causal which may imply that the transformation cannot be realised in the time domain.

Another problem is a cross-over effect that often occurred when the frequency functions $U_{ij}(\omega)$ are transformed to the time domain. At a cross-over frequency, the order of importance of two independent sources changes. This is indicated by a crossing in the plot of the singular values. Since the SVD is calculated frequency line by frequency line, cross-over effects cause discontinuities in the calculated $\sigma_i(\omega)$ and $U_{ij}(\omega)$ functions. For a simple case with 2 singular values, the cross-over effect is shown in figure 4.20. For data sets involving multiple singular values, multiple cross-overs occur which must be detected such that continuity of the singular-value functions can be assured. The cross-over effect was detected by looking at the transformation matrices for two adjacent frequencies, $[\mathbf{U}(\omega_n)]$ and $[\mathbf{U}(\omega_{n+1})] = [\mathbf{U}(\omega_n + \Delta\omega)]$, as explained below.

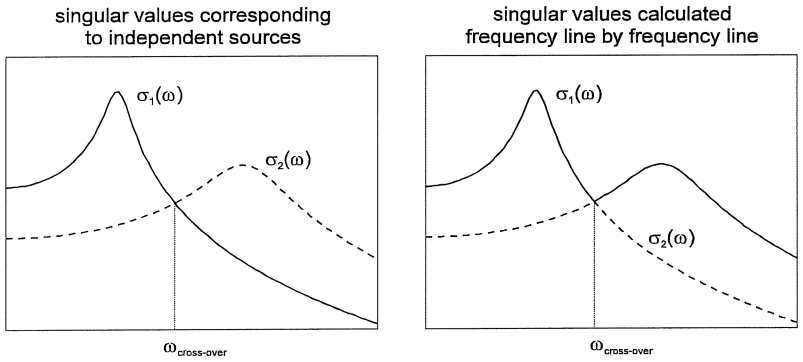

Figure 4.20. Cross-over effect.

As each transformation matrix is orthonormal,

$$\left[\mathbf{U}(\omega_n)\right]\left[\mathbf{U}(\omega_n)\right]^H = [\mathbf{I}] \quad \text{and} \quad \left[\mathbf{U}(\omega_{n+1})\right]\left[\mathbf{U}(\omega_{n+1})\right]^H = [\mathbf{I}]. \tag{4.11}$$

When the functions $U_{ij}(\omega)$ are smooth functions of frequency, the cross-product of two transformation matrices for adjacent frequency lines also approximates a unity matrix :

$$\left[\mathbf{U}(\omega_n)\right]\left[\mathbf{U}(\omega_{n+1})\right]^H \approx [\mathbf{I}]. \tag{4.12}$$

When a cross-over occurs between frequency lines ω_n and ω_{n+1}, it is reflected in the matrix of singular values since two singular values will change position mutually. In the matrix of singular vectors, the two corresponding columns are switched :

$$\left[\Sigma(\omega_n)\right] = \begin{bmatrix} \ddots & & \\ & \sigma_i(\omega_n) & 0 \\ & 0 & \sigma_j(\omega_n) \\ & & \ddots \end{bmatrix} \tag{4.13a}$$

$$\left[\Sigma(\omega_{n+1})\right] = \begin{bmatrix} \ddots & & \\ & \sigma_j(\omega_{n+1}) & 0 \\ & 0 & \sigma_i(\omega_{n+1}) \\ & & \ddots \end{bmatrix} \tag{4.13b}$$

$$\left[\mathbf{U}(\omega_n)\right] = \left[\cdots \vdots \mathbf{U}_i(\omega_n) \quad \mathbf{U}_j(\omega_n) \vdots \cdots\right] \tag{4.14a}$$

$$\left[\mathbf{U}(\omega_{n+1})\right] = \left[\cdots \vdots \mathbf{U}_j(\omega_{n+1}) \quad \mathbf{U}_i(\omega_{n+1}) \vdots \cdots\right] \tag{4.14b}$$

As a result of this, the cross-product of the two transformation matrices approximates a unity matrix with two columns switched :

$$\left[\mathbf{U}(\omega_n)\right]\left[\mathbf{U}(\omega_{n+1})\right]^H \approx \begin{bmatrix} \ddots & & \\ & 0 & 1 \\ & 1 & 0 \\ & & \ddots \end{bmatrix} \tag{4.15}$$

Detecting cross-over, and rearranging the singular values accordingly, can impossibly be realised without human interaction. This makes it impossible to implement the frequency domain technique in real time.

Time domain data enhancement

To overcome the shortcomings of the frequency domain technique, an on-line time domain technique for data enhancement is proposed now. The technique is inspired by the work of Moonen [251]. The aim is to find a transformation matrix $[\mathbf{T}(k)]$ such that the virtual reference signals are defined as :

$$[\mathbf{x}^{\circ}(k)]_{N_S \times k} = [\mathbf{T}(k)]^T_{N_S \times P} [\mathbf{x}(k)]_{P \times k} . \tag{4.16}$$

With : $[\mathbf{x}(k)]_{P \times k} = [\mathbf{x_1}(k) \quad \cdots \quad \mathbf{x_P}(k)]^T$ the original reference signals,

$[\mathbf{x}^{\circ}(k)]_{N_S \times k} = [\mathbf{x}^{\circ}_{\mathbf{1}}(k) \quad \cdots \quad \mathbf{x}^{\circ}_{\mathbf{N_S}}(k)]^T$ the virtual reference signals,

$[\mathbf{x_i}(k)]_{1 \times k} = [x_i(1) \quad \cdots \quad x_i(k)]$ the i-th original reference signal,

$[\mathbf{x}^{\circ}_{\mathbf{i}}(k)]_{1 \times k} = [x^{\circ}_i(1) \quad \cdots \quad x^{\circ}_i(k)]$ the i-th virtual reference signal,

until time step k,

and $[\mathbf{T}(k)]$ a transformation matrix that transforms the set of P original reference signals into a set of N_S independent virtual reference signals at time step k.

The independence of a set of time signals can be evaluated by looking at the covariance matrix. For the original reference signals, this covariance matrix is determined as :

$$[\mathbf{COV_{xx}}(k)]_{P \times P} = [\mathbf{x}(k)]_{P \times k} [\mathbf{x}(k)]^T_{k \times P}$$

$$= \begin{bmatrix} \sum_{n=0}^{k} (x_1^2(n)) & \cdots & \sum_{n=0}^{k} (x_1(n) x_P(n)) \\ \vdots & \ddots & \vdots \\ \sum_{n=0}^{k} (x_P(n) x_1(n)) & \cdots & \sum_{n=0}^{k} (x_P^2(n)) \end{bmatrix} . \tag{4.17}$$

$[\mathbf{COV_{xx}}(k)]$ is a real symmetric matrix with variances of reference signals as diagonal elements and covariances between two reference signals as off-diagonal elements.

If the covariance matrix of a set of signals is diagonal, the signals are independent, since the covariance function between every pair of signals is then equal to zero.

The covariance matrix for the virtual reference signals then equals :

$$\begin{aligned}\left[\mathbf{COV}_{\mathbf{x}^\circ\mathbf{x}^\circ}(k)\right]_{N_S\times N_S} &= \left[\mathbf{x}^\circ(k)\right]_{N_S\times k}\left[\mathbf{x}^\circ(k)\right]^T_{k\times N_S} \\ &= \left[\mathbf{T}(k)\right]^T_{N_S\times P}\left[\mathbf{x}(k)\right]_{P\times k}\left[\mathbf{x}(k)\right]^T_{k\times P}\left[\mathbf{T}(k)\right]_{PxN_S} \\ &= \left[\mathbf{T}(k)\right]^T_{N_S\times P}\left[\mathbf{COV}_{\mathbf{xx}}(k)\right]_{P\times P}\left[\mathbf{T}(k)\right]_{P\times N_S}.\end{aligned} \tag{4.18}$$

The covariance matrix of the reference signals can be diagonalised by means of a singular value decomposition. Since $\left[\mathbf{COV}_{\mathbf{xx}}(k)\right]$ is symmetric, the left and right eigenvectors are equal :

$$\left[\mathbf{COV}_{\mathbf{xx}}(k)\right]_{P\times P} = \left[\mathbf{u}(k)\right]_{P\times P}\left[\Sigma(k)\right]_{P\times P}\left[\mathbf{u}(k)\right]^T_{P\times P}. \tag{4.19}$$

With : $\left[\Sigma(k)\right]_{P\times P}$ the diagonal matrix with the singular values in descending order,

$\left[\mathbf{u}(k)\right]_{P\times P}$ the orthonormal matrix $\left(\left[\mathbf{u}(k)\right]\left[\mathbf{u}(k)\right]^H = \left[\mathbf{I}\right]\right)$ with singular vectors as columns.

With N_S significant singular values, $\left[\mathbf{COV}_{\mathbf{xx}}(k)\right]$ can be approximated by a truncated sum :

$$\begin{aligned}\left[\mathbf{COV}_{\mathbf{xx}}(k)\right]_{P\times P} &\approx \sum_{i=1}^{N_S}\left(\sigma_i(k)\left[\mathbf{u}_\mathbf{i}(k)\right]_{P\times 1}\left[\mathbf{u}_\mathbf{i}(k)\right]^T_{1\times P}\right) \\ &= \left[\mathbf{u}(k)\right]_{P\times N_S}\left[\Sigma(k)\right]_{N_S\times N_S}\left[\mathbf{u}(k)\right]^T_{N_S\times P}.\end{aligned} \tag{4.20}$$

If now the matrix of singular vectors is taken as the transformation matrix (4.16) :

$$\left[\mathbf{T}(k)\right] = \left[\mathbf{u}(k)\right], \tag{4.21}$$

the covariance matrix of these virtual reference signals becomes :

$$\begin{aligned}\left[\mathbf{COV}_{\mathbf{x}^\circ\mathbf{x}^\circ}(k)\right]_{N_S\times N_S} &= \left[\mathbf{x}^\circ(k)\right]_{N_S\times k}\left[\mathbf{x}^\circ(k)\right]^T_{k\times N_S} \\ &= \left[\mathbf{u}(k)\right]^T_{N_S\times P}\left[\mathbf{COV}_{\mathbf{xx}}(k)\right]_{P\times P}\left[\mathbf{u}(k)\right]_{P\times N_S} \\ &\approx \left[\Sigma(k)\right]_{N_S\times N_S}.\end{aligned} \tag{4.22}$$

Thus virtual reference signals obtained in this way are independent.

So far, a technique has been proposed to transform a set of k time samples of references in a set of k time samples of virtual references. The transformation is determined such that it orthogonalises all reference vectors until time instant k and is therefore guaranteed to be causal. However, it does not guarantee orthogonality at time instant $(k+1)$ and therefore it must be determined at each time instant, after which the virtual references can be calculated. For real time control applications, an on-line technique is needed which directly transforms each new sample of the references to a new sample of virtual reference signals.

Suppose a new time sample of reference signals $[\mathbf{n}(k+1)]$ arrives at time step $(k+1)$. The new set of reference signals is :

$$[\mathbf{x}(k+1)]_{P\times(k+1)} = [\mathbf{x}(k) \quad \mathbf{n}(k+1)]. \tag{4.23}$$

Where $[\mathbf{n}(k+1)]_{P\times 1} = [x_1(k+1) \quad \cdots \quad x_P(k+1)]^T$ is the new sample of (original) reference signals.

The new covariance matrix of the reference signals is :

$$\begin{aligned}[\mathbf{COV}_{\mathbf{xx}}(k+1)]_{P\times P} &= [\mathbf{x}(k+1)]_{P\times(k+1)}[\mathbf{x}(k+1)]^T_{(k+1)\times P} \\ &= [\mathbf{COV}_{\mathbf{xx}}(k)]_{P\times P} + [\mathbf{n}(k+1)]_{P\times 1}[\mathbf{n}(k+1)]^T_{1\times P}.\end{aligned} \tag{4.24}$$

A preliminary covariance matrix $[\mathbf{C}]$ of the virtual reference signals can be defined, analoguous to (4.22):

$$\begin{aligned}[\mathbf{C}(k+1)]_{N_S\times N_S} &= [\mathbf{u}(k)]^T_{N_S\times P}[\mathbf{COV}_{\mathbf{xx}}(k+1)]_{P\times P}[\mathbf{u}(k)]_{P\times N_S} \\ &= [\mathbf{COV}_{\mathbf{x}^\circ\mathbf{x}^\circ}(k)]_{N_S\times N_S} + [\mathbf{u}(k)]^T_{N_S\times P}[\mathbf{n}(k+1)]_{P\times 1}[\mathbf{n}(k+1)]^T_{1\times P}[\mathbf{u}(k)]_{P\times N_S} \\ &\equiv [\Sigma(k)]_{N_S\times N_S} + [\mathbf{u}(k)]^T_{N_S\times P}[\mathbf{n}(k+1)]_{P\times 1}[\mathbf{n}(k+1)]^T_{1\times P}[\mathbf{u}(k)]_{P\times N_S}.\end{aligned} \tag{4.25}$$

$[\mathbf{C}(k+1)]$ is not necessarily diagonal because of the extra term that corresponds to the new sample. It can be partially diagonalised by a Givens-like [250] rotation $[\mathbf{R}(k+1)]$ that makes the off-diagonal element C_{pq} with the largest absolute value (of all elements in $[\mathbf{C}(k+1)]$, i.e. $C_{pq}(k+1) = \max_{\substack{i=1\cdots N_S-1 \\ j=(i+1)\cdots N_S}} \{|C_{ij}(k+1)|\}$) equal to zero.

The transformation matrix $[\mathbf{R}(k+1)]$ is defined as :

$$[\mathbf{R}(k+1)] = \begin{array}{c} \\ \text{row } p \\ \\ \text{row } q \\ \\ \end{array} \begin{bmatrix} 1 & 0 & & \cdots & & & 0 \\ 0 & \ddots & & & & & \\ & & cos\,\alpha & & sin\,\alpha & & \\ \vdots & & & 1 & & & \vdots \\ & & -sin\,\alpha & & cos\,\alpha & & \\ & & & & & \ddots & 0 \\ 0 & & & \cdots & & 0 & 1 \end{bmatrix} \tag{4.26}$$

such that it realises a rotation of the (p,q)-plane over an angle α. The rotation angle which makes $C_{pq}(k+1)$ equal to zero is determined by :

$$tan(2\alpha) = \frac{2C_{pq}(k+1)}{C_{pp}(k+1) - C_{qq}(k+1)} \Rightarrow tan(\alpha) = \frac{-1 \pm \sqrt{1+tan^2(2\alpha)}}{tan(2\alpha)}. \tag{4.27}$$

The new, partially diagonalised covariance matrix of the virtual reference signals yields :

$$\begin{aligned} \left[\mathbf{COV}_{\mathbf{x}^\circ\mathbf{x}^\circ}(k+1)\right]_{N_S \times N_S} &= \left[\mathbf{R}(k+1)\right]^T_{N_S \times N_S} \left[\mathbf{C}(k+1)\right]_{N_S \times N_S} \left[\mathbf{R}(k+1)\right]_{N_S \times N_S} \\ &= \left[\mathbf{R}(k+1)\right]^T_{N_S \times N_S} \left[\mathbf{u}(k)\right]^T_{N_S \times P} \left[\mathbf{COV}_{\mathbf{xx}}(k+1)\right]_{P \times P} \left[\mathbf{u}(k)\right]_{N_S \times P} \left[\mathbf{R}(k+1)\right]_{N_S \times N_S}, \end{aligned} \tag{4.28}$$

where the incorporation of the rotation transformation determines the new transformation matrix :

$$\left[\mathbf{u}(k+1)\right]_{P \times N_S} = \left[\mathbf{u}(k)\right]_{PxN_S} \left[\mathbf{R}(k+1)\right]_{N_S \times N_S}. \tag{4.29}$$

It is important to note that the new transformation matrix is still orthonormal.

By choosing the '+'-sign in (4.26), α is constrained to $-45^\circ \le \alpha \le 45^\circ$ and it converges to $\alpha = 0$ when the transformation matrix converges to a constant matrix. Choosing the '-'-sign yields $45^\circ \le \alpha \le 90^\circ$ or $-90^\circ \le \alpha \le -45^\circ$. This converges to $\alpha = \pm 90^\circ$, which results in a continuous permutation of 2 columns of the covariance matrix. For a discussion of the convergence properties of recursive SVD algorithms, refer to [251]. The error propagation due to successive Givens rotations is discussed in [252].

In a practical application it is advisable to introduce a forgetting factor. As can be seen from (4.25), the magnitude of the diagonal elements of the

covariance matrix will continuously increase since the additional term has positive diagonal elements.
To avoid numerical problems, a forgetting factor is introduced :

$$\begin{aligned}\left[\mathbf{COV}_{\mathbf{X}^\circ\mathbf{X}^\circ}(k+1)\right]_{N_S\times N_S} &= \beta\left[\mathbf{R}(k+1)\right]^T_{N_S\times N_S}\left[\mathbf{COV}_{\mathbf{X}^\circ\mathbf{X}^\circ}(k)\right]_{N_S\times N_S}\left[\mathbf{R}(k+1)\right]_{N_S\times N_S} \\ &+\left[\mathbf{u}(k+1)\right]^T_{N_S\times P}\left[\mathbf{n}(k+1)\right]_{P\times 1}\left[\mathbf{n}(k+1)\right]^T_{1\times P}\left[\mathbf{u}(k+1)\right]_{N_S\times P}\end{aligned} \tag{4.30}$$

To conclude, a technique has been proposed to generate real-time independent virtual references by taking linear combinations of the original references. The transformation matrix which realises this is updated every time step. The update consists of a postmultiplication of the transformation matrix of the previous time step, with a Givens-like rotation matrix which is chosen such that is zeroes the largest off-diagonal element of the covariance matrix of the virtual references. This covariance matrix is also determined recursively (4.30).
In order to start with a set of independent virtual references, the transformation matrix should in theory be initialised as the matrix with the first N_S singular vectors, and the covariance matrix as the matrix with the first N_S singular values, obtained from an exact SVD of a certain time block of the original references.
Experiments have shown (refer to paragraph 4.4.4) that this exact SVD is not necessary and that it is possible to start from scratch, i.e. to initialise the transformation matrix as a unity matrix and the covariance matrix as a zero matrix. Care should be taken to extract the singular vectors corresponding to the largest N_S diagonal elements of the covariance matrix as they appear after a certain number of recursion steps. These are not necessarily the first singular values in this case.

To comply with the notations used in chapter 2, the vector of the virtual references used for control is defined as follows :

$$\left[\mathbf{X}^\circ(k)\right] = \left[\mathbf{X}_1^\circ(k)^T\ \mathbf{X}_2^\circ(k)^T\ \cdots\ \mathbf{X}_{N_S}^\circ(k)^T\right]^T \tag{4.31}$$

where $\left[\mathbf{X}_\mathbf{n}^\circ(k)\right] = \left[x_n^\circ(k)\quad x_n^\circ(k-1)\quad \cdots\quad x_n^\circ(k-L_{cf}-1)\right]^T$ for n = 1, 2, ..., N_S.
In the remainder of this section, (4.31) is referred to as "the virtual reference signals".

4.4.3 Enhancement of the convergence speed of the adaptive control algorithm due to the virtual reference technique

The LMS algorithm is sometimes associated with a certain deterioration in performance for problems with a large spread between the eigenvalues of the input autocorrelation matrix **R** [109] [253]. In general, it can be shown [109] that for stationary input and sufficiently small μ, the speed of convergence of the algorithm is dependent on the ratio of the largest to smallest eigenvalue (i.e., the *eigenvalue spread*) of the matrix **R**.
This is explained as follows : when plotting the Mean Square Error as a function of the iteration number, "modes of convergence" will appear which decay exponentially. The decay rate of the slowest mode of convergence is inversely proportional to λ_{min}, the smallest eigenvalue of **R**. On the other hand, the maximum convergence rate μ is limited by $1/\lambda_{max}$ [109]. Thus, as the eigenvalue spread of **R** increases, the convergence speed of the LMS algorithm decreases. The eigenvalues of **R** are determined by the spectral content of the reference signals. Whereas a reference signal with a flat energy spectrum (white noise signal) indicates fast convergence, a reference spectrum with a large dynamic range will lead to slow convergence.

Transform-domain LMS algorithms

In order to eliminate the potential deficiency of the LMS algorithm, an *ideal orthogonalised LMS algorithm* has been proposed in [109]. The basic idea behind this algorithm is that the input to the LMS algorithm should be prefiltered such that it becomes orthogonal (i.e. every sample is independent from the previous one). The orthogonalisation matrix that is used is $\mathbf{R}^{-1/2}$ and hence this algorithm assumes perfect knowledge of the input auto-correlation matrix, which implies such an algorithm is not able to be implemented practically (it is analysed in [109] because it is important from a theoretical point of view).
In fact, the orthogonalised LMS algorithm which is presented in [109], is identical to the Karhunen-Loéve transform (KLT), which is actually the classic benchmark for the Transform-domain adaptive algorithms discussed in [253 - 255]. The KLT (or orthogonalised LMS) performs an exact decorrelation of the input data by projecting them onto the eigenvectors of their auto-correlation matrix. It is thus an optimal transform, but it requires *a priori* knowledge of these eigenvectors. Transform-domain circumvent this requirement by using other transformation, such as the discrete Fourier transform (DFT-LMS), the discrete cosine transform (DCT-LMS), the

Hartley transform (DHT-LMS), etc. Five orthogonal transforms are discussed in [254] in terms of convergence characteristics and computational complexity. The transform-domain approach has been applied to the (single-channel) filtered-X LMS algorithm in [148]. No general theory exists that demonstrates the superiority of one such transform over another. The DFT-LMS, first introduced in [253], is perceived as the simplest algorithm of the family because of the exponential nature of the DFT (and because of the strong intuition scientists have developed about the Fourier transform).

It is important to note that the transform-domain approach is essentially a two-stage approach : the inputs are pre-processed with a unitary data-independent transformation, followed by a power normalisation stage. This DCT/DFT procedure can be illustrated geometrically [255]. The cost function that is optimised by the LMS algorithm is a quadratic function of the filter weights that represents a hyper-ellipsoid in the L_{cf}-dimensional weight space. A unitary transform of the inputs rotates this hyper-ellipsoid and brings it into approximate alignment (perfect alignment for KLT) with he co-ordinate axes. The power normalisation stage that follows the DFT/DCT is a transformation that, while preserving the elliptical nature of the cost functions, forces it to cross all the co-ordinate axes at the same distance form the centre. This operation is not unitary, and it changes the eigenvalue spread (it almost always improves it). The performance of transform-domain algorithms depends for a part on the orthogonalisation capabilities of the transformation : the better the alignment of the hyper-ellipsoid with the co-ordinate axes, the more efficient the power normalisation will be. However, the essential part of the procedure is the normalisation stage ([254], p. 477) : "it is significant to note that no convergence rate improvement can be realised *without* power normalisation". The need to continuously track the power in the transformed inputs increases the computational complexity of these algorithms.

At this point, it is interesting to note the apparent similarity between the transform-domain algorithms (more specifically, the KLT) and the RLS algorithm. As the RLS algorithm recursively forms an estimate of $\mathbf{R}^{-1}$ (which comes down to implicitly whiten the input), it achieves near optimum convergence. Unfortunately, the computation required for the RLS algorithm is not easily carried out in real-time and it is sensitive to numerical instability.

The problem that is envisaged here implies two major complications in the sense that multiple references are involved (transform-domain algorithms

deal with 1 reference) and that the filtered-X LMS algorithm is used. The filtered-X LMS algorithm differs from the conventional LMS algorithm in that the reference signals (here : virtual references) are pre-filtered by a model of the secondary paths (the transfer function from the controller output to the error sensor) in order to ensure convergence of the algorithm in the presence of secondary paths. Unlike the single channel LMS algorithm, the convergence behaviour of the multiple-channel Filtered-X LMS algorithm for an arbitrary wideband signal is difficult to analyse. In chapter 2, it was mentioned that the convergence rate is determined *(i)* by the delays caused by the physical separation of secondary sources and error microphones and *(ii)* by the eigenvalue spread of the input autocorrelation matrix of the filtered reference signals [126] [256]. In order to avoid slow modes of convergence it is thus of prime importance to get rid of the extremely small eigenvalues of the input autocorrelation matrix of the filtered reference signals.
Particularly in the case of active control of road noise, this autocorrelation matrix is often ill-conditioned [233] and hence various solutions have been proposed in literature to solve this problem. Sano *et al.* propose to use the RLS algorithm in [236], and the filtered-X LSL algorithm in [237], instead of the commonly used filtered-X LMS algorithm. The patent claimed by Freymann in [238] essentially comes down to improving the convergence speed of the filtered-X LMS algorithm by inserting a whitening filter after the reference sensor [24]. This was realised by the inverse auto-correlation function of the reference signal and hence relates to the KLT technique. Masaichi [249] proposed the frequency domain technique which was discussed (and shown to be inferior to the time domain technique developed here) in paragraph 4.4.2. Kim *et al.* [257] propose a new "constraint" filtered-X LMS algorithm which in essence identical to the extended filtered-X LMS algorithm described in paragraph 2.3.3. It is interesting to note that the constraint filtered-X LMS algorithm is found to have an improved convergence speed in [257], whereas the same algorithm showed identical convergence properties as the filtered-X LMS algorithm in [100] (p. 57) for an identical application (...).

The virtual reference technique

The technique of virtual references presented here, orthogonalises the reference signals and removes all the linear dependent signals from the virtual reference set. The virtual references are decorrelated in space (the different references are independent), but not in time (the samples of a virtual reference signal are not independent in time). Removing $(P - N_S)$ virtual references that yield zero or near-zero diagonal entries in $\mathbf{COV}_{\mathbf{x^o x^o}}$ implies that $(P - N_s) \times L_{cf}$ near-zero eigenvalues are removed from the autocorrelation matrix of the virtual references $\mathbf{E}\{\mathbf{X}^o(k)\mathbf{X}^o(k)^T\}$ (note that this does not change the eigenvalue spread of the virtual references that are retained). Similarly, $(P - N_S) \times L_{cf} \times M \times N$ near-zero eigenvalues are removed from the input autocorrelation matrix of the filtered virtual references (defined in analogy with $\mathbf{R} = \mathrm{E}\{\mathbf{X}^f(k)\mathbf{X}^f(k)^T\}$). Thus it may be anticipated that the convergence speed is enhanced by removing the extremely slow modes of convergence of the algorithm.

However, the secondary path filters often give much spectral coloration to the references [256] and thus some degree of correlation is introduced between the filtered virtual references. Compared to $\mathbf{E}\{\mathbf{X}^o(k)\mathbf{X}^o(k)^T\}$, the input autocorrelation matrix of the filtered virtual references will typically have a range of significantly smaller eigenvalues (i.e. there are generally more than $(P - N_S) \times L_{cf} \times M \times N$ near-zero eigenvalues). More, and smaller eigenvalues are introduced in the case of lightly damped secondary paths compared to more heavily damped systems. Hence, though filtering the references is necessary in the presence of secondary paths, it may slow down the convergence rate of the Filtered-X LMS algorithm. In the application presented here, it was observed that this latter effect did not completely deteriorate the increase in convergence speed achieved by using virtual references instead of the original reference set. To this aim, the input autocorrelation matrix of the (filtered) original references of the laboratory test (explained in the next paragraph) was calculated (10.000 averages, 19 10^9 flops) and compared to the (filtered) virtual reference. The first matrix was found to have much more eigenvalues which were several orders of magnitude smaller than the smallest eigenvalues of the second matrix.

4.4.4 Application of the virtual reference technique to the active control of road noise

Validation on laboratory test data

In a first instance, a laboratory test was performed, generating a data set on which the virtual references technique could be validated. To this aim, four shakers were mounted to the four wheel hubs exciting the car wheels in vertical direction. As the car was excited while the car was standing on the laboratory floor, the tires were left into place, and thus a certain degree of non-linearity was introduced.
All four shakers were driven with the same white noise signal (band-limited white noise in a frequency range 0 - 400 Hz). The original reference set was constituted of four vertical-accelerations measured at the four wheels. The sound field inside the car cabin was evaluated using Bruel & Kjær ½-inch condenser microphones (type 4188). The location of these microphones was determined in paragraph 4.2. A time domain data set was acquired at a sample frequency of 1024 Hz.
Not surprisingly, application of the recursive algorithm described in paragraph 4.4.2, revealed that only 1 virtual reference was sufficient to describe the noise source. The singular values of the virtual references' covariance matrix are shown as a function of time in figure 4.21. In figure 4.22, the multiple coherence between the original references and the rear left microphone is compared to the multiple coherence between the virtual reference that was retained and the rear left microphone. Both curves do not exactly match due to system non-linearities. However, it is clear that almost identical information is carried within one single virtual reference.

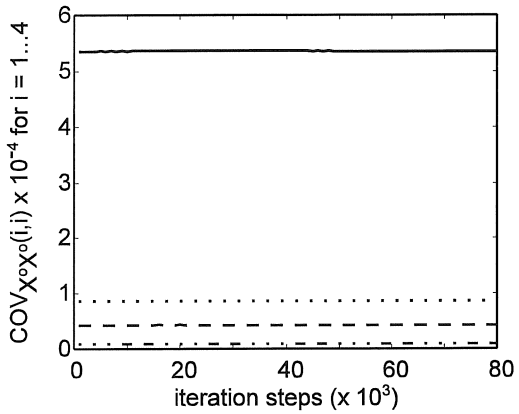

Figure 4.21. Diagonal elements of $COV_{X^oX^o}$ as a function of time.

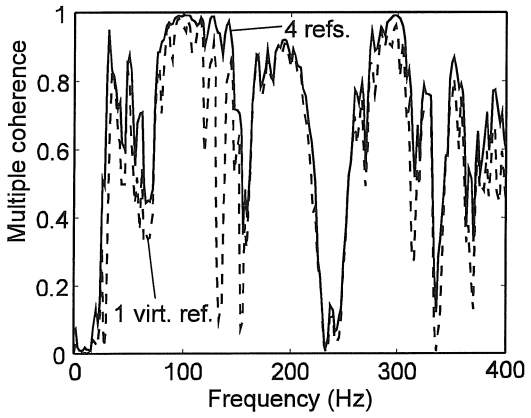

Figure 4.22. Multiple coherence between the rear left microphone and (i) 4 original references and (ii) 1 virtual reference.

In figure 4.23, the largest off-diagonal element of the virtual references' covariance matrix is shown as a function of time. The figure illustrates that the covariance matrix is nearly diagonal (note different scaling of the y-axis). Figure 4.24 presents the evolution of the Givens rotation angle during the first 300 iteration steps. Relatively large corrections are applied in the first few iteration steps (near to 45 degrees, which is the maximum rotation angle), after which the rotation angle rapidly decreases and converges to zero.

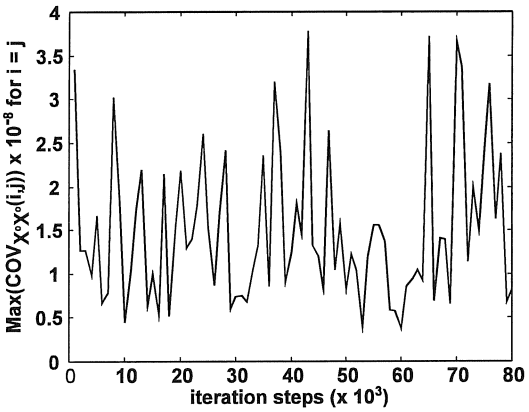

Figure 4.23. Largest off-diagonal element of $COV_{X^cX^c}$ during recursion.

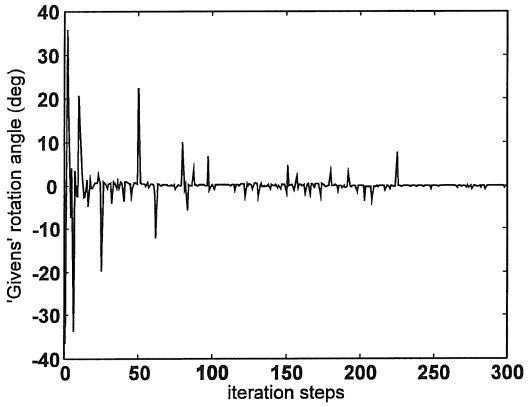

Figure 4.24. Evolution of the rotation angle of the unitary transform during the first 300 iterations.

Road test data, including simulation of active control of structure borne road noise

A second set of time domain data was generated by driving the test car at 90 km/h over a rough road. An extended set of reference signals, consisting of the acceleration measured in three directions at each wheel, was recorded on a 16-channel DAT-tape together with four microphone signals measured at locations specified in the laboratory test. The data set was then analysed using the recursive algorithm.

In figure 4.25, the two largest diagonal elements of the (diagonalised) covariance matrix of the virtual references are shown as a function of time for two initial covariance matrices : (*a*) the matrix of singular values obtained from an exact SVD of the original reference signals, (*b*) the 12×12 null matrix. The figure demonstrates that the result obtained with initial condition (*b*) converges to condition (*a*). In contrast to the laboratory tests that were performed in stationary conditions, the diagonal elements of the covariance matrix vary as a function of time.

Figure 4.26 graphically represents the order of magnitude of the covariance matrix obtained after 80.000 iteration steps. Though it is clear that the first two virtual references need to be retained, it is not obvious which of the remaining diagonal elements need to be considered as being significant or not. In order to determine the number of virtual references that needs to be retained, both the cumulated power of the virtual references and the multiple coherence between the virtual reference set and the rear left microphone were calculated. The cumulated power of the r-th virtual reference was

calculated as the ratio between the sum of the r largest diagonal elements and the sum of all diagonal elements of the covariance matrix. From figure 4.27 it is clear that more than 75 % of the total cumulated power is carried within the first four virtual references.

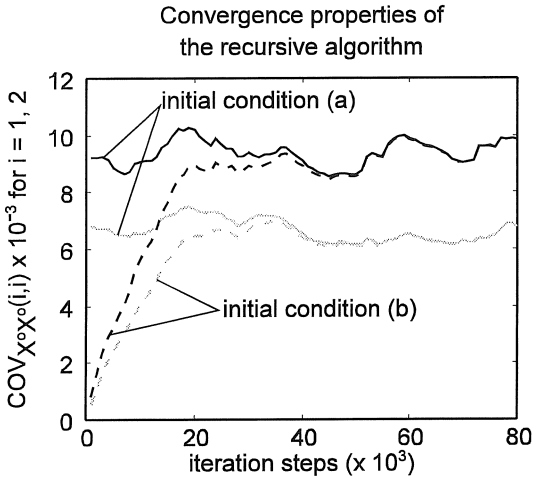

Figure 4.25. Evolution of the two largest diagonal elements of $COV_{X^eX^e}$ for an initial COV equal to (a) $O_{12 \times 12}$ and (b) $\Sigma_{12 \times 12}$

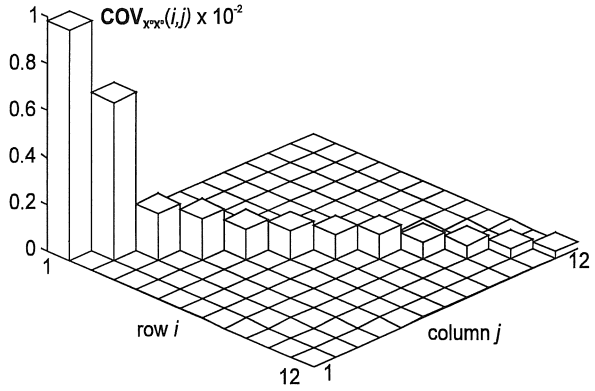

Figure 4.26. The elements of the covariance matrix of the virtual references after 80.000 iteration steps.

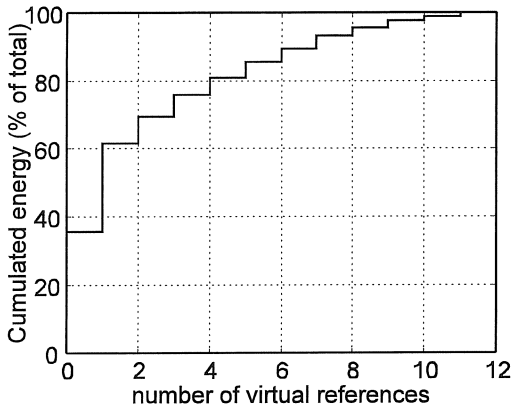

Figure 4.27. Cumulated engergy (i.e. ratio between the energy in first n virtual refs. and the total energy) as function of number of virtual refs.

Figure 4.28 presents the multiple coherence between the reference set and the rear left microphone for (*a*) twelve original references, (*b*) four main virtual references, (*c*) an arbitrary selection of four of the original references.

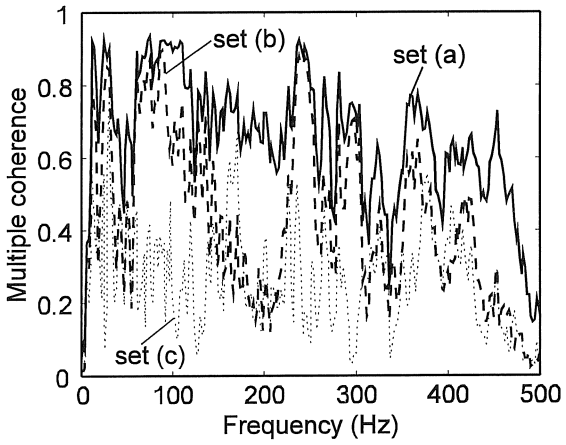

Figure 4.28. Multiple coherence between rear left microphone and (a) 12 original, (b) 4 virtual, and (c) 4 arbitrary original references.

The coherence obtained with set (*c*) indicates that such limited reference sets are not useful for active control purposes. However, due to the imperfect match of the curves for set (*a*) and (*b*), the usefulness of the virtual reference set may be questionable as well. Therefore, both the

extended original reference set (*a*) and the four main virtual references (*b*) were used to simulate the noise reduction achieved with a control configuration aimed at the reduction of road noise in a car that is driven on rough asphalt at 90 km/h.
The simulation tool is described in paragraph 4.2.6. A control configuration with 4 control loudspeakers and 4 error microphones is simulated. The synthesised sound pressure level (SPL) at the rear left microphone obtained after 80,000 iteration steps with and without control is presented in figure 4.29. Both reference sets yield nearly identical noise reductions (an average of 8 to 9 dB noise reduction in the frequency band 75 - 105 Hz). This is explained by the fact that the sound spectrum inside the car cabin of the test car is dominated by two "booms", viz. in the frequency ranges 75 - 105 Hz and 225 - 275 Hz. As these booms dominate the objective function, the adaptive controller converges to a setting that maximises the noise reduction in these frequency bands primarily. Therefore, it is most important to maximise the multiple coherence of the reference set at "booming" frequencies. The selected virtual reference set yields multiple coherence values comparable to the complete original reference set in the frequency bands of interest (compare figure 4.28 to 4.29).

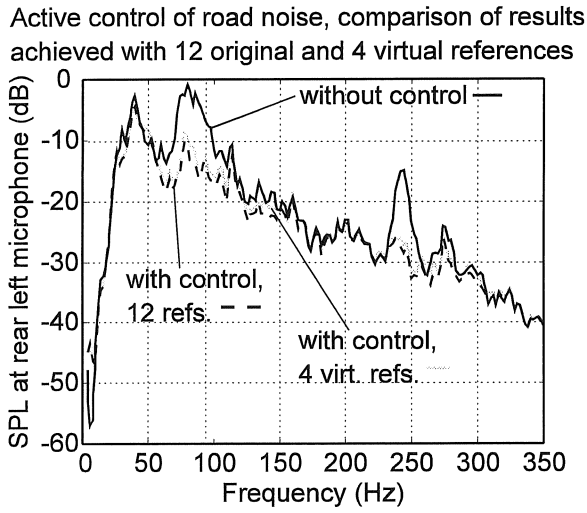

Figure 4.29. Result of simulation of active control of road noise using the original and virtual (reduced) reference sets.

Discussion

1. With a set of the four "best" original references, a maximum reduction of 6 dB could be achieved in the same frequency band. This set was selected by simulating the control performance for all possible sets of four references, which is an involving procedure which will need to be repeated regularly in the case where the "best" set of physical transducers would be a function of the operating conditions. The real-time virtual reference estimation scheme performs a similar task automatically. Moreover, the algorithm will always converge to the best solution when the operating conditions would change.
2. Application of the technique of virtual references explicitly assumes that the given problem can be considered as a linear combination of multiple uncorrelated sources. More specifically in the case of road noise, system linearity is questionable, which explains the apparent loss of coherence if even the least significant virtual references are omitted from the set.
3. The selection of the original reference set remains very important. If the original reference set does not appropriately capture all the disturbance sources, the sound field which needs to be controlled would contain contributions from disturbances which do not contribute to the references. This could be avoided by decoupling the microphone signals into uncorrelated noise sources, indicating which is the number of uncorrelated phenomena dominating the sound field. The same number of independent sources should then be found in the reference set.

4.5 CONCLUSIONS

An new control approach has been presented to actively control road noise using vibration actuators which change the vibration behaviour of the car body such that structure-borne road noise inside this car body is reduced. The control algorithm is a filtered-X LMS adaptive feedforward scheme.
The control approach has been validated in laboratory and by means of numerical simulations. Using a single-channel control configuration using one control actuator and one error microphone, a sound pressure reduction of more than 10 dB has been achieved in the presence of a single primary disturbance (generated by an electrodynamic shaker, connected to a rear wheel of the demonstrator car).
A simulation tool has been presented to predict the control performance for multi-channel control of road noise inside the car cabin of a car driving on a

coarse road. The simulation tool has been used to optimise the control configuration for the active structural acoustic control of structure-borne road noise inside a car driven on a coarse road.
Road tests have been performed, yielding 6.9 dB reduction in the frequency range from 75 to 115 Hz at the error microphone and 6.1 dB reduction at the passenger's ear.
This chapter also presents an new approach to the optimisation of the reference set for broadband feedforward control of sound and vibration in the presence of multiple, uncorrelated primary sources. A real-time algorithm is presented that generates a set of orthogonal virtual references out of a given set of reference signals. The technique simplifies controller design in the sense that, primarily, a reduced set of virtual references is sufficient to yield comparable control performance. Hence controller dimensions (and thus memory requirements for implementation), and the computational burden, reduce accordingly. Secondly, it was shown that convergence speed of the adaptive Filtered-X LMS algorithm is enhanced.
Confirmation is given by means of a numerical simulation of an active control configuration aimed at reducing structure-borne road noise in a car cabin. A reduced set of references yields nearly identical noise reductions as the original extended reference set.
The increase of the computational burden due to the integration of the on-line generation of virtual references into the control algorithm, is not analysed here. As the recursive procedure lends itself well to parallel implementation, extremely high throughput can be provided by implementation of the algorithm on customised systolic computing systems [251].

CHAPTER 5

PRACTICAL IMPLEMENTATION OF ACTIVE CONTROL SYSTEMS

5.1 INTRODUCTION

The design and development of dedicated software and customised hardware, such as actuators, sensors and DSPs, has not been dealt with in this thesis. Basically, for proof-of-principle experiments, the control actuator which is used is not always relevant. If the control strategy requires selective control of the structural modes, this may be realised in hardware (by designing a specific actuator, as described in paragraph 5.2.2) or alternatively in software (by using a modal model as a basis for the synthesis of the digital controller). The applications described in the previous chapters have made use of point force actuators. Laboratory instruments (electrodynamic shakers) have been used in chapter 3, specifically designed inertia shakers have been used in chapter 4. This kind of hardware is perfectly suited for laboratory tests or system demonstrations

but would never make it to commercial systems. The feasibility, performance and cost effectiveness of fully operational active control systems is strongly dependent on the use, and eventually the development, of the appropriate components. The aim of this chapter is to provide somewhat more information about the practical limitations encountered in the implementation phase of an active control system, and about the available new technology.
In paragraph 5.2, an overview is presented of the research work which focuses on the instrumentation required to implement the active control strategies. Commonly known "traditional" sensors, such as microphones and accelerometers, and control sources, such as loudspeakers, are not considered in this overview (although they have been further developed to some extent to better suit the application [259 - 261]). This paragraph rather presents some examples of a new generation of actuators and sensors. Paragraph 5.3 deals with the electronics design, processor choice and programming issues. Unlike other active control system components such as transducers, the electronic hardware implementation usually comes down to selecting the appropriate processor type from the range of DSPs available on the market. Though the electronic requirements of an active noise or vibration control system in terms of computational requirements, dynamic range, distortion and throughput, need to be considered seriously, very little is written on that subject. This paragraph presents a summary of the conclusions drawn from our own experience, and from the available literature.

5.2 ACTUATOR AND SENSOR TECHNOLOGY FOR ACTIVE CONTROL

5.2.1 Distributed sensors

The piezoelectric effect in quartz, and in a number of natural an synthetic single-crystal materials, has widely been used in force cells and accelerometers. The piezoelectric effect in polymers has received attention since the 1960s, and a breakthrough came in 1969, with the discovery of the strong piezoelectric effect in polyvinylidenefluoride (PVDF). PVDF is a semicrystalline polymer ; thermal poling or corona poling (i.e. a discharge with a needle electrode at a distance of a few centimetres) will orient the molecular dipoles in the crystalline parts and thus yield a permanent

polarisation. PVDF exhibits considerably stronger piezoelectric activity than other polymers, and compared to other piezoelectric materials (piezo-crystals, piezoelectric ceramics) it has unique properties such as flexibility, ruggedness, low acoustic impedance, and availability as thin film (from 50 μm). The latter property makes PVDF very useful as a sensor in ASAC.

Basically, to resolve an individual mode or a combination of modes using film sensors, it must be possible to vary the charge-generating capacity of the sensor over the spatial duration of the mode (the characteristics of the variation are dependent upon the target mode). If the mode is one-dimensional, such as a beam mode, then the modal displacements amplitude can be measured using a two-dimensional sensor : one dimension to measure over the spatial duration of the mode, one dimension to accommodate the required variation in charge producing capacity. If a PVDF film is positioned on the surface of a structure with a shape defined by a shape function $\Gamma(x, y)$ and a predetermined polarisation profile $P_o(x, y)$, the electrical response of the sensor can be expressed in terms of the vibration response of the structure [47] as

$$q(t) = \frac{h_p + h_s}{2} \int_A P_o(x, y)\Gamma(x, y)\left(e_{31} \frac{\partial^2 w}{\partial x^2} + e_{32} \frac{\partial^2 w}{\partial y^2} + e_{36} \frac{\partial^2 w}{\partial x \partial y} \right) dxdy \,. \quad (5.1)$$

In this expression, h_p and h_s are the thickness of the piezo-film and the substrate, respectively, e_{31}, e_{32}, and e_{36} are the stress per charge constants in units C/m^2 and $q(t)$ is the electrical response in terms of charge C. The measured voltage is dependent upon the capacitance of the sensor and the impedance of the instrumentation used to make the measurement. Equation (5.1) shows that by placing the sensor along the length of the beam (the spatial duration of the mode), and by varying the width over this duration, the charge producing capacity of the sensor can be prescribed.

If the target structure is two-dimensional, such as a plate, then the above discussion seems to indicate that a three-dimensional sensor would be required to resolve a (two-dimensional) mode. That is, the entire structure would have to be covered in piezo-electric polymer film and the thickness of the film varied to alter the charge-producing capacity over this duration. the requirement that the entire structure be covered in film to resolve one mode is clearly impractical. Snyder *et al.* [262] show that two-dimensional modes can also be resolved using multiple strip sensors (each individual strip sensor can discriminate between modes in one dimension but all modes

in the other direction will contribute to its response) in a modal filtering arrangement.

Modal domain optical fibre sensors were used in a control configuration to suppress the acoustic radiation from a vibrating beam [263] and a simply supported plate [264]. Briefly, a modal domain optical fibre sensor consists of a section of optical fibre attached to the structure, a coherent light source, and a photodetector. The geometry of the fibre and the wavelength of the source are chosen such that two electromagnetic modes propagate in the fibre. These two modes interfere with each other to generate an intensity pattern at each cross section which varies as a function of the length of the fibre. Since the fibre is attached to the structure, the strain at the surface of the structure is transferred to the fibre. When the fibre is strained the intensity of the light at the fibre endface changes in a predictable way (the direct effect of axial strain in the optical fibre is threefold : the length of the fibre changes, the geometry changes, and the indices of refraction change ; i.e. the so-called photo-elastic effect). Thus the sensor responds to strain in the structure. The sensor can also be configured to sense structural variables directly, such as modal amplitudes, by varying the transfer coefficient of the strain from the structure to the fibre as a function of the length of the fibre according to prespecified weighting functions.
Optical fibre sensors have certain advantages for instrumenting structural control systems. They are low power, light weight, low mass, and EMI insensitive. The sensors can also be attached to or embedded in a structure. However, because the sensor is of the interferometric type, the output of the sensor has a sinusoidal nonlinearity. The sensor nonlinearities imposes some restrictions on the performance of the control system in which they are used. These effects are studied in [265], and region of linear operation in terms of the optical fibre sensor parameters is identified.

5.2.2 Distributed actuators

Lead zirconate titanate (PZT) is a ceramic substance which can by made piezoelectric by poling. As PZT exhibits a very strong piezoelectric effect, the material has been the preferred piezoelectric ceramic, used in piezostack actuators (paragraph 5.2.3) and distributed PZT patches which are easily to attach to any structure. These actuators have attracted significant attention because of their distributed character of actuation which allows them to be tailored to selectively reduce structural modes with little control spillover

[191 - 192]. Piezo-actuators also have several other inherent advantages over conventional actuators because they are relatively inexpensive, space efficient, lightweight, and they do not require a back reaction.

An extensive study of the optimal design of piezo-actuators for vibration control is presented in [266]. In contrast to PVDF, PZT actuators are difficult to manufacture in sheets large enough to fully cover a substructure. Though PVDF films are 30 times more compliant that PZT, and have a lower electromechanical coupling factor, they are also used as actuators in some specific applications [62] [267]. While it is generally believed that PZT actuators are superior to PVDF, it is possible to compare quantitatively the performance difference between both actuator types [268]. PVDF has almost an order of magnitude lower piezoelectric strain constant[1] than PZT. On the other hand, the maximum allowable electric field strength of PVDF is almost one hundred times larger than that of PZT. Thus the maximum free piezoelectric strain for PVDF may be expected to be ten times larger that PZT. The maximum bending moment in the substructure (which result from bonding the piezo-actuator to the structure), however, is also a function of the elastic material properties of the actuator. In that respect, PZT actuators compensate the small free piezoelectric strain with a high stiffness.

When calculating the effective bending moment as a function of the piezo-actuator thickness (for constant substructure thickness) using the maximum allowable electric field strengths, it is observed that the maximum bending moment for PVDF is approximately four times larger than for PZT. However, to achieve this, the optimal thickness of the PVDF actuator is approximately five times that of the PZT actuator. While the optimal thickness of PZT actuators for application on steel and aluminium substructures are readily available, using PVDF in these cases would require a PVDF actuator which is approximately 4 to 5 mm thick. However, even for suboptimal PVDF thickness, the effective bending moment induced by a PVDF actuator appears to be comparable to that of a PZT actuator with the same thickness. Nevertheless, it must be noted that PVDF requires 100 times higher voltages and has substantially higher mechanical damping. Due to the latter property, heat builds up quickly which may cause the

---

[1] The strain in the x- and y-direction of an unconstrained piezo-electric actuator by applying a voltage over its surface electrodes (z-direction) is expressed as a function of the applied voltage, V, the piezoelectric strain constant, d_{31} and the thickness, t, of the material in the z-direction : $\varepsilon_x = \varepsilon_y = \frac{d_{31}}{t} V$.

piezoelectric properties to diminish over time. This may become an important disadvantage for PVDF actuators for applications which require substantial control energy.
It must be noted that piezoelectric devices act mainly as a capacitive load, for which the power supply must be specifically designed in order not to limit the performance at high frequencies where high current at relatively high voltage is required.

5.2.3 Point force actuators

Classical point force actuators are electrodynamic shakers. For active control applications, however, reaction-mass (or inertia) shakers are more practical because they require only one-point mounting. Inertia shakers contain an internal reaction mass which is accelerated by an actuator (which results in a reaction force that acts on the base of the inertia shaker). The output force of the inertia shaker, at a frequency ω_o, is

$$\omega_o^2 \, \Delta l \, m_r , \tag{5.2}$$

where m_r is the reaction mass and Δl is the stroke of the actuator.
Clearly, in order to limit the total weight of the actuator, the stroke of the actuator must be maximised if the actuator has to operate at low frequencies. It has been shown [269] that if the reaction mass is strongly constrained, the best actuator principle is a voice-coil configuration (figure 5.1) because they allow several millimetres of linear motion. The design of an inertia shaker using a voice-coil actuator is discussed in detail in [72].

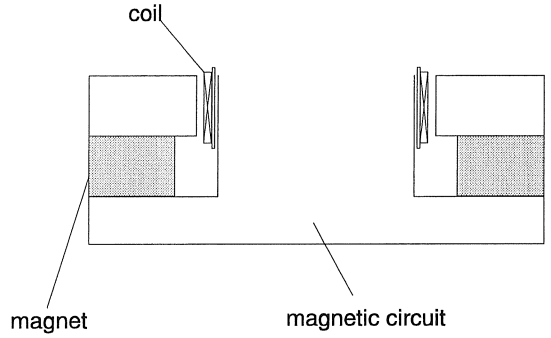

Figure 5.1. Voice-coil actuator. The reaction mass can be connected to the coil.

Variable reluctance (moving armature) electrodynamic actuators (figure 5.2), which are capable of generating much higher forces, are constrained in this sense because the maximum stroke of the actuator is relatively limited. However, as these devices are extremely rugged, do not use permanent magnets (which are expensive and sensitive to temperature) and can operate at high forces without forced cooling, substantial effort has been put in the development of inertia shakers based on this principle [270 - 271].

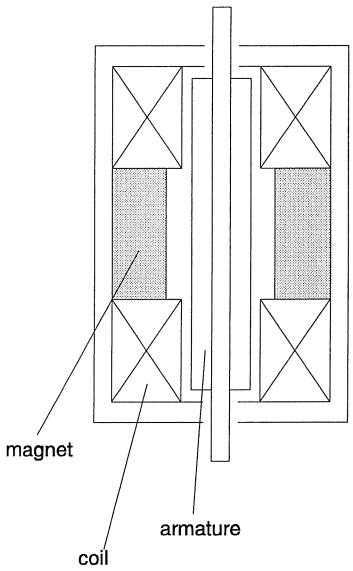

Figure 5.2. Moving armature actuator. Can be designed to incorporate a reaction mass.

A typical performance curve of such type of inertia shaker shows that the generated force is limited at low frequencies (but increases with frequency) by the available motion of the reaction mass which is set by the magnetic gap. In the mid frequency range, the force is limited by saturation of the magnetic circuit. At higher frequencies the force is generally reduced due to voltage limitations of the power amplifier which drives the actuator.
A variable reluctance actuator is inherently non-linear because it has a square law output force to input current relationship. Non-linear devices are often approximately linearised by operating them in a small dynamic range around an equilibrium point. In order to increase the available linear dynamic range, the actuator can be linearised by means of a local feedback control loop, as proposed in [271]. The local feedback loop was realised

using a DSP. This solution, however, makes the design more complicated and expensive. In [270], the authors have taken the approach of using two opposing electromagnets and differentially biasing them (with a permanent magnet) to achieve both linearity and large dynamic range. The proposed configuration cancels the non-linear components due to the quadratic term in the input-output relationship (there remains another source of non-linearity due to the varying air gap). However, such a device is unstable because the balance of forces due to magnetic flux alone creates a negative spring about the equilibrium position. To stabilise the system, a mechanical spring is used which provides a net positive spring rate (furthermore, the spring introduces a mechanical resonance which can be used to enhance the actuator response at a specified frequency).

The inertial shakers with actuators which are based on electromagnetic driving forces are typically limited in bandwidth. In order to increase the bandwidth of the inertial actuators, piezoelectric stack actuators have been considered which can provide very high forces at high frequencies. Piezoelectric stack electrodes are a laminate of several alternating layers of ceramics and electrodes. The more layers, the larger the stroke of the actuator but for practical applications the actuator length is usually constrained (actuator length in the product range in [272] is limited to 65 mm). A disadvantage of piezo-actuators is their limited stroke (typically 10 to 80 μm), which makes them undesirable for low frequency applications. This problem can partly be solved by using a lever mechanism as in [273]. In practice, however, this leads to additional problems such as resonance in the lever mechanism, wear, tolerances, etc.

Magnetostrictive actuators, using new materials such as Terfenol-D, have almost the same characteristics as piezostacks but at moderate voltages and at lower prices. General characteristics of magnetostrictive actuators are discussed in [274]. A magnetostrictive material expands when it is exposed to a magnetic field (the inverse magnetostrictive effect allows to use the device as a sensor and actuator at the same time). The magnetostrictive strain depends only on the magnitude of the applied magnetising field, not on its sign. Therefore, the material is magnetically biased for transducer applications. A typical magnetostrictive actuator (figure 5.3) consists of a Terfenol-D rod, an annular permanent magnet which is axially magnetised (to supply the bias magnetic field) and a coil, which provides the magnetising field used to actively control the magnetostrictive strain.

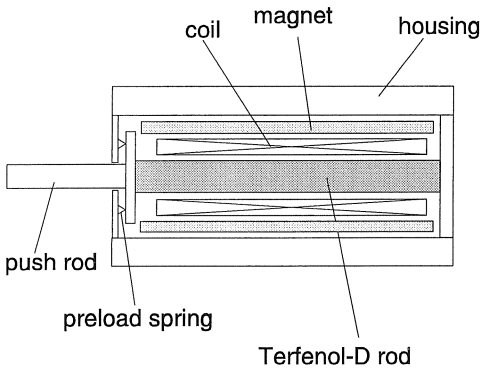

Figure 5.3. Basic magnetostrictive actuator configuration.

A magnetostrictive inertia shaker, designed for high frequency applications, is presented in [275]. The paper illustrates which trade offs must be faced when designing this particular type of actuator. First of all, the bandwidth of the actuator is determined by the inductance of the coil providing the magnetic field. At high frequencies, the impedance of the coil is dominated by the inductance and thus significant increases in drive voltage are required to produce the required forces. One way to alleviate this requirement is to increase the diameter of the coil wire and reduce the number of turns. This, however, increases the required current. Therefore, the authors have preferred to introduce a mechanical resonance in the actuator at the required frequency band. Thus it was possible to provide about 935 N at 1900 Hz while consuming 3.5 A at 33 V peak. A second parameter of the actuator to be set is the length. A longer Terfenol-D element provides more stroke, and thus more output force at a given frequency. The reaction mass, for a fixed force requirement, is inversely proportional to the actuator length. Since the actuator mass, which should be as small as possible, is dominated by the reaction mass, the actuator length should be as large as possible. In practice, however, the length cannot be much greater than the diameter since that would cause mechanical problems with bending moments (furthermore there are generally not only mass constraints but also space limitations). The authors of [275] have considered the heat dissipation in the actuator to fix the maximum length of the actuator. Heat dissipation is an important issue as the dissipated hysteresis power must be conducted through the Terfenol-D rod. The average temperature of the Terfenol-D rod must however be constrained because the magnetostrictive strain decreases substantially above 100° C.

Though the actuator, described in [275], exhibits an unusually large force-to-mass (0.590 kg) and force-to-volume ratio (74 mm long and 44 mm in diameter), it is important to stress the fact that it operates at a mechanical resonance at relatively high frequency. The same values can impossibly be obtained at low frequencies. The maximum stroke that can be achieved with a Terfenol-D actuator of length l is about $8 \times 10^{-4}\ l$. This assumes that it is run far into the saturated non-linear regime. Staying within the -relatively-linear regime reduces the maximum stroke to $3 \times 10^{-4}\ l$.

5.2.4 Alternative loudspeaker systems

Basically, any structure which is equipped with actuators in order to control the structural vibration and hence to control sound waves, can be considered as a loudspeaker. From that perspective, (flat) panels, which are driven by piezoceramic patch actuators, represent the ideal loudspeaker configuration because they can easily be integrated (in walls, existing acoustic linings, etc.). Such configuration has been presented and analysed extensively. A further development of this idea is presented in [277]. In this paper, a composite panel is presented in which a single sheet piezoceramic sensor and actuator are embedded. The target applications are spacecraft or launch vehicle structures which consist of a series of thin composite panels that are clamped around their individual boundaries by a frame. These structures are typically light-weight and hence susceptible to vibration excitation. The damping of the dominating modes of this "intelligent" composite panel is increased by a digital H_∞ controller. The combination of the controller and the composite panel is optimised as a whole. Using a composite material instead of an isotropic material has significant advantages because the structural behaviour of isotropic panels (of fixed size) can only be changed by changing the thickness. In the case of a composite, the number of layers, the stacking sequence of the filaments, and the fibre orientation in the various layers can be optimised such that control performance (and robustness) is maximised while the controller order is minimised. The paper first presents control results for a non-optimised, 5-layer composite panel of dimension $300 \times 300 \times 1$ mm. The embedded sensor and actuator are a piezoceramic sheet of dimension $30 \times 70 \times 0.25$ mm. An eighth order controller was required to achieve vibration attenuation in the 150 - 350 Hz frequency range. Then, an optimisation procedure is presented which aims at optimising the distribution of the panel eigenfrequencies in the considered

frequency range. In this optimisation, an 8-layer composite is considered. The material used for the structural lamina is GUBD 3105, which is a glass-epoxy composite. The optimisation parameters are the orientation of the four outer layers (2 at each side) with respect to the four middle layers. Different optimal configurations were found for the frequency range 0 - 300 Hz and 350 - 550 Hz.

A conventional configuration for a flat panel loudspeaker is the electrostatic loudspeaker. An alternative electrostatic flat panel loudspeaker, which does not require high driving voltage, is presented in [278] (figure 5.4). The loudspeaker uses an ElectroMechanical Film (EMF), which is a thin (30 to 100 μm), flexible, electret film in which microscopic air bubbles are embedded. It is coated with metal electrode layers. The film thickness can be controlled by applying a voltage to the electrodes (typical response about 1 nm/V [279]), and inversely the EMF generates electrical charge when a force acts on its surfaces. In the EMF panels, a dual-layer EMF is fixed between two porous support panels with evaporated metal electrodes inside. The support panels contain cavities at the EMF side which allow a normal motion of the EMF. The support panels are made of sintered plastic powder such that they are transparent on audio frequencies. When alternating voltage is applied between the electrodes on the EMF and the electrodes on the support panels, the EMF is forced in a normal motion in the cavities between the support plates. When driven with 30 V (RMS) signal input, a 410 $\times$ 310 mm flat panel loudspeaker yields maximum 95 dB sound pressure level at 1 m distance above the panel (at 4000 Hz) [280].

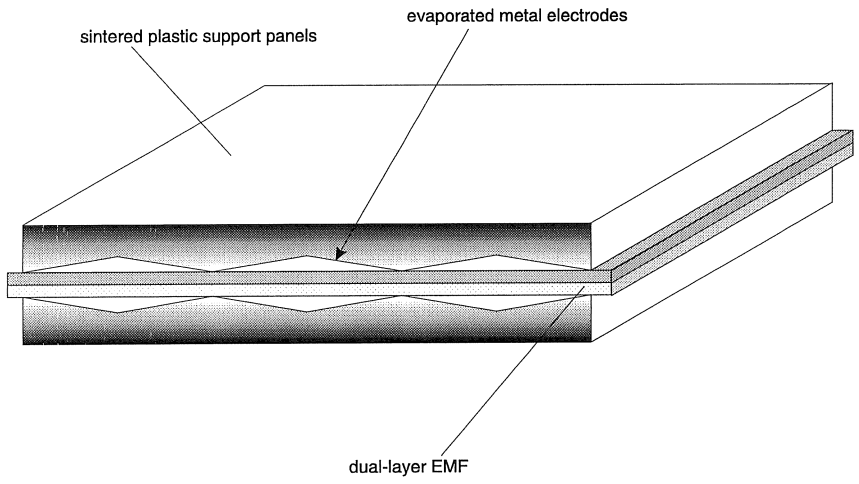

Figure 5.4. EMF acoustic actuator.

5.3 ELECTRONICS DESIGN AND SOFTWARE DEVELOPMENT

5.3.1 General considerations

The development of dedicated digital control hardware is only rarely reported in literature. One example is the QuietChip, presented in [165], which is a multi-chip module that has been designed for the special needs of active control systems. The QuietChip features a Motorola 96002 (32-bit, 40 Mflops) DSP, on-chip memory, one 16-bit A/D and one 16-bit D/A, digital I/O and optional tachometer input. The bus configuration allows 12 QuietChips to be run in parallel.
In an early stage of the control system development, however, it is common practice to configure a DSP-based development system by selecting from the available product range of DSP-carrier boards, I/O-boards, etc. This choice is becoming more and more complicated with the ever increasing number of possible configurations which have become available (PC-based, VME-based, etc.). Furthermore, although the DSP architecture was intended for signal-processing and thus intrinsically different from microprocessor architecture [282], general purpose microprocessors (RISC or CISC) have evolved to a performance level where today they can perform many tasks that would previously have required DSPs (at the same time DSPs are moving from their original "niche" applications to more mainstream applications). Nevertheless, the DSP approach still seems to be the processor architecture of choice for a vast range of applications [283]; this certainly applies to active control. However, due to the rate at which new systems are continuously being released, it is practically impossible to present a market overview (it would be outdated before it gets to publication). Therefore we will satisfy with discussing the most important specifications which need to be considered in the selection of the digital control configuration.

Analog input and output

The digital controller is "connected" to the sensors and actuators through Analog-to-Digital converters (ADC) and Digital-to-Analog converters (DAC), respectively. The functional dynamic range of these devices is determined by their noise floor and the maximum input value. The dynamic range is often expressed in dB, and is related to the number of bits, N : the Signal to Noise Ratio, SNR, for a full-scale sine wave input is equal to

$(6.02N + 1.76)$dB [284]. A correction factor must be used for broadband signals because the have a higher peak-to-rms ratio (a different crest factor) than sinusoids (a peak-to-rms ratio of 3:1 for bandlimited Gaussian noise is a useful approximation [285]). The necessary dynamic range is determined by the application. For most applications, a 12-bit converter will do ; in the case of the ANRAVA project, on the other hand, we have observed significant changes in the signals' dynamic range in different operating conditions (changing from smooth asphalt to pavement, for example). For a system on which an adaptive feedforward controller is implemented, it is also important to take into account the different requirements of the reference and the error signals. When cancellation starts, the errors decrease substantially, whereas the references maintain the same level, or even increase when there is feedback from the control sources.

Apart from the number of bits, it is also essential to consider the converter type. Care must be taken, when selecting a converter, that the delay introduced is acceptable for the application. For example, Sigma-Delta converters, by their very nature introduce a delay onto the converted signal. This is due to the fact that the signal is first over-sampled and then filtered. It is this filter that introduces the delay, which can be of the order of 20 ms [286]. The actual delay depends on the specific converter and the mode of operation. The advantages of Sigma-Delta converters are that they have very good noise performance and are very good for audio work, however the introduced delay makes these converters unsuitable for real-time applications, like control systems (despite the fact that they are the cheapest). Successive approximation converters can operate at sample frequencies up to 1 MHz and therefore they are a good compromise (flashing converters are even faster but they are much more expensive). In the ANRAVA project, successive approximation converters have been used providing a maximum sampling rate of 200 kHz on the inputs and 500 kHz on the outputs. Needless to say that the speed of the converters is often not the major constraint on the controller bandwidth.

Another issue associated with sampling is the use of anti-aliasing filters (on the inputs) and reconstruction filters (on the outputs). The anti-aliasing filter is used to satisfy the Nyquist criterion and should provide signal attenuation at $f_s/2$, where f_s is the sample frequency of the controller. The reconstruction filter avoids high-frequency components to be excited by the sharp transitions of the output signal of the DAC. Both filters, however, introduce delays in the control loop. These delays are determined by the cut-off frequency, the type of filter (Butterworth, Bessel, ..) and the filter order. An

obvious solution is to increase the sample frequency, which allows to shift the filter cut-off frequencies far outside the control bandwidth. Increased sample frequency, however, reduces the time available for the computation of the control signal and moreover, it requires longer filters to model the same transfer function to the same accuracy. Therefore, the right balance must be found between filter order, cut-off frequency, and sample frequency[2]. Most commercially available I/O boards provide on-board settable filters. If the available processor allows, more flexibility can be provided by over-sampling and digital filtering on the DSP.
Total Harmonic Distortion of the ADC or DAC is not usually an issue in the electronic design as it is often much better than that offered by the control transducers [285].

Processor choice

Apart from their internal (memory and bus) configuration, DSPs can be discriminated by the type of arithmetic performed. The two main types are fixed point and floating point arithmetic. In fixed-point arithmetic, the decimal point always stays at the same digit. Arithmetic overflow and underflow can thus occur and constant attention to scaling is necessary. Software development is easier for floating-point chips because designers can just concern themselves with the algorithm and not the nature of the data. The architecture also contains other features, besides the floating point capability, that simplify programming. Thus, an algorithm developed in floating-point in a high-level language can be easily ported to such a device. On the other hand, floating-point is generally more complex and slower.
Comparable performance of floating-point processors (w.r.t. fixed-point) will always be associated with a higher cost and therefore fixed-point implementation of algorithms for active control have received continuous interest. Apart from round-off errors due to the possible time variation is the dynamic range of the input signals, the filtered-X LMS is intrinsically not so well suited for fixed-point implementation. Fixed-point processing of small adjustments (which occur when the filters are nearly converged) shortens the significant word length of the differences to be added to the coefficients of the adaptive filters. The resulting error may help to improve the convergence speed of very slowly converging modes in some applications ;

[2] In that respect, the sigma-delta converters may seem an ideal solution because they have built-in anti-aliasing filters. The settings of these filters, however, are predetermined and hence may not be optimal.

in other circumstances, however, it can deteriorate the control performance. To solve this problem, a "polarised-g" INLMS algorithm is presented in [287] which provides almost the same convergence properties on a 16-bit fixed-point DSP as the filtered-X NLMS algorithm implemented in floating-point arithmetic.

Another important feature of the processor is its (in)ability to communicate with other processors. For very computationally intensive applications it may be necessary to run a few DSPs in parallel. While it is in principle possible to exchange data over the (PC or VME) bus of the host system, there are other options which are much less time consuming.
First of all, it is advisable to use a processor type which is conceived for this kind of operation, i.e. a processor which is designed with a number of communication ports through which it can transfer/receive data to/from alike processors. A typical example is the Texas Instruments TMS320C40 processor (competitor Analog Devices has its "SHARC" ADSP21060). While at first glance this processor doesn't seem to have improved significantly over its predecessor, the TMS320C30 (the first release of the 32-bit, floating point, C40 provided 40 Mflops whereas the 32-bit, floating point C30 provided 33 Mflops), its six high-speed communication ports (20 Mbits/s) allow to realise very efficient multiprocessor configurations. This is the main reason why the C40 was chosen as the platform on which the software code for the ANRAVA project was developed. The maximum configuration which was implemented in the laboratory experiments was a control system with 2 references, 2 control actuators, and 2 error microphones. This application was implemented on a single processor, and a processor from the C30 family might have been used as well in this stage. The final control system, however, involved 6 references, 6 control actuators, and 4 error microphones. This application required 3 processors running in parallel. Since the control software had been implemented on a C40 processor from the first stage, it could easily be ported to the multi-processor system and still run very efficiently.
The 20 Mbit/s specification of the communication channels is only valid after the communication has been set up. Therefore, a second improvement may result from using shared memory which can be accessed by different processors. This feature is provided on the MDC40YS-module (manufactured by LSI), which features two C40 processors, each with local memory but with access to shared memory. Compared to internal or local memory, this type of memory typically has a relatively long access time (1 or 2 wait states access time must be taken into account). However, setting

up a communication links creates a delay which is of the order of 1 μs, whereas 2 wait states at 50 MHz (clock frequency of the C40 module) amounts to a 40 ns delay. Even when taking into account some degree of arbitration to avoid simultaneous access by different processors, a shared memory configuration yields a positive balance in performance (not in price).

5.3.2 Software code optimisation

DSPs are the most efficient and cost-effective solution for active control applications because they have a function-specific instruction set : single-cycle multiplication, multiplication with accumulation, single-cycle fetch of two operands for sum-of-products calculations, etc. At the same time the instruction set is more limited than that of a generic microprocessor. In order to fully exploit the power of DSP architectures, greater awareness is demanded of the DSP programmer than for non-DSP processors. A few major issues which have to be considered in order to streamline the software code are presented here. Detailed program optimisation will not be discussed because it is very processor-specific (optimisation for the TMS320C10 and C20 can be found in [288], the TMS320C30 is dealt with in [289]).

A first remark pertains to the triggering of the conversion on the ADCs and DACs. While most of these devices allow to be triggered through software, it is advisable not to use this option and define the trigger by hardware settings (set a counter period in the clock register and generate an interrupt when the counter reaches zero). This way, *sampling jitter* is avoided. Sampling jitter occurs when the assumption of a constant sampling period is not fulfilled. When the ADCs or DACs are triggered by software, the trigger event is often programmed to follow a certain sequence of operations of a recurrent loop. As the execution of the loop cannot be guaranteed always to be finished in exactly the same time (e.g. due to sequences containing if-then-else conditions), sampling jitter will inevitably occur. Sampling jitter leads to distortion of the spectrum. In an LTI control system, this would result in small loss of performance. In an adaptive system, however, the performance loss can be significant and in severe cases may result in instability [285].

The optimisation of software code can in principle be performed at different levels. The DSP program is usually written in C and then translated by a compiler (which is processor-specific) in DSP-readable and -executable code (assembly language). General rules to optimise the C-code are : combine all operations on the same variable, use circular arrays, minimise the operands of a function, etc. However, when generating and running DSP-code which are generated from C-programs, one will generally achieve very low performance. In our experiments, a maximum of 4 Mflops could be achieved on a 40 Mflops device. The DSP-code was generated using TI's "optimising" compiler. In practice, however, it was observed that DSP-code which was generated with this compiler, did not use the very efficient instructions such as simultaneous fetch of two operands or the parallel execution of an addition and a multiplication, even if the operation which was programmed in C-code was perfectly suited for that. Getting the most out of DSPs therefore implies working at assembly language level. In general it is not necessary to program the complete algorithm in assembly, but to optimise the time-critical parts. A good starting point is to write the algorithm in C-code first, and then to work on the output of the compiler. With this approach, we have been able to attain almost 40 Mflops. Note that theoretically, the code may also be optimised by using optimised software libraries, such as SPOX® or the examples provided in [290], and by including these functions in the C-code. The LMS-algorithm will normally be provided by these libraries; other versions such as filtered-X or Normalised LMS, however, will need to be programmed from scratch.

Another important factor in the optimisation of the computational efficiency is the location of the code and the data. For the execution of the program, the DSP disposes of cache memory, which is high-speed memory linked to the CPU. Executable code is preferably optimised in length such that it can be stored in cache memory. Data memory is divided into internal memory (located on the DSP-chip), and external memory (partly located on a local bus, partly on a global bus). Both internal and external memory may be zero wait state memory, but the fact that external memory is accessed over a bus leads to additional delay. The location of data in memory is therefore determined by the length of the variables and the frequency with which they appear in the algorithm. In the case of the filtered-X LMS algorithm, the control filters are preferably located in the internal memory because they appear in the calculation of the control signal and in the update. The compiler will generally take care that variables which are larger than the internal memory size can be located in the internal memory and "spill over" into external memory but it is inefficient to do so.

The effect of both assembly language and memory map optimisation has been demonstrated in [291]. A simple program, realising the scalar product of two vectors, was implemented using a version obtained from a C-program and a second version which was written in assembly directly. The location of the operands was varied : both in internal memory (the benchmark, achieving the factory performance spec); one of both in internal, the other in external memory; both in external memory but one on the local bus and one on the global bus or both on the local bus. The "C-version" was found to be consistently slower than the "assembly-version". As for the memory mapping of the variables, there is little difference between reading data over the same external bus if the external memory is zero wait state but performance is significantly degraded for one wait state memory. If one operand is held in internal memory and the other in external, it seemed to be important which of them appeared first in the assembly command.

Finally, when distributing a program over several processors, it is important to *(i)* minimise the exchange of data and *(ii)* optimise the I/O with peripheral devices (ADC and DAC, the host PC, ...). In the ANRAVA project, the first objective was realised by performing all computation related to two control outputs on one DSP of the Quad-DSP board (6 control actuators, 3 DSPs). The fourth DSP was used for communication with the industrial PC, such as transferring control filter coefficients to the PC and receiving commands from the operator (start/stop, freeze convergence process, ...). If there is a difference in performance between the DSPs, the slowest processor should be used for this task as I/O is typically a slow process.

CHAPTER 6

GENERAL CONCLUSIONS

6.1 CONCLUSIONS FROM THE RESEARCH WORK

This thesis is mainly concerned with developing active control strategies to cope with structure-borne noise. In noise and vibration control literature, these control strategies are categorised as Active Structural Acoustic Control (ASAC). This approach has been chosen because it can be shown that ASAC is superior to Active Vibration Control (AVC), which aims at reducing vibration levels of the structure-borne noise source, both in performance and efficiency. The various ways to realise ASAC are explained in the first chapter which presents a state of the art of the current research in the field of ASAC.

The second chapter gives an overview of the control theory. The essential trade-offs which need to be considered in the design of the controller are

discussed. The overview starts from fundamental relations established in the "classical" control theory. Thus, the necessary basis is provided for the development of the control strategies presented in the subsequent chapters. Feedback and feedforward control are first dealt with separately ; both are illustrated with a practical example. The differences between the two control strategies are pointed out, but special attention is paid to the apparent equivalences which seem to exist between feedback and feedforward. From the discussion, it follows that it is more relevant to distinguish between LTI (linear time invariant) and adaptive control strategies, rather than to distinguish between feedback and feedforward.

Chapter 3 presents a feedback control strategy for ASAC. The controller is synthesised in the state space, and guarantees the reduction of the total sound power which is radiated by a vibrating structure. The control configuration is based on vibration sensors (accelerometers) to measure, and point force actuators to control the structural response of the system. A model for the vibro-acoustic behaviour of the system is included in the controller such that an ASAC approach can be realised. This implies that the controller will not necessarily aim at reducing the vibration levels measured at the feedback sensors. This approach is different from other approaches which aim at designing sensors which provide a feedback signal to the controller that is in some way proportional to the sound power radiated and thus must be minimised. In those applications, the vibro-acoustic system model is included in the design of the sensor. Though those sensors actually realise a very high level of integration -part of the signal conditioning is realised in the sensor- the performance of the resulting control configuration is inherently sensitive to system changes. Including the vibro-acoustic model in the synthesis of the controller, on the other hand, provides additional flexibility in the sense that the changes to the software code are more easily realised than changes to the design of the transducers (in case of significant variation in the dynamic behaviour of the system).
The important contribution of this work lies in the fact that it introduces a powerful tool for system identification, namely a subspace identification procedure, in the design of the controller. Through this approach, it is possible to deal with what is recognised by other researchers to be the most intricate part of the controller design procedure. Though our results were published only recently, we have already been contacted by researchers from several institutes, asking for more information about our approach. To our knowledge, the application of the control approach to the practical

example which is presented here, the active control of sound radiated from an elastic rectangular plate, is unique.

The development of ASAC system for the reduction of structure-borne road noise in a passenger car is presented in chapter 4. This application was dealt with in the framework of a Brite-Euram project "ANRAVA" and demonstrates that ASAC can also yield satisfying control performance in the case of complex control problems. The controller which was developed by KULeuven in this project, has been used by one of the project partners in a following project (with a French car maker whose name we cannot reveal) where it even performed better. The research approach, which has been presented on a number of conferences, has been adopted by other researchers dealing with structure-borne noise inside a high-speed passenger train.
The chapter also deals with an advanced signal processing algorithm, applicable to any problem involving multiple uncorrelated noise sources. The algorithm basically transforms a given set of reference signals for feedforward control to a reduced set of so-called virtual references which carry the same information as the original set of references. Working with a reduced set of virtual references allows to reduce the complexity of the controller and moreover it was shown to enhance the convergence properties of the adaptive feedforward controller. Simulations, based on data acquired during road tests performed with the active road noise control system, show that the approach works very efficiently in this practical example.

Chapter 5 presents an overview of the research work which deals with developing appropriate hardware for the implementation of active control systems. Apart from giving an overview, the chapter also illustrates that there are basic constraints which need to be met before an active control strategy can be put to practice.

6.2 EPILOGUE

It is not irrational to expect a researcher to be concerned with the relevance of his work. In this particular research work that question is directly related to the relevance of active control in the field of noise and vibration suppression. Indeed, though abundant theoretical and experimental proof has been given to illustrate the potential of an "active" approach to control

of noise and vibration, it is the market that evaluates whether that solution is worth the money. In that sense, public awareness over the unhealthy repercussions of loud noise is essential for a further growth in popularity in active noise and vibration control systems.

But apart from the fact that active control achieves larger noise and vibration reductions at low frequencies, there are additional features which make it worthwhile considering the technique. First of all, compared to passive measures, active control can yield similar -or better- performance and at the same time reduce the energy loss due to the noise and vibration suppression of the disturbance. A first example, which is taken from research work performed at our own laboratory, is an active muffler [294]. An active muffler is a device which aims at attenuating engine exhaust noise. It consists of an electrically driven valve, in series with a volume, with which the flow to the exhaust outlet can be regulated such that only the mean flow passes through it and that fluctuations of flow are buffered in the volume. The active control system consumes approximately 1 kW, which is significantly less than a conventional muffler, which typically consumes 5 kW in a standard passenger car. A second example is given in [33] (p. 64), where the power consumption of an active engine mount is compared to the estimated power consumption of balancer shafts. Balancer shafts rotate in the inverse direction of the engine crankshaft in order to reduce 2nd order vibration of 4 cylinder engines. Balancer shaft systems consume an increasing amount of power as a function of rotational speed of the engine, the maximum power consumption at 6000 rpm may exceed 1.5 kW. The active engine mount, which has performance advantage at low engine speeds and idle, was expected to consume approximately 45 W.

Secondly, some of the compromises which must be made in machine design can be alleviated by using active control. Machine mounts, for example, could be made much stiffer -and thus low-frequency oscillations could be avoided- if an actuator is used in parallel to deal with vibration transmission at high frequency ([12] p. 139). Similarly, the bushings used in a car suspension could optimised for road handling only, if an active control system takes care of the acoustic (dis)comfort due to the vibration transmission through the bushings to the car cabin.

Thirdly, as the governing control algorithm is most often realised by software code running on a digital controller, the dynamic behaviour of an active control system can easily be tuned to fulfill various requirements [295]. A straightforward example is the modification of the sound field inside a car cabin such that the engine can be made to sound like any desirable car (such that a Fiat Cinquecento could be made to sound like a

Ferrari, for example). A more relevant application could be to tune the sound perceived in a car corresponding to the subjective evaluation of different peoples. This would solve the practical problem that the sound quality norms are known to vary over the different continents (e.g. Asia vs. Europe). Product differentiation would then be realised by providing a different ROM-chip in the control module, rather than to provide cars with different acoustic lining, different tires, or other components which determine the subjective evaluation of a car.

However, when considering the applications listed in the appendix of this thesis, there seems to be a imbalance between the number of publications on active control per year (several hundreds) and the number of applications resulting from that research work. This suggests the conclusion that a lot of research in active control is not even aimed at developing a particular application or product. This is partly true. Active control is the ideal playing ground for researchers working in the field of structural dynamics and control ; a perfect touchstone for any new development in system identification, control theory, signal processing, materials research, etc. While (government) money invested in research on active control is partly justified in that respect because it generates an additional "market pull" in related research areas, this practice may also degrade the research on active control to a "bonfire of the vanities" for researchers who want to show off rather than to solve practical problems.

Nevertheless, active control is not a marketable product on its own. People cannot simply buy active control components and apply them in the way they would apply acoustic absorbing material[1]. To date, an active control solution involves a substantial engineering effort and skill to make it work - in the first place- and to maximise its performance/cost ratio. It has not yet been possible to provide active control systems as an option in CAE-software dealing with analysis of noise and vibration problems. In that respect, passive and active control often seem to be worlds apart, instead of complementary such that optimal performance can be achieved by the well-balanced application of both principles. One major step still to be taken is

[1] An exception might be the "smart foam", as it is presented in [1]. Current application of that concept seems to evolve towards a classical ANC configuration [296], however, and not towards a stand-alone device which maximises the absorption of acoustic energy at its surface.

the further integration of the active control approach, earlier in the product development stage.

APPENDIX

NON-EXHAUSTIVE LIST OF PRODUCTS AND APPLICATIONS

A lot of the active control examples which are dealt with in literature are concerned with relatively simple systems, such as beams, plates, cylinders, laboratory simulations of duct noise (using loudspeaker as disturbance source), etc.

In this appendix, reference is given to "real-life" applications. In this overview, two main categories are distinguished : *applications* of active control, and active control *products*. The former group comprises all research work concerned with developing demonstration prototype active control systems. The latter group consists of active control systems, or products involving active control technology, which are available on the market. In this group, a few companies will be mentioned as well which provide consulting services in the domain.

A general overview of application fields of active control has already been given in chapter 1. The appendix complements the overview with a number

of specific examples. Additional overviews of applications are also presented in [68] (chapter 9) and [297] (pp. 550 - 925).

APPLICATIONS

The automotive and aerospace business has always showed an interest in the research on active control. The most obvious reason is the potential weight (and thus fuel) savings that may result from applying active control. Inversely, the large potential market (and the associated return in case of success) seems to have motivated researchers to study on active control systems for vibration and noise abatment in these transportation vehicles.

Active suspensions to control vehicle body motion are a straightforward example. Mercedes Benz AG has applied the technology both to a C-class passenger car [298] and a super-high decker O 404 coach [299]. In contrast to systems developed for Formula 1 cars, these systems were not developed to increase cornering speed etc., but they were specifically aimed at increasing handling safety and ride comfort. Semi-active suspensions, which rely on tunable dampers, have been studied because they offer satisfying performance at a reasonable cost and power consumption. An interesting concept are the tunable dampers using electrorheological [300] or magnetorheological [301] fluids.

Active control of car interior noise is a second major research topic. An overview of research opportunities is given in [302]. Research on *Active control of engine noise* has been carried out both at research institutes [303] and large automotive companies [304]. For an overview of research concerned with road noise, refer to chapter 4. Noise due to airconditioning systems is considered in [305]. Aerodynamically induced car interior noise is a fairly new topic which is dealt with in [306]. Different "electronic mufflers" developed by NCT, Elesa, Gillet, the University of Poitiers, Freyman, and Lotus, are discussed in [307]. The overview also pays attention to semi-active systems, which rely on adapting the passive exhaust system to different engine conditions for the best acoustic behaviour. In fact, an adaptable engine exhaust silencer was already patented in 1971.

Different approaches to *active cancellation of aircraft interior noise* are summed up in [308]. Three different type of systems are distinguished by the actuators and sensors used for control. The "Active Noise Control"

systems use microphones to detect cabin sound, and speakers to eliminate it. "Active Structural Control" systems use inetial actuators to control the vibration of the fuselage, whereas "Active Isolation Systems" are said to use active mounts to control noise and vibration at the interface between disturbance sources and the fuselage. The two latter systems use microphones and accelerometers to monitor noise and vibration. Results from demonstration systems are discussed as an example of each of those systems.

Active control of duct noise seems to be a relatively mature application at this moment, which is illustrated by the fact that a large number of systems have already been installed in industry (refer to next section). It must be noted that reduction of duct noise is relatively easily achieved as long as the sound field in the duct can be assumed to be 1-dimensional (plane waves travelling down the duct). When the duct diameter increases, transversal modes appear in the frequency range of interest, which requires multiple speakers and error microphones. An interesting example is the active multichannel muffler, developed for the ventilation system of the Paris underground [309]. The duct has a square section (4 m^2) and behaves more as a room than as a wave guide. The active control system therefore uses 6 loudspeakers and 6 microphones.

An interesting application of the research on active control of double panel partitions is the *actively controlled double-glazing window*, as presented in [19] and [310]. Standard loudspeakers are used in [19], a particular loudspeaker is developed in [310] such that it fits in a standard double glazing window with a "normal" air gap.

Transformer noise is actually an application with great potential for active control as the noise source is per definition a harmonic low frequency source (fundamental frequency 50 or 60 Hz, in most cases only the first four harmonics are prominent). Achieving global reduction in the case of large size transformers, however, is not evident. An overview of the relevant issues associated with the implementation of active transformer noise control systems is presented by Angevine (a leading researcher in this field) [311].

Recent overviews of applications of active control have been made by Tichy [21] and Kam [312]. In the latter paper, some examples have been taken from research for *military applications* and were not published previously.

E.g., a system for machinery raft isolation in ships is discussed which has shown the capability to selectively isolate raft resonant modes and control independently the force pattern output at the base. Another example is an adaptive wing design to improve the performance of aircraft (a fighter aircraft is shown in the figure). The adaptive wing has : (1) wing twist shape memory alloy (SMA) actuators to enhance lift in multiple flight regimes, (2) leading edge and trailing edge control surfaces using SMA and piezoelectric composite actuators to achieve minimum drag and maximum lift, (3) wing surface coated with polymer material to actively reduce drag and noise generated by turbulence, and (4) embedded fiber-optic sensor arrays for real-time aerodynamic pressure measurements.

PRODUCTS

Apart from the research on practical applications of active control, it is perhaps even more interesting to have a look at the wide range of "active control products" which are (or have been) available on the market. These products originate either from companies which aim at commercialising active control products only, such as NCT (Noise Cancellation Technologies), or Digisonix ; or from companies which have introduced active control technology in their existing product range. An example is the *active headset* : Bose Corp. is producing a headset for use by pilots in small passenger airplanes and helicopters [314] ; on the other hand, NCT and ANVT (Active Noise Vibration Technologies, a company which does not longer exist) have seperately introduced active control headsets for airline passengers annoyed by the drone of jet engines [8]. The NCT *NoiseBuster*™ analog headset is said to be the lowest priced active headset currently on the market [315]. More interestingly, a variation of this headset is sold for use with the Magnetom Magnetic Resonance Imaging (MRI) scanner developed by Siemens Medical Systems. The search for higher-resolution images in the medical profession had resulted in the use of powerful electromagnets ; the noise levels of an MRI system, however, has increases in proportion. Where there used to be a compromise between the quality of the MRI image and the noise it makes, patients can now enjoy music while high-quality cross-section images are taken by the MRI scanner. A wide range of active headsets is also sold by TechnoFirst under the product name *NoiseMaster*™ [316].

Another product which has been developed by TechnoFirst is the ANCAS® seat (Active Noise Controller for Aircraft Seat) which is a noise attenuation system integrated into the passenger seat, aimed at improving the acoustic comfort within a wide frequency band [317]. The system does not need external synchronisation and therefore it is well suited for retrofit. The product is the result of a collaboration between TechnoFirst and Dassault Electronique (manufacturer of aeronautical and electronic equipment) and will be commercialised by Dassault Electronique.

The ANCAS seat is just a first example in a long row of active and semi-active control systems implemented in commercial aircraft. NCT has developed an active sound control system for Saab Aircraft AB using loudspeakers and microphones installed in the cabin. The first aircraft to be delivered to a customer market with the system fitted as standard was the Saab 2000 (in 1994), shortly followed by the Saab 340*plus*, and the Alenia ATR42-500 [318]. The system is be installed by Ultra Electronics (formerly Dowty). With this system, Saab Aircraft was the first airframer to introduce an active noise cancellation system.
A more recent system, which has now been launched on the de Havilland DASH-8 200, 300 and 400 aircraft, utilises active tuned vibration attenuators attached to the fuselage frames in the region around the propellor plane to provide forces to the frames to oppose the deflections of the fuselage caused by the propeller excitation [319]. Active control systems are also expected to be standard fitted to the King Air, the Twin Commander, and the Canadair Challenger aircraft.
The *Aviation Week & Space Technology* journal reports about a system using Active Tuned Mass Absorbers (ATMAs) for reducing cabin noise which will be installed in a Midwest Express DC-9-30 as soon as the FAA Parts Manufacturers Aproval and Suppl. Type Certificate is received [320]. the ATMAs are designed to cancel the high noise levels in the back of the DC-9 due to its rear-mounted jet engines and replace the four passive-tuned vibration absorbers per engine that are standard on the DC-9s. The system will be installed by Barry Controls and was developed in collaboration with Hood Technology Corporation (company of von Flotow) [321] and was said to outperform loudspeaker systems developed by competitors for the same aircraft in terms of system complexity (lower) and reduction (larger).

Commercially available *active suspensions* have been supplied both by Nissan and Toyota in the past who have been offering cars fitted with such suspension to the Japanese domestic market [322]. The currently available

Citroen Xantia *ACTIVA* uses two hydraulic pistons (one in the front, one in the rear) acting between the torsion bar and the car body to keep the car horizonal during cornering. Though the system works in parallel to the passive system, it is not a semi-active system because it does not work on adapting damper rates (which system is found in a lot of other cars).
Nissan has offered in *active interior-quieting* system as an option in the 1992 Bluebird in Japan. It was the first system of its kind to be installed in a production vehicle and was aimed at reducing engine noise at speeds between 3000 and 5000 rpm.
Active mufflers for internal combustion engines have not yet made it to mass production, though some isolated implementations have been reported (NCT has installed an electronic muffler on a stationary Detroit Diesel 6V-92 450-horsepower engine [314]).

Standard, modular *active control systems for duct noise*, which are available from different manufacturers (*NoiseEater*™ by NCT [323], *Eolane* by TechnoFirst [324], DigiDuct by Digisonix [325]), have been developed for the retrofit market and are designed to allow easy placement in existing HVAC (Heating, Ventilation, Air Conditioning) installations. Active duct silencer have the ability to provide low frequency noise control without obstructing air flow or adding significant weight or bulk.
Larger industrial air treatment systems often involve more engineering. The critical part of such systems is not the control strategy (which is relatively standard, using an upstream reference microphone, control loudspeakers and a downstream error microphone) but the shielding of the hardware to corrosive particles which are floating in the gases and the temperature to which the microphones and speakers are exposed. Another effect which shortens the life of a loudspeaker is the magnitude of the noise level that has to be generated. In general it is unwise to drive a speaker at its maximum capability and the number of speakers should be increased if the magnitude of the noise level would require a single speaker to be driven with a deflection which is larger than half its rated maximum. In the first implementations, an average speaker in a low-frequency industrial apllication lasted only one year before it had to be replaced. This aspect has been looked upon carefully and lifespan of these components has been significantly increased since then [92].

Digital Controllers, dedicated to active control applications, have appeared on the market since a few years. Digisonix has designed the *DigiWare*® development system for active control application research and

development. The software (operated from Windows 3.1 or Win95 on PC) and hardware (C40 board) package combines Digisonix' proprietary active control technology with user friendly application development tools to allow customers to engineer their application. Similarly, TechnoFirst has brought a range of controllers to the market which are based on the control system which was developed for internal use (*NOVACS*™, *NOVACS Lite*™, *ANCOM*™, *ACTA*™ [326]). The *EZ-ANC* active noise control development system by Causal Systems [327] is a somewhat more modest software and hardware package. The product is aimed at demystifying the field of active noise control and to make it accessible to engineers; researchers; consultants; and industrial product designers. It is based on a stand-alone digital signal processing board, with a wide range of control algorithms pre-programmed, which communicates with a PC through a serial port connection. Because of its relatively large group delay (approximately 30 sample periods) it is not suited for broadband applications.

A vibration problem which is of particular relevance in Japan is the vibration induced in tall buildings by *earthquakes and strong winds*. Though the idea of solving that problem by active control was already raised in the 1950s, it was thanks to the technological advances that the concept has evolved in a number of response-controlled buildings. In 1989 An active control system was installed on a building to verify the reliability of the system against earthquakes and strong winds. Test data showed that the system was very effective and interest in the concept has increased enormously in Japan. Today a wide range of control systems for buildings are developed and commercialised by the Kajima Technical Research Institute [328].

A very interesting application of active vibration control is found in the so-called *smart ski* [329]. The ski, which is sold by K2 (a major ski manufacturer), has a laminated body in which a piezoelectric ceramic actuator is embedded which damps the shocks and vibrations of the ski. The smart ski is said to provide improved control on fast downhill runs where it gives enhanced stability in carving quick turns on hard snow. The ski itself was actually designed to be a very versatile ski and therefore it was made relatively short. The disadvantage of short skis, however, is that they vibrate at high speeds. The piezoceramic actuators were then used to damp the first vibrational mode of the ski. The actuator was not driven to counteract vbration but to dissipate mechanical energy as heat in a resistive shunt. The shunt circuit was optimised to provide the right amount of damping because

it was observed that the ski was called unresponsive when too much damping was introduced. The actuator is a PZT QuickPack® strain actuator [330], provided by ACX™, a firm which was founded in 1992 to develop and commercialise smart materials and Smart Structures technology.

Some other products or products under developments are mentioned in [315] and [325]. NCT announced in 1994 it would be producing an actively quieted kitchen hood, which, besides having sharply reduced noise levels, has achieved a 10 - 30 % reduction in energy use. Similar systems were said to be pursued for use in vacuums, air conditioners, microwaves, computers and other household appliances. Furthermore, NCT has been field testing an active muffler for buses in three US cities. Commercial development of an active control system for the reduction of noise generated by large transformers was also said to be worked at by NCT. The system uses piezoceramic actuators to induce vibration into the skin of the transformer and cancels noise in any direction and it is not susceptible to ambient noises such as wind. NCT was also aiming at releasing in mid-1994 a system that removes siren noise from radio transmissions that originate in emergency vehicles. Further developments of that technique might be useful in a variety of different applications including cellular and telephone systems, fax and modem transmissions, voice recognition systems and other areas where signal-to-noise ratio improvement is important. A similar idea is worked upon by Digisonix to improve communications in a car interior by the so-called Digital Voice Enhancement (DVE) system.

Consulting services for active control are offered by numerous companies. In fact, most of the companies like NCT, Digisonix, etc., have started from that kind of work. E.g., Digisonix is a subsidiary of Nelson Industries, Inc., a leading supplier of complete exhaust and filtration systems for a wide variety of applications. The early success of commercial applications of active control has prompted Nelson to create Digisonix, Inc., as a subsidiary to further develop, apply and market this technology. Part of Digisonix' well developed technology is currently being applied through exclusive licences : in aerospace, by Lord Corporation, the leading worldwide supplier of vibration control products in the aerospace industry ; Ford holds a license of Digisonix' patents relating to automotive applications. Similarly, NCT has granted a license to Ultra Electronics for the installation of the ANC system in the Saab 2000 (and other) aircraft after NCT had completely developed the system.

Alpine Electronics, Inc., which is basically a car audio manufacturer, has developed a digital (adaptive feedforward) controller for use in automobile interior quieting systems. Alpine Electronics does not plan to market complete automobile ANC systems, but wants to provide the ANC controller to other companies [330].
Consulting services are also offered by BBN (Bolt Beranek & Newman, mainly involved with military applications [331]), Adaptive Audio Inc. (consulting services in active noise and vibration control and signal processing [332]), Cooper Tire and Rubber (supplier of automotive tires and engine mounts, now also developing active control systems for automobiles, aircraft, and office environments [332]), and many, many others.

BIBLIOGRAPHY

[1] Fuller, C.R., Bronzel, M.J., Gentry, C.A., and Whittington, D.E., 1994, "Control of sound radiation/reflection with adaptive foams," *Proc. NoiseCon 94*, Ft. Lauderdale, FL, 1 - 4 May 1994, pp. 429 - 436.

[2] Eriksson, L.J., 1994, "Recent Trends in the Development of Active Sound and Vibration Control Systems," *Proc. NoiseCon 94*, Ft. Lauderdale, FL, 1 - 4 May 1994.

[3] Bernhard, R.J., 1994, "The state of the art of active-passive noise control," *Proc. NoiseCon 94*, Ft. Lauderdale, FL, 1 - 4 May 1994, pp. 421 - 428.

[4] Ahmadian, M., Song, X., and Reichert, B., 1997, "Semiactive Control of Structural Resonance," *Proc. 11th Symp. Struct. Dyn. and Contr.*, VPI & SU, Blacksburg, VA, 12 - 14 May 1997.

[5] Ahmadian, M., Song, X., and Reichert, B., 1997, "Semiactive Control of Multibody Systems," *Proc. 11th Symp. Struct. Dyn. and Contr.*, VPI & SU, Blacksburg, VA, 12 - 14 May 1997.

[6] Spencer, B.F., Sain, M.K., and Dyke, S.J., 1997, "Semi-Active Control of Civil Engineering Structures," *Proc. 11th Symp. Struct. Dyn. and Contr.*, VPI & SU, Blacksburg, VA, 12 - 14 May 1997.

[7] Weltin, U., Feurer, G., 1991, "Aktive Aggregatlagerungen," *Fortschritte der Farhzeugtechnik*, **10**, Wallentowitz, Vieweg, Braunschweig (in German).

[8] O'Connor, L., 1994, "Generating the sounds of silence," *Mech. Eng.*, April 1994, pp. 54 - 58.

[9] Tichy, J., 1994, "Achievements and tasks for active noise control," *Proc. NoiseCon 94*, Ft. Lauderdale, FL, 1 - 4 May 1994, pp. 309 - 314.

[10] Uosukainen, S., 1997, "Modified JMC Method in Active Control of Sound," *ACUSTICA - acta acustica*, **83**, pp. 105 - 112.

[11] Nelson, P.A., and Elliott, S.J., 1986, "The minimum power output of a pair of free field monopole sources," *J. Sound and Vib.*, **105**, pp. 173 - 178.

[12] Jenkins, M.D., Nelson, P.A., Pinnington, R.J., and Elliott, S.J., 1993, "Active isolation of periodic machinery vibrations," *J. Sound and Vib.*, **166**(1), pp. 117 - 140.

[13] Darlington, P., and Avis, M.R., 1996, "Noise control in resonant soundfields using active absorbers," *Proc. InterNoise 96*, Liverpool, England, 30 July - 1 August 1996, pp. 1121 - 1126.

[14] Darlington, P., 1996, "Active boundary control of enclosed sound fields," *Proc. InterNoise 96*, Liverpool, England, 30 July - 1 August 1996, pp. 1127 - 1132.

[15] Burdisso, R.A., and Fuller, C.R., 1992, "Theory of feedforward controlled system eigenproperties," *J. Sound and Vib.*, **153**(3), pp. 437 - 451.

[16] Burdisso, R.A., and Fuller, C.R., 1992, "Dynamic behavior of structural-acoustic systems in feedforward control of sound radiation," *J. Acoust. Soc. Am.*, **92**(1), pp. 277 - 286.

[17] Elliott, S.J., 1993, "Active control of structure-borne noise", *Proc. of the Institute of Acoustics*, Vol. 15 Part 3, pp. 93-119.

[18] Tsahalis, D.T., Katsika, S.K., and Manolas, D.A., 1993, "A Genetic Algorithm for Optimal Positioning of Actuators in Active Noise Control : Results from the ASANCA project," *Proc. of Inter-Noise 93*, Leuven, Belgium, August 24 -26, pp. 83 - 88.

[19] De Fonseca, P., Dehandschutter, W., Sas, P., and Van Brussel, H., 1996, "Implementation of an active noise control system in a double-glazing window," *Proc. ISMA 21 - Noise and Vib. Eng.*, Leuven, Belgium, 18 - 20 Sept. 1996, pp. 377 - 388.

[20] Mangiante, G., 1997, Description of the patent by H. Coanda, *to be published in Int. J. of Act. Contr.*

[21] Tichy, J., 1995, "Applications for active control of sound and vibration," *Proc. InterNoise95*, Newport Beach, CA, 10 - 12 July 1995, pp. 17 - 28.

[22] Guicking, D., 1993, "Active noise control - A review based on patent specifications," *Proc. Noise-93*, St. Petersburg, Russia, 31 May - 3 June 1993, pp. 153 - 158.

[23] Elliott, S.J., and Nelson, P.A., 1993, "Active Noise Control," *IEEE Signal Processing Magazine*, **Oct. 1993**, pp. 12 - 35.

[24] Guicking, D., 1996, "Active control of vibration and sound -an overview of the patent literature," *Proc. ISMA 21 - Noise and Vib. Eng.*, Leuven, Belgium, 18 - 20 Sept. 1996, pp. 199 - 220.

[25] Guicking, D., 1988, "Active Noise and Vibration Control," Annotated reference bibliography, 3rd ed.

[26] Guicking, D., 1991, "Active Noise and Vibration Control," Annotated reference bibliography, 1st supplement to 3rd ed.

[27] "Glossary of terms in acoustics," *definitions proposed by Noise/News Int.*, Sept. 1995, pp. 162 - 167.

[28] Marulo, F.S., Lecce, L., Buono, G., Carbone, A., and Canciaruso, N., 1985, "Theoretical studies of frame applied dynamic absorbers to reduce vibration and noise of turboprop aircraft," *Aerotecnica Missili e Spazio*, **64** (4).

[29] Sutton, T.J., Elliott, S.J., Brennan, M.J., and Heron, K.H., 1996, "Active isolation of noise transmission through a helicopter gearbox support strut using multiple magnetostrictive actuators," *Proc. ISMA 21 - Noise and Vib. Eng.*, Leuven, Belgium, 18 - 20 Sept. 1996, pp. 315 - 328.

[30] Gardonio, P., Elliott, S.J., and Pinnington, R.J., 1996, "Active control of structural vibration transmission from a vibrating rigid body to a flexible panel using two active mounts," *Proc. ISMA 21 - Noise and Vib. Eng.*, Leuven, Belgium, 18 - 20 Sept. 1996, pp. 233 - 246.

[31] Ghesquiere, H., Friot, E., and Albarrazin, A., 1994, "Active noise control for reducing booming noise in cars," *IMechE* 1994, pp. 191 - 198.

[32] von Flotow, A., 1997, "Methods of active vibration isolation," plenary speech, *ACTIVE 97*, Budapest, Hungary, 21 - 23 August 1997.

[33] Quinn, D.C., 1992, "Automotive Active Engine Mount Systems," *ATZ/MTZ Sonderheft Motor und Umwelt '92*, pp. 62 - 64.

[34] Fuller, C.R., Hansen, C.H., and Snyder, S.D., 1991, "Active control of sound radiation from a vibrating rectangular panel by sound sources and vibration inputs : an experimental comparison," *J. Sound and Vib.*, **145**(2), pp. 195 - 215.

[35] Naghshineh, K., and Koopmann, G.H., 1992, "A design method for achieving weak radiator structures using active vibration control," *J. Acoust. Soc. Am.*, **92**(2, Pt. 1), pp. 856 - 869.

[36] Wang, B-T., and Fuller, C.R., 1991, "Evaluation of different forms of cost functions in the design of active structural-acoustic control systems," *Proc. Noise-Con 91*, Tarrytown, NY, 14 - 16 July 1991, pp. 291 - 298.

[37] Siano, D., Concilio, A., Viscardi, M., and Lecce, L., 1997, "Sound-vibration link analysis in a fuselage cavity for active control (ASAC) specification,", *Proc. InterNoise 97*, Budapest, Hungary, 25 - 27 August 1997, pp. 493 - 496.

[38] Meirovitch, L., and Thangjitham, S., 1990, "Active Control of Sound Radiation Pressure," *Trans. ASME, J. Vib. and Acoust.*, **112**, pp. 237 - 244.

[39] Meirovitch, L., and Thangjitham, S., 1992, "Control of Sound Radiating from an Orthotropic Plate," *Trans. ASME, J. Vib. and Acoust.*, **114**, pp. 531 - 539.

[40] Fahy, F., 1985, "Sound and Structural Vibration," Academic Press, London, pp. 69.

[41] Fuller, C.R., and Burdisso, R.A., 1991, "A Wavenumber Domain Approach to the Active Control of Structure-borne Sound," *J. Acoust. Soc. Am.*, **148**, pp. 355 - 360.

[42] Wang, B-T., 1997, "Optimal location of PZT actuator for the PVDF based wavenumber sensing approach in active sound radiation control," *Proc. ACTIVE 97*, Budapest, Hungary, 21 - 23 August 1997, pp. 719 - 732.

[43] Thi, J., Unver, E., and Zuniga, M., 1991, "Comparison of design approaches in sound radiation suppression," *Proc. Conf. Recent Advances in Active Control of Sound and Vib.*, Blacksburg, VA, 15 - 17 April 1991, pp. 534 - 551.

[44] Clark, R.L., and Fuller, C.R., 1991, "Active structural acoustic control with adaptive structures including wavenumber considerations," *Proc. Conf. Recent Advances in Active Control of Sound and Vib.*, Blacksburg, VA, 15 - 17 April 1991, pp. 507 - 524.

[45] Clark, R.L., and Saunders, W.R., 1993, "An Intelligent Systems Approach to Active Structural Acoustic Control," *Proc. 1993 SAE Noise and Vib. Conf.*, Traverse City, MI, 15 - 18 May 1995, pp. 153 - 177.

[46] Mathur, G.P., and Tran, B.N., 1991, "A study of structural control of plate transmission loss using wavenumber analysis," *Proc. Conf. Recent Advances in Active Control of Sound and Vib.*, Blacksburg, VA, 15 - 17 April 1991, pp. 552 - 563.

[47] Lee, C.K., and Moon, F.C., 1990, "Modal Sensors/Actuators," *J. Applied Mechanics*, **57**, pp. 434-441.

[48] Snyder, S.D., Tanaka, N., Kikushima, Y., 1996, "The Use of Optimally Shaped Piezo-electric Film Sensors in the Active Control of Free Field Structural Radiation, Part 1 : Feedforward Control," *Trans. of the ASME, J. of Vibrations and Acoustics*, **117**, pp. 311 - 322.

[49] Snyder, S.D., Tanaka, N., Kikushima, Y., 1996, "The Use of Optimally Shaped Piezo-electric Film Sensors in the Active Control of Free Field Structural Radiation, Part 2 : Feedback Control," *Trans. of the ASME, J. of Vibrations and Acoustics,* **118**, pp. 112-121.

[50] Friot, E., 1997, "Optimal feedback control of a radiating plate under broadband acoustic loading," *Proc. ACTIVE 97*, Budapest, Hungary, 21 - 23 August 1997, pp. 873 - 884.

[51] Baumann, W.T., Saunders, W.R., and Robertshaw, H.H., 1991, "Active suppression of acoustic radiation from impulsively excited structures," *J. Acoust. Soc. Am.,* **90** (6), pp. 3202 - 3208.

[52] Baumann, W.T., Ho, F-S., Robertshaw, H.H., 1992, "Active Structural Acoustic Control of Broadband Disturbances," *J. Acoust. Soc. Am.* **92** (No. 4, Pt. 1), pp. 1998 - 2005.

[53] Thomas, D.R., and Nelson, P.A., "Active Control of Turbulent Boundary Layer Noise in Aircraft," *Proc. 15th AIAA Aeroacoustics Conf.*, Oct. 25 - 27, 1993, Long Beach, CA, paper AIAA-93-4423.

[54] Thomas, D.R., and Nelson, P.A., "Feedback Control of Sound Transmission through Stiff Lightweight Partitions," *Proc. Inter-Noise 94,* Yokohama, Japan, August 29 - 31, 1994, pp. 1283 - 1286.

[55] Thomas, D.R., and Nelson, P.A., "The Application of an Implicit Self Tuning LQG Algorithm to the Active Control of Sound

Transmission," *Proc. ACTIVE 95*, Newport Beach, CA, July 06 - 08, 1995, pp. 299 - 310.

[56] Mørkholt, J., 1997, "Sensitivity to plant modelling uncertainties in optimal feedback control of sound radiation from a panel," *Proc. ACTIVE 97*, Budapest, Hungary, 21 - 23 August 1997, pp. 893 - 904.

[57] Faust, M., Wiedemann, B., Müller, G., and Baier, H., 1997, "A state-space formulation of coupled structure-acoustic vibrations for active control simulations applied to a cavity enclosed by a sandwich cylinder," *Proc. ACTIVE 97*, Budapest, Hungary, 21 - 23 August 1997, pp. 391 - 403.

[58] Maillard, J.P., and Fuller, C.R., 1997, "Active control of sound radiation from cylinders with piezo-electric actuators and structural acoustic sensing," *Proc. ACTIVE 97*, Budapest, Hungary, 21 - 23 August 1997, pp. 1021 - 1034.

[59] Elliott, S.J., and Johnson, M.E., 1993, "Radiation modes and the active control of sound power," *J. Acoust. Soc. Am.* **94**(4), pp. 2194 - 2204.

[60] Sung, C.C., and Huang, C.Y., 1997, "Comparison of active control effects in terms of structural and radiation modes for transmitted sound power through a thin plate," *Proc. ACTIVE 97*, Budapest, Hungary, 21 - 23 August 1997, pp. 1049 - 1062.

[61] Johnson, M.E., and Elliott, S.J., 1993, "Volume velocity sensors for active control," *Proc. Inst. of Acoust.*, pp. 411 - 420.

[62] Pan, X., Sutton, T.J., and Elliott, S.J., 1997, "Active control of harmonic sound transmission through a double-panel partition using a distributed PVDF actuator," *Proc. ACTIVE 97*, Budapest, Hungary, 21 - 23 August 1997, pp. 1063 - 1076.

[63] Geib, W., 1990, "Noise and Vibration : Conflicting requirements of components and overall vehicle behaviour," ***VDI BERICHTE* 791**, pp. 3 - 38.

[64] Sehrndt, G.A., and Van den Brulle, P., 1994, "Noise generation of foundry machines and definition of reproducible operating conditions," *Proc. InterNoise 94*, Yokohama, Japan, 29 - 31 August 1994, pp. 471 - 474.

[65] Moorhouse, A.T., and Gibbs, B.M., 1994, "Structure-borne sound power emission from a resiliently mounted machine," *Proc. 3rd Int. Congr. Air- and Structure-Borne Sound and Vib.*, Montreal, Canada, 13 - 15 June 1994, pp. 225 - 228.

[66] Botteldooren, D., 1993, "Feasibility Study of Active Control of Noise Perceived by Operators of Large Agricultural Machines," *Noise Control Eng. J.*, May-June 1993, pp. 221 - 229.

[67] Thomas, D.R., 1992, "The active control of the transmission of sound," *PhD. Thesis*, ISVR, Univ. Southampton, UK.

[68] Kuo, S.M., Morgan, D.R., 1996, "Active Noise Control Systems - Algorithms and DSP Implementations," John Wiley & Sons, New York.

[69] David, J., 1994, "Algorithms for analysis and design of robust controllers," *PhD. thesis*, KULeuven, Dept. ESAT.

[70] Skogestad, S., and Postlethwaite, I., 1996, "Multivariable feedback control - Analysis and Design," *John Wiley & Sons*, West Sussex, England.

[71] Åström, K.J., Wittenmark, B., 1984, "Computer controlled Systems - Theory and Design," Prentice-Hall, Englewood Cliffs, New Jersey, pp. 36 - 65.

[72] She, T., 1992, "Active vibration control by eigenstructure assignment," *PhD. thesis*, KULeuven, Dept. Mech. Eng.

[73] McFarlane, A.G., and Postlethwaite, I., 1977, "The generalized Nyquist stability criterion and multivariable root loci," *Int. Journ. Contr.*, **26**, pp. 265 - 278.

[74] Dailey, R.L., Lecture Notes for the "Workshop on H_∞ and μ Methods for Robust Control," *1991 IEEE Conf. on Decision and Control*, Dec. 9 - 10, 1991, Brighton, England, pp. 6 - 11.

[75] Doyle, J.C., and Stein, G., 1981, "Multivariable feedback design : Concepts for a classical/modern synthesis," *IEEE Trans. Aut. Contr.*, **AC-26**, pp. 4 - 16.

[76] Stein, G., and Athans, M, 1987, "The LQG/LTR Procedure for Multivariable Feedback Control Design," *IEEE Trans. on Aut. Cont.*, **AC-32** (2), pp. 105 - 114.

[77] Anderson, B.D.O., Moore, J.B., 1989, "Optimal Control, Linear Quadratic Methods," *Prentice-Hall International*, Englewood Cliffs.

[78] Kwakernaak, H., Sivan, R., 1972, "Linear Optimal Control Systems," *John Wiley & Sons,* New York.

[79] Åström, K.J., Hagander, P., and Sternby, J., 1984, "Zeros of Sampled Systems," *Automatica*, **20** (1), pp. 31 - 38.

[80] Åström, K.J., Wittenmark, B., 1984, "Computer controlled Systems - Theory and Design," Prentice-Hall, Englewood Cliffs, New Jersey.

[81] Franklin, G.F., and Powell, J.D., "Digital Control of Dynamic Systems," Addison-Wesley, 1980.

[82] Doyle, J.C., Stein, G., 1979, "Robustness with Observers," *IEEE Transactions on Automatic Control*, Vol AC-24, No. 4, August 1979, pp. 607 - 611.

[83] Neto, A.T., Dion, J.M., and Dugard, L., 1992, "Robustness bounds for LQ Regulators," *IEEE Trans. Aut. Contr.*, **AC-37**, pp. 1373 - 1377.

[84] Postletwhaite, I., 1991, "Robust control of multivariable systems using H_∞ optimisation," *Journal A*, **32** (4), pp. 8 - 19.

[85] Zames, G., 1981, "Feedback and optimal sensitivity : Model reference transformations, multiplicative seminorms, and approximate inverses," *IEEE Trans. Aut. Contr.*, **AC-26**, pp. 301.

[86] Kwakernaak, H., 1993, "Robust Control and H_∞ Optimisation - Tutorial Paper," *Automatica*, **29** (2), pp. 255 - 273.

[87] Francis, B.A., 1987, "A Course in H_∞ Control Theory," *Springer-Verlag*, Berlin-Heidelberg.

[88] Doyle, J.C., Glover, K., Khargonekar and Francis, B., 1989, "State-space solutions to standard H_∞ and H_2 control problems," *IEEE Trans. Aut. Contr.*, **AC-34**, pp. 831 - 847.

[89] Packard, A., and Doyle, J.C., 1993, "The Complex Structured Singular Value," *Automatica*, **29** (1), pp. 71 - 109.

[90] Eriksson, L.J., 1991, "The Continuing Evolution of Active Noise Control with Special Emphasis on Ductborne Noise," *Proc. 1st Conf. Recent Advances in Active Control of Sound and Vib.*, Blacksburg, VA, 15 - 17 April 1991, pp. 237 - 245.

[91] Billet, Y., 1997, "Active Feedback Noise Control of Lightly Damped Cavities," Thesis 97ER01, KULeuven, Faculty of Engineering, Dept. of Mech. Eng., div PMA.

[92] Leventhall, H.G., Wise, S.S., 1996, "Experience of active control of noise from HVAC and industrial equipment," *Proc. ISMA 21 - Noise and Vib. Eng.*, Leuven, Belgium, 18 - 20 Sept. 1996, pp. 329 - 340.

[93] Hull, A.J., Radcliffe, C.J., and Southward, S.C., 1993, "Global Active Noise Control of a One-Dimensional Acoustic Duct Using a Feedback Controller," *Trans. ASME, J. Dyn. Syst., Meas., and Contr.*, **115**, pp. 488 - 494.

[94] Bai, M.R., Shieh, C., and Lee, D., 1995, "Development of a modal LQG active noise canceler," *Proc. ACTIVE 95*, Newport Beach, CA, 6 - 8 July 1995, pp. 911 - 920.

[95] Nonami, K., Fan, Q.U., and Nakano, M., 1996, "Active noise control of one-dimensional duct using H_∞ control theory," *Proc. InterNoise 96*, Liverpool, UK, 30 July - 2 August 1996, pp. 1045 - 1050.

[96] Mehta, P., Zheng, Y., Hollot, C.V., and Chait, Y., 1996, "Active noise control in ducts : feedforward/feedback design by blending H_∞ and QFT methods," *Proc. 13th Triennial IFAC World Congr.*, **2d-17 2**, San Francisco, CA, pp. 291 - 296.

[97] Meirovitch, L., 1990, "Dynamics and Control of Structures," John Wiley & Sons Inc., US.

[98] Meirovitch, L., Baruh, H., Öz, H., 1983, "A Comparison of Control Techniques for Large Flexible Systems," *AIAA J. Guidance*, Vol. 6, No. 4, pp. 302 - 310.

[99] Åström, K.J., and Wittenmark, B., 1989, "Adaptive Control", *Addison-Wesley*, Reading (MA).

[100] Bronzel, M., 1993, "Aktive Beeinflussung nicht-stationärer Schallfelder mit adaptiven Digitalfiltern," *PhD. Dissertation*, Univ. Göttingen (in German)

[101] Ljung, L., Morf, M., and Falconer, D.D., 1978, "Fast calculation of gain matrices for recursive estimation schemes," *Int. J. of Control*, **27**, pp. 1-19.

[102] Kalman, R.E., 1960, "A New Approach to Linear Filtering and Prediction Problems," *Trans. ASME, J. Basic Eng.*, **82**, pp. 35 - 45.

[103] Carayannis, G., Manolakis, D., Kalouptsidis, N., 1983, "A fast sequential algorithm for least-squares filtering and prediction," *IEEE Trans. Acoust., Speech and Sign. Proc.*, **ASSP-31** (6), pp. 1394 - 1402.

[104] Cioffi, J.M., Kailath, T., 1984, "Fast recursive least squares transversal filters for adaptive filtering," *IEEE Trans. Acoust., Speech and Sign. Proc.*, **ASSP-32** (6), pp. 304 - 338.

[105] Schirmacher, R., Auspitzer, T., Guicking, D., 1993, "Fast algorithms for active adaptive control of nonstationary sound fields," *NAG journaal*, **120**, pp. 41 - 55.

[106] Widrow, B., Walach, E., 1996, "Adaptive Inverse Control," *Prentice-Hall, Inc.*, USA.

[107] Schütze, H., Ren, Z., 1991, "Easy and Effective Stabilization Measure for Fast Recursive Least Squares Algorithms for Adaptive Transversal Filters," *Electronics Letters,* **27** (16), pp. 1397 - 1399.

[108] Widrow, B., Stearns, S.D., 1985, "Adaptive Signal Processing," *Prentice-Hall*, Inc., Englewood Cliffs.

[109] Widrow, G., and Walach, E., 1984, "On the Statistical Efficiency of the LMS Algorithm with Nonstationary Inputs," *IEEE Trans. on Information Theory*, **IT-30** (2), pp. 211 - 221.

[110] Macchi, O., 1995, "Adaptive Processing", John Wiley & Sons, Chichester, UK.

[111] Boucher, C.C., Elliott, S.J., and Nelson, P.A., 1993, "Fast algorithms for multichannel feedforward adaptive control," *Proc. of Inter-Noise 93*, Leuven, Belgium, August 1993, pp. 739 - 742.

[112] Marshall, D.F., and Jenkins, W.K., 1992, "A Fast Quasi-Newton Adaptive Filtering Algorithm," *IEEE Trans. Sign. Proc.*, **18**, pp. 33 - 42.

[113] Bershad, N.J., and Macchi, O., 1989, "Comparison of RLS and LMS algorithms for tracking a chirped sinusoid," *Proc. ICASSP*, Glasgow, May 1989, pp. 896 - 899.

[114] Eriksson, L.J., 1985, "Active Sound Attenuation Using Adaptive Digital Signal Processing Techniques," *PhD. Thesis*, Univ. of Wisconsin-Madison.

[115] Eriksson, L.J., 1992, "Active Noise Control," in *Noise and Vibration Control Engineering*, Edited by Beranek, L.L., and Vér, I.L., *John Wiley & Sons, Inc.,* New York, pp. 565 - 583.

[116] Eriksson, L.J., 1991, "Development of the Filtered-U Algorithm for Active Noise Control," *J. Acoust. Soc. Am.,* **89** (1), pp. 257 - 265.

[117] Haykin, S., 1991, "Adaptive Filter Theory," *Prentice-Hall,* Englewood Cliffs, NJ.

[118] Regalia, P.A., 1995, "Adaptive IIR Filtering in Signal Processing and Control," *Marcel Dekker, Inc.,* New York, NY.

[119] Bao, C., 1994, "Adaptive algorithms for active noise control and their applications," *PhD. Thesis,* KULeuven, Belgium.

[120] Widrow, B., Schur, D., and Shaffer, S., 1981, "On adaptive inverse control," in *Conf. Rec. of 15th Asilomar Conf. on Circuits, Systems and Computers,* Santa Clara, CA (Nov. 1981), pp. 185 - 189.

[121] Burgess, J.C., 1981, "Active adaptive sound control in a duct : A computer simulation," *J. Acoust. Soc. Am.*, **70** (3) , pp. 715 - 726.

[122] Elliott, S.J., Stothers, I.M., Nelson, P.A., 1987, "A Multiple Error LMS Algorithm and Its Application to the Active Control of Sound and Vibration," *IEEE Trans. on Acoustics, Speech, and Sig. Proc.,* **ASSP-35** (10), pp. 1423 - 1434.

[123] Elliott, S.J., and Nelson, P.A., 1993, "Active Noise Control," *IEEE Signal Processing Magazine*, **Oct. 1993**, p. 26.

[124] Snyder, S.D., and Hansen, C.H., 1992, "Design considerations for active noise control systems implementing the multiple input, multiple output LMS algorithm," *J. Sound and Vib.*, **159**, pp. 157 - 174.

[125] Chen, G., Sone, T., and Abe, M., 1996, "Effects of multiple secondary paths on convergence properties in active noise control systems with LMS algorithm," *J. Sound and Vibr.*, **195** (1), pp. 217 - 228.

[126] Elliott, S.J., Boucher, C.C., and Nelson, P.A., 1992, "The behaviour of a multiple channel active control system," *IEEE Trans. Sign. Proc.,* **40**, pp. 1041 - 1052.

[127] Kurisu, K., 1996, "Effect of the difference between error path C and its estimate $\hat{C}$ for active noise control using Filtered-X LMS algorithm," *Proc. InterNoise 96*, Liverpool, UK, 30 July - 2 August, pp. 1041 - 1044.

[128] Boucher, C.C., Elliott, S.J., and Nelson, P.A., 1991, "The effect of modelling errors on the performance and stability of active noise control systems," *Proc. 1st Conf. Recent Advances in Active Control of Sound and Vibration,* 15 - 17 April 1991, Blacksburg, VA, pp. 290 - 301.

[129] Jolly, M.R., and Rossetti, D.J., 1995, "The effects of model error on model-based adaptive control systems," *Proc. ACTIVE 95*, Newport Beach, CA, 6 - 8 July 1995, pp. 1107 - 1116.

[130] Saito, N., Sone, T., Ise, T., and Akiho, M., 1995, "Conditions for optimal on-line identification of secondary paths in active noise control systems," *Proc. ACTIVE 95*, Newport Beach, CA, 6 - 8 July 1995, pp. 1141 - 1148.

[131] Douglas, S.C., and Olkin, J.A., 1993, "Multiple-input, multiple-output, multiple-error adaptive feedforward control using the Filtered-x Normalised LMS algorithm," *Proc. 2nd Conf. Recent Advances in Active Control of Sound and Vibration,* Blacksburg, VA, 28 - 30 April 1993, pp. 743 - 754.

[132] Mathews, V.J., and Xie, Z., 1993, "A Stochastic Gradient Adaptive Filter with Gradient Adaptive Step Size," *IEEE Trans. Sign. Proc.*, **41** (6), pp. 2075 - 2087.

[133] Shan, T.J., and Kailath, 1988, "Adaptive Algorithms with an Automatic Gain Control Feature," *IEEE Trans. Circuits and Systems*, **35** (1), pp. 122 - 126.

[134] Nelson, P.A., and Elliott, S.J., 1990, "Active Control of Sound," *Academic Press*, London.

[135] Dehandschutter, W., and Van Cauter, R., 1995, BE-ANRAVA project, Internal Report BE-5391-TR-6.1-K-01.

[136] Stothers, I.A., Quinn, D.C., and Saunders, T.J., 1995, "Computationally efficient LMS based hybrid algorithm applied to

the cancellation of road noise," *Proc. ACTIVE 95*, Newport Beach, CA, 6 - 8 July 1995, pp. 727 - 734.

[137] Elliott, S.J., and Rafaely, B., 1997, "Frequency-domain adaptation of feedforward and feedback controllers," *Proc. ACTIVE 97*, Budapest, Hungary, 21 - 23 August 1997, pp. 771 - 787.

[138] Shen, Q., and Spanias, A., 1992, "Time and Frequency domain X-Block LMS algorithms for single channel active noise control," *Proc. 2nd Int. Congr. Recent Developments in Air- and Structure-Borne Sound & Vibration*, pp. 353 - 360.

[139] Shen, Q., and Spanias, A., 1993, "Frequency domain adaptive algorithms for multi-channel active sound control," *Proc. 2nd Conf. Recent Advances in Active Control of Sound and Vibration,* Blacksburg, VA, 28 - 30 April 1993, pp. 755 - 766.

[140] Chen, C-H., 1993 "Integrated design methods for motion control systems," *PhD. Thesis*, KULeuven, Belgium.

[141] Torfs, D., 1995 "High performance motion control in the presence of structural flexibilities - An engineering approach," *PhD. Thesis*, KULeuven, Belgium.

[142] Van den Braembussche, P., Swevers, J., and Van Brussel, H., 1997, "Selection of weighting fucntions for H_∞ synthesis for robustness against varying load for machine axes with linear motor," *submitted to Trans. ASME.*

[143] Rubak, P., and Johansen, L.G., 1997, "Active noise cancelling in headsets : limitations caused by non-minimum phase transfer function of the cancelling sound source," *Proc. ACTIVE 97*, Budapest, Hungary, 21 - 23 August 1997, pp. 457 - 466.

[144] Burdisso, R.A., Vipperman, J.S., and Fuller, C.R., 1993, "Causality analysis of feedforward-controlled systems with broadband inputs," *J. Acoust. Soc. Am.* **94** (1), pp. 234-242.

[145] Brokish, C.W., 1994, "Causality constraints of adaptive active control algorithms," *Proc. of Noise-Con 94*, Ft. Lauderdale, Florida, 1994 May 01-04, pp. 325-330.

[146] S. Suzuki, T. Hayashi, 1994, "A study on the causality problem in active noise control," *Proc. InterNoise 94*, Yokohama, Japan, August 29-31, pp. 1213-1216.

[147] Nelson, P.A., Hammond, J.K., Joseph, P., and Elliott, S.J., 1990, "Active control of stationary random sound fields", *J. Acoust. Soc. Am.* **87** (3), pp. 963-975.

[148] Paillard, B., Le Donh, C.T., Berry, A., and Nicolas, J., 1995, "Accelerating the convergence of the Filtered-X LMS algorithm

through transform-domain optimisation," *Mech. Syst. and Sig. Proc.*, **9** (4), pp. 445 - 464.

[149] Nelson, P.A., Sutton, T.J., and Elliott, S.J., 1990, "Performance limits for the active control of random sound fields from multiple primary sources", *Proc. of the IOA*, 12, Part 1, pp. 677 - 678.

[150] Ross, C.F., 1980, "Active Control of Sound," *Ph.D. thesis*, University of Cambridge.

[151] Guicking, D., 1995, Remark during plenary speech "Active Control of Road Noise" by R. Bernhard on *ACTIVE 95*, Newport Beach, CA, 6 - 8 July 1995.

[152] Arruda, J.R., Dehandschutter, W., and Sas, P., "Active vibration control in finite plates using a structural power flow approach," accepted for publication in *Acta Acustica united with Acustica*.

[153] Noiseux, D. U., 1970, "Measurement of Power Flow in Uniform Beams and Plates," *J. Acoust. Soc. Am.*, **47** (1, Pt. 2), pp.238-247.

[154] Pascal, J.-C., Loyau, T., and Carniel, X., 1993, "Complete Determination of Structural Intensity in Plates Using Laser Vibrometers," *J. Sound and Vib.*, **161**(3), pp. 527-531.

[155] Miller, D. W., Hall, S. R., and von Flotow, A. H., 1990, "Optimal Control of Power Flow at Structural Junctions," *J. Sound and Vib.*, **140**(3), pp.475-497.

[156] Tanaka, N., Snyder, S. D., Kikushima, Y., and Kuroda, M., 1994 "Vortex structural power flow in a thin plate and the influence on the acoustic field," *J. Acoust. Soc. Am.*, **96**(3), pp.1563-1574.

[157] Gibbs, G. P., Fuller, C. R., and Silcox, R. J., 1995, "Active Control of Flexural and Extensional Power Flow in Beams Using Real Time Wave Sensors," *Proc. ACTIVE 95,* Newport Beach, CA, 6 - 8 July 1995, pp.909-925.

[158] Pan, X., Hansen, C.H., Snyder, S.D., 1995, "Power Transmission Characteristics in an Actively Controlled Semi-Infinite Plate," *Int. J. Act. Contr.*, **1**(2).

[159] Nelson, P. A., Curtis, A. R. D., Elliot, S. J., Stothers, I. M., and Bullmore, A. J., 1987, "The Minimum Power Output of Free Field Point Sources and the Active Control of Sound," *J. Sound and Vib.*, **116**, pp.397-414.

[160] Arruda, J. R. F., and Mas, P., "Predicting and Measuring Flexural Power Flow in Plates," *Proc. the 2nd. Int. Conf. on Vibration Measurements by Laser Techniques*, Ancona, Italy, September 1996.

[161] Tanaka, N., Kikushima, Y., and Kuroda, M., 1995, "Active Wave Control of a Distributed Parameter Beam (On The Optimal Feedback

Control)," *Proc. ACTIVE 95*, Newport Beach, CA, 6 - 8 July 1995, pp.127-138.

[162] Halkyard, C. R. and Mace, B. R., 1995, "Structural Intensity in Beams - waves, transducer systems and conditioning problems," *J. Sound and Vib.*, **185**(2), pp.279-298.

[163] Pavic, G., 1995, "Comparison of Different Strategies of Active Vibration Control," *Proc. ACTIVE 95*, Newport Beach, CA, 6-8 July 1995, pp.197-208.

[164] Burdisso, R.A., and Fuller, C.R., 1994, "Design of active control systems using eigenanalysis," *Proc. 3rd Int. Congr. Air- and Structure-Borne Sound and Vib.*, Montreal, Canada, 13 - 15 June 1994, pp. 1341 - 1358.

[165] Berkman, E.F., and Bender, E.K., 1997, "Perspectives on Active Noise and Vibration Control," *Sound and Vib.* 30th Anniversary Issue, Jan. 1997, pp. 80 - 94.

[166] Olson, H.F., and May, E.G., 1953, "Electronic sound absorber," *J. Acoust. Soc. Am.*, **25**, pp. 1130 - 1136.

[167] Rood, G.M., "Introduction of Active Noise Reduction Systems in the Harrier GR5/AV8B," *Course on Active Control of Sound and Vibration*, ISVR, Southamption, 22 - 24 March 1993.

[168] Hong, J., and Bernstein, D.S., 1995, "A comparison of fundamental properties of feedback and feedforward control : Bode integral constraints and spillover," *Proc. ACTIVE 95*, Newport Beach, CA, 6 - 8 July 1995, pp. 929 - 940.

[169] Hu, J-S., 1996, "Feedforward and Feedback Control Strategy for Active Noise Cancellation in Ducts," *Trans. ASME, J. Dyn. Syst., Meas., and Contr.*, **118**, pp. 372 - 378.

[170] Burke, M.J., 1993, "State space modelling of tonal adaptive controllers," *Proc. 2nd Conf. Recent Advances in Active Control of Sound and Vib.*, Blacksburg, VA, 28 - 30 April 1993, pp. 15 - 25.

[171] Doelman, N.J., 1993, "On the optimal design of a controller for the active reduction of random noise," *Proc. 2nd Conf. Recent Advances in Active Control of Sound and Vib.*, Blacksburg, VA, 28 - 30 April 1993, pp. 26 - 37.

[172] Berkman, E.F., Coleman, R.B., and Owen, A.A., 1995, "Trade-off between using the feedforward Widrow filtered-X LMS algorithm and a compensator/regulator feedback algorithm for narrowband control," *Proc. ACTIVE 95*, Newport Beach, CA, 6 - 8 July 1995, pp. 1149 - 1159.

[173] Elliott, S.J., Sutton, T.J., Rafaely, B., and Johnson, M., 1995, "Design of feedback controllers using a feedforward approach," *Proc. ACTIVE 95*, Newport Beach, CA, 6 - 8 July 1995, pp. 863 - 874.

[174] Brown, D.E., and Cabell, R., 1993, "An application of filtered-X techniques and neural networks to the active control of non-linear systems," *Proc. 2nd Conf. Recent Advances in Active Control of Sound and Vib.*, Blacksburg, VA, 28 - 30 April 1993, pp. 3 - 14.

[175] Bozich, D.J., and MacKay, H.B., 1991, "Neurocontrollers applied to real-time vibration cancellation at multiple locations," *Proc. 1st Conf. Recent Advances in Active Control of Sound and Vib.*, Blacksburg, VA, 28 - 30 April 1993, pp. 326 - 357.

[176] Wu, A.T., Ju, M.S., and Tsuei, Y.G., 1993, "Comparison of fuzzy logic and self-tuning adaptive control of single-link flexible arm," *Mechatronics*, **3**(4), pp. 451 - 464.

[177] Babb, M., 1993, "Neural Nets - No Hype, Please," *Control Engineering*, pp. 49.

[178] Hunt, K.J., Sbarbaro, D., Zbikowski, R., and Gawthrop, P.J., 1992, "Neural Networks for Control Systems - A survey," *Automatica*, **28**(6), pp. 1083 - 1112.

[179] Arruda, J.R.F., Moreira, F.J.O., and Pereira, A.K.A, 1997, "Comparing feedback vibration control and feedforward power-flow-based control strategies using a simple plate example," *Proc. ACTIVE 97*, Budapest, Hungary, 21 - 23 August 1997, pp. 75 - 92.

[180] Sas, P., Augusztinovicz, F., "Pressure gradient acoustic intensity measurements," *Proc. ISAAC 3, Advanced Techniques in Applied and Numerical Acoustics*, September 21-22, 1992, Leuven, Belgium.

[181] P. Sas, J.P. Coyette, "Numerical solution methods for vibro-acoustic radiation problems," *Proc. ISAAC 7, Advanced Techniques in Applied and Numerical Acoustics*, September 16-17, 1996, Leuven, Belgium.

[182] Francis, B.A., 1987, "A course in H_∞ Control Theory," *Springer-Verlag Berlin, Germany*, chapter 7, pp. 84 - 104.

[183] Van Overschee, P., De Moor, B., Dehandschutter, W., Swevers, J., 1997, "A Subspcae Algorithm for the Identification of Discrete Time Frequency Domain Power Spectra," *accepted for publication in IFAC Automatica*.

[184] Dehandschutter, W., Henrioulle, K., Swevers, J., Sas, P., Van Overschee, P., 1997, "Feedback control of broadband sound radiation from a rectangular plate," *Proc. of the 11th VPI & SU Symposium on Dynamics and Control of Structures*, May 11 - 14, Blacksburg, VA.

[185] Bhat, R.B., Mundkur, G., 1991, "Vibration of plates using plate characteristic functions obtained by reduction of partial differential equation," *Journal of Sound and Vibration* **161** (1), pp. 157 - 171.

[186] Kim, S.J., Jones, J.D., 1991, "A study of actuators for active control of distributed elastic systems," *Proc. Of Noise-con 91*, July 14-16, Tarrytown, New York, pp. 283 - 290.

[187] Maidanik, G., 1974, "Vibrational and radiative classifications of modes of a baffled finite panel," *Journal of Sound and Vibration* **34** (4), pp. 447 - 455.

[188] Heylen, W., Lammens, S., Sas, P., 1995, "Modal Analysis Theory and Testing," KULeuven, Belgium.

[189] Wang, B-T., Burdisso, R.A., Fuller, C.R., "Optimal placement of piezoelectric actuators for active control of sound radiation from elastic plates," *Proc. of Noise-Con 91*, Tarrytown, New York, July 14-16, 1991, pp. 267-274.

[190] De Fonseca, P., Dehandschutter, W., Sas, P., Van Brussel, H., "Optimisation of sensor and actuator locations in active noise and vibration control applications," *Proc. of ACTIVE 97*, Budapest, Hungary, 21 - 23 August 1997, pp. 649 - 664.

[191] Bailey, T., and Hubbard Jr., J.E., 1985, "Distributed Piezoelectric-Polymer Active Vibration Control of a Cantilever Beam," *J. Guidance, Control and Dynamics,* **8** (5), pp. 605 - 611 en

[192] Burke, S., Hubbard Jr., J.E., 1988, "Distributed Actuator Control Design for Flexible Beams," *Automatica* **24** (5), pp. 619 - 627.

[193] Dailey, R.L., in Video Course of "Workshop on H_∞ and μ Methods for Robust Control," *1991 IEEE Conf. on Decision and Control*, Dec. 9 - 10, 1991, Brighton, England.

[194] Doyle, J.C., and Stein, G., 1981, "Multivariable feedback design : concept for a classical/modern synthesis," *IEEE Trans. Autom. Control,* **AC-25**, pp. 4-16.

[195] Steinbuch, M., Bosgra, O.H., 1994, "Robust performance H_2/H_∞ optimal control," *33rd IEEE Conf. on Decision and Control,* Dec. 14-16, Orlando, FL.

[196] Kaminer, I., Khargonekar, P.P., and Rotea, M.A., 1993, "Mixed H_2/ H_∞ Control for Discrete-time Systems via Convex Optimization," *Automatica,* **29** (1), pp. 57-70.

[197] Rafaely, B., Garcia-Bonito, J., and Elliott, S.J., 1997, "Feedback control of sound in headrest," *Proc. ACTIVE 97*, Budapest, Hungary, 21 - 23 August 1997, pp. 445 - 456.

[198] Abramovitz, M., Stegun, I.A., 1965, "Handbook of Mathematical Functions," Dover Publications, New York.

[199] Van Niekerk, J.L., Tongue, B.H., Packard, A.K., 1995, "Active Control of a Circular Plate to Reduce Transient Noise Transmission," *J. of Sound and Vib.*, **183** (4), pp. 643 - 662.

[200] Giebeler, W-R., and Booz, G., 1994, "Acoustic Behaviour as Objective in Vehicle Body Development," *Proc. Numerical analysis in automotive engineering*, VDI-Tagung Würzburg, 26 - 27 Sept. 1994, pp. 237 - 252 (in German).

[201] Vandeurzen, U., Leuridan, J., Bakkers, W., Roesems, D., 1994, "Technology Trend for Vibro-Acoustic CAE Used in Vehicle Development," *Proc. Numerical analysis in automotive engineering*, VDI-Tagung Würzburg, 26 - 27 Sept. 1994, pp. 253 - 266.

[202] Otto, N.C., and Feng, B.J., 1994, "Automotive Sound Quality in the 1900's," *Proc. 3rd Int. Congr. Air- and Structure-Borne Sound and Vib.*, Montreal, Canada, 13 - 15 June 1994, pp. 635 - 638.

[203] Kim, J., 1996, "Sound Quality in Cars Assessment and Engineering Solutions : Impulsive Sound Transmission through a Car Bulkhead," *ISVR Contract Report* 96/13, BRE 7796, 7.4/04/07.

[204] George, A.R., and Carr, J.F., 1995, "Recent advances in understanding automobile aerodynamic noise," *Proc. First Joint CEAS/AIAA Aeroacoust. Conf.*, München, Germany, 12 - 15 June 1995, paper CEAS/AIAA-95-004.

[205] Zorea, S.I., 1994, "Interior automobile aerodynamic noise measured in a controlled wind flow," *Proc. 3rd Int. Congr. Air- and Structure-Borne Sound and Vib.*, Montreal, Canada, 13 - 15 June 1995, pp. 643 - 646.

[206] Wyckaert, K., Hendricx, W., 1993, "Characterisation of the Structure-Borne Road Noise Problem, Task 2.1 : Interior Noise Analysis," ANRAVA Technical Report BE-5931-TR-2.1-L-01.

[207] Roggenkamp, T.J., Kompella, M.S., and Bernhard, R.J., 1994, "Development of experimentally based structural/acoustic automobile tire noise models," *Proc. Noise-Con94*, Ft. Lauderdale, FL, 1 - 4 May 1994, pp. 111 - 116.

[208] Stevenson, D.C., 1976, "Some effects of tyre tread and road surface on road noise," *J. Sound and Vib.*, **48**(4), pp. 561 - 564.

[209] Meiarashi, S., Ishida, M., Nakashiba, F., and Niimi, H., 1994, "Noise reduction factors of drainage asphalt pavement," *Proc. InterNoise 94*, Yokohama, Japan, 29 - 31 August 1994, pp. 423 - 426.

[210] Iwai, S., Miura, Y., Koike, H., and Levy, G., 1994, "Influence of porous asphalt pavement characteristics on the horn amplification of tire/road contact noise," *Proc. InterNoise 94*, Yokohama, Japan, 29 - 31 August 1994, pp. 431 - 434.

[211] Toyoda, T., Komatsu, N., Noge, S., and Yoshikawa, 1994, "Cabin noise in car on cruising the porous asphalt pavement," *Proc. InterNoise 94*, Yokohama, Japan, 29 - 31 August 1994, pp. 439 - 442.

[212] Sandberg, U., 1997, "A new porous pavement with extended acoustical lifetime and useful even on low-speed roads," *Proc. InterNoise 97*, Budapest, Hungary, 25 - 27 August 1997, pp. 99 - 104.

[213] Targeted Research Action Environmentally Frienldy Vehicles, Cluster Noise and Vibration Suppression Technologies, Annual review meeting November 27 - 28 1996.

[214] Sutton, T.J., Elliott, S.J., and Saunders, T.J., 1997, "Transmission of road noise through a vehicle damper," *Proc. ATA 5th Int. Conf.*, Firenze, Italy, 26 - 28 February 1997.

[215] Hendricx, W., and Vandenbroeck, D., "Suspension Analysis in View of Road Noise Optimisation,"

[216] van der Linden, P.J., and Fun, J.K., 1993, "Using Mechanical-Acoustic Reciprocity for Diagnosis of Structure Borne Sound in Vehicles," *Proc. 1993 SAE Noise and Vib. Conf.,* May 1993, Traverse City, MI, pp. 625 - 630.

[217] Ochsner, S.D., and Bernhard, R.J., 1995, "Application of a component mobility technique to automotive suspension systems," *Noise Control Eng. J.*, **43**(3), pp. 73 - 82.

[218] Dong, B., Green, M., Voutryas, M., Bremner, P. and Kasper, P., "Road Noise Modelling Using Statistical Energy Analysis Method," *Proc. 1995 SAE Noise and Vib. conf.*, Traverse City, MI, 15 - 18 May 1995, pp. 761 - 766.

[219] Johnson, R., 1995, "Sound Quality Team Tackles Road Noise," *Sound and Vib.*, March 1995, pp. 6 - 12.

[220] Göhlich, D., and Köder, B., 1993, "Structure-borne sound transmission calculation of elastomeric elements," *Proc. VDI-Tagung Berechnung im Automobilbau*, pp. 213 - 235.

[221] V. Moreggia, 1994, Market Analysis, *internal communication in the framework of the ANRAVA project.*

[222] Dehandschutter, W., Van Cauter, R., and Sas, P., 1995, "Active control of simulated structure borne road noise using force actuators," *Proc. 1995 SAE Noise and Vib. Conf.,* Traverse City, MI, 15 - 18 May 1995, pp. 737 - 747.

[223] Dehandschutter, W., Van Cauter, R., and Sas, P., 1995, "Active structural acoustic control of structure borne road noise : theory, simulations and experiments," *Proc. ACTIVE 95*, Newport Beach, CA, 6 - 8 July 1995, pp. 735 - 746.

[224] Wyckaert, K., Dehandschutter, W., and Banfo, G-L., 1995, "Active vibration control of rolling noise in a passenger car : performance evaluation of actuator and feedback sensor configuration," *Proc. ACTIVE 95*, Newport Beach, CA, 6 - 8 July 1995, pp. 755 - 766.

[225] Dehandschutter, W., Sas, P., and Banfo, G-L., 1996, "Active control of rolling noise in a passenger car through structural and acoustic control," *Proc. ISMA 21 - Noise and Vib. Eng.*, 18 - 20 Sept. 1996, p. 401 - 412.

[226] Dehandschutter, W., and Sas, P., 1998, "Active control of structure-borne road noise using vibration actuators," *Trans. ASME J. Vib. and Acoust.* **120**, Jan. 1998.

[227] Sutton, T. J., Elliott, S. J., and Moore, I., 1991, "Use of nonlinear controllers in the active attenuation of road noise inside cars", *Proc. Conf. Recent Advances in Active Control of Sound and Vib.*, Blacksburg, VA, 15 - 17 April 1991, pp. 682-690.

[228] Sutton, T.J., Elliot, S.J., Malcom McDonald, A., and Saunders, T.J., 1994, "Active Control of Road Noise inside Vehicles", *Noise Control Eng. J.*, **42**(4), pp. 137 - 147.

[229] Ferren, W. B., and Bernhard, R.J., 1991, "Active Control of Simulated Road Noise," *Proc. 1991 SAE Noise and Vib. Conf.*, Traverse City, MI, 13 - 16 May 1991, pp. 69 - 82.

[230] Heatwole, C.M., Dian, X., and Bernhard, R.J., 1993, "Parameter Studies of Active Control of Road Noise in Automobiles", *Proc. of 2nd Conf. on Recent Advances in Active Control of Sound and Vib.*, Blacksburg, Virginia, 28 - 30 April 1993, pp. 813 - 825.

[231] Heatwole, C.M., Dian, X., and Bernhard, R.J., 1993, " Determination of the number of input transducers required for active control of road noise inside automobiles," *Proc. Noise-con 93*, Williamsburg, Virginia, 2 - 5 May 1991, pp. 207 - 211.

[232] Heatwole, C.M., and Bernhard, R.J., 1994, "Prediction of Multiple-Input Active Control of Road Noise in Automobile Interiors", *Proc. of Noise-Con 94*, Ft. Lauderdale, Florida, 1-4 May 1994, pp. 367-372.

[233] Bernhard, R.J., 1995, "Active Control of Road Noise inside Automobiles," *Proc. ACTIVE 95*, Newport Beach, CA, 6 - 8 July 1995, pp. 21 - 33.

[234] Guicking, D., Bronzel, M., and Bohm, W., 1991, "Active adaptive noise control in cars," *Proc. Conf. Recent Advances in Active Control of Sound and Vib.*, Blacksburg, VA, 15 - 17 April 1991, pp. 657 - 670.

[235] Bronzel, M., 1993, "Aktive Beeinflussung nicht-stationärer Schallfelder mit adaptiven Digitalfiltern," *Ph.D. Thesis*, Drittes Physikalisches Institut, University of Göttingen (in German).

[236] Sano, H., Adachi, S., and Kasuya, H., 1995, "Active Noise Control based on the RLS algorithm for an automobile," *Proc. of ACTIVE 95*, Newport Beach, CA, 1995 July 6 - 8, pp. 891 - 898.

[237] Sano, H., Adachi, S., and Kasuya, H., 1997, "Application of a Least Squares Lattice Algorithm to Active Noise Control for an Automobile," *Trans. of the ASME, J. of Dyn. Syst., Meas., and Contr.*, **119**, pp. 318 - 320.

[238] Freymann, R. et al., 1995, "Vorrichting zur aktiven akustischen Schall-kompensation in Hohlräumen eines Kraftfahrzeuges," European Patent Appl. No. 0649129 A2. Prior. (D) : Oct. 13, 1993. Pbl. : April 19, 1995.

[239] Sano, H., and Adachi, S., 1997, "Two-degree-of-freedom active control of road noise inside automobiles," *Proc. ACTIVE 97*, Budapest, Hungary, 21 - 23 August 1997, pp. 543 - 556.

[240] Schirmacher, R., Hölz, G., Redmann, M., and Scheuren, J., 1997, "Active noise and vibration control for a high speed railcar : a case study," *Proc. ACTIVE 97*, Budapest, Hungary, 21 - 23 August 1997, pp. 557 - 564.

[241] Wyckaert, K., Hendricx, W., 1994, "Transmission path analysis in view of active cancellation of road induced noise in automotive vehicles", *Proc. InterNoise 94*, 29 - 31 August 1994, Yokohama, Japan, pp. 653-656.

[242] Wyckaert, K., Hendricx, W., 1993, "Characterisation of the Structure-Borne Road Noise Problem, Task 2.5 : Vibration Transmission Path Identification," ANRAVA Technical Report BE-5931-TR-2.5-L-01.

[243] Wyckaert, K., Van der Auweraer, H., and Hermans, L., 1995, "An approach for the simulation of active control sensor and actuator configurations for rolling noise reduction in automotive vehicles," *Proc. ACTIVE 95*, Newport Beach, CA, 6 - 8 July 1995, pp. 747 - 754.

[244] Shoji, A., Watanabe, Y., and Hamada, H., 1997, "Subjective evaluation of the effects for active noise control," *Proc. InterNoise 97*, Budapest, Hungary, 25 - 27 August 1997, pp. 533 - 536.

[245] Van der Auweraer, H., and Wyckaert, K., 1996, "Sound Quality : perception, analysis and engineering," *Proc. ISAAC 7 - Advanced Techniques in Applied and Numerical Acoustics*, KULeuven, Belgium, 16 - 17 Sept. 1996.

[246] van den Berg, F., 1996, "Laagfrekwent geluid - een onderschat probleem," *GELUID*, **1,** pp. 14 - 18.

[247] Dehandschutter, W., Van Herbruggen, J., Swevers, J., and Sas, P., 1997, "Real-time enhancement of reference signals for feedforward control of random noise due to multiple uncorrelated sources," *IEEE Trans. on Sign. Proc.*, **46**(1), Jan. 1998.

[248] Otte, D., Van den Auweraer, H., Leuridan, J., 1992, "The use of multivariate correlation techniques for vibro-acoustic experimental data analyis", *Proc. ISMA 17,* Course on Advanced Techniques in Applied Acoustics, Pt. II.

[249] Masaichi, A., 1995, "Virtual reference signals for active road noise cancellation in a vehicle cabin," *Proc. 1995 SAE Noise and Vib. Conf.*, Traverse City, MI, 15 - 18 May 1995, Vol 2, pp. 747 - 752.

[250] Golub, G.H., et al., 1989, "Matrix computations", *The John Hopkins Univerity Press*, Baltimore and London, pp 201 - 209.

[251] Moonen, M., 1990, "Jacobi-type updating algorithms for signal processing, system identification and control," *PhD. Thesis*, Dept. ESAT, KULeuven, Belgium.

[252] Wilkinson, J.H., 1965, "The algebraic eigenvalue problem," *Claredon Press*, Oxford, England, pp. 131 - 139.

[253] Narayan, S. S., Peterson, A. M., Narasimha, M. J., 1983, "Transform Domain LMS Algorithm," *IEEE Trans. Acoustics, Speech, and Sig. Proc.,* **ASSP-31**(3), pp. 609 - 615.

[254] Marshall, D.F., Jenkins, W.K., and Murphy, J.J., 1989, "The Use of Orthogonal Transforms for Improving Performance of Adaptive Filters," *IEEE Trans. Circuits and Systems*, **36**(4), pp. 474 - 483.

[255] Beaufays, F., 1995, "Transform-Domain Adaptive Filters : An Analytical Approach," *IEEE Trans. Sig. Proc.*, **43**(2), pp. 422 - 431.

[256] Chen, G., Sone, T., and Abe, M., 1996, "Effects of multiple secondary paths on convergence properties in active noise control systems with LMS algorithm," *J. Sound and Vib.*, **195**(1), pp. 217 - 228.

[257] Kim, H-S., Park, Y., and Sur, K-H., 1996, "Active noise control of road booming noise with constraint multiple filtered-X LMS algorithm," *Proc. InterNoise 96*, Liverpool, UK, 30 July - 1 August 1996, pp. 1155 - 1158.

[258] Gray, R.M., 1972, "On the Asymptotic Eigenvalue Distribution of Toeplitz Matrices," *IEEE Trans. Information Theory*, **IT-18**(6), pp. 725 - 730.

[259] Blondel, L.A., and Elliott, S.J., 1996, "Non-linearities in tuned loudspeaker enclosures for active noise control," *Proc. ISMA21 - Noise and Vibration Eng.*, Leuven, Belgium, 18 - 20 September 1996, pp. 341 - 352.

[260] Maier, R., Pucher, M.J., and Bschorr, O., 1996, "Active Resonator for Noise Control," *Proc. ISMA21 - Noise and Vibration Eng.*, Leuven, Belgium, 18 - 20 September 1996, pp. 353 - 364.

[261] Carme, Ch., Derrien, D., and Valentin, G., 1997, "The ANCAS seat : extension and industrial applications," *Proc. ACTIVE 97*, Budapest, Hungary, 21 - 23 August 1997, pp. 381 - 390.

[262] Snyder, S.D., Tanaka, N., Burgemeister, K., and Hansen, C.H., 1995, "Direct-sensing of global error criteria for active noise control," *Proc. ACTIVE 95*, Newport Beach, CA, 6 - 8 July 1995, pp. 849 - 860.

[263] Lindner, D.K., Baumann, W.T., Ho, F-S., and Bielecki, E., 1991, "Modal domain optical fiber sensors for control of acoustic radiation," *Proc. Conf. Recent Advances in Active Control of Sound and Vib.*, Blacksburg, VA, 15 - 17 April 1991, pp. 839 - 850.

[264] Masson, P., and Berry, A., 1996, "Active Structural Acoustic Control using Straing Sensing," *Proc. of Fourth Int. Congress on Sound and Vibration*, St-Petersburg, Russia, 24-27 June 1996, pp. 453-560.

[265] Lindner, D.K., Zvonar, G.A., Baumann, W.T., Delos, P.L., 1993, "Nonlinear Effects of a Modal Domain Optical Fiber Sensor in a Vibration Suppression Control Loop for a Flexible Structure," *Trans. of the ASME, J. of Vibration and Acoustics*, **115**, pp. 120-128.

[266] Kim, S.J., and Jones, J.D., 1991, "Optimal design of piezoactuators for active noise and vibration control," *AIAA J.* **29**(12), pp. 2047 - 2053.

[267] Newman, M.J., 1991, "Distributed active vibration controllers," *Proc. Conf. Recent Advances in Active Control of Sound and Vib.*, Blacksburg, VA, 15 - 17 April 1991, pp. 379 - 392.

[268] Kim, S.J., and Jones, J.D., 1991, "Optimizing of piezo-actuator/substructure coupling for ative noise and vibration control," *Proc. Conf. Recent Advances in Active Control of Sound and Vib.*, Blacksburg, VA, 15 - 17 April 1991, pp. 78 - 91.

[269] Gugsch, M, 1994, "Selection of the Actuator Principle," ANRAVA Internal Report, BE-5931-TR-5.1.1-Me-01.

[270] Murray, B.S. 1995, "A compact force generator for active vibration control," *Proc. ACTIVE 95*, Newport Beach, CA, 6 - 8 July 1995, pp. 817 - 826.

[271] Gennesseaux, A., 1993, "Research for New Vibration Isolation Techniques : From Hydro-Mounts to Active Mounts," *Proc. 1993 SAE Noise and Vib. Conf.,* May 1993, Traverse City, MI, pp. 491 - 499.

[272] Piezosystem Jena, Product information, Präzisionselemente GmbH.

[273] Ushijima, T., and Kumakawa, S., 1993, "Active Engine mount with Piezo-Actuator for Vibration Control," *Proc. 1993 SAE Int. Congr. and Expo.*, Detroit, MI, 1 - 5 March 1993, paper 930201.

[274] Goodfriend, M.J., and Shoop, K.M., 1992, "Adaptive characteristics of the magnetostrictive alloy, Terfenol-D, for active vibration control," *J. Intell. Mat. Syst. and Struct.* **3**, pp. 245.

[275] Fenn, R.C., Avakian, K.M., Boudreau, D.J., Gerver, M.J., and Torti, R.P., 1994, "Low mass, high reliability magnetostrictive reaction mass actuators," *Proc. ASME Conf. Act. Contr. Vib. and Noise*, DE-Vol. 75, pp. 457 - 464.

[276] ETREMA Terfenol-D Magnetostrictive Actuators, Product information, ETREMA Products, Inc.

[277] Resch, M., Jeger, M., and Elspass, W.J., 1996, "Optimal design of laminated plates for active vibration control," *Proc. ISMA21 - Noise and Vib. Eng.*, Leuven, Belgium, 18 - 20 September 1996, pp. 283 - 294.

[278] Antila, M., Muurinen, T., Linjama, J., and Nykänen, H., 1997, " Measurement methods of flat panel electromechanical film loudspeakers," *Proc. ACTIVE 97*, Budapest, Hungary, 21 - 23 August 1997, pp. 607 - 618.

[279] Messet, O., "Electromechanical film, EMF," VTT Chemical Technology.

[280] Antila, M., 1997, "Product Information Sheet," VTT Manufacturing Technology.

[281] Sessler, G.M., 1981, "Piezoelectricity in polyvinylidenefluoride," *J. Acoust. Soc. Am.* **70**(6), pp. 1596 - 1608.

[282] Gunn, L., 1989, "DSP uproots traditional analog jobs," *Electronic Design*, Sept. 28, pp. 49 - 52.

[283] Wright, A., 1995, "DSPs drive data acquisition and analysis," *Scientific Computing World*, June, pp. 31 - 36.

[284] N., 1995, "Practical Analog Design Techniques," *Analog Devices Technical Reference Books*, Prentice-Hall.

[285] Goodman, S.D., 1993, "Electronic design considerations for active noise and vibration control systems," *Proc. 2nd Conf. on Recent Advances in Active Control of Sound and Vib.*, Blacksburg, VA, 28 - 30 April 1993, pp. 519 - 526.

[286] Edwards, J., 1994,"Using Analog Daughter Modules and AMELIA," *Loughborough Sound Images Application Note*.

[287] Fujii, K., Yamaguchi, A., Furuya, H., and Ohga, J., 1997, "An adaptive algorithm for active noise control system by a fixed point processing type DSP," *Proc. ACTIVE 97*, Budapest, Hungary, 21 - 23 August 1997, pp. 1163 - 1170.

[288] Allie, M.C., Bremigan, C.D., Eriksson, L.J., and Greiner, R.A., 1988, "Hardware and Software Considerations for Active Noise Control," *IEEE Int. Conf. Acoust., Speech and Sign. Proc.*, New York, N.Y., 11 - 14 April 1988.

[289] Jain, Y., 1991, "Getting more out of DSPs," *Machine Design*, March 21, pp. 185 - 188.

[290] Papamichalis, P.E., 1990, "Digital Signal Processing Applications with the TMS320 Family - Volume 3," *Prentice Hall*, Englewood Cliffs, NJ.

[291] "DSP Performance Measurements," *DSPLink* **10**, 1994, p. 6.

[292] Doyle, J.C., Francis, B.A., and Tannenbaum, A.R., 1992, "Feedback Control Theory," *Macmillan Publ. Comp.*, New York, NY.

[293] Freudenberg, J.S., and Looze, D.P., 1985, "Right Half Plane Poles and Zeros and Design Tradeoffs in Feedback Systems," *IEEE Trans. Aut. Contr.*, **AC-30** (6), pp. 555 - 565.

[294] Boonen, R., and Sas, P., 1997, "Design of an active noise cancellation device for internal combustion engines," *Proc. ACTIVE 97*, Budapest, Hungary, 21 - 23 August 1997, pp. 499 - 512.

[295] Eatwell, G.P., 1995, "Active Control of Sound Quality," *Proc. InterNoise 95*, Newport Beach, CA, 10 - 12 July 1995, pp. 521 - 525.

[296] Fuller, C.R., Guigou, C., and Gentry, C.A., 1996, "Foam-PVDF smart skin for active control of sound," *Proc. SPIE Conf. Smart Struct. and Mat.*, San Diego, CA, 27 - 29 February 1996, pp. 26 - 37.

[297] *Noise and Vibration Worldwide*, June 1997, p. 13, Book review of : Hansen, C.H., and Snyder, S.D., 1997, "Active control of noise and vibration."

[298] *Act. Sound & Vib. Contr. News* **2** (5), May 1995, p. 1.

[299] *dSPACE News*, Dec. 1996, p. 3

[300] "Shock absorber uses electrorheological fluid," *Automot. Eng.* **100** (6), June 1992, pp. 27 - 30.

[315] Hulings, W.J., 1994, "Noise Cancellation Technologies, Inc. - Products and Developments," *Proc. InterNoise 94*, Yokohama, Japan, 29 - 31 August 1991, pp. 2201 - 2202.
[316] "TechnoFirst Headset Series," Product information sheet, TechnoFirst.
[317] "ANCAS," Product information sheet, TechnoFirst.
[318] Powers, J.C., 1994, "Regional Aircraft Are Breaking The Barrier Of Sound," *Regional Air Int.*, April 1994, pp. 16 - 21.
[319] Ross, C.F., and Purver, M.R., 1997, "Active cabin noise control," *Proc. ACTIVE 97*, Budapest, Hungary, 21 - 23 August 1997, pp. XXXIX - XLVI.
[320] Lavitt, M.O., 1997, "Active Absorbers Cancel Aircraft Engine Noise," *Aviation Week & Space Techn.*, Feb. 1997, p. 68.
[321] von Flotow, "Methods of active vibration isolation," plenary speech on *ACTIVE 97*, Budapest, Hungary, 21 - 23 August 1997.
[322] "Nissan and Toyota adopt active suspension on production cars," *Automot. Eng.*, Dec. 1989, pp. 86 - 90.
[323] "NoiseEater enters Europe," *Noise & Vib. Worldwide*, April 1995, p. 19.
[324] "Eolane concept," Product information sheet, TechnoFirst.
[325] "Digisonix® Technology and Active Sound and Vibration Control," *Noise & Vib. Worldwide*, Jan. 1997, pp. 10 - 14.
[326] "Active controllers series," Product information sheet, TechnoFirst.
[327] "EZ-ANC - Active Noise Control Development System," Product information sheet, Causal Systems.
[328] Kobori, T., 1997, "Structural control of buildings under earthquakes and strong winds," *Proc. ACTIVE 97*, Budapest, Hungary, 21 - 23 August 1997, pp. III - XV.
[329] Ashley, S., 1995, "Smart skis and other adaptive structures," *Mech. Eng.* **117**(11), pp. 76 - 81.
[330] Quickpack® Piezoelectric actuators, Product information sheet, ACX™ - Active Control eXperts.
[331] "BBN...Solving Noise and Vibration Problems," Company information sheet.
[332] *Active Sound & Vib. Contr. News*, Sept. 1996, p. 1.
[333] *Active Sound & Vib. Contr. News*, Feb. 1997, pp. 1 - 2.
[334] DIGISONIX Newsletter, Summer/Fall, 1990, p. 1.

[301] Wereley, n.M., 1997, "Experimental validation of Electrorheological and Magnetorheological Fluid-Based Dashpot Damper Models," *Proc. 11th Symp. on Struct. Dyn. and Contr.*, Blacksburg, VA, 12 - 14 May 1997.

[302] Bremigan, C.D., Eriksson, L.J., Eppli, R.J., and Stroup, E.S., 1995, "Future of active sound and vibration control in vehicles," *Proc. ACTIVE 95*, Newport Beach, CA, 6 - 8 July 1995, pp. 791 - 802.

[303] Van Overbeek, M.W., 1993, "Active reduction of periodic noise in the interior of a delivery van," *NAG journaal*, **120**, pp. 25 - 39.

[304] Uchida, H., Nakao, N., and Butsuen, T., "High performance system to control interior engine noise," *Mazda Motor Corporation.*

[305] Polisset, C., and Bordeneuve-Guibe, J., 1995, "Insonorisation of a car air conditioning system : Active noise control approach using numveric simulations," *Proc. ACTIVE 95*, Newport Beach, CA, 6 - 8 July 1995, pp. 779 - 790.

[306] Heatwole, C.M., Franchek, M.A., and Bernhard, R.J., 1997, "Active Control of Wind Noise Using Robust Feedback Control," *Proc. 1997 SAE Noise and Vib. Conf*, Traverse City, MI, 20 - 22 May 1997, pp. 165 - 175.

[307] "Advanced exhaust silencing," *Automot. Eng.*, Feb. 1993, pp. 13 - 16.

[308] Trego, L.E., 1994, "Noise and Vibration Control," *Aerospace Engineering*, Sept. 1994, pp. 10 - 12.

[309] Montassier, A., and Carme, Ch., 1997, "Active multichannel muffler for the ventilation system of Paris underground," *Proc. InterNoise 97*, Budapest, Hungary, 25 - 27 August 1997, pp. 497 - 501.

[310] Carme, Ch., Montassier, A., and Rehfeld, M., 1997, "Active double-glazing windows," *Proc. InterNoise 97*, Budapest, Hungary, 25 - 27 August 1997, pp. 489 - 492.

[311] Craig, S.E., and Angevine, O.L., 1995, "Active control of hum from large power transformers - The real world," *Proc. 2nd Conf. on Recent Advances on Active Control of Sound and Vib.*, Blacksburg, VA, 28 - 30 April 1993, pp. 279 - 290.

[312] Kam, W., 1995, "Applications of active control,"*Proc. ACTIVE 95*, Newport Beach, CA, 6 - 8 July 1995 (late paper).

[313] Jessel, M., 1988, "25 years with active noise control/ A survey and comments with reference to Guicking's bibliography and "Field reshaping theory," *Proc. InterNoise 88*, Avignon, France, 30 August - 1 Sept. 1988, pp. 953 - 958.

[314] O'Connor, 1991, "Putting a Lid On Noise Pollution," *Mech. Eng.*, June 1991, pp. 46 - 51.